The role and regulation of voltage-gated potassium channels in vascular smooth muscle

Tammaro, Paolo

Award date:
2003

Awarding institution:
University of Bath

THE ROLE AND REGULATION OF VOLTAGE-GATED POTASSIUM CHANNELS IN VASCULAR SMOOTH MUSCLE

Submitted by Paolo Tammaro
For the degree of PhD
of the University of Bath
2003

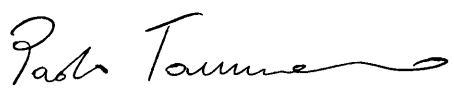

ProQuest LLC
789 East Eisenhower Parkway
P.O. Box 1346
Ann Arbor, MI 48106-1346

[...] tenebras necessest
non radii solis neque lucida tela diei
discutiant, sed naturae species ratioque.

Lucretius, De rerum natura I 146-148

Acknowledgments

I would like to thank my supervisor, Dr Sergey V Smirnov, for his enthusiasm and support throughout this research. As well as for his guidance and precious criticism, I would like to thank him for having had confidence in me; for this, his kindness and friendship I am sincerely grateful.

I am also grateful to many colleagues - too many to name - in the Pharmacology and Vascular Pharmacology Unit. I would also like to thank Amy L. Smith and Richard A. Firth for reading of my work.

Special thanks go to Dr Oscar Moran, for his supervision during the time spent at the National Research Council in Genoa, Italy, and for one of many unforgettable discussions about science and philosophy. I am also indebted to Dr Michael Pusch for his valuable advice, teaching and critical comments. I would like to thank Professor Franco Conti for his kind hospitality at the Institute of Biophysics. Professor Tetsuro Ishii was an invaluable *sensei* during the time I spent at King's College in London.

I am grateful to my supervisor Dr Sergey V.Smirnov to allow me to present part of the data describing two populations of SMCs in rat conduit pulmonary artery in Chapter 5, section 5.3.1. I also wish to thank Miss Amy L. Smith and Mr Simon R. Hutchings for their contribution (< 20-25%) to experimental results presented in Chapter 3 (Figs. 3.2 and 3.3) and Chapter 4 (Fig. 4.1), respectively.

Finally, I wish to express my gratitude to the British Heart Foundation for having supported my research and myself over the last three years.

Abstract

K^+ channels play a pivotal role in the regulation of excitation-contraction coupling in vascular smooth muscle cells (SMCs). The relative distribution of various types of K^+ channel in different parts of the circulatory system and the mechanisms of their regulation remain poorly understood. The aim of my work was to study the physiological role, molecular identity and mechanisms of regulation of Kv currents (I_{Kv}) in the rat vasculature. Using patch-clamp recordings, isometric-tension measurements, biochemical and immunocytochemical techniques I found that:

1. I_{Kv} is the predominant K^+ current controlling the resting potential and phenylephrine-induced oscillatory activity in rat aortic SMCs (RASMCs) and is composed predominantly of the Kv2.1 α-subunit.

2. A novel mechanism of regulation of Kv channels by intracellular Mg^{2+} was discovered in rat aortic and conduit pulmonary arterial SMCs. I_{Kv} steady-state activation and inactivation were modulated in a specific manner, depending on the type of I_{Kv} and SMCs studied.

3. In contrast to SMCs, Mg^{2+}-dependent changes in voltage-dependent characteristics of two Kv α-subunits (Kv1.5 and Kv2.1) expressed in *Xenopus* oocytes were similar and described in terms of interaction of Mg^{2+} with intracellular negative surface charges according to the Gouy-Chapman theory, suggesting SMC-specific Mg^{2+}-dependent modulation of Kv channels.

4. A physiological role for this effect was confirmed in functional experiments using endothelium-denuded rat aortic rings, in which KCl-induced isometric contractions were potentiated in Mg^{2+}-loaded arteries.

5. I_{Kv} voltage-dependent characteristics were also modulated by specific PKC inhibitors, bisindolilmalimide I and chelerythrine, in RASMCs. Immunoblot analysis confirmed the presence of PKCα, PKCδ and PKCζ, but not PKCε, isoforms in the rat aorta. Immunocytochemical images showed that PKCα was localised near the plasmalemma, while PKCδ was detected near the nucleus, suggesting that PKCα is the most likely isoform to control I_{Kv} in RASMCs.

In conclusion, my findings indicate that Kv channels play an important role in the regulation of vascular function in the rat and that their activity is modulated by intracellular Mg^{2+} and PKC.

Contents

Abbreviations and symbols

Abbreviations

ACh	acetylcholine
4-AP	4-aminopyridine
ATP	adenosine trisphosphate
BSA	bovin serum albumin
BIM	bisindolylmaleimide I
BK_{Ca}	large conductance Ca^{2+}-activated K^{+} channel
cAMP	3',5'-adenosine monophosphate
cGMP	3',5'-guanosine monophosphate
C-	carboxi terminus
CAM	cellular adhesion molecule
CACC	Ca^{2+}-activated Cl^{-}-Channels
ChTx	charybdotoxin
CICR	calcium induced calcium release
C_m	cell capacitance
CNG	cyclic nucleotide-gated channels
CPA	cyclopiazonic acid
Cx	connexin
DAG	diacylglicerol
DILT	diltiazem
DMSO	dimethylsulphoxide
DTx	α-dendrotoxin
EC	endothelial cell
EDHF	endothelium-derived hyperpolarizing factor
EDRF	endothelium-derived relaxing factor
EGTA	ethylenediaminetetra acetic acid
ET	endothelin
G protein	heterotrimeric guanine nucleotide-binding protein
GDP	guanodine diphosphate
GHK	Goldman-Hodgkin-Katz equation

GTP	guanosine triphosphate
HEPES	N-2-hydroxythylpiperazine-N-2-ethanesulphonic acid
HH-model	Hodgkin-Huxley model
K_{ATP}	ATP sensitive K^+ channel
K_{ir}	inwardly rectifier K^+ channel
Kv	voltage-gated K^+ channel
IbTx	iberiotoxin
IP_3	inositol 1,4,5-triphosphate
$I_{Cl(Ca)}$	Ca^{2+} activated Cl^- current
I_{Kv}	voltage gated K^+ current in RASMCs
I_{K1}	Kv1 type of K^+ current in rat conduit PASMCs
I_{K2}	Kv2 type of K^+ current in rat conduit PASMCs
MLC	myosin light chain
MLCK	myosin light chain kinase
N-	amino terminus
NO	nitric oxide
NSC	non-selective cation channels
OW	oscillatory wave
PASMC	pulmonary artery smooth muscle cell
PE	phenylephrine
PKA	cAMP dependent protein kinase
PKC	protein kinase C
PKG	cGMP dependent protein kinase
PIP_2	phospshatidil inositol di-phosphate
PLC	phospholipase C
PMA	phorbol 12-myristate 13-acetate
PMCA	plasmalemma Ca^{2+} ATPase
PP2A	protein phosphatase 2A
PSS	physiological salt solution
R	regression coefficient
RASMC	rat aortic smooth muscle cell
ROCC	receptor operated cation channel
SERCA	sarcoplasmic-endoplasmic Ca^{2+} ATPase
s.e.m.	standard error of mean

SDS-PAGE	sodium dodecil sulphate polyacrylamide gel electrophoresis
SMC	smooth muscle cell
SOCC	store operated cation channel
SUR	regulatory sulphonylurea receptor
TEA	tetraethylammonium
TEVC	two electrodes voltage clamp
TM	trans-membrane
TRPC	transient receptor potential channel
VACC	volume-activated Cl^- channel
VDCC	voltage dependent calcium channel
VIP	vasoactive intestinal peptide
VRAC	volume-regulated anion channels
VSMC	vascular smooth muscle cell

Symbols

B_{Mg}	fraction of channels blocked by Mg^{2+}
δt	empirical delay in activation onset
E_K	K^+ equilibrium potential given by the Nernst equation
F	Faraday constant (9.6485×10^4 C mol^{-1})
γ	single channel conductance
g_K	peak I_{Kv} conductance
G_{max}	maximum whole-cell conductance
k_a	activation *e*-fold slope
Kd	apparent dissociation constant
k_h	inactivation *e*-fold slope
k_{+1}	apparent rate constant of drug interaction with the Kv channel
k_{-1}	apparent rate constant of drug dissociation with the Kv channel
i	single channel conductance
I'	asymptotic maximal current at a given potential
IC_{50}	concentration required to evoke 50% of a maximum response
I_{leak}	leak current
I'_{Kv}	leak-corrected peak current
I_{NORM}	normalised peak current

I_{peak}	current amplitude measured at the test pulse
$\hat{I}_{peak}$	test current amplitude measured following the most hyperpolarised V_c
I_{ss}	non-inactivating current component
$I(t)$	current as a function of time
Ψ_i	inner surface potential
ψ_o	outer surface potential
Pa	channel probability to be activated
P_{block}	Boltzmann factor in equation [6.7]
Pi	channel probability to be inactivated
Po	channel open probability
δ	relative electric distance
t	time
T	temperature in Kelvin
$t_{1/2}$	half time of the maximal Kv current amplitude
τ_a	time constant of current activation
τ_d	drug-induced time constant
τ_i	time constant of current inactivation
V_a	half-activation potential
ΔV_a	relative change in V_a
V_c	conditioning potential
V_h	half-inactivation potential
ΔV_h	relative change in V_h
V_m	membrane potential
z	ion valence

It should be mentioned that some symbols such as A and B are omitted from this list since they have different meanings (which are defined in the text) in different equations.

Chapter 1

Introduction

1.1. Vascular smooth muscle

Smooth muscle is a major component of blood vessels as well as of a number of internal organs, e.g. the walls of the uterus, gastrointestinal tract and airways. Blood vessels include arteries and veins which carry blood away and return it to the heart, respectively. In general, blood vessels are characterised by three layers: *tunica adventitia*, *tunica media* and *tunica intima* (Fig. 1.1). Smooth muscle cells (SMCs) are localised in the intermediate layer (*tunica media*) and are organised in a variable number of sheets (from 1 to 6) depending on the vessel diameter. Cells are interconnected to each other by gap junctions acting as a low resistance pathway allowing a rapid spread of electrical signals throughout the vessel wall. The luminal (*tunica intima*) and external (*tunica adventitia*) layers are composed of non-SMC types. Fibroblasts, mast cells, macrophages and unmyelinated nerve fibers are present in the *adventitia*, while the *intima* consists of a monolayer of endothelial cells. Vascular SMCs (VSMCs) have an elongated (at least 50 μm) double spindle shape and a diameter of ~5 μm (Casella & Taglietti, 1996; Aaronson & Ward, 1999).

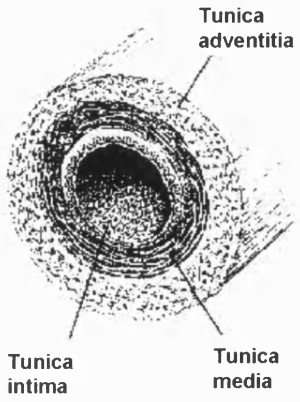

Figure 1.1 Schematic representation of a section of a generic blood vessel. Adapted form (Casella & Taglietti, 1996)

1.1.1 Histology of the blood vessels

1.1.1.1 Arteries

Arteries are classified into three types according to their size: large (or elastic) arteries; medium (or muscular or distributive) arteries; and small arteries or arterioles, which are less than 0.5 mm in diameter in humans. A characteristic feature of arteries, regardless of size, is a well-defined lumen, rounded or oval, maintained by the muscularity of the vessel wall (Aaronson & Ward, 1999; Casella & Taglietti, 1996; Levick, 1995).

Large arteries

The aorta (the biggest vessel in the body) and its branches (brachiocephalic, subclavian, pulmonary, beginning of common carotid and iliac) are distinguished by their pronounced elasticity. This allows them to smooth out the large fluctuations in blood pressure created by the heart activity. During systole, their elastic laminae are stretched thereby reducing blood pressure. During diastole, the elastic rebound helps to maintain arterial pressure (Aaronson & Ward, 1999; Casella & Taglietti, 1996; Levick, 1995).

Tunica intima represents a large subendothelial layer, which grows with age or pathological conditions (arteriosclerosis) in large arteries. Both connective tissue and smooth muscle are present in the intima. The border of the intima is delineated by the internal elastic membrane (Aaronson & Ward, 1999; Casella & Taglietti, 1996; Levick, 1995).

Tunica media is the thickest of the three layers in large arteries. The well-defined rounded lumen of the vessel is maintained by the muscularity of the vessel wall. The smooth muscle cells are arranged perpendicularly to the vessel axis. They secrete elastin in the form of sheets, or lamellae, which are fenestrated to facilitate diffusion (Jacob *et al.*, 2001). The number of lamellae increases with age (few at birth, 40-70 in adult) and in pathological conditions such as hypertension (Jacob *et al.*, 2001). The presence of lamellae and a relatively large size of the media layer are the most typical histological characteristic of elastic arteries. It is noteworthy that in addition to elastin, SMCs also secrete reticular and fine collagen and proteoglycans (Jacob *et al.*, 2001; Casella & Taglietti, 1996).

Tunica adventitia is a relatively thin connective tissue layer. Fibroblasts are the predominant cell type, and many macrophages are also present. Collagen fibres predominate and elastic fibres (not lamellae) are also present. Collagen fibres in the adventitia play an important role to prevent elastic arteries from stretching beyond their physiological limits during systole. Blood vessels (which are called *vasa vasorum* from the Latin "vessels of the vessels") supplying the adventitia and the outer media are also present. The inner part of the media layer is supplied from the lumen of the vessel via pinocytic transport (Aaronson & Ward, 1999; Casella & Taglietti, 1996; Levick, 1995).

Medium arteries

Medium (muscular or distributive) arteries have less elastic tissue than large arteries, the most abundant constituent of the tunica media is SMCs (Aaronson & Ward, 1999; Casella & Taglietti, 1996; Levick, 1995).

Tunica intima is thinner than in large arteries presenting fewer SMCs and less elastic tissue. The outer part of the intima is defined by a prominent internal elastic membrane (not obscured by elastic lamellae as in large arteries). The basement membrane of the endothelium may rest directly on the internal elastic membrane. The tunica intima increases in thickness with age, and may also become expanded by lipid deposits (Proudfoot & Shanahan, 2001; Levick, 1995).

Tunica media has predominantly SMCs and little elastic material. As in large arteries, no fibroblasts are present. Elastic fibres (few), collagen, and ground substance are produced by SMCs. These are arranged perpendicularly to the main axis of the vessel and their contraction helps maintain blood pressure (Aaronson & Ward, 1999; Levick, 1995).

Tunica adventitia mainly composed of collagen fibres, secreted by fibroblasts. Elastic fibres are also present. Concentration of such fibres at the inner boundary of the adventitia is called the external elastic membrane. The external elastic membrane is not as prominent as the internal, and disappears as arteries become smaller. The tunica adventita is relatively larger than in elastic arteries, it can be up to the same size as the media. Adipose cells may be present (Wilcox & Scott, 1996).

Small arteries

The general construction of small arteries is very similar to that of muscular arteries. The media contains SMCs and has up to 6 layers of SMCs. The number of layers reduced as the arteries get smaller, the smallest arterioles have 1-2 layers of smooth muscle cells. The adventitia becomes thinner and the external elastic membrane disappears. The intima becomes smaller and the internal elastic membrane also eventually disappears. Small arteries also maintain their shape, and tend to be round or oval (Aaronson & Ward, 1999; Casella & Taglietti, 1996; Levick, 1995).

1.1.1.2 Veins

Like arteries, veins are classified as large, medium and small. Although the same layers (intima, media and adventitia) are present, they are often not as well defined as in arteries. An important difference between arteries and veins is the thickness of their walls and the relative amount of muscle tissue (tunica media). In vessels of comparable size, arteries have thicker walls and a much larger media than veins. In veins, the adventitia is larger than the media. Because of these features, veins do not retain their shape. They often do not maintain a well-define circular cross section after dissection. Veins also have less elastic tissue than in arteries. Even in larger veins, the internal elastic membrane may be poorly developed or absent. Vein valves, which prevent the backflow of blood especially in lower parts of the body, are also present in many large veins. Veins often run in close proximity to their arterial counterparts (Aaronson & Ward, 1999; Casella & Taglietti, 1996; Levick, 1995).

1.1.2 Hystology of arteries in phatological conditions

Normal histology of a vessel wall includes components of smooth muscle cells, elastin, and collagen making up the three tunicae. Any alteration in these key components will ultimately lead to hardening, thickening and loss of elasticity of the vessel walls causing illness and death. Atherosclerosis is a general term used to describe these changes. It should be mentioned, however, that dysfunctions of the vessel wall constituents, such as endothelial cells dysfunctions are involved in other pathological conditions such as hypertention, diabetes and hypercholesterolemia (Levick, 1995; Nilius & Droogmans,

2001). Arteriosclerosis or atheroma is the most common type of atherosclerosis that effects medium and large arteries (Willeit & Kiechl, 2000). Atheroma is a lipid depositional desease of subendothelial space in the walls of the arteries. The atheromatous plaques narrow the arterial lumen, causing tissue ischaemia and vascular thrombosis (van Hinsbergh, 1992). Changes in the arterial wall morphology including thickening and reorganization of the tunica intima, excess synthesis of collagenous matrix and deposition of lipids already occur in the childhood/adolescence in humans (van Hinsbergh, 1992; Willeit & Kiechl, 2000). Several models have been proposed to explain the progression from such precursor lesion to the actual atherosclerosis (Ross, 1999). Endothelial dysfunction is considered to be the main cause that provokes a series of structural and functional changes (Celermajer, 1997) including insufficient production of nitric oxide (NO) by endothelial cells (ECs) results in increased adhesion and aggregation of platelets. Leakage of the endothelial barrier and an up-regulation in the expression of cellular adhesion molecules (VCAM-1, ICAM-1) and selectins lead to the accumulation of monocytes (macrophages) and lipids in the subendothelial space (Willeit & Kiechl, 2000; van Hinsbergh, 1992). In this compartment native low density lipoproteins (LDL, a large -total molecular mass ~ 3000 kDa- complex of cholesterol molecules bound to a single protein carrier) are subjected to a series of postsecretory (oxidative) changes that target them for rapid uptake by macrophages (Steinberg *et al.*, 1989). Moreover, oxidized LDL display a chemiotactic effect on blood monocytes, facilitate the entry of lipoproteins by cytotoxic endothelial injury and give rise to SMCs migration and proliferation (Quinn *et al.*, 1987). Another important feature in the process of atherogenesis in the production of cytokines, chemokines and growth factors by vascular cells and a consequent inflammatory response (Ross, 1999).

1.2 Force generation in smooth muscle

The primary role of smooth muscle is to generate force. In blood vessels, the degree of contraction governs arterial resistance and venous distensibility. The amount of force produced by a smooth muscle cell therefore needs to be finely regulated. Despite the diversity of extracellular contractile stimuli, a rise in concentration of free Ca^{2+} ($[Ca^{2+}]_i$) is the predominant intracellular signal responsible for activation of the contractile machinery of the cell.

The most striking feature of smooth muscle, when compared with cardiac and skeletal fibers, is the absence of visible cross striation (hence the name "smooth"). Ultrastructural studies show filamentous structures in the cytoplasm of SMCs that lack the regular geometric organisation present in striated muscle. The contractile machinery in smooth muscle is mainly made up of actin (thin filaments) and myosin (thick filaments). Thin filament-associated proteins (e.g. caldesmin, calponin) are also present and may play a modulatory role in the contractile process (Stromer, 1998). Actin filaments are not only involved in the contractile process but also in the formation of cytoskeletal structures. Connection between the contractile apparatus and the cytoskeleton occurs at cytoplasmic dense bodies, structures rich in α-actinin, which are distributed in the cytoplasm in a regular 3-dimensional arrangement (Stromer, 1998). Actin and myosin filaments are the motor elements that lead to contraction by sliding along each other, similarly to that which occurs in cardiac and skeletal muscles (Stull *et al.*, 1991; Allen & Walsh, 1994). There are however important specific features occurring in smooth muscle. Increase in $[Ca^{2+}]_i$ determines contraction not by directly activating actin-myosin interaction but via phosphorylation of myosin filaments. The first step in this process is activation of calmodulin by Ca^{2+}. Calmodulin, when associated with Ca^{2+} (4 Ca^{2+} bind to a single molecule of calmodulin), activates myosin light chain kinase (MLCK). MLCK is a serine/threonine kinase which phosphorylates the myosin light chain filaments making them active and able to interact with the actin thin filaments forming actomyosin complexes. In low $[Ca^{2+}]_i$ myosin phosphatases are activated causing MLC dephosphorylation, dissociation of actomyosin complex and muscle relaxation (Rembold & Murphy, 1993). Schematically the process of smooth muscle contraction-relaxation cycle can be presented as following:

Relaxation Contraction

$$\text{Actin+MyosinLC-OH} + MgATP_2 \leftrightarrow \text{ActomyosinLC-O-}PO_3^{2-} + MgADP^- + H^+$$

1.3 Types of contractile and relaxing stimuli

Stimuli that act directly on vascular smooth muscle can be broadly grouped into three categories.

1) Agents acting at G-protein linked receptors. The majority of vasoconstrictors such as α-adrenoreceptor agonists, angiotensin II, serotonin or vasopressin and vasodilators such as β-adrenoreceptor agonists, vasoactive intestinal peptide or calcitonin gene-related peptide all stimulate G-protein linked receptors which act as transducers from the ligand-receptor complex to a multitude of intracellular events (e.g. Ca^{2+} release from intracellular Ca^{2+}-stores, increase in concentration of cyclic nucleotides or activation of K^+ channels) (Large, 2002; Beech *et al.*, 2001).

2) Growth factors. Vascular growth factors such as platelet-derived growth factor and epidermal grow factor can affect vascular tone as well as acting as mitogens for VSMCs (Berk & Alexander, 1989). The majority of growth factors act by binding to and thus causing dimerisation of transmembrane receptors with intrinsic tyrosine kinases activity. Dimerisation triggers trans-autophosphorylation of tyrosine residues in the intracellular domain of the receptor leading to activation of a variety of signalling molecules (Schlessinger & Ullrich, 1992).

3) Transmural pressure. Wall tension or stretch is also a stimulus for contraction. It can occur as a result of activation of ion channels by stretch, stretch induced production of vasoconstrictors or growth factors (Li & Xu, 2000; Rubanyi *et al.*, 1990) or activation of signalling enzymes (Osol, 1995).

1.4 Regulation of intracellular calcium concentration

An increase or decrease $[Ca^{2+}]_i$ is the principal mechanism that initiates contraction or relaxation in smooth muscle. Resting cytoplasmic $[Ca^{2+}]_i$ is maintained at very low levels (around 100 nM) creating more than 10,000 fold gradient with the extracellular space, which contains about 1.6 mM Ca^{2+} (Himpens *et al.*, 1992). Two main mechanisms contribute to the increase in $[Ca^{2+}]_i$: 1) Ca^{2+} release from intracellular Ca^{2+}

stores or Ca^{2+} entry from extracellular space through receptor- or store- operated Ca^{2+} permeable channels in response to neurotransmitters or hormones, termed *pharmacomechanical coupling*, and 2) entry of Ca^{2+} from the extracellular space into SMCs through voltage-dependent Ca^{2+} channels (VDCCs), termed *excitation-contraction coupling*. The reuptake of Ca^{2+} back into the sarcoplasmic reticulum by sarcoplasmic/endoplasmic reticulum Ca^{2+}-ATPase (SERCA) and Ca^{2+} extrusion into extracellular medium by plasmalemmal Ca^{2+}-ATPase and Na^{+}/Ca^{2+} exchanger are the main mechanisms responsible for lowering $[Ca^{2+}]_i$ and subsequent relaxation of VSMCs (Mueller & van Breemen, 1979). Changes in ion channel conductance leading to corresponding changes in the cell membrane potential are central elements in excitation-contraction coupling. Most VSMCs are "electrically silent" (i.e. do not generate action potentials) and changes in membrane potentials occur in the form of gradual membrane depolarisation or hyperpolarisation which requires a coordinate action of several types of K^{+} and Ca^{2+} channels. Membrane depolarisation activates VDCCs which allows extracellular Ca^{2+} to enter the cell and thus initiate contraction. At rest changes in the relationship between smooth muscle membrane potential and arterial tone occur very rapidly, so that even membrane depolarisation of a few millivolts can open enough VDCCs to initiate significant Ca^{2+} influx to cause contraction of VSMCs and significant changes in blood vessel diameter (Brayden & Nelson, 1992; Nelson *et al.*, 1990b). When Ca^{2+} channels open, $[Ca^{2+}]_i$ can rise to near micromolar levels leading to activation of contraction and other intracellular processes. There is evidence that Ca^{2+} is compartmentalised within the SMCs and that localised increases in $[Ca^{2+}]_i$ may play an important role in, for example, modulation of ion channel activity (Nelson *et al.*, 1995).

It is worth mentioning that pharmacomechanical and excitation-contraction coupling coexist and interplay in smooth muscle. The relative importance of the two mechanisms in a particular type of smooth muscle can be investigated using specific pharmacological agents. For example, nifedipine, an inhibitor of VDCCs, virtually abolished KCl or agonist-induced contraction in certain tissues such as the guinea-pig ileum. However, in others, for instance the mouse anococcygeus, nifedipine had relatively little effect, pointing towards a role for the pharmacomechanical pathway (Gibson *et al.*, 1994). It should be mentioned however, that in the latter tissue, nifedipine did produce some reduction in the response to contractile agonists, suggesting that VDCCs also contributed to the overall contraction. Opening of VDCCs

can be also caused by membrane depolarisation mediated by activation of Ca^{2+}-dependent Cl^- conductance due to Ca^{2+}-release from intracellular Ca^{2+}-stores. At the same time, the depletion of the sarcolasmic reticulum, via a still unknown mechanism, activates store-operated Ca^{2+} channels in the plasma membrane allowing Ca^{2+} entry and maintenance of smooth muscle tone (Gibson *et al.*, 1998).

1.4.1 Intracellular calcium stores

Intracellular Ca^{2+}-stores play a crucial role in the regulation of $[Ca^{2+}]_i$ in the cytoplasm of VSMCs. The effective permeability of the intracellular Ca^{2+}-store is determined by the balance between uptake into and efflux from Ca^{2+} stores. Efflux from the stores into the cytoplasm occurs through Ca^{2+}-selective ion channels located in the sarcoplasmic reticulum (Somlyo *et al.*, 1985). Two types of channels have been described in the sarcolemmal membrane of smooth muscle: inositol 1,4,5-triphosphate (IP_3) -sensitive channels (IP_3-receptors) and ryanodine-sensitive channels (Ry-receptor) and a number of pieces of evidence suggest that IP_3- and Ry-receptors could be localised in particular regions within the cell (Nixon *et al.*, 1994; Lesh *et al.*, 1998). The IP_3-receptor has been isolated from porcine aortic smooth muscle (Islam *et al.*, 1996) and is a glycoprotein consisting of a single polypeptide chain. The functional IP_3-receptor is a tetramer and opens in response to IP_3 biding. IP_3 is produced in response to agonist stimulation of plasmalemmal receptors coupled to phospholipase C (PLC). PLC hydrolyses the membrane lipid phophatidylinosotol4,5 bisphosphate (PIP_2) to IP_3 and diacylglycerol (DAG), both of which are intracellular messengers. The physiological role of Ry-receptors is less clear. This channel is sensitive to Ca^{2+}, adenine nucleotides, Mg^{2+} and pH. Ry-receptors are activated by caffeine which causes transient contraction in vascular smooth muscle (Jaggar *et al.*, 2000). It is believed that Ry-receptors play an important role in Ca^{2+}-induced Ca^{2+}-release (CICR), since they are activated by elevated $[Ca^{2+}]_i$. Uptake into stores is via a Ca^{2+}-ATPase probably of the SERCA 2 subtype. Activity of SERCA is regulated by phospholamban, cAMP-dependent protein kinase (PKA) and by cGMP-dependent protein kinase (PKG) (Colyer, 1998). The endoplasmic reticulum Ca^{2+}-ATPase can also be blocked irreversibly by thapsigargin (Lytton *et al.*, 1991) and reversibly by cyclopiazonic acid (Seidler *et al.*, 1989).

1.4.2 Calcium efflux from smooth muscle cells

VSMCs extrude Ca^{2+} into the extracellular medium via the plasmalemmal Ca^{2+}-ATPase (PMCA) (Himpens *et al.*, 1995) and the Na^{+}/Ca^{2+} exchanger (Gonzalez *et al.*, 1996; Ashida & Blaustein, 1987). The major contribution is from PMCA, which is also regulated by calmodulin, cAMP- and cGMP- dependent kinases (Zylinska *et al.*, 1998). Na^{+}/Ca^{2+} exchanger might be important in determining local changes in $[Ca^{2+}]_i$, since these proteins are unevenly distributed on the plasmalemma (Moore *et al.*, 1993; Ashida & Blaustein, 1987).

1.5 Ion channels expressed in vascular smooth muscle cells

There are four major classes of ion channels ubiquitously present in VSMCs which play an important role in the regulation of vascular excitability and in the mediation of the action of vasoactive substances. These are K^{+} channels, voltage-dependent Ca^{2+} channels, Cl^{-} channels and non-selective cation channels. Na^{+} channels have also been found in some types of VSMCs. In this section, I will focus mainly on structural and functional characteristics of K^{+} and VDCCs, due to their relevance to my thesis. Other classes of ion channel will be discussed more briefly.

1.5.1 Potassium channels

The resting membrane potential measured using microelectrode techniques in arteries *in vitro* is between –50 and –70 mV depending on the vascular bed. The nearness of the resting potential to the equilibrium K^{+} potential (calculated according to the Nernst equation to be between –82 and –84 mV with physiological K^{+} intracellular and extracellular concentrations of 130-140 mM and 5 mM, respectively) means that K^{+} permeability is mainly responsible for setting the resting potential in VSMCs (Hirst & Edwards, 1989b; Nelson *et al.*, 1990b; Hirst & Edwards, 1989a; Nelson *et al.*, 1990a; Nelson *et al.*, 1990a).

Arterial SMCs express four main types of K^{+} channels: voltage-gated (Kv), Ca^{2+}-activated (K_{Ca}), ATP-dependent (K_{ATP}) and inwardly rectifying K^{+} (K_{ir}) channels

(Nelson & Quayle, 1995). Also, the presence of two-pore domain TASK-like K^+ channels (Patel & Honore, 2001) has been reported in rabbit and rat pulmonary arteries (Gurney *et al.*, 2002). K^+ channels represent one of the major targets for various endogenous vasodilators. For example, it is well documented that β-adrenoreceptor agonists, calcitonin-gene related peptide and nitric oxide increase the open probability of potassium channels such as K_{ATP} or BK_{Ca} either directly or by elevating cytoplasmic cyclic nucleotide levels (Standen & Quayle, 1998). Additionally, a number of therapeutically important vasoactive drugs such as the K^+ channels openers cromakalim and nicorandil, which open K_{ATP} channels, and thiazide diuretics, which open BK_{Ca} channels, are also used as potent vasodilators (Lawson, 2000). The relative expression and contribution of K^+ channels to the control of the cell membrane potential differs in various vascular beds. In addition, the four classes of K^+ channels also vary in their molecular structure (Fig. 1.2), resulting in different biophysical and pharmacological properties. Therefore the current view of the molecular structure, distribution and functional role of each type of K^+ channel in VSMCs will be briefly considered below.

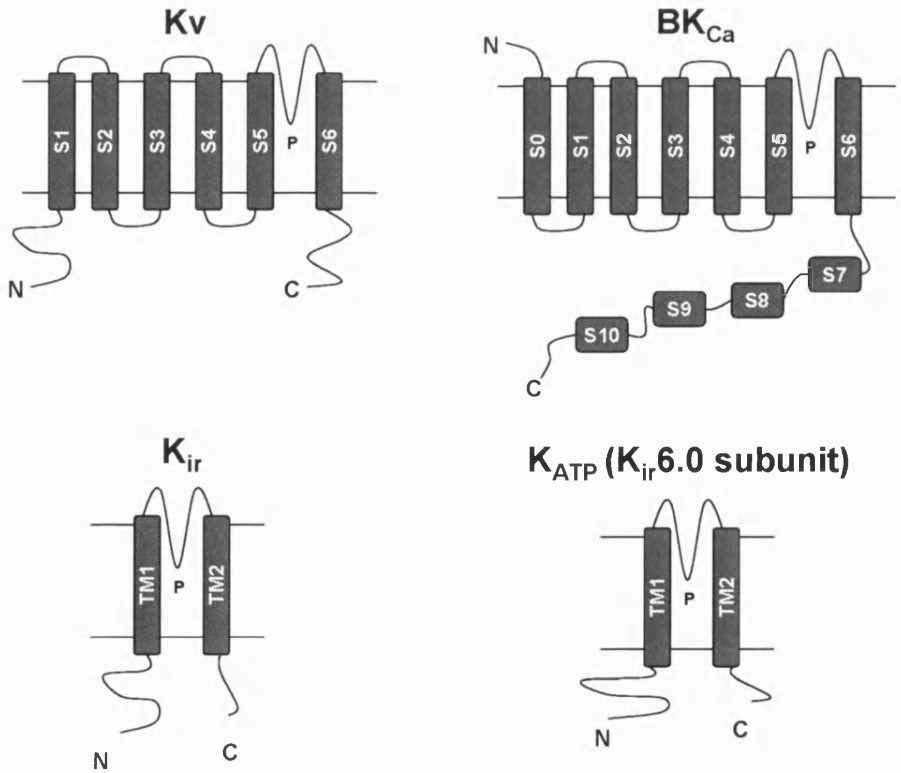

Figure 1.2. Membrane topologies of the pore forming subunit of the K^+ channels expressed in VSMCs.

1.5.1.1 Calcium activated potassium channels

The Ca^{2+}-activated K^+ channels (K_{Ca}) are a structurally diverse group of K^+ channels that share the common feature of being activated by increase in the intracellular Ca^{2+} concentration (occurring during e.g. receptor-mediated Ca^{2+}-release from intracellular Ca^{2+}-stores) (Vergara *et al.*, 1998). K_{Ca} channels are divided in three major types, which can be distinguished electrophysiologically by their different single channel conductances as large, intermediate and small conductance K_{Ca} channels. All these three types of K_{Ca} channels have been found in vascular smooth muscle (Brayden & Nelson, 1992b; Neylon *et al.*, 1999; Van & Lazdunski, 1992) although their precise molecular identity is not always clear.

The three K_{Ca} subtypes also exhibit specific voltage and pharmacological sensitivities and have different functional roles. The maxi K_{Ca} or BK_{Ca} channel is characterised by a 100-250 pS single-channel conductance in symmetrical K^+ solution. It is activated by both depolarisation and by micromolar $[Ca^{2+}]_i$ (Faraci & Heistad, 1998). The small (SK_{Ca}; 5-20 pS) and intermediate (IK_{Ca}; 20-80 pS) conductance K_{Ca} channels are not voltage sensitive and are activated by intracellular Ca^{2+} within the submicromolar range (Vergara *et al.*, 1998). BK_{Ca} channels are blocked by low concentrations of TEA, iberiotoxin and charybdotoxin (ChTx) but are unaffected by apamin, a peptide isolated from the honeybee venom. In contrast, SK_{Ca} channels are insensitive to TEA, and are blocked by apamin. IK_{Ca} channels are insensitive to apamin but blocked by ChTx and clotrimazole (Vergara *et al.*, 1998).

Molecular structure of K_{Ca} channels

It is generally accepted that BK_{Ca} channels are tetramers consistings of four α and four β subunits (Knaus *et al.*, 1994b). The α subunit is believed to be formed by 7 transmembrane (TM) domains (S0-S6), with an extracellular amino- (N-) and intracellular carboxy- (C-) termini (Fig. 1.2) (Wallner *et al.*, 1996). The C-terminus is composed of four domains and contains the Ca^{2+} binding site, although its precise location has not yet been identified. The S4 segment, as in the case of Kv channels (see below), contains positively charged residues and acts as a voltage sensor. The S5-S6 loop forms the channel pore and contains the K^+ selectivity filter. The extracellular N-

terminus and the first, S0, transmembrane domain are required for β-subunit modulation (Wallner *et al.*, 1996). The BK_{Ca} β-subunit is formed by two transmembrane domains linked by a large extracellular domain and with cytosolic N- and C-termini. The BK_{Ca} β-subunit confers a greater Ca^{2+}- and voltage- sensitivity to the α-subunit (McManus *et al.*, 1995). In addition, the presence of the BK_{Ca} β-subunit increases sensitivity to certain toxins such as charybdotoxin (ChTx) (Knaus *et al.*, 1994a).

Althought they have no significant amino acid homology except within the putative pore region, hydrophobicity analysis suggests that SK_{Ca} and IK_{Ca} have similar topology to that of Kv channels. IK_{Ca} and SK_{Ca} channels have six putative transmembrane domains and a hairpin loop linking TM5 and TM6 that is thought to form part of the pore and also have intracellular N- and C- termini. The N- terminus is shorter in IK_{Ca} channels. The fourth TM domain resembles the S4 voltage sensor of Kv channels although it contains only three positively charged residues instead of 7 found in the Kv channels. Despite the presence of positive charges, the IK_{Ca} and SK_{Ca} channels, however, display only a limited voltage dependency. Half maximal activation of SK_{Ca} channel by intracellular Ca^{2+} is ~ 0.3 μM thus about 10 times more sensitive than BK_{Ca} (Vergara *et al.*, 1998). Analysis of the steepness of the relationship between Ca^{2+}, suggest that 4 Ca^{2+} are required for channel activation. Ca^{2+} ions do not bind directly to the intracellular domains of the channel (Ca^{2+} binding domains are in fact missing) but they interact with calmodulin that is constitutively bound to the channel (Xia *et al.*, 1998). IK_{Ca} channel display a similar sensitivity to intracellular Ca^{2+} than SK_{Ca} however, the relationship between channel activation and $[Ca^{2+}]_i$ is less steep, suggesting that fewer ions are required to be bound for channel activation to occur (Fanger *et al.*, 1999).

Functional role of K_{Ca} channels in vascular smooth muscle

A number of observations suggest that BK_{Ca} channels are involved in setting the resting potential and modulating the excitability of some types of VSMCs. Application of tetraethylammonium (TEA), a non-selective BK_{Ca} channel inhibitor, caused depolarisation and generation of an action potential in a variety of arteries (Hirst & Edwards, 1989). Brayden and Nelson (1992) showed that elevation of luminal pressure caused vasoconstriction and depolarization in rabbit cerebral arteries (Brayden &

Nelson, 1992a). Under these conditions TEA and ChTx caused further depolarization and development of tension, not seen at low pressures. The authors therefore argued that BK_{Ca} channels serve as a negative feedback mechanism to control myogenic tone in these arteries. Recently, using a more selective BK_{Ca} blocker iberiotoxin (IbTx), it was demonstrated that application of IbTx induced contraction of non-stimulated coronary (Marijic *et al.*, 2001) and middle cerebral (Long *et al.*, 2000) arteries, suggesting that BK_{Ca} conductance is involved in the control of the resting membrane potential in these VSMCs. It has been demonstrated that BK_{Ca} are activated by cGMP-dependent protein kinase, advocating a possible involvement in NO-dependent relaxation of blood vessels (Schubert & Nelson, 2001). It has also been proposed that activation of BK_{Ca} channels by local release of Ca^{2+} from ryanodine-sensitive Ca^{2+}-stores during Ca^{2+}-sparks is responsible for vasorelaxation (Jaggar *et al.*, 1998). On the other hand, Cheong *et al.* (2002) have shown that the apparent threshold for Kv channel activation in rabbit cerebral arterioles was ~20 mV more negative than that of BK_{Ca} channel (Cheong *et al.*, 2002). Moreover, the diameter of the arterioles was decreased by 3,4-diaminopyridine, a non-selective inhibitor of Kv channels, but not by penitrem A, a selective inhibitor of BK_{Ca} channels (Cheong *et al.*, 2002), suggesting that Kv channels also play an important role in the regulation of the resting membrane potential in resistance vessels.

Many vasoconstrictors (e.g. noripinephrine, angiotensin II, andothelin, and serotonin) depolarize vascular smooth muscle (Nelson *et al.*, 1990) via inhibition of BK_{Ca} channels. Thus, angiotensin II and the tromboxane A_2 agonist (U-46619) have been shown to inhibit K_{Ca} channels from coronary artery smooth muscle (Scornik & Toro, 1992; Toro *et al.*, 1990). Also, stimulation of muscarinic receptors in airway and colonic smooth muscle inhibited K_{Ca} channels (Cole *et al.*, 1989; Kume & Kotlikoff, 1991).

Activation of K_{Ca} channels on the other hand will hyperpolarize smooth muscle, causing relaxation. The observed stimulation of K_{Ca} channels in airways smooth muscle by β-adrenergic stimulation might have a role in the β-adrenergic bronchodilation (Kume *et al.*, 1989). This activation of K_{Ca} channels in airways smooth muscle and coronary artery smooth muscle seems to be mediated by activation of PKA or by a direct activation of G protein pathway (Kume *et al.*, 1992; Kume *et al.*, 1989; Sadoshima *et al.*, 1988; Scornik *et al.*, 1993). Other pieces of evidence suggest that NO can directly

activate K_{Ca} channels in aortic smooth muscle (Bolotina *et al.*, 1994) and vasorelaxation of mesenteric arteries in response to NO also appears to involve activation of K_{Ca} channels (Cowan *et al.*, 1993; Khan *et al.*, 1993).

1.5.1.2 Inwardly rectifier channels

Molecular structure of K_{ir} and K_{ATP} channels

K_{ATP} and K_{ir} channels belong to the same family of the inwardly rectifying K^+ channels (Reimann & Ashcroft, 1999). K_{ir} and K_{ATP} channels possess only two putative transmembrane domains, TM1 and TM2, linked by a loop which is referred to as the "pore loop" or H5 region. The pore loop, which determines the selectivity of the channel for K^+, displays significant homology to the pore loop of other K^+ channels. Therefore, two TM domains of K_{ir} and K_{ATP} correspond to the S5 and S6 domains of the Kv channels. There is no equivalent to the S4 ("voltage-sensor") domain of the voltage gated K^+ channels in the structure of inward rectifying channels which explains a weak voltage dependence of both K_{ir} and K_{ATP} channels (compare the corresponding structures of Kv and K_{ir} in Fig. 1.2). Both the N- and C- termini of K_{ir} are located in the cytoplasm. As in the case of the BK_{Ca} channel, the functional K_{ir} channel is formed by 4 subunits generally belonging to the same family, although heteromultimerisation is also possible (Kofuji *et al.*, 1995; Krapivinsky *et al.*, 1995). K_{ATP} channels are composed by members of the inward rectifier genes belonging to the $K_{ir}6.x$ subfamily and a regulatory sulphonylurea receptor (SUR) subunit forming an octameric (4x4) channel complex (Reimann & Ashcroft, 1999). The C-terminus of Kir6.2 appears to be essential for the interaction with the SUR subunit (Tucker *et al.*, 1997). SUR subunits are members of the ABC-transporter superfamily. Hydropathy analysis suggests that they contain several transmembrane domains (currently believed to be 17). There are two large intracellular loops that contain consensus sequences for nucleotide binding which play a role in the regulation of K_{ATP} channel activity. There are at least two different sulphonylurea receptor genes (SUR1 and SUR2) and further diversity is created by alternative splicing of SUR2 (reviewed in Ashcroft & Gribble, 1998). SUR1 is expressed primarily in pancreatic β-cells and in the brain, whereas SUR2A is expressed in cardiac and skeletal muscle, and SUR2B is found in smooth muscle (Clapp & Tinker, 1998).

Kir6.x/SUR complexes are sensitive to intracellular concentration of ATP (Inagaki *et al.*, 1996). An increase in intracellular ATP concentration will shut down the channel causing membrane depolarisation, while a depletion of ATP inside the cell will cause an opposite effect on K_{ATP} channel current and membrane potential. Therefore, activation of K_{ATP} channels will be controlled by the balance between ATP and ADP inside the cell. This balance is determined by intracellular metabolism and can be altered in pathological states, leading to altered excitability of VSMCs (Shieh *et al.*, 2000; Ashcroft, 2000).

All K_{ir} and K_{ATP} channels show inward rectification (i.e. the membrane current evoked by a given hyperpolarisation from the potassium equilibrium potential (E_K) is grater than the one elicited by a depolarization of the same amplitude). Inward rectification results from a voltage-dependent block by intracellular Mg^{2+} (Matsuda *et al.*, 1987) or polyamines (e.g. spermine (Lopatin *et al.*, 1994) by a mechanism that involves the movement of the blocking particle into the channel open pore by membrane depolarization. Those K_{ir} that exhibit strong inward rectification (e.g. K_{ir} 2.1 and K_{ir} 3.1) also show an apparent time-dependent activation on hyperpolarisation, whereas a weak inward rectifier (e.g. K_{ir} 1.1 and K_{ir} 6.2) turns on instantaneously. The apparent activation kinetics of strong inward rectifier results from a time-dependent un-block of the channel on membrane hyperpolarisation.

Functional role of K_{ir} channels in vascular smooth muscle

K_{ir} channels are ubiquitously present in endothelial cells (Nilius & Riemann, 1990). K_{ir} channels were also described in some VSMCs, particularly in cerebral (Edwards *et al.*, 1988b) and coronary (Xu *et al.*, 1999) arteries and in submucosal arterioles (Edwards & Hirst, 1988), contributing to the control of the resting potential and its alteration in response to changes in extracellular K^+. The K_{ir} channels conduct inward current at membrane potential negative to the E_K and smaller outward current at membrane potential positive to E_K (Nelson & Quayle, 1995). It should be stressed that only the latter current is physiologically relevant since the membrane potential in vivo can not go to values more negative than E_K. Importantly, the activity of K_{ir} channels is a function of both membrane potential and extracellular K^+ concentration (Edwards *et al.*, 1988b). As $[K^+]_o$ is changed, the channel conducts inward current at membrane potentials

negative to the new E_K, while the outward current remains small. The control of the channel activity by $[K^+]_o$ is a unique feature of K_{ir} channel since for other K^+ channels (i.e. Kv and K_{Ca}) changes in the reversal potential caused by physiological changes in $[K^+]_o$ changes do not change the voltage range over which the channels are active.

K_{ir} channel can be blocked by extracellular Ba^{2+} in voltage dependent manner with a dissociation constant in the micromolar range (Quayle *et al.*, 1993). Due to this high sensitivity, Ba^{2+} can be used as a useful "pharmacological" tool for the investigation of the physiological role of this channel. Cs^+ can also block K_{ir} channels but with an dissociation constant of ~1.6 mM at +50 mV (Quayle *et al.*, 1993). Glibencalmide (a selective blocker of K_{ATP} channels) as well as the K_{Ca} blocker charybdotoxin (100 nM) have little effect (at 10 μM) on K_{ir} in cerebral arteries (Quayle *et al.*, 1993).

K_{ir} in smooth muscle are implicated in several important physiological functions. The K_{ir} channel is more active at negative membrane potential and is therefore a good candidate for regulating the membrane potential of VSMCs in arteries in the absence of stimuli (e.g. pressure or presence of vasoconscritors) for depolarisation. The membrane potential of arterial SMCs at low transmural pressure (i.e. <20 mm Hg) measured in vitro ranges between –75 and –60 mV (reviewed in Nelson *et al.*, 1990). In non-pressurised rat cerebral arterioles low Ba^{2+} concentration (0.1-0.5 mM) caused depolarisation and inhibition of K_{ir} currents (Hirst *et al.*, 1986). However, 50 μM Ba^{2+} has little effect on the membrane potential of rabbit cerebral arteries (Brayden, 1990). Thus membrane potential, transmural pressure, vasonstrictors and vasodilators have an impact on the contribution of K_{ir} to the resting membrane potential.

The mechanism of increase in blood flow to various organs in relation to their metabolic condition is considered to be associated with the release of metabolites form the tissues near to the vessel. A number of possible vasodilators have been proposed as candidate including H^+, adenosine and K^+. For example, in the cerebral circulation, an increase in the extracellular K^+ concentration within few mM (1-15 mM) causes dilation of small arteries (Kuschinsky *et al.*, 1972). K^+ can be released as a consequence of neuronal activity and may be one of the factors that increase local cerebral blood flow during increased cerebral activity (Kuschinsky *et al.*, 1972). Extracellular K^+ dilates arteries by at least two mechanisms: activation of the Na-K pump and activation of K_{ir} channels.

Several piece of evidence point out the importance of K_{ir} channels in K^+-induced dilations. For example, an increase in $[K^+]_o$ from 5 to 10 mM hyperpolarized rat cerebral arteries (Edwards *et al.*, 1988a). This hyperpolarisation was prevented by application of Ba^{2+}. Similar increases in $[K^+]_o$ have also been shown to dilate pressurised rat cerebral arteries (McCarron & Halpern, 1990), but not in the presence of 10 μM Ba^{2+}, while dilation still occur in the presence of other K^+ channels inhibitors or a various receptor antagonists.

Functional role of K_{ATP} channels in vascular smooth muscle

The presence of K_{ATP} channel in VSMCs has been demonstrated by application of K_{ATP} channels openers (e.g. the clinically and experimentally used diazoxide, minoxidil sulphate, cromakalim and pinacidil), which produced hyperpolarisation in single SMCs and relaxation in intact arterial preparations (e.g. Clapp *et al.*, 1993; Davie *et al.*, 1998, reviewed in Quayle *et al.*, 1997). These responses were also prevented by selective K_{ATP} channels inhibitors such as the sulfonylureas glibenclamide and tolbutamide. It is noteworthy that application of K_{ATP} channel inhibitors *per se* do not generally affect the basal arterial tone, suggesting that K_{ATP} channels are not active at rest. However, K_{ATP} channels are activated by vasodilators such as the calcitonin gene-related peptide (Quayle *et al.*, 1994) or during hypoxia and acidosis (Quayle *et al.*, 1997), indicating their contribution to the excitability of VSMCs increased under these conditions.

1.5.1.3 Volatge-gated potassium channels (Kv)

Molecular structure and diversity of Kv channels

At least 11 sub-families of voltage dependent K^+ channel genes have been identified in mammalian cells, including Kv (Kv1.0 to Kv9.0), as well as KvLQT and EAG subfamilies (reviewed in Jan & Jan, 1992 and Hille, 2001). Each sub-family consists of individual members termed α-subunits. Each functional channel is composed of four α-subunits and the basic structure of the α-subunit (Fig. 1.2) is well conserved with ~70% homology within and ~40% between different sub-families. Further diversity is possible due to the formation of heteromeric channels that comprise of two or more different α-subunits and also by co-assembly with auxiliary intracellular β-subunits.

Heteromerisation of Kv α-subunits is possible only between members of the same subfamily (Christie *et al.*, 1990). Each α-subunit has six transmembrane domains (S1-S6), connected by hydrophilic loops exposed to the intracellular and extracellular compartment. Every Kv α-subunit also has cytoplasmic amino- and carboxy-termini. One of the membrane spanning domains (the S4) is charged, having a basic amino acid (lysine or arginine) every third residue. The S4 region of the Kv α-subunit is the voltage sensor for the channel (Jiang *et al.*, 2003). In response to depolarisation, the S4 segment is displaced outward across the membrane, giving rise to a gating current and triggering the conformational change that opens the channel pore (Bezanilla, 2002). The permeation pathway is formed, in part, by the region linking the S5 and S6, called the H5 or pore region. Kv channels essentially display two main modes of inactivation: fast and slow. The cytoplasmic N-terminus is responsible for the fast inactivation (thus also termed "N-type" inactivation). The N-type inactivation is a characteristic property of fast inactivating A-currents, which are encoded by Kv α-subunits belonging to various Kv sub-families (e.g. Kv1.4 and Kv4.x). N-type inactivation involves the most distal part of the N terminus acting as a "ball" which can swing into the channel pore and block K^+ efflux (Armstrong *et al.*, 1973; Hoshi *et al.*, 1990). Some Kv do not inactivate rapidly and are termed delayed rectifier. Delayed rectifier channels maintain a fairly constant current for hundreds of ms before inactivation occur. They are characterised by an additional form of inactivation that involves residues in the C-terminus of the protein ("C-type" inactivation). C-type inactivation was first described in mutant channels lacking the N-terminal inactivation (Hoshi *et al.*, 1991). It now clear that C-type inactivation involves residues at the outer mouth of the pore whose rearrangement would cause occlusion of the pore (Liu *et al.*, 1996).

Auxiliary Kv β-subunits are protein with a molecular mass of about 40 kDa (as opposed to the ~350kDa of a α subunit tetramer). Hydrophobicity plots indicate that they are probably cytoplasmic. It has also been demonstrated that the stoichiometry of association with the α-subunits is 1:1 (Parcej *et al.*, 1992). At least four different classes of Kv β-subunit genes (Kvβ1 – Kvβ4) have been identified and further diversity is generated by alternative splicing. Not all combinations of α-and β-subunit are possible, since each type of Kv β-subunit does not associate with all types of Kv α-subunit (the opposite is also true) (Shamotienko *et al.*, 1997). Co-expression of any Kv β-subunit with a compatible pore forming α-subunit, enhances the K^+ current amplitude by

promoting the surface expression of the α-subunit (Shi *et al.*, 1996). Kv β1-subunits also modify the inactivation properties of some members of the Kv1 sub-family. This is due to the presence of a protein domain in the Kv β1-subunit that can act as a "ball peptide" blocking Kv channels in a similar way as occurs in A-type currents (Rettig *et al.*, 1994). In contrast, Kv β2 –subunits do not affect the inactivation properties but can increase the density of Kv channel currents (Shi *et al.*, 1996).

Functional role of Kv channels in vascular smooth muscle

Kv channels are constitutively expressed in the vasculature and generally encode a slowly inactivated outward delayed rectifier current. Delayed rectifier currents have been described in various vascular beds, including coronary (Volk *et al.*, 1991), cerebral (Knot & Nelson, 1995; Hirst *et al.*, 1986), renal (Gelband & Hume, 1992), mesenteric (Smirnov & Aaronson, 1992) and pulmonary (Clapp & Gurney, 1991) circulations. However, the presence of fast inactivating outward currents have also been demonstrated (Beech & Bolton, 1989; Smirnov & Aaronson, 1992). Voltage-clamp experiments revealed that the delayed rectifier currents diverged in their electrophysiological and pharmacological characteristics among different types of VSMCs (Kuriyama *et al.*, 1995), although evidence for the existence of Kv current subtypes within the same vessel have also been presented (Archer *et al.*, 1996; Smirnov *et al.*, 2001). In addition, Kv channel expression can change significantly during vascular development (Guo *et al.*, 1997; Belevych *et al.*, 2002). Up to now, the physiological role of Kv channel currents has mainly been investigated using pharmacological tools such as aminopyridines like 4-aminopyridine (4-AP) and 3,4-diaminopyridine, non-selective Kv channel blockers which effectively inhibit all Kv channel currents with different potency (Rudy, 1988; Kuriyama *et al.*, 1995). 4-AP caused membrane depolarisation and vasoconstriction in pulmonary arteries (Smirnov *et al.*, 1994; Archer *et al.*, 1998), where Kv channel currents are predominantly expressed (Yuan *et al.*, 1993; Smirnov *et al.*, 1994). Aminopyridines also constricted rabbit cerebral (Robertson & Nelson, 1994), porcine coronary (Kuromaru & Sakai, 1986) and dog coronary (Nakazawa & Mustafa, 1988) arteries. These data imply an important contribution of Kv channels to the regulation of the resting potential at least in these types of VSMCs. It is noteworthy that some blood vessels, particularly veins, generate

action potentials. In these tissues, Kv channels could also be involved in the repolarising phase of the action potential (Beech & Bolton, 1989).

Pathophysiological role of Kv channels in vascular smooth muscle

In addition to a physiological relevance, it is worth mentioning that altered expression and regulation of Kv channels play a role in a variety of pathological conditions. Kv channels have been shown to play an important role during hypoxic pulmonary vasoconstriction (e.g. Coppock *et al.*, 2001). Kv channel gene and protein expression, as well as functional activity of Kv currents were suppressed in pulmonary arterial myocytes during chronic hypoxia (Smirnov *et al.*, 1994; Wang *et al.*, 1997). It has also been shown that 4-AP, but not paxilline or low dose of TEA or glibenclamide, reversed the reduced response to KCl, phenylephrine (PE) or prostaglandin $F_{2\alpha}$ during pneumonia in rats, suggesting that 4-AP sensitive currents could be involved in this process (Yaghi *et al.*, 2002). A 4-AP sensitive component of the whole-cell K^+ current was also increased in rat coronary arterial SMCs after 3 weeks exposure of the animals to carbon monoxide. The augmented 4-AP sensitivity was associated with an increased expression of Kv channel proteins, suggesting an involvement of Kv conductance in this pathologiocal state (Barbe *et al.*, 2002).

It has been proposed that K^+ efflux from the cell is an essential prerequisite for apoptotic volume decrease and a role for Kv channels in this process demonstrated (Yu & Choi, 2000). Also, cellular K^+ loss via BK_{Ca} channels was associated with apoptosis in rat pulmonary SMCs (Krick *et al.*, 2001). It has been demonstrated that the Kv2.1 channel is involved in the development of apoptosis in mammalian cortical neurons (Pal *et al.*, 1915; Krick *et al.*, 2001). Recently Ekhterae et al. (2001) found that overexpression of the anti-apoptotic protein Bcl-2 decreases both current density and Kv1.1, Kv1.5 and Kv2.1 mRNA production in pulmonary arterial myocytes, suggesting an involvement of Kv channels in apoptosis in this tissue (Ekhterae *et al.*, 2001).

In conclusion, Kv channels play an important role in both physiological and patho-physiological conditions, being involved in the regulation of membrane potential and the basal tone of blood vessels. Kv channel expression varies in different vascular beds, and can be altered during normal vascular development and in pathological conditions.

The understanding of the molecular identity of Kv channels and of the mechanisms which regulate their expression and function in various vascular beds are key questions in modern cardiovascular physiology. It is noteworthy that together with a pharmacological approach to the investigation of the molecular nature and role of Kv channels in various vascular beds, molecular cloning, determination of molecular structure and hetreologous expression of potassium channels, enabled the biophysical and pharmacological characterisation of various Kv properties, thus providing a "molecular database" for comparison with native Kv currents.

1.5.2 Voltage dependent calcium channels

VDCCs are classified as T, L, N, P/Q and R types on the basis of their sensitivity to pharmacological blockers, selectivity to divalent cations, single channel conductance, kinetics and voltage dependence. Opening of VDCCs is strongly voltage dependent. They are mostly closed at potentials more negative than the resting potential and open only in response to depolarisation. On the basis of their voltage dependency of activation, the VDCCs can be divided into low and high threshold activated channels. Thus, T-type VDCCs open in response to small membrane depolarisations, while the L, N, P/Q and R types require stronger depolarisation to be activated.

Various types of high-threshold VDCCs have a distinct pharmacological profile. For example, L-type channels are selectively blocked by phenylalkylamines (e.g. verapamil), benz(othi)azipines (e.g. diltiazem) and dihydropyridines (e.g nifedipine), while the N-type VDCCs are blocked by two toxins extracted from the fish-hunting cone shell *Conus geographus* (the GVIA and MVIIA ω-conotoxins). ω-agatoxin (extracted form the spider *Agelenopsis aperta*) potently blocks P-type channels and, with lower affinity, the Q-type VDCCs (see for review Hockerman *et al.*, 1997).

VDCCs also differ in their degree of inactivation. For example, the T-type channels inactivate rapidly and completely at positive potentials, whereas L-type channels inactivate more slowly. The single channel conductance also varies. Commonly, the single channel current is recorded in the presence of Ba^{2+} instead of Ca^{2+}, since the use of Ba^{2+} reduces the inactivation and increases the current amplitude in some types of VDCCs, making single channel recording easier. Thus, T-type channels have a single

channel conductance of ~ 8 pS while L-type channels has a 15-28 pS conductance in 80-110 mM Ba^{2+} (Benham *et al.*, 1987; Yatani *et al.*, 1987; Ganitkevich & Isenberg, 1990; Nelson *et al.*, 1990a), and the conductance of N-type is between these values. L-type VDCCs have a wide distribution being found in skeletal, cardiac and smooth muscle as well as in a number of other tissues. T-type channels are found in cardiac muscle, in some types of nerve cells and in smooth muscle. In contrast, the N- and P/Q-types are mainly confined to the nervous system. The property of inactivation in L-type VDCCs is enhanced by the presence of intracellular Ca^{2+} (Brehm & Eckert, 1978). This feature has a possible functional importance, providing an intrinsic negative feedback mechanism that limits Ca^{2+} entry in the cell. The other types of Ca^{2+} channels primarily exhibit a voltage dependent inactivation.

Molecular structure of voltage dependent calcium channels

The skeletal muscle L-type channel was the first of the VDCCs to be cloned (Curtis & Catterall, 1984). The L-type channel is composed of 5 subunits, α_1, α_2, β, δ and γ, arranged in a 1:1:1:1:1 stoichiometry. α_2 and δ subunits are derived from the proteolytic cleavage of the same gene product, while the other subunits are encoded by separate genes. Hydrophobicity analysis and the location of putative glycosilation sites indicate that α_1, δ and γ subunits have transmembrane domains. The γ-subunit acts as an anchor for the extracellular α_2 subunit while the β-subunit is cytoplasmic. At least 7 α_1-subunit genes have been identified and further diversity is made possible by alternative splicing (Snutch & Reiner, 1992; Zhuchenko *et al.*, 1997). The α_1-subunit has 4 homologous repeats (I-IV), each repeat consists of 6 putative transmembrane domains and a loop linking the TM5 and TM6 that dips back into the membrane forming the conducting pore. The TM4 domain contains positive charges and is believed to form the voltage sensor. The proteins structures involved in the voltage dependent inactivation are still not well identified although it has been demonstrated that residues in the sixth transmembrane domain of the repeat I, as well as residues in the cytoplasmic loop between the repeat I and II, are important (Herlitze *et al.*, 1997). There are two hypothesis for the Ca^{2+}-dependent inactivation observed in L-type VDDCs: 1) Ca^{2+} could activate a Ca^{2+}- dependent phosphatase (calcineurin) that dephosphorylates the channel causing its "run-down" (Chad & Eckert, 1986); 2) Ca^{2+} "gates" the channel by binding to the channel protein in an intracellular domain. A possible Ca^{2+} binding site (a

domain of the "E-F hand" type) has been identified at the C-terminus of the α_1-subunit (de LeonM *et al.*, 1995). How Ca^{2+} binding could result in the channel closure is still unknown.

Physiological role of voltage dependent calcium channels in vascular smooth muscle

Ca^{2+} entry through VDCCs is one important pathway by which Ca^{2+} enters VSMCs from the extracellular medium. The ability of drugs such as verapamil, diltiazem or dihydropyridines, to block this channel account for their vasoactive action (reviewed in Hughes, 1995). Two types of VDCCs, high threshold activated, L-type, and low-threshold activated, T-type, have been described in a variety of SMCs (e.g. Sturek & Hermsmeyer, 1986; Benham & Tsien, 1987; Aaronson *et al.*, 1988). While the L-type VDCC seems to be ubiquitous in all vessels studied, the T-type is less frequently found in the vasculature (Akaike *et al.*, 1989; Loirand *et al.*, 1989). Although their precise physiological effects in vascular smooth muscle is not clear (Triggle, 1998), they might play a role in cell proliferation (Richard *et al.*, 1992) and at early stages of postnatal development in rat ileal SMCs (Smirnov *et al.*, 1992).

L-type Ca^{2+} current has also been observed in *quasi*-physiological Ca^{2+} concentration (1.5-2.5 mM) in a number of VSMC preparations (Benham *et al.*, 1987; Aaronson *et al.*, 1988; Matsuda *et al.*, 1990; Smirnov & Aaronson, 1992). It had an half activation potential around –10 mV and an average maximal amplitude of 15-50 pA at room temperature. However, the actual Ca^{2+} influx *in vivo*, is likely to be underestimated since the Q_{10} for the peak current is 1.6 in rabbit coronary artery (Matsuda *et al.*, 1990) and the peak current could reach values up to 500 pA in rat portal vein myocytes at 37 °C (Loirand *et al.*, 1989). As reviewed by Aaronson and Smirnov (Aaronson & Smirnov, 1996) and based on experimental data from Gollasch *et al.*, (1992), which estimated the flux of Ca^{2+} through a single open L-type Ca^{2+} channel as $5.7x10^5$ ions/s in VSMCs, the influx of Ca^{2+} at physiological membrane potential can be calculated as follows. Considering a channel open probability of 0.002 and a channel density of 1000 channels per cell, Ca^{2+} influx would be ~ $1.5x10^6$ ion/s. Taking into account the Q_{10} of 1.6 and an estimated single cell volume of 10^{-9} cm^3, the Ca^{2+} at –60 mV could elevate $[Ca^{2+}]_i$ by 2.5 μM/s (not taking into account Ca^{2+} buffering inside the cell or extrusion of Ca^{2+} from the cytoplasm). A membrane depolarisation of 10 mV should double the

open probability of L-type window current (Smirnov & Aaronson, 1992), resulting in an increase in the Ca^{2+} influx by a further 2.5 μM/s. This estimation suggests that Ca^{2+} influx through L-type VDCCs is strongly sensitive to small changes in membrane potential near the cell resting potential (Smirnov & Aaronson, 1992; Nelson *et al.*, 1990a).

1.5.3 Non-selective cations channels

Ca^{2+} can enter SMCs not only via VDCCs but also through non-selective cation channels, which are generally permeable to both monovalent and divalent cations. Two types of non-selective cation channels have been described in smooth muscle: the receptor-operated cation channels (ROCCs) and the store-operated cation channels (SOCCs) (Gibson *et al.*, 1998; Large, 2002). The existence of receptor-gated ion channels, responsible for Ca^{2+} influx directly or indirectly via membrane depolarisation and activation of VDCCs, was proposed in SMCs more than 30 years ago (Somlyo & Somlyo, 1968; Bolton, 1979). Since then, receptor-operated cation currents have been reported in a variety of vascular beds following activation of a range of receptors. ATP, externally applied, has been shown to cause a rapid, transient membrane depolarisation of ear artery smooth muscle caused by a non-selective cation conductance with significant Ca^{2+} permeability (Benham & Tsien, 1987). Similar responses to ATP, mediated by P2X receptors, have been reported in other preparations (e.g. neuronal cells) (Khakh, 2001). In addition, noradrenaline, released from sympathetic nerves and acting on α-adrenoreceptors, also produced membrane depolarisation of the rabbit ear artery by activation of a non-selective cation current (Amedee *et al.*, 1990). This current, also observed in a number of other preparations, displays strong inward rectification at positive membrane potentials as well as a reduction of the conductance at negative voltages giving an "s" shape to the current-voltage relationship (Large, 2002).

SOCCs are activated by the depletion of Ca^{2+} from intracellular Ca^{2+} stores. Although the mechanism of activation of SOCCs is unknown, it seems clear that SOCCs are not directly activated by variations in $[Ca^{2+}]_i$. Although our knowledge on the electrophysiology, pharmacology and molecular identity of these channels is less progressed than that of VDCCs, in the recent years several advances have been made

indicating that mammalian homologues of the transient receptor potential channel (TRPC) gene family, originally described in *Drosophila*, could be responsible for ROCCs and SOCCs in VSMCs. It is interesting to mention that the general molecular structure of the TRPC proteins is believed to be similar to that of Kv channels but lacking the positive charges in the segment corresponding to the Kv voltage sensor. This difference could account for a limited voltage dependence observed in currents mediated by ROCCs and SOCCs.

1.5.4. Chloride channels

Cl^- conductance has an important influence on membrane potential in VSMCs (Kozlowski, 2000), although its importance in different vascular beds can vary. The major Cl^- channel current present in vascular smooth muscle appears to be Ca^{2+}-activated Cl^- current ($I_{Cl(Ca)}$) (Pacaud *et al.*, 1992) (Klockner, 1993). It should be mentioned, however, that voltage dependent large conductance (~300 pS) Cl^- channels have been described in cultured vascular and colonic myocytes (Sun *et al.*, 1992). The first observation of $I_{Cl(Ca)}$ in smooth muscle was done by Byrne and Large (1987) in rat anococcygeus muscle stimulated with norepinephrine. The current showed a reversal potential equal to the Cl^- equilibrium potential and was activated by agents that induced an increase in $[Ca^{2+}]_i$. Moreover the response to norepinephrine was greatly reduced by removal of extracellular Ca^{2+}. These observations lead to the conclusion that this Cl^- current was Ca^{2+}-activated (Byrne & Large, 1987). These results were subsequently confirmed in experiments where Cl^- currents and changes in $[Ca^{2+}]_i$ were simultaneously measured using patch clamp recording and Ca^{2+} imaging techniques (reviewed in Large & Wang, 1996). $I_{Cl(Ca)}$ is activated by several neurotransmitters and neuropeptides acting on α-adrenoreceptors, purinoreceptors and muscarinic receptors coupled to PLC via G-protein mediated pathways. Therefore, activation of $I_{Cl(Ca)}$ by these vasoactive agents is likely to be due to a corresponding increase in $[Ca^{2+}]_i$ leading to membrane depolarisation, opening of VDCCs and initiation of muscle contraction. Little is known about the molecular structure of Ca^{2+}-activated Cl^- channels in VSMCs, although a Ca^{2+}-activated Cl^- channel has been isolated from bovine bronchial epithelial cells (Ran & Benos, 1992) and the corresponding gene cloned (Cunningham *et al.*, 1995).

1.5.5 Sodium channels

Voltage-gated Na^+ channels are composed of a channel forming α-subunit and up to 4 β-subunits (Yu & Catterall, 2003). The α-subunit when expressed in hetrerologous systems is alone sufficient to form a functional Na^+ channel. The β-subunits can enhance the Na^+ current density via a not well-defined mechanism or modulate the properties of inactivation of the channel (Tammaro *et al.*, 2002; Moran *et al.*, 2003). The α-subunit is formed by four homologous repeats (I-IV). Hydropathy analysis suggests that each repeat contains six transmembrane segments (S1-S6) and cytoplasmic N- and C- termini. The S4 segment is considered, in analogy with the S4 of Kv channels, to act as voltage-sensor. The extracellular loop between the S5 and S6 dips down into the membrane and contribute to forming the channel pore. The cytosolic linker between repeats II and IV plays a key role in the inactivation process (for review see Yu & Catterall, 2003).

There is little evidence that tetrodotoxin-sensitive Na^+ channels, such as those found in neurons, cardiac or skeletal muscle are present in smooth muscle. However, relatively non-selective channels permeable to mono- and divalent cations (see above) may contribute to increased Na^+ permeability. Tetrodotoxin-sensitive voltage-gated Na^+ currents have been described in rat azygous vein (Sturek & Hermsmeyer, 1986) and in rabbit pulmonary artery (Okabe *et al.*, 1988), where it was suggested to play a role in the generation of spontaneous activity.

The schematic diagram in Fig. 1.3 summarises the contribution of ion channels to the control of cell excitability and $[Ca^{2+}]_i$ in VSMCs.

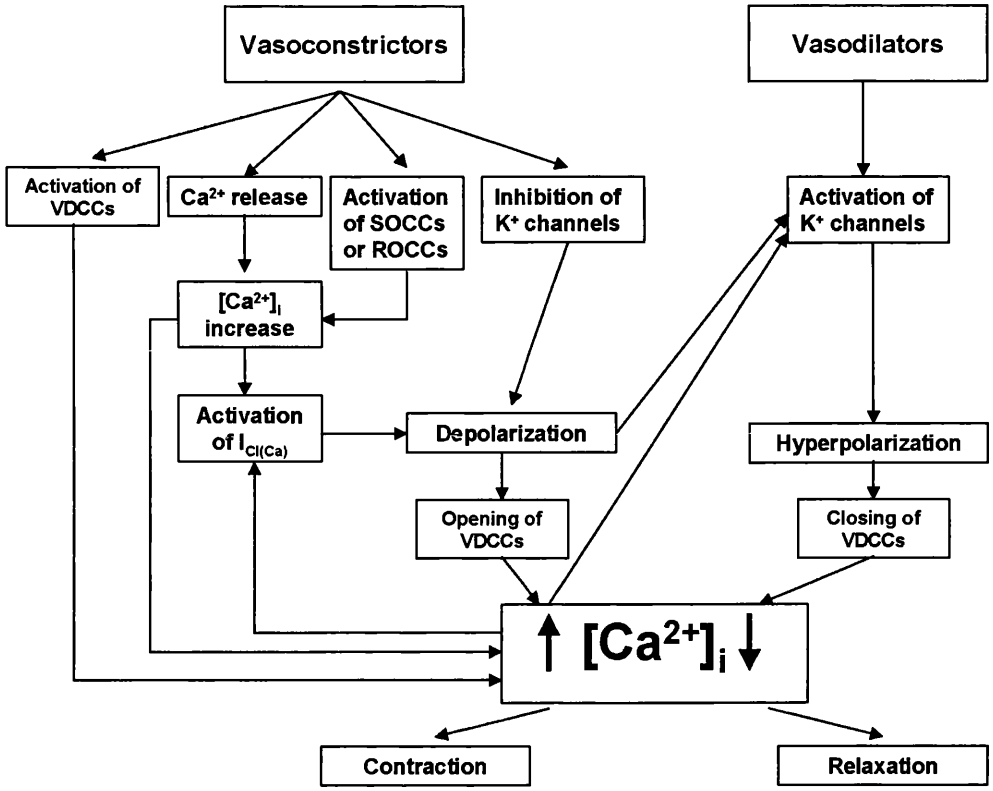

Figure 1.3. Summary of the relationships between ion-channels and intracellular Ca^{2+}-stores in the regulation of the contractile tone in VSMCs. (Adapted from Aaronson & Smirnov, 1996).

1.5.6 Membrane potential and regulation of arterial tone

The resting potential of each cell is based on two processes: passive movement of ions across the cell membrane according to their electrochemical gradient and active movement of ions against their electrochemical gradient. The first process occurs through ion channels, while the latter is carried out by ionic pumps (e.g. Na^{2+}/K^{+} pump, molecular "devices" that couple the energy of hydrolysis of ATP with the transport of ions across the cell membrane).

Membrane potential of smooth muscle cells of arteries and arterioles spans from –40 and –60 mV under condition of normal intravascular pressure (Brayden & Nelson, 1992; Harder, 1984; Nelson *et al.*, 1990b). However, membrane potentials measured in vivo are in the range of –40 and –55 mV (Neild & Keef, 1985; Hirst & Edwards, 1989; Nelson *et al.*, 1990b). These values of membrane potential are significantly more positive than the K^{+} equilibrium potential (predicted by the Nernst equation to be ~-80

mV in physiological K^+ concentrations), suggesting that the K^+ conductance does not dominate entirely at rest. The membrane potential of arterial smooth muscle might be more positive to E_K because the Cl^- conductance is relatively high in these cells (Hirst & Edwards, 1989), driving the resting potential towards the Cl^- equilibrium potential (E_{Cl} = ~-30 mV).

The membrane potential of smooth muscle in the arterial wall is an important regulator of the vascular tone. At rest the relationship between the smooth muscle membrane potential and the arterial tone is very steep with a few millivolts changes in membrane potential resulting in significant changes in the vessel diameter (Brayden & Nelson, 1992; Nelson *et al.*, 1990b). Membrane potential of vascular smooth muscle, falling in the range in which Ca^{2+} influx through voltage-dependent Ca^{2+} channels (VDCCs) is strongly voltage dependent (between -40 and –50 mV), modulating vascular tone (Nelson *et al.*, 1990b). In addition, changes in membrane potential could also modulate Ca^{2+} entry via Na^{2+}/Ca^{2+} exchanger (Nelson *et al.*, 1990b) and/or by controlling IP_3-dependent Ca^{2+}-release via the voltage dependence of IP_3 production (Ganitkevich & Isenberg, 1993).

The steep relationship between the vessel tone and the cell membrane potential is likely to originate from the steep potential dependency of the open probability of VDCCs. 3-mV changes in the resting membrane potential can affect Ca^{2+} influx of about two-fold (Nelson *et al.*, 1990b). Thus, it not surprising that any pharmacological agents, which affect ion channel activity at rest, could have an impact on the vessel contractile state. For example, activation of K^+ channels would cause membrane hyperpolarisation and vasodilation and a decrease in blood pressure. Thus, cromakalim, a specific K_{ATP} channel opener, hyperpolarized a pressurised middle cerebral artery by ~15 mV and caused significant dilation. On the contrary, inhibition of K^+ channels generally causes smooth muscle membrane depolarisation and vasoconstriction. For example, charibdotoxin, a specific K_{Ca} blocker, depolarised a pressurized middle cerebral artery by ~7 mV and caused significant vasoconstriction (Brayden & Nelson, 1992).

At the physiological resting membrane potential of -60 to -40 mV, and considering an E_K of ~ -80 mV, a constant passive outward movement of K^+ can be expressed by the following relation:

$$I_K = \gamma N P_o (V_m - E_K), \qquad [1.1]$$

where I_K is the whole cell K^+ current, γ is the single K^+ channel conductance, N is the number of channel per cell, Po is the channel open probability (i.e. the fraction of time in which the channel is open), and V_m is the membrane potential. As reviewed by Nelson and Quayle (1995), an estimate of number of channels per cell in arterial smooth muscles ranges from ~100-500 for K_{ATP} and K_{ir} channels to 1000-10000 for K_v and K_{Ca} channels. Indeed, in rat aortic smooth muscle cells (RASMC) the estimated number of channels per cell can be lower: considering a Kv current of ~3.5 pA/pF at 0 mV (Belevych *et al.*, 2002), a average cell capacitance of ~ 13 pF (Belevych *et al.*, 2002), a *Po* at 0 mV of ~ 0.4 (Belevych *et al.*, 2002) and an assumed single channel conductance of 20 pS (Nelson *et al.*, 1990a), the estimated number of Kv channels per RASMC according to the equation [1.1] results to be ~ 90. It is worth stressing that *Po* can be either constant with the V_m (as is the case for K_{ATP} channels) or change with the V_m (Kv channels) and/or with other factors such as $[Ca^{2+}]_i$ (K_{Ca} channels).

Very few K^+ channels need to open to produce significant membrane hyperpolarization, since the resting slope resistance is high in smooth muscle cells, equal to ~ 11 GΩ in RASMCs (Belevych *et al.*, 2002). According to other studies (Nelson & Quayle, 1995; Nelson *et al.*, 1990b) this concept can be illustrated by a simple parallel conductance model. The membrane potential in RASMCs can be seen as the result of two parallel conductance pathways, a selective K^+ conductance (G_K), representing the various K^+ channels and a leakage pathways (G_L), accounting for Cl^-, Na^+ and Ca^{2+} conductances with a reversal potential of 0 mV. According to this model, V_m can be expressed as:

$$V_m = \frac{G_K}{(G_K + G_L)} E_K, \qquad [1.2]$$

where E_K, the potassium equilibrium potential, is considered equal to –83 mV.

Assuming a input resistance of 11 GΩ (i.e. a G_L of 110 pS) and resting V_m of – 60 mV the calculated G_K results to be 287 pS. An increase of G_K of 19 pS (e.g as a consequence of an increase of *Po* for Kv from 0.01 to 0.02) would cause the hypothetical RASMC membrane potential to hyperpolarize by 1.4 mV, a change sufficient to produce

significant impact on voltage dependent Ca^{2+} entry (Nelson *et al.*, 1990b). This hyperpolarization could therefore reduce the force and increase blood vessel diameter. A vasodilation could lead to significant increase of blood flow, since the flow is related to the fourth power of the radius. Therefore, low levels of K^+-channels activation could cause significant vasodilation.

1.6 Ion channels expressed in vascular endothelium

Endothelial cells (ECs) are a multifunctional cell type. They perform different tasks depending on their localisation in the vascular beds, regulating many fundamental processes in the cardiovascular system, such as the control of blood flow and blood pressure (by changing the diameter of arteries and arterioles through production of various vasorelaxing and vasoconstricting substances), coagulation, platelet aggregation, vessel permeability, wound healing and angiogenesis (Levick, 1995; Casella & Taglietti, 1996). In microvascular beds, ECs also regulate the permeation of various metabolites, gasses, autocrine and paracrine factors (Levick, 1995; Casella & Taglietti, 1996).

This multitide of functions, are mediated by the production and release of a variety of vasoactive substances that affect the cells in the vessel wall, including ECs themselves. These agents includes nitric oxide (NO or endothelium-derived relaxing factor, EDRF), endothelium-derived hyperpolarizing factor (EDHF), heparin (which contributes to the creation of an anticoagulative surface for blood flow), various prostaglandins, endotelins (ET), natriuretic peptide, small signalling molecules (e.g. substance P), ATP, growth factors, steroids, and even large proteins such as receptors and proteins involved in the blood clotting cascade (e.g. ectonucleotiases) (Levick, 1995; Aaronson & Ward, 1999; Inagami *et al.*, 1995).

ECs not only responds to humoral substances, which act via receptor stimulation at their luminal or abluminal sides, but also to mechanical stimuli such as changes in the flow rate (shear stress) or blood pressure (biaxial tensile stress) (Davies, 1995). Secretory signals also originate from cell-cell contacts with other cells (e.g blood cells) and extracellular matrix proteins (Levick, 1995; Aaronson & Ward, 1999).

The mechanisms which regulate production and release of vasoactive substances from ECs are still only partially understood. It is well known, however, that their production and release is initiated by Ca^{2+}-dependent processes. Ion channels play a pivotal role in the transduction of the above-mentioned signals into cellular responses. Ion channels directly activated by agonists or by mechanical forces can provide direct pathways for Ca^{2+} entry and be therefore responsible for the mechano-sensor properties of ECs that control cell responses to hemodynamic forces and to volume-regulatory events during cell division, angiogenesis, and wound healing. Other channels (such as K^+, Cl^- or non-selective cation channels) can modulate the resting potential thus altering the driving force for Ca^{2+} entry (i.e. the difference between the membrane potential and the equilibrium potential for Ca^{2+}, see e.g. Nilius & Droogmans, 2001; Nilius *et al.*, 1997; Nilius & Riemann, 1990).

1.6.1 Membrane potential in endothelial cells

The membrane potential of vascular ECs as well as their cell capacitance and input resitance varies greatly among different vascular beds depending on conditions of cell isolation and culturing. Values of membrane potentials span from –10 to –70 mV while the cell capacitance and input resistance vary from 40 to 60 pF and from 1 and 5 GΩ respectively in cultured non-confluent macrovascular ECs (reviewed in Nilius & Droogmans, 2001). Confluent cells have a higher cell capacitance (up to 160 pF) and lower input resistance 0.01-0.4 GΩ (Vargas *et al.*, 1994) due to the presence of electrical couplings between neighboroughing ECs created by gap-junction channels. Differences in membrane potential also depend on the cell type being generally more negative in macrovascular than in microvascular ECs (Daut *et al.*, 1994; Vargas *et al.*, 1994; Zunkler *et al.*, 1995). Moreover, the membrane potential in confluent ECs (which are electrically coupled) is more negative than in non-confluent cells (Vargas *et al.*, 1994; Zunkler *et al.*, 1995), indicating a correlation between electrogenesis and the level of confluence.

K^+ channels play an important role in the control of the resting potential only in one group of ECs, termed K^+-type ECs. The resting membrane potential of the K^+-type is between –70 and –60 mV and is mainly controlled by K_{ir} channels. In another group of ECs, where Cl^- conductances are dominating (termed Cl^--type ECs), the resting

potential is between –40 and –10 mV, which is close to the Cl^- equilibrium potential (~ -30 mV in physiological Cl^- concentrations), suggesting that Cl^- channels are active under resting conditions in these cells (Nilius & Riemann, 1990; Nilius *et al.*, 1997; Nilius & Droogmans, 2001).

In addition to a role for K^+ and Cl^- conductances, the hyperpolarisation induced by decreased extracellular Na^+ suggests that either a Na^+-selective or non-selective cation conductance contributes to the resting permeability (Himmel *et al.*, 1993; Marchenko & Sage, 1993; Miao *et al.*, 1993; Vargas *et al.*, 1994).

It is noteworthy that a contribution to the resting membrane potential may be attributed to electrogenic pumps such as the Na^+/K^+ ATPase (Daut *et al.*, 1994; Nag, 1990; Oike *et al.*, 1993).

1.6.2 Ion channels on vascular endothelial cells

ECs are classified as "non-excitable cells", thus they are unable to exhibit action potential-like electrical activity. Although the presence of voltage-gated channels in ECs has been occasionally detected, it is generally accepted that their functional role in this cell type is minor (Nilius & Riemann, 1990; Nilius *et al.*, 1997).

1.6.2.1 Potassium channels

K_{ir} channels

K_{ir} is one of the most important channel controlling the resting potential in ECs. They conduct inward currents at potentials more negative than the K^+ equilibrium potential (E_K) but allow the passage of a much smaller current at potential positive than E_K. It should be mentioned however, that these channels may not be ubiquitously present in ECs (Nilius & Droogmans, 2001). When present, K_{ir} mainly determines the resting potential of ECs (Fransen *et al.*, 1995). Interestingly, together with a role in setting the membrane potential, K_{ir} channels are also sensitive K^+ "sensors". A small increase in extracellular K^+ concentration (e.g. as a result of activation of BK_{Ca} channels) shifts E_K to more positive values and thereby increases the conductance of K_{ir}. This enhancement

in K_{ir} conductance is sufficient to overcome the depolarising action of the volume-regulated anion channels (VRAC) and to bring the membrane potential to more negative values (Nilius *et al.*, 1997).

The single channel K_{ir} conductance in ECs varies between 23 to 30 pS in symmetrical K^+ solutions (e.g. Elam & Lansman, 1995; Inazu *et al.*, 1994; Kamouchi *et al.*, 1997b; Nilius *et al.*, 1993c; Pennefather & DeCoursey, 1994; Silver & DeCoursey, 1990; Silver *et al.*, 1994). Typical feature of this channel is the increase in single channel conductance in the presence of elevated extracellular K^+ (Silver *et al.*, 1994). Extracellular Ba^{2+}, TEA and Cs^+ all block K_{ir} (Leung *et al.*, 2000; von *et al.*, 1996). Extracellular Mg^{2+} causes time-dependent block at negative potentials, which can be antagonised by extracellular K^+. At positive potentials, intracellular Mg^{2+} also induces a time- and voltage-dependent block (reviewed in (Hille, 2001).

K_{ir} channels are also regulated by metabolism, since intracellular ATP prevents their run-down in the whole cell mode, while the reduction in intracellular ATP or hypoxic conditions promotes run-down of the current in ECs (Kamouchi *et al.*, 1997b). Okadaic acid (a protein phosphatase inhibitor) also prevents run-down of K_{ir}, while protamine (an activator of protein phosphatase 2A (PP2A)), has an opposite effect. Phosphorylation of K_{ir} seems to be essential to maintain its functional activity and its run-down is probably due to dephosphorylation by phosphatase PP2A (Kamouchi *et al.*, 1997b).

It is noteworthy that K_{ir} in capillary and microvascular ECs is inhibited by the vasoactive agonists such as angiotensinII, vasopressin, vasoactive intestinal peptide (VIP), endothelin (ET1) and histamine (Hoyer *et al.*, 1991; Nilius *et al.*, 1993c; Pasyk *et al.*, 1992; Zhang *et al.*, 1994). A similar effect has been observed in the presence of GTPγS (a non-hydrolyzable GTP analogue) in the patch pipette solution (Hoyer *et al.*, 1991; Kamouchi *et al.*, 1997b). This inhibition was probably due to activation G-protein, which may mediate this inhibitory action by modulating PPA2.

The molecular identity of K_{ir} channels in ECs have been identified as the $K_{ir}2.1$ (Forsyth *et al.*, 1997).

K_{ATP} channels

K_{ATP} channel currents were observed in ECs cultured from the rat aorta and brain micro-vessels in the absence of ATP in the intracellular pipette solution (Janigro *et al.*, 1993). Under this condition (which mimicked low intracellular ATP contents observed during ischemic/hypoxic conditions), both whole cell and single channel currents were increased. Currents recorded in inside-out patches were inhibited by the K_{ATP} channel inhibitor glibenclamide or ATP and activated by K_{ATP} channel opener pinacidil (Janigro *et al.*, 1993). Currents with similar characteristics have been observed in other preparation such as, e.g., rabbit aortic ECs (Katnik & Adams, 1995; Katnik & Adams, 1997). In coronary capillary ECs, low concentrations of the K_{ATP} channel opener diazoxide caused a large glibenclamide-sensitive hyperpolarization and induced a rapid Ca^{2+} transient followed by a sustained increase in $[Ca^{2+}]_i$. This high sensitivity to diazoxide has been interpreted as a novel type of K_{ATP} channel composed of a novel combination of K_{ir} and sulfonylurea receptor (SUR) subunits (Langheinrich *et al.*, 1998). Both $K_{ir}6.1$ and $K_{ir}6.2$ were detected in freshly isolated ECs form capillaries from guinea pig heart. It is not know if homo- or hetero-meric $K_{ir}6.1/6.2$ channels assemble with SUR2B in vascular ECs (Schnitzler *et al.*, 2000). Also, endothelium-dependent vasodilatation of coronary micro-vessels in response to abluminal increase in osmolarity is significantly attenuated by glibenclamide, but not by inhibition of Ca^{2+}-activated K^+ channels by iberiotoxin (Ishizaka & Kuo, 1997). It has to be mentioned however, that physiological significance of K_{ATP} channels in all types of ECs is still to be confirmed experimentally.

K_{Ca} channels

The initial response of ECs to most stimuli is an increase in $[Ca^{2+}]_i$ that is due to an influx of Ca^{2+} proportional to its the electrochemical gradient which is primarily regulated by the membrane potential. The depolarising action of Ca^{2+} influx on the membrane potential is antagonised by the activation of Ca^{2+}-dependent K^+-channels, which increase open probability in the presence of elevated $[Ca^{2+}]_i$ causing membrane hyperpolarisation. Different types of Ca^{2+}-activated K^+ channels exist and have been found in ECs. They differ in their single channel conductance and sensitivity to Ca^{2+} and membrane potential. Thus, there are large- (BK_{Ca}), intermediate- (IK_{Ca}) and small-

(SK_{Ca}) conductance Ca^{2+}-activated K^+ channels. However the relative expression of these channels in ECs greatly varies in the various vascular beds.

The expression of BK_{Ca} channel with unitary conductance ranged between 165 and 240 pS has been demonstrated in cultured ECs (e.g (Haburcak *et al.*, 1997; Hoyer *et al.*, 1994; Kamouchi *et al.*, 1997a; Ling & O'Neill, 1992; Rusko *et al.*, 1992; Suh *et al.*, 1999). Rusko *et al.*, 1992 also reported a 220 pS BKCa channel in freshly isolated rabbit aortic ECs (Rusko *et al.*, 1992). A fast elevation of $[Ca^{2+}]_i$ during stimulation with vasoactive agonists induces a fast increase in the probability of channel being open. The open probability is also increased at positive potentials. It is noteworthy, however, that the BK_{Ca} β-subunit, which is a modulator of the Ca^{2+} sensitivity of the α subunit, has not been found in ECs (McManus *et al.*, 1995; Tanaka *et al.*, 1997). Interestingly, Edwards et al. showed that K^+ efflux via endothelial BK_{Ca} might activate K^+-sensitive smooth muscle K_{ir} channels and induce hyperpolarisation and act as endothelium-derived hyperpolarizing factor (EDHF) in some types of ECs (Edwards *et al.*, 1998).

Medium conductance Ca^{2+}-activated K^+ channels, IK_{Ca} channels, present properties of inward rectification and have a conductance of about 15 pS in normal physiological K^+ concentrations (Ling & O'Neill, 1992; Sauve *et al.*, 1988; Vaca *et al.*, 1992). IK_{Ca} are activated by IP_3-mediated Ca^{2+} release induced by agonists such as bradykinin, acetylcholine and ATP (Sauve *et al.*, 1990). ET-1 and ET-3 activate IK_{Ca} channels in brain microvascular endothelium via endothelin-A receptors (Van *et al.*, 1995). The pharmacology of IK_{Ca} is not very well characterised. Charibdotoxin and quinine can efficiently inhibit IK_{Ca} and BK_{Ca} (Ling & O'Neill, 1992; Sauve *et al.*, 1990; Van *et al.*, 1995). Noxius-toxin (a toxin extracted from *Centuroides* scorpion toxin Vaca *et al.*, 1993) potently and specifically block IK_{Ca}. Both the electrophysiological and pharmacological profile of the IK_{Ca} current in ECs suggests that the recently cloned hIK (Ishii *et al.*, 1997) and mIK (Vandorpe *et al.*, 1998) can be possible molecular candidates.

Small-conductance Ca^{2+}-activated K^+ channels, SK_{Ca}, have a conductance of about 10 pS in asymmetrical physiological K^+ concentrations (Groschner *et al.*, 1992; Muraki *et al.*, 1997). Unlike BK_{Ca} these channels lack of voltage dependence. They also lack of

putative Ca^{2+} intracellular binding domains. Gating of SK_{Ca} involves a Ca^{2+} dependent interaction of calmodulin with the C-terminal domain of the α-subunit and is mediated by binding of Ca^{2+} to the first and second EF hands motifs in the N-terminus domain of calmodulin (Keen *et al.*, 1999). They are blocked by apamin, clotrimazole and D-tubocuranine (Groschner *et al.*, 1992). The K^+ efflux through both IK_{Ca} and SK_{Ca} could acts as EDHF in the rat mesenteric arterial bed (Dora *et al.*, 2003; Dora & Garland, 2001).

1.6.2.2 Ion channels mediating calcium entry

Due to the absence of VDCCs, the Ca^{2+} influx in ECs is carried out by non voltage-dependent cation channels. Ca^{2+} entry in ECs occurs via different pathways and their mechanism of activation is still elusive (Nilius & Droogmans, 2001). It is likely, theat endothelial Ca^{2+} entry channels belong to the family of TRP (transient receptor potential) channels (Clapham, 2004) which comprises of both non-selective cation channels (NSC) (which display a limited selectivity for the various cations), receptor operated cation channels (ROCCs) and the more Ca^{2+}-selective store-operated cation channels (SOCCs). Activation of these channels occurs via both G-protein coupled receptors and receptor tyrosine kinases. In addition, P2X receptors (purinergic ligand gated receptor channel complex) may provide alternative pathways for Ca^{2+} entry in ECs (Yamamoto *et al.*, 2000). These mechanisms are important for maintaining long-lasting response of EC, such as Ca^{2+}-dependent synthesis and release of NO, secretion of vasoactive compounds, and also growth factor dependent stimulation of ECs differentiation (Nilius & Droogmans, 2001).

Non-selective cation channels:

-Receptor operated cation channels:

Various functionally different cation channels activated by binding of an agonist to its membrane receptor have been described in ECs (Groschner *et al.*, 1994; Jow & Numann, 2000; Kamouchi *et al.*, 1999; Nilius *et al.*, 1993b; Nilius *et al.*, 1997). Most of these channels are activated through mechanisms involving activation of PLC. Interestingly TRP3 and 6, which have been found in endothelium (Freichel *et al.*, 1999), are non-selective ROCCs (Clapham, 2004). Endothelial ROCCs can also be activated

by an increase in $[Ca^{2+}]_i$ providing a positive feedback on their own activation. Ca^{2+}-permeable NSCs activated by vasoactive agonists have been identified in freshly isolated ECs from umbilical veins (Nilius, 1990; Nilius *et al.*, 1993a; Nilius *et al.*, 1997) and their biophysical properties characterised in detail in cell culture. The channel displayed a conductance of about 25 pS and was permeable for Na^+ Cs^+ and Ca^{2+} (Jow & Numann, 2000; Kamouchi *et al.*, 1999; Nelson *et al.*, 1990). The current slowly activated during agonist stimulation and can be recorded only in presence of physiological $[Ca^{2+}]_i$. Interestingly, store depleting substances, such as SERCA inhibitors (e.g thapsigargin), can also activate this NSC. It is noteworthy that another non-selective cation conductance of 44 pS, which was activated by intracellular Ca^{2+}, has also been described (Baron *et al.*, 1996). This channel had a permeability ratio for Ca^{2+} versus Na^+ of 0.7 and was maximally activated at $[Ca^{2+}]_i$ = 0.7 μM. A non-selective, agonist-induced current, which was activated by $[Ca^{2+}]_i$ and suppressed by inhibitors of the cyclooxygenase pathway, has also been described in aortic ECs (Himmel *et al.*, 1994).

-Redox NSC:

An activation of a 28 pS conductance by oxidant stress (which induces superoxide anions) was observed in a calf pulmonary artery endothelial cell line. This channel was equally permeable for Na^+, K^+ and Ca^{2+}. Oxidised glutathione, a cytosolic product of oxidant methabolism, activated these channels, whereas reduced glutathione had the opposite effect (Koliwad *et al.*, 1996). Based on common gating properties, TRP3 was proposed as a molecular candidate for this channel (Balzer *et al.*, 1999).

-Cyclic nucleotide-gated channels (CNG):

CNG channels are characterised by a C-terminal binding site for cyclic nucleotides. They are directly gated by binding of cAMP or cGMP and also open in response to hyperpolarized membrane potentials. The CNG channels display a conductance of 20 pS for monovalent cations and are also Ca^{2+} permeable (Hille, 2001).

A CNG1 member has been cloned in vascular endothelium. It is expressed in aortas and mesenteric arteries and forms a non-selective cation channel that may be responsible for a Ca^{2+} entry involved in the regulation of arterial diameter (Yao *et al.*, 1999). It has been proposed that an increase in $[Ca^{2+}]_i$ caused by ROCCs or SOCCs Ca^{2+} entry upon agonist stimulation activates endothelial NO-sythase (eNOS) in rat pulmonary ECs,

which in turn enhances NO levels, stimulates soluble guanylate cyclase, and increases cGMP levels, thus causing activation of CGN channels and depolarisation of ECs (Wu *et al.*, 2000). This depolarisation exerts a negative feedback on the Ca^{2+} entry via ROCCs/SOCCs.

Store-operated calcium channels

Intracellular Ca^{2+} stores depleting agents such as cyclopiazonic acid (CPA) or thapsigargin can activate a Ca^{2+} influx pathway in ECs (for review see Dolor *et al.*, 1992). This influx is apparently controlled by the degree of the emptiness of intracellular Ca^{2+} stores. Although the mechanism which links the influx of Ca^{2+} with the status of the intracellular stores is not completely understood (Clapham, 2004), it is believed that it constitutes the major Ca^{2+} entry during agonist stimulation (Parekh & Penner, 1997).

SOCCs present a higher selectivity for Ca^{2+} than ROCCs. The best-studied SOCCs is a so-called Ca^{2+}-activated Ca^{2+} channel (CRAC). CRAC displays high selectivity for Ca^{2+} and has a single channel conductance of 30 pS (Kerschbaum & Cahalan, 1999). Activation of CRAC current in response to bradykinin has been observed in bovine aorta ECs (Mendelowitz *et al.*, 1992). CRAC-like currents have also been identified in other ECs after depleting intracellular Ca^{2+} stores by either a high concentration of a Ca^{2+} buffer BAPTA, IP_3, or by extracellular application of ionomycin, or via administration of the SERCA blocker thapsigargin (Fasolato & Nilius, 1998; Gericke *et al.*, 1993a; Gericke *et al.*, 1993b; Oike *et al.*, 1994b).

1.6.2.3 Chloride channels

Anion channels are ubiquitously present in ECs. Two principal classes of Cl^- channels have been described in ECs: Ca^{2+}-activated Cl^- channels (CACC) and volume – activated Cl^- channels (VACC). In addition, high-conductance Cl^- channels, which are not regulated either by Ca^{2+} or by changes in cell volume, have been observed in excised patches but not in the cell-attached or whole cell mode recordings from ECs (Groschner & Kukovetz, 1992). Small conductance cAMP-regulated CFTR channels are generally not present in ECs, although abnormal vessel permeability has been observed in patients with cystic fibrosis (Denning *et al.*, 1992; McCannel *et al.*, 1992).

Changes in cell volume activate large whole-cell currents with densities up to 120 pA/pF at +100 mV (Fransen *et al.*, 1995; Szucs *et al.*, 1996a; Szucs *et al.*, 1996b) that is about 10 times larger than a corresponding current density for the CACC. The volume-regulated current is not Ca^{2+}-activated but requires intracellular ATP. Activation is also voltage independent and slow inactivation at positive potentials is typical (Szucs *et al.*, 1996a). Changes in both cell volume and cell shape are stimuli for activation of this conductance (Oike *et al.*, 1994a; Ueda *et al.*, 1990). A possible molecular candidate for this channel is the volume- and voltage- dependent ClC-2 channel (Grunder *et al.*, 1992; Thiemann *et al.*, 1992).

Histamine, as well as other agonists, such as ATP and thrombin, activates CACC (Groschner *et al.*, 1994; Himmel *et al.*, 1994; Watanabe *et al.*, 1994; White & Brock, 1994; Yumoto *et al.*, 1994). CACC is characterised by slow activation at positive potentials, outward rectification and sensitivity to N-phenyl-anthranilic acic, 4,4'-diisothiocyanostilbene-2,2'-disulfonate, Zn^{2+} and calmodulin antagonists (Groschner *et al.*, 1994; Watanabe *et al.*, 1994). Activation of these currents requires intracellular ATP (Watanabe *et al.*, 1994), while PKC activation inhibits CACC, suggesting that diacylglycerol (DAG), which is generated during agonist stimulation, may produce a negative feedback on CACC via a PKC-dependent mechanism (White & Brock, 1994).

1.6.2.4 Mechano-sensitive channels

ECs are constantly exposed to mechanical forces due to changes in blood flow (shear stress) and transmural pressure (biaxial tensile stress) (Malek & Izumo, 1994). The mechanical stress results in activation of mechano-sensitive channels (reviewed in Sackin, 1995). How these channels can detect changes in membrane tension is still a matter of debate but a direct involvement of cytoskeletal structures in these responses have been proposed (Davies, 1995; Davies & Tripathi, 1993; Malek & Izumo, 1994). Activation of cytoskeletal tyrosine kinases (Malek & Izumo, 1994) or 42 and 44 Kda MAP kinases (Tseng *et al.*, 1995) by shear stress also cannot be ruled out.

-Channel activated by tensile stress:
Tensile stress (experimentally generated by application of negative pressure to the patch pipette) activates channels permeable for monovalet cations and Ca^{2+} in ECs from the

pig aorta (Lansman *et al.*, 1987). Stretch-activated non-selective cation channels have also been described in miscrovascular endocardium ECs (Hoyer *et al.*, 1994; Popp *et al.*, 1992). It was also proposed that the increase in $[Ca^{2+}]_i$ associated with these stretch-activated currents could be sufficient to activate BK_{Ca} channels, leading to membrane hyperpolarisation and providing a positive feedback for Ca^{2+} entry by increasing its driving force (Hoyer *et al.*, 1994).

-Channels activated by shear stress:

Response to shear stress are likely to have a more relevant physiological meaning than responses to tensile stress in ECs (Davies, 1995). Various K^+ channels display sensitivity to mechanical stimulations. Changes in the frequency of the heartbeat, producing changes in the shear stress, activate SK_{Ca} and BK_{Ca} but not K_{ATP} channels. Differently, changes in the rate of shear stress from a variation of the viscosity do not affect SK_{Ca} channels, but have an impact on K_{ATP} and BK_{Ca} channels (Hutcheson & Griffith, 1994). Opening of these K^+ channels results in hyperpolarisation in native (Nakache & Gaub, 1988) and cultured (Jacobs *et al.*, 1995) ECs. Interestingly, cGMP and NO seem to be involved in the activation of shear stress-dependent K^+ channels (Hassessian *et al.*, 1993; Ohno *et al.*, 1993). Shear stress also activates cation channels which are about 12 times more permeable for Ca^{2+} than for Na^+ (Schwarz *et al.*, 1992b). Modulators of the cytoskeleton, such as cytochalasin B which prevent microtubule polymerisation, increased the sensitivity of ECs to shear stress (Schwarz *et al.*, 1992a; Schwarz *et al.*, 1992b). Shear stress activated Ca^{2+} influx was completely blocked by removal of sialic acid in the glycocalyx of ECs (Hecker *et al.*, 1993).

1.6.2.5 Gap junction channels

Gap junctions formed by connexins are abundant both between ECs and also between ECs and SMCs (Davies *et al.*, 1988). Gap junction channels allow direct electrical and metabolic communications between cells. At least three isoforms of connexins (Cx37, Cx40, Cx43) have been found in ECs. Cx43 is prevalently expressed in macrovascular rather than microvascular ECs; however some ECs can also express Cx37 and Cx40 (Dejana *et al.*, 1995; Little *et al.*, 1995). Connexins form functional gap junction channels between ECs that can be disrupted by uncoupling agents such as heptanol (Dejana *et al.*, 1995; Reed *et al.*, 1993). Functional channels are formed between

identical isoforms although further diversity is made possible by heteromeric combinations. Interaction does not occur between Cx40 and Cx43 isoforms, but it is possible between Cx40 or Cx43 or Cx37 (Bruzzone *et al.*, 1993). Expression of connexins depends on the functional states of ECs and is also regulated by mechanical forces. Low shear stress induces expression of gap junction channels, while high shear stress and aging have opposite effects (Dejana *et al.*, 1995; Okano & Yoshida, 1993; Xie & Hu, 1994).

Electrical coupling between ECs (Miao *et al.*, 1993) have a role in the electrotonic spread of electrical signals along the wall of the vessel. The electrical coupling between ECs and SMCs via low-resistance gap junction channel (Beny, 1990; Davies *et al.*, 1988) could be functionally relevant in small arterioles where a large total surface of ECs contacts a much smaller surface of SMCs, allowing an efficient modulation of the smooth muscle membrane potential by the ECs (Daut *et al.*, 1994). Interestingly, other observations suggest that agonist-induced hyperpolarisation of ECs does not spread electrotonically to the smooth muscle cells (Beny, 1990), while the opposite process, the electrotonic spread from smooth muscle to adiacent ECs, does take place (Beny & Pacicca, 1994; Marchenko & Sage, 1994).

1.6.3 Functional role of endothelial ion channels

1.6.3.1 Calcium signalling

Regulation of the intracellular Ca^{2+} concentration is probably the most important function of ion channels in ECs. Two types of Ca^{2+} signals can be seen in ECs: $[Ca^{2+}]_i$ oscillations and a biphasic increase in $[Ca^{2+}]_i$ consisting of a fast peak followed by a long-lasting plateau (e.g.(Jacob *et al.*, 1988). Low concentrations of an agonist (e.g acetylcholine, ATP, histamine or bradykinin) often induce oscillations of $[Ca^{2+}]_i$ (Jacob *et al.*, 1988), whereas a biphasic rise in $[Ca^{2+}]_i$ prevails at higher concentrations (Nilius *et al.*, 1993b). The fast transient Ca^{2+} peak is due to release of Ca^{2+} from IP_3-sensitive intracellular Ca^{2+} stores, whereas Ca^{2+} enrty from the extracellular space via SOCCs account for the plateau-like phase. Plasmalemmal ion channels thus provide a direct influx of Ca^{2+} and tune the driving force for the Ca^{2+} influx.

Agonist- or shear stress- induced Ca^{2+} entry is related to the membrane potential (which determined the driving force for the Ca^{2+}). Generally, shear stress or Ca^{2+} mobilising agonists activate K^+ channels (BK_{Ca}, SK_{Ca}, K_{ATP}) and cause membrane hyperpolarization of ECs thereby enhancing Ca^{2+} influx (Benzing *et al.*, 1999; Bhullar *et al.*, 1998; Birnbaumer *et al.*, 1996; Clark *et al.*, 1995; Emeis *et al.*, 1997; Graier *et al.*, 1998; Graier *et al.*, 1995). In many cases, an initial hyperpolarisation is followed by depolarisation via activation of NSC channels, which could limit the extent of Ca^{2+} entry by decreasing a driving force for Ca^{2+} (Bkaily *et al.*, 1993; Feron *et al.*, 1997; Kajimura & Curry, 1999). Interestingly, a similar mechanism for modulation of the Ca^{2+} driving force has also been hypothesised for Cl^- channels. ATP and histamine-induced and store operated Ca^{2+} entries can be inhibited by Cl^- channel blockers or by a shift of the Cl^- equilibrium potential towards more positive values (Hosoki & Iijima, 1994; Hosoki & Iijima, 1995; Yumoto *et al.*, 1994). Depolarisation of ECs membrane potential caused by an increase of K^+ concentration or by pharmacological blockage of K^+ channels decreased the plateau phase of the Ca^{2+} signal upon stimulation with ATP or bradykinin and, as a consequence, reduced the production and release of NO and PGI_2 (both require an increased intracellular Ca^{2+} level) (Busse *et al.*, 1991; Inagami *et al.*, 1995).

This interplay between ion channels, membrane potential and Ca^{2+} influx may also be relevant for generation of Ca^{2+} oscillations in ECs. Stimulation with ATP or histamine (Jacob *et al.*, 1988) causes Ca^{2+} release and is often accompanied by mirrored oscillatory changes in membrane potential due to activation of BK_{Ca} channels (Nilius & Droogmans, 2001). These Ca^{2+} oscillations are merely due to periodic discharges of intracellular Ca^{2+} stores (Jacob *et al.*, 1988; Nilius *et al.*, 1997). These hyperpolarisations increases the driving force for Ca^{2+} entry.

1.6.3.2 Vessel Permeability

One of the most important roles for ECs is the regulation of the exchange of solutes, proteins and endocytosed particles between blood and tissue. This transport is partially mediated by changes in the paracellular permeability of the endothelial layer. Some agonists (e.g. thrombin or histamine which transiently increase $[Ca^{2+}]_i$) induce a mirrored short-lasting increase in vascular permeability, while others (e.g. cytokines,

growth factors) induce more persistent changes. It is believed that the increase in permeability is caused by changes in cytoskeleton and cell-cell coupling (Dejana *et al.*, 1995). ECs hydraulic permeability, especially in the micro-vascular beds, is modulated by Ca^{2+} entry (involving a Ca^{2+}/calmodulin-dependent non-VSMC isoform of MLCK, Verin *et al.*, 1998, which in turn is driven by the membrane potential, He & Curry, 1991; He & Curry, 1994). Modulation of Ca^{2+} entry, via SOCC-dependent or independent mechanisms, and the control of Ca^{2+} influx by the electrochemical driving force, might be responsible for this regulation of permeability (He & Curry, 1994).

1.6.3.3 Cell-cell contacts

A multitude of stimuli originating by cell adhesion have an effect on the phenotype and functional properties of ECs (Albelda & Buck, 1990). For example, contacts of ECs with other cell types circulating in the blood such as lymphocytes, T-helper cells, tumor cells or antigen-presenting ECs) and extracellular matrix proteins are modulated by intracellular Ca^{2+} (Pfau *et al.*, 1995). Elevation of $[Ca^{2+}]_i$ also enhances the ability of ECs to adhere to other cells (Leavesley *et al.*, 1993; Pili *et al.*, 1993). Ca^{2+} influx is also activated by binding of ECs to matrix proteins (fibronectin and vitronectin), as was demonstrated with integrin monoclonal antibodies (Schwartz *et al.*, 1993). This Ca^{2+} entry strongly depends on β1 and β3 intergrins and the β2 integrin cellular adhesion molecules ICAM-1 (Pfau *et al.*, 1995). The influx pathway however seems to be different from the agonist-induced Ca^{2+}-entry. An intergin-associated protein (IAP-50) physically bound at β3 has been proposed to function as Ca^{2+}-entry channel (Schwartz *et al.*, 1993).This signalling pathway is linked to the generation of IP_3 (Pfau *et al.*, 1995) and might be related to the mechanisms proposed for the TRP activation.

1.6.3.4 Volume regulation

VACC contribute to the regulatory volume decrease. Cell swelling is the triggering signal for a series of events, including the activation of Cl^- channels. It is not certain however whether the Cl^- channels activation is directly involved in regulatory volume changes that occur in ECs e.g during metabolic activity, secretion or pathophysiological conditions. Co-activation of K^+ and Cl^- channels sets the membrane potential to a value between the two reversal potential (i.e. ~ -80 and ~ -30 mV respectively) and governs

Ca^{2+} entry by affecting the driving force for Ca^{2+} ions (Hosoki & Iijima, 1994; Hosoki & Iijima, 1995; Oike *et al.*, 1994b). VACC in ECs are also involved in the transport of small organic molecules such as taurine, aspartate, gluconate (but not arginine), and this might be important in non-saturable Na^+-independent endothelial transport.

1.6.3.5 pH regulation

Agonist stimulation and changes in cell shape give rise to substantial Cl^- currents in ECs (estimated to be ~ 100 pA/pF) (Oike *et al.*, 1994b; Szucs *et al.*, 1996a; Szucs *et al.*, 1996b; Ueda *et al.*, 1990). This current might produce relevant changes in the intracellular or intercellular Cl^- concentrations. These local changes in $[Cl^-]$ could affect other Cl^--dependent transport mechanism such as the Cl^- exchanger and the Na^+-K^+-$2Cl^-$ co-transporter, which are important intracellular pH regulators. They might also affect a Cl^-- and GTP-dependent plasma membrane protein kinase (Treharne *et al.*, 1994) giving rise investigated signalling pathways which have still to be fully investigated.

1.6.3.6 Cell proliferation and differentiation

A role for ion channels in the modulation of progression through cell cycle is well known. Block of K^+ channels and cell depolarisation induce G1 arrest in several cell types (Wonderlin & Strobl, 1996; Neylon, 2002). There are evidence that blockers of volume-sensitive Cl^- channels such as tamoxifen or quinine, also suppress the growth of ECs (Voets *et al.*, 1995). This Cl^- current might therefore be involved in the regulation of cell proliferation via a mechanism that is linked to the volume and/or pH regulation or to a fine-tuning of the driving force for Ca^{2+} entry, which is important at the Ca^{2+}-dependent cell cycle control point (i.e. between G1 and S phases), also thought to be mediated by these channels. Interestingly, angiogenesis (i.e. formation of new blood vessels) is inhibited by various blockers of VRCC (Manolopoulos *et al.*, 2000). Also, the functional expression of volume-activated Cl^- channels appears to change if cells switch from proliferation to differentiation (Voets *et al.*, 1995) further supporting the role of VRCCs in the regulation of EC growth.

1.7 Regulation of K^+ channels

Due to their ability to influence the membrane potential and thus the contractile activity of VSMCs, K^+ channels can be an important target for regulation by various intracellular and extracellular stimuli. Vasoactive substances either circulating in the blood or released from endothelial cells and other non-SMCs, including perivascular nerves, can affect the activity of K^+ channels (Standen & Quayle, 1998; Beech *et al.*, 2001).

1.7.1 Regulation of K^+ channels by vasoactive substances

A number of vasodilators act via G-protein coupled receptors linked to activation of adenylate cyclase causing an increase in intracellular cAMP and subsequent activation of PKA. This pathway has been shown to modulate various types of K^+ channels. For example, activation of K_{ATP} channels occurs in response to calcitonin gene-related peptide, adenosine and isoprenaline in mesenteric and coronary arteries (Miyoshi & Nakaya, 1993; Quayle *et al.*, 1994; Wellman *et al.*, 1998). Agonist dependent activation of K_{ATP} was abolished by PKA inhibitors such as Rp-cAMPS, H8 or H89 and PKA inhibitory peptides. In addition, a PKA catalytic subunit applied intracellularly activated K_{ATP} channels in both whole cell and excised patches isolated from pig coronary artery SMCs (Wellman *et al.*, 1998). Isoprenaline has been reported to activate BK_{Ca} channel in rat aorta, porcine coronary and guinea pig basilar arteries via a mechanism involving PKA-dependent phosphorylation (Sadoshima *et al.*, 1988; Minami *et al.*, 1993; Song & Simard, 1995). It was proposed that activation of BK_{Ca} channels in VSMCs may also occur via a direct interaction of the G-protein α-subunit with the channel (Scornik *et al.*, 1993). Evidence for regulation of Kv channels by PKA is scarce and limited to essentially a single study showing that activation of β-adrenoreceptors stimulates Kv currents in rabbit portal vein SMCs via a PKA-dependent mechanism (Aiello *et al.*, 1995).

Many vasoconstrictors also act via G-protein coupled membrane receptors which, when activated, lead to the production of two second messengers, IP_3 and DAG. DAG is a potent activator of PKC. It has been previously demonstrated that activation of PKC causes an inhibition of K_{ATP} and BK_{Ca} currents in VSMCs. K_{ATP} currents were inhibited

by angiotensin II (Miyoshi & Nakaya, 1991; Kubo *et al.*, 1997), endothelin (Miyoshi *et al.*, 1992), vasopressin (Wakatsuki *et al.*, 1992) and noradrenaline, histamine, serotonin and neuropeptide Y (Bonev & Nelson, 1996), via PKC-mediated mechanisms. BK_{Ca} channels from coronary artery SMCs incorporated into lipid bilayer have been reported to be inhibited by angiotensin II (Toro *et al.*, 1990). Kv currents were inhibited by activation of a histamine H_1 receptor agonist in rabbit portal vein (Ishikawa *et al.*, 1993). Also, in rabbit portal vein, Kv currents were inhibited by activation of PKC (Aiello *et al.*, 1996), in contrast to PKA which activated this current (Aiello *et al.*, 1995). However, in rat pulmonary arterial myocytes, activation of PKC by arachidonic acid resulted in an increase of I_{Kv} (Aaronson & Smirnov, 1996b). It is noteworthy that cloned Kv1.5, Kv1.3 and Kv2.1 channels, which are expressed in VSMCs, contain consensus sites for PKC-mediated phosphorylation (Martel *et al.*, 1998; Williams *et al.*, 2002; Murakoshi *et al.*, 1997).

Some vasodilators activate guanylate cyclase and increase intracellular levels of cyclic GMP leading to activation of cGMP-dependent protein kinase (PKG). It has been shown that NO can activate BK_{Ca} channels via activation of PKG-mediated pathways since the effect was mimicked by application of a PKG catalytic subunit on inside-out patches from cerebral artery (Robertson *et al.*, 1993). Kubo et al. (1994) reported evidence of activation of K_{ATP} channels by PKG in cultured SMCs from thoracic aorta (Kubo *et al.*, 1994). On the other hand, a direct effect of NO on BK_{Ca} currents has also been shown (Bolotina *et al.*, 1994). In addition, in tracheal SMCs it has been proposed that PKG does not activate the channel directly but through activation of protein phosphatases that would, in turn, dephosphorylate and activate the channel (Zhou *et al.*, 1996).

Oxygen is an essential element for normal cell activity and is delivered to tissues with the blood. Reduction in partial oxygen tension causes significant effects on the vasculature. Hypoxia generally causes vasodilatation in systemic blood vessels so that blood flow and gas exchange in tissues is enhanced. On the other hand, pulmonary vasoconstriction in response to hypoxia has the physiological significance to reduce the blood flow to poorly oxygenated alveoli. Although the precise mechanisms are not known, it is believed that K^+ channels are involved in both processes. Changes in oxygen tension affects intracellular metabolism and may also influence the activity of

K^+ channels. In isolated VSMCs both inhibition of intracellular metabolism and hypoxia itself can activate K_{ATP} channels (Beech *et al.*, 1993; Dart & Standen, 1995; Zhang & Bolton, 1995). This effect could be due to a reduction of the cellular ATP:ADP ratio or due to a undefined oxygen sensing mechanism linked to the channel. Since hypoxia is associated with elevated $[Ca^{2+}]_i$, BK_{Ca} channels can also be activated, as found in portal vein SMCs (Miller *et al.*, 1993; Yuan *et al.*, 1996). BK_{Ca} activity is also modulated by changes in cellular redox state (Park *et al.*, 1995). Kv channels have been demonstrated to play a central role in acute (Post *et al.*, 1992) and chronic (Aaronson *et al.*, 1994; Archer *et al.*, 2001) hypoxic pulmonary vasoconstriction. Interestingly, an oxygen sensitivity by the Kv2.1/Kv9.3 (Patel *et al.*, 1997), Kv1.2 (Conforti *et al.*, 2000) and the Kv3.1b (Patel & Honoré, 2001) channels has been reported. These Kv homo- and hetero-tetramers are thought to be involved in responses to acute hypoxia in pulmonary arterial SMCs (Coppock *et al.*, 2001), however, the mechanisms by which changes in oxygen tension alter their activity remain unknown.

1.7.2 Regulation by intracellular divalent cations

The importance of Ca^{2+} and Mg^{2+} as regulators of vascular tone is well documented (Nelson *et al.*, 1990b; Altura & Altura, 1984; Takaya *et al.*, 2000). An increase of $[Ca^{2+}]_i$ not only initiates contraction but also triggers many other biochemical events necessary for excitation contraction coupling of smooth muscle. An increase in $[Mg^{2+}]_i$ enhances enzymatic activity responsible for signal transduction and regulates bioenergetics and ion transport (Takaya *et al.*, 2000). It is noteworthy that in contrast to the intracellular Ca^{2+} homeostasis our knowledge on the mechanisms of regulation of $[Mg^{2+}]_i$ is limited (Altura & Altura, 1984). Interestingly, in VSMCs it has been reported that during agonist stimulation there is not only an increase in $[Ca^{2+}]_i$ but also an increase in $[Mg^{2+}]_i$ (Okada *et al.*, 1992), suggesting that increases in both the divalent cations may play a significant role in agonist-induced contraction.

Various types of K^+ channels are inhibited by intracellular divalent cations in a number of different preparations. One example of intracellular divalent cation inhibition is the property of inward rectification. Inward rectification is believed to be due to block of the outward movement of K^+ through K^+ channels by intracellular divalent (Matsuda *et al.*, 1987; Mazzanti & DiFrancesco, 1989; Gelband & Hume, 1992) and monovalent

(Harvey & Ten, 1989; Forsythe *et al.*, 1992) cations which are driven into the open channel pore by membrane depolarisation.

Changes in the intracellular ionic composition can also affect the voltage dependency of voltage-gated channels by screening fixed negative charges at the intracellular side of the cell membrane, thereby modifying the local electric field sensed by the channel voltage sensor (McLaughlin *et al.*, 1971; Hille *et al.*, 1975).

1.8 Aims and Objectives

To summarise, K^+ channels in general and Kv channels in particular, play a crucial role in the regulation of excitation-contraction coupling in VSMCs. The relative contribution of Kv currents to the control of excitability varies in different vascular beds. The molecular identity of functional Kv channels in the vasculature is still generally unknown. Also, mechanisms that regulate Kv currents in VSMCs remain poorly understood. Preliminary work leading to this project, suggested that Kv channel currents could be a major contributor to the whole cell K^+ current in rat aortic SMCs and could be regulated in a complex manner via involvement of PKC and possibly other intracellular factors.

Two experimental models, the rat aorta and rat conduit pulmonary artery as representatives of two different circulatory beds, were chosen for this project. The preliminary data leading to this project demonstrated that Kv channel current is relatively homogenious in aortic SMCs, whereas two cell sub-types expressing different Kv channels were found in the rat conduit pulmonary artery. It is noteworthy, that one type of Kv current in pulmonary SMCs has similar electrophysiological and pharmacological profile to that in rat aortic SMCs. Therefore, rat aortic and conduit pulmonary SMCs represent an exceptional experimental model allowing investigation and comparison of mechanisms of regulation of different Kv channels in different vascular beds, thus enlightening the fundamental principles of Kv channel function in the vasculature. This knowledge will also provide the basis for our understanding of abnormal changes in the mechanisms of regulation of function and expression of Kv channels, which could occur in various pathological conditions (e.g. hypertension), altering pharmacological responsiveness and contractile reactivity of blood vessels from different circulations.

Therefore, the main aim of my thesis was to investigate the contribution of the Kv current to the whole cell K^+ current in the rat aortic and conduit pulmonary SMCs, its physiological importance in vascular function and mechanisms which control its activity.

The objectives were initially set as follows:

1. To characterise electrophysiological and pharmacological properties of the Kv current in single rat aortic SMCs using the patch clamp technique and compare those with Kv currents in rat main pulmonary SMCs.

2. To identify the Kv channel α-subunits expressed in aortic tissue and in rat aortic SMCs using western blot, immunocytochemistry and confocal imaging.

3. To investigate the role of Kv channels in intact aortic preparations using isometric tension measurements and selective K^+ channel inhibitors.

4. To investigate mechanisms of regulation of rat aortic Kv channel currents by protein kinases, focusing on various PKC isoforms expressed in rat aorta.

It is noteworthy that during the course of my project I found a novel modulatory effect of intracellular Mg^{2+} on Kv currents in rat aortic SMCs. Therefore, the effect of intracellular Mg^{2+} on two types of Kv currents in rat conduit pulmonary arterial SMCs were also investigated. Also, in collaboration with Dr Oscar Moran and Professor Franco Conti (Institute of Biophysics, CNR, Genoa, Italy), I studied the effect of intracellular Mg^{2+} on two different Kv channels, Kv1.5 and Kv2.1, expressed in *Xenopus* oocytes.

In this thesis, discussion to each of the points listed above is given at the end of each corresponding chapter and summary of my major findings are given in "Summary and Conclusion".

Chapter 2

Materials and Methods

2.1 Solutions

Table 2.1. Composition of solutions for contraction experiments

Reagents (mM)	**Krebs**	**Na^+-free buffer**	**Mg^{2+}-loading buffer**	**Na^+-buffer**
NaCl	118	-	-	140
$NaHCO_3$	25	-	-	-
KCl	4.7	-	6	6
$CaCl_2$	2.5	2	-	2
$MgSO_4$	1.2	-	-	-
$MgCl_2$	-	1.2	30	1.2
EGTA	-	-	0.1	-
HEPES	-	5	5	5
NMDG	-	140	110	-
Glucose	11.7	11.7	11.7	11.7
pH	7.4	7.2 (HCl)	7.2 (HCl)	7.2 (KOH)

Table 2.2. Composition of solutions for cell isolation and oocyte preparation

Reagents (mM)	PSS [1]	Ca^{2+} -free PSS	Barth solution [2]	Ca^{2+} -free Barth [2]	Skinning solution [2]
NaCl	130	130	84	84	-
KCl	5	5	10	10	20
K-aspartate	-	-	-	-	200
$CaCl_2$	1.5	-	0.6	-	-
$MgCl_2$	1.2	1.2	-	-	1
$NaHCO_3$	-	-	2.5	2.5	-
$Ca(NO_3)_2$	-	-	6.5	6.5	-
Tris-HCl	-	-	7.5	7.5	-
HEPES	10	10	-	-	10
EGTA	-	-	-	-	10
Glucose	10	10	-	-	-
pH	7.2 (NaOH)	7.2 (NaOH)	7.4	7.4	7.4

[1] PSS- Physiological Salt Solution

[2] Solutions used for handling *Xenopus* oocytes

Table 2.3. Composition of solutions for electrophysiological recordings

	VSMCs	***Xenopus* Oocytes**			
	whole-cell configuration	**inside-out configuration**			
Reagents (mM)	**Intracellular (pipette)**	**Extracellular (pipette)**	**Intracellular (bath)**		**NFR[1] (bath)**
			"0 Mg"	**"10 Mg"**	
NaCl	10	115	-	-	112.5
KCl	110	2.5	120	120	2.5
$CaCl_2$	0.5	1.8	-	-	1.8
$MgCl_2$	0-10	-	-	10	-
Tris-HCl	-	-	20	10	-
HEPES	10	10	-	-	10
EGTA	10	-	2	2	-
pH	7.2 (KOH)	7.4 (NaOH)	7.4 (NaOH)	7.4 (NaOH)	7.4 (NaOH)

[1]NFR –Normal Frog Ringer-

Krebs solution (Table 2.1) was used for contraction experiments. HEPES-based buffers were used to investigate the effect of intracellular Mg^{2+} on KCl-induced contraction in endothelium-denuded rat aortic preparations. In Na^+-free and 30 mM Mg^{2+}-loading buffers NaCl was replaced with 140 and 110 mM N-methyl-D-glucamine (NMDG), respectively. The removal of Na^+ was essential for Mg^{2+} loading since Mg^{2+}-Na^+ exchanger was inhibited under these conditions and worked in reverse, when extracellular Mg^{2+} was increased pumping Mg^{2+} in to the cell (Handy *et al.*, 1996). Contraction experiments in Mg^{2+}-loaded aortic rings were also performed in Na^+-free buffer in order to retain a high Mg^{2+} concentration inside the cell. Imipramine, which is thought to inhibit Na^+-Mg^{2+} exchanger (Handy *et al.*, 1996), was not used, since preliminary findings showed that this drug at a concentration of 200 μM inhibited KCl- or PE- induced contraction. This effect was also not reversible.

Solutions containing various concentrations of KCl had the same composition except that the amount of NaCl was reciprocally reduced when KCl was increased to achieve a required K^+ concentration. Appropriate volumes of tetraethylammonium chloride (TEA, 2 M stock) or 4-aminopyridine (4-AP, 0.5 M stock solution, pH adjusted to 7.4 with HCl) were added directly to the organ bath to achieve a required final concentration of the drug.

PSS (Table 2.2) was used as extracellular recording solution for experiments involving whole-cell configuration in VSMCs.

Intermediate concentrations of $MgCl_2$ for the inside-out intracellular recording solution were obtained by mixing the "0 Mg" and "10 Mg" solutions (Table 2.3) in corresponding proportions.

The free $[Ca^{2+}]$ in the pipette (intracellular) solution was calculated using the program Maxchelator (Stanford University, CA, USA). In the "whole cell intracellular" solution, pH was adjusted to 7.2 with KOH (~850 μl KOH 1M per 50 ml pipette solution) giving a final concentration of K^+ equal ~ 135 mM.

2.2 Materials and reagents

All chemicals, enzymes for cell isolation and K^+ channel inhibitors were purchased from BDH Merck (UK) or Sigma unless indicated otherwise. cDNA for the Kv2.1 channel was kindly provided by Dr Rolf H. Joho (University of Texas, Southwestern Medical Center) and Dr Martin Stocker (University College London).

2.3 Tissue dissection and preparation

2.3.1 Rat vasculature

Male Wistar rats (weight 225-300 g) were killed by cervical dislocation in accordance with UK Home Office guidelines. The chest was open at the level of the diaphragm and the rib cage cut with scissors. Heart and lungs were removed *en block* before removing the thoracic part of the aorta. Tissues were immediately placed in 5-20 ml of PSS solution at room temperature. The thoracic aorta and external (main extra-lobar) pulmonary arteries were then mechanically cleaned of the adhering connective tissue and cut into rings (~ 2-2.5 mm width). This operation was carried out under a stereo-microscope (Leica, zoom 2000) with the aid of fine forceps and scissors. When required, the intimal surface of the vessel was gently rubbed with horsehair to remove the endothelium.

2.3.2 Xenopus Oocytes

The *Xenopus* oocyte expression system was used to study the effect of intracellular Mg^{2+} on the properties of Kv1.5 (Snyders *et al.*, 1993) and Kv2.1 (Frech *et al.*, 1989) channels. Ovarian lobes were surgically extracted from the South African frog *Xenopus Leavis* under anesthesia (20-40 min in Tricaine solution, 2.5 g/l) and transferred into a perti dish containing Barth solution. The follicular cell layer was removed after incubation in Ca^{2+}-free Barth solution containing collagenase (1 mg/ml, Type II) for 2-3 hours under continuous gentle shaking. To stop the enzymatic reaction, oocytes were washed in Barth solution where the presence of 0.6 mM Ca^{2+} inhibited the activity of collagenase. Only healthy looking oocytes, that possessed an intact vitelline membrane and a regular spherical shape were selected for microinjection. The experiments in

Xenopus oocytes were performed in collaboration with Dr Oscar Moran and Professor Franco Conti at the Institute of Biophysics of the National Research Council in Genoa, Italy. All experimental procedures were performed in accordance with European rules (86/609/CEE) and have been approved by the local health board (A.S.L. n3, Genova).

2.4 Isolation of single vascular smooth muscle cells

Pieces (1-3 mm^2) of aortic or pulmonary arteries were kept in normal PSS (Table 3.1) on ice for 30 min and then transferred to nominally Ca^{2+}-free PSS for 10 min at 37°C. After incubation, pieces of tissue were transferred into 3 ml of Ca^{2+}-free PSS containing collagenase Type XI (1 mg/ml) for 10 min at 37°C. The tissue was then transferred to 3 ml of pre-warmed PSS solution containing papain (1 mg/ml) and 1 mM dithiothreitol (DTT). DTT, a reducing agent, was used to activate papain. After incubation for 10 min at 37°C, the segments were gently triturated in 3-4 ml of Ca^{2+}-free PSS and then were put into a fresh papain-containing solution. The treatment was repeated two more times. The resulting three volumes were combined, filtered through 95μm nylon mesh and centrifuged at 1100×*g* for 5 min. The cell pellet was initially re-suspended in Ca^{2+}-free PSS (0.5 ml). Ca^{2+} concentration was increased gradually by a consecutive addition of three volumes of PSS (0.5 ml each) in 5 min intervals. The cell suspension thus obtained was maintained at +4°C and cells were used on the same day. Single smooth muscle cells had an elongated spindle-shape and were able to contract reversibly upon the approach of the patch pipette filled with high K^+ solution or ATP-containing solution.

2.5 Isometric tension measurements in the rat aorta

Aortic rings (isolated as described in section 2.3.1) were mounted in a 18 ml organ bath between two metal hooks, connected to a piezoelectric force transducer and to a micromanipulator respectively. Tissue was firstly equilibrated in Krebs solution aerated with 95% O_2/5% CO_2 under a resting tension of 1 g for 60 min at 37°C and was then stimulated with three subsequent applications of 2.5 μM phenylephrine (PE) followed by washing with Krebs solution before starting each experiment. Contraction was

measured using Biegestab K30 piezoelectric force transducer (Hugo Sack Elektronics, Germany), MacLab/4s recording unit and Chart v3.6/s software (ADI Instruments, UK) and expressed in grams of tension. Data were sampled at 40 Hz. When indicated, endothelium was removed by gentle rubbing of the vessel lumen with a horsehair and its removal was verified by the absence of relaxation to 10 μM acetylcholine (ACh) in arteries preconstricted with 2.5 μM PE. Each experimental protocol was repeated in preparations isolated from at least three animals, unless stated otherwise.

2.6. Electrophysiological recordings

2.6.1 Mechanical set-up and electrical recordings

The patch clamp set-up requires mechanical stability and electrical shielding (Neher & Sakmann 1995; Ogden, 1994; Moran, 1996).

The recording chamber, a micromanipulator (Sutter Instruments, U.K.) used to control the movement of the patch clamp pipette and an inverted microscope (Nikon, Japan) were mounted on an anti-vibration table and surrounded by a Faraday cage. Optimal electrical shielding was obtained by connecting the individual items of the set-up to a single ground point, avoiding current ("ground") loops between the instruments. Membrane currents were measured in the whole-cell or inside-out excised patch configuration of the patch clamp technique (Hamill *et al.*, 1981), using an Axopatch-200B amplifier (Axon Instruments). Current signals were sampled at 20 kHz and low pass filtered with a 4-pole Bessel filter at 5 kHz (a frequency 4 times lower that of sampling). Pulse stimulation and data acquisition used 16 bit D-A and A-D converters and were controlled by a Personal Computer with pClamp 8.02 software (Axon Instruments, Foster City, CA) or Pulse-PulseFit software package (Heka Elektronik, Lambrecht, Germany).

2.6.2. Pipette fabrication

Table 2.4. Types of glass used for pipette fabrication

	Glass	$\varnothing_I$ (mm)	$\varnothing$o (mm)	Resistance (MΩ)	Manufacturer
Whole cell	Borosilicate	0.86	1.5	3.0-4.5	Sutter Instruments
Patch ins-out	Aluminiumsilicate	1.2	1.6	1-3	Hilgenberg
TEVC*	Borosilicate	1.17	1.5	0.6-1	Harvard Apparatus
Injection glass	Borosilicate	1.6	2	-	Hilgenberg

*Two-electrode voltage-clamp

Three types of glass capillaries were used for the different recording conditions (Table 2.4). According to the melting temperature the capillaries' glass can be classified as soft (soda glass), hard (borosilicate glass) and extra hard (aluminium glass) (1995). Selection of the glass was made by optimising between the requirement for low noise-recording characteristics (e.g. hard glass has a higher resistance and lower dielectric constant and therefore low noise) and the facility to work with each type of glass (e.g. with soft glass it is easier to achieve a desired profile of the pipette tip). After having been cut to an appropriate length, the edges of the glass capillary tubes were rounded using a Bunsen burner to mechanically protect the Ag/AgCl electrode in the pipette holder. Pipettes were pulled with a two steps vertical puller (Narishige PC-10). In inside-out experiments, to improve noise characteristics and reduce the tip capacity, pipette tips were coated with Sylgard®, a low dielectric and highly hydrophobic polymer. Sylgard® was applied as near as possible to the pipette tip. A hot air stream induced polymerisation of the polymer. Pipettes for whole cell and two electrode voltage clamp (TEVC) experiments, were made from borosilicate capillary glass containing a thin filament to facilitate filling with the pipette solution. To smooth and clean the surface of the pipette tip and improve the patch formation, the tip of each patch pipette was fire-polished by bringing it close to a hot platinum wire of a microforge (Narishige MF-830) before use. Patch pipettes were fabricated on the day of experiment and stored in a closed container. Both the pipette and reference electrodes were made from a silver wire (diameter of 0.01 mm) covered with silver chloride. The wire converts the ionic current into electronic current in the metal, according to $Cl^- + Ag \leftrightarrow AgCl + e^-$ reaction occurring at the liquid/metal interface. A liquid junction

potential between the two electrodes, caused by the unequal mobility of the ions in the pipette and bath solution, (Barry & Lynch, 1991; Neher, 1992), was routinely compensated before starting each experiment.

2.6.3 Whole-cell recording from vascular smooth muscle cells

A drop of cell suspension was placed in a chamber of ~ 100-200 µl and left for ~ 5 min for cells to adhere to the glass surface. During the experiment the chamber was continually superfused (~1 ml/min) with PSS or test solutions via a 5-barrel pipette. Experiments where carried out at room temperature. The holding potential was maintained at -80 mV unless otherwise stated. The pipette access resistance was always less than 15 MΩ. If the in-series-resistance was above 10 MΩ, it was electronically compensated between 70% and 85% with the built-in compensation circuit of the amplifier (Axopatch 200B, Axon instruments, Foster City, CA). At the beginning of each experiment the capacitative transient in response to a 10 mV depolarising step (filtered at 50 kHz and sampled at 200 kHz) was recorded. The cell membrane capacitance was then calculated from the area under the capacitative transient divided by the pulse voltage amplitude. Electrophysiological recordings were taken at least 5 min after establishing the whole-cell configuration. This time was considered to be long enough to allow equilibration of the pipette solution with cell interior (Hille, 2001).

2.6.4 Inside-out recordings from Xenopus oocytes membrane patches

For inside-out recordings from *Xenopus* oocytes, the holding potential was manteined at –120 and –100 mV for Kv2.1 and Kv1.5 channels, respectively. Measurements were taken in a 1 ml chamber under continuous perfusion of solutions at a flow of 0.5-1.5 ml/min via a 9 barrel rapid switch perfusion system (Rapid Solution Changer, Bio-Logic Science Instruments). The bath temperature (measured with a small thermistor of Ø 0.2 mm), was kept between 19±1.5 °C using a Peltier cell.

2.6.5 Two-electrode voltage clamp from Xenopus oocytes

TEVC experiments were performed exclusively to monitor the expression of Kv1.5 and Kv2.1 channel currents in the injected oocytes. Non-injected oocytes were also used as negative control. Oocytes were positioned in a recording chamber of ~120 µl and

continually perfused with the NFR solution (Table 2.3) at a flow rate of 1-1.5 ml/min. Whole-oocyte currents were measured with a standard TEVC (see (Stuhmer, 1992)), using a homemade high-voltage feedback amplifier. Electrode pipettes, made from borosilicate glass, were filled with 3 M KCl. Reference electrodes were made from Ag/AgCl pellets and connected to the perfusion bath via agar bridges. Stimulation and data acquisition were controlled by a Macintosh microcomputer (Cupertino, CA) interfaced to the voltage-clamp amplifier with a 16-bit AD/DA converter (Instrutech, Elmond, NY), using the Pulse-PulseFit software package (Heka Elektronik, Lambrecht, Germany). Currents were filtered at 5-kHz with a 4-pole low-pass Bessel filter (Ithaco, Ithaca, NY) and sampled at 20kHz.

2.6.6 Electrophysiological stimulation protocols

To enable comparison of the voltage-dependent parameters of I_{Kv} under different treatment conditions and in different types of VSMCs, identical voltage protocols were used. The description of these protocols is detailed in this section. To avoid unnecessary repetition, in the results I will only refer to the name of the corresponding protocol used.

2.6.6.1 Current-Voltage relationship protocol (I-V protocol) and measurement of the Kv channel conductance

I_{Kv} was recorded using 300 ms depolarising steps applied between –90 and +100 mV in 10 mV increments from the holding potential of -80 mV. In order to construct the steady-state activation dependence, the peak current amplitude had to be measured. Since the current amplitude tends to decrease with time, particularly at positive potentials, the onset of I_{Kv} measured at each potential was fitted with a single exponential function:

$$I(t) = a\exp\left(\frac{-t}{\tau_a}\right) + B, \qquad [2.1]$$

where *I(t)* is the current as a function of the time *t*, τ_a is the time constant of activation, *a* is a scaling factor and *B* is the asymptotic value. *B* was taken as estimation of the peak current at a given membrane potential. The method is independent of the type of model chosen for activation, gives a good approximation of the current kinetics in RASMCs

and therefore represents a convenient manner to quantitatively describe the activation rate and determine the peak current amplitude.

The current amplitude derived was leak corrected and the peak I-V relationship was constructed for I_{Kv} in each cell. Leak currents were calculated from the slope resistance measured at negative potentials (between –90 and –60 mV), where activation of I_{Kv} channel was negligible. The slope resistance, a, was obtained from the following equation:

$$I_{leak}(V_m) = aV_m + b, \qquad [2.2]$$

where b is the intercept with the V_m axis.

The leak-corrected peak current I'_{Kv} at each V_m was then calculated as:

$$I'_{Kv}(V_m) = I_{Kv}(V_m) - I_{leak}(V_m) \qquad [2.3]$$

The peak I_{Kv} conductance ($g_K(V)$) at each test potential (V_m) was then calculated assuming a linear (Ohmic) relationship between the current amplitude and the membrane potential, using the following equation:

$$g_k(V) = \frac{I'_{Kv}(V)}{V_m - E_K}, \qquad [2.4]$$

where E_K is the K^+ equilibrium potential given by the Nernst equation:

$$E_K = \frac{RT}{zF}\ln\left(\frac{[K^+]_o}{[K^+]_{in}}\right), \qquad [2.5]$$

where R is the gas constant (1.987 cal mol^{-1} K^{-1}), T is room temperature expressed in Kelvin (295°), z is the valence of the ion and F is the Faraday constant (9.6485 x 10^4 C mol^{-1}). $[K^+]_0$ = 5 mM and $[K^+]_{in}$ = 135 mM are the external and pipette concentrations of K^+, respectively, giving E_K = - 83.25 mV.

The normalised peak conductance-potential relationship was fitted with the Boltzmann equation:

$$g_K(V) = G_{max} \Big/ \left\{1 + \exp\left[\left(V_a - V_m\right) \Big/ k_a\right]\right\}, \qquad [2.6]$$

where $g_K(V)$ is the peak conductance at a given potential (V_m), G_{max} is the maximum whole-cell conductance at the most hyperpolarised test-pulse potential, V_a is the half activation potential (the potential at which 50% of the channels are activated) and k_a is the slope factor determining how steeply the activation curve changes with voltage. The

Boltzmann relation describes the voltage-dependence of channel gating and the slope factor k_a is related to the equivalent number of charges on the channel protein that move in the membrane voltage field to give rise to channel opening.

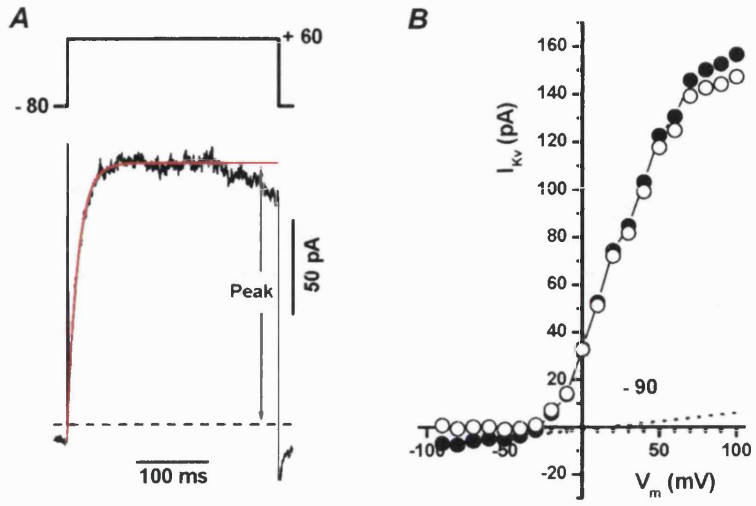

Figure 2.1. *A* shows the peak determination of I_{Kv} recorded from a representative RASMC (C_m = 10.7 pF) in response to 300 ms depolarisation to +60 mV. The upper panel illustrates the stimulation protocol. The dashed line in *A* is the zero current. The red line is a single exponential fit (eq. [2.1]) of the current trace with time constants and an asymptotic (peak) value equal to 14.5 ms and 139.5 pA, respectively. ***B*** shows an example of the I-V relationships for the peak I_{Kv} (filled circles), measured at various potentials and for I_{Kv} corrected for a linear leak (open circles). Dotted line represents a linear leak current with a slope a = 14.2 GΩ and b = 0.07 mV derived from the fit of the current between –90 and –60 mV according to the equation [2.2].

2.6.6.2 Measurements of the steady-state activation of heterologously expressed Kv channels (I-V tail protocol)

Steady-state activation dependences for Kv1.5 and Kv2.1 channels expressed in *Xenopus* oocytes were constructed from "tail" current amplitude measured using the following voltage protocol. The patch was held at a holding potential of –100 mV for the Kv1.5 and –120 mV for the Kv2.1 channel. Kv currents were elicited every 2 (Kv1.5) and 5 s (Kv2.1) by a 50 ms (Kv1.5) or 100 ms (Kv2.1) step depolarisation. Voltage steps were applied between -100 to +50 mV (Kv2.1) or between -90 to +10 mV (Kv1.5) in 5 (Kv1.5) or 10 mV (Kv2.1) increments. The membrane potential was then set to –40 mV for 20 ms to measure the tail currents following the activation of the Kv channels during the first depolarising step (Fig. 2.2*A*). The amplitude of the tail current,

measured at –40 mV immediately after the first depolarisation, is proportional to the number of channels open at the end of the first step and then declines exponentially as channels close or deactivate. The current amplitude at the beginning of the tail pulse to –40 mV can be considered equal to:

$$I_{tail} = N\gamma P_{o(p)}(-40 - E_K), \qquad [2.7]$$

where N is the number of potassium channels, γ is the single channel conductance, $P_{o(p)}$ is the channel open probability at the end of the test pulse (p) and E_K is the K^+ equilibrium potential.

Plotting the normalised tail current amplitude (I_{NORM}) against the voltage of the first step, will therefore give a measure of the channels open probability as a function of the voltage (Fg 2.2*B*). This relationship can be fitted with the Boltzmann function of the form:

$$I_{NORM} = 1 \Big/ \left\{ 1 + \exp\left[\left(V_a - V_m \right) \Big/ k_a \right] \right\}, \qquad [2.8]$$

where V_a, k_a, and V_m, have the same meaning described previously.

In the experiments on *Xenopus* oocytes, subtraction of linear current responses was carried out using a standard P/4 protocol (Heinemann, 1995). Briefly, in the voltage range where voltage dependent channels are not active (i.e. potential = V holding), a series of scaled down pulse protocols were applied 4 times and the resulting currents averaged, scaled and subtracted from the current elicited by the main test pulse.

In the experiments on *Xenopus* oocytes I preferred to determine the steady state activation using the I-V tail protocol because the results are independent of possible differences in the driving force at different voltages. One uncertainty associated with this procedure is that the degree of a slow (C-type) inactivation during the prepulse is neglected. However, in both channels tested, C-type inactivation during the prepulse duration used was either absent or of irrelevant amplitude. It is noteworthy that native Kv currents, especially in the rat aortic myocytes, in contrast to heterlogously expressed currents in the *Xenopus* oocyets, have relatively small tail current amplitude. Proper analysis of tail currents in these types of cells would require averaging more than 3 identical recordings at each potential. This would significantly prolong the duration of each individual experiment and therefore has not been performed routinely in native

cells. Pulmonary arterial SMCs, which have a substantially larger current, showed a strong accumulation of K^+ even in single cell, which alter E_K (Smirnov & Aaronson, 1994). For this reason, the tail current protocol also cannot be properly applied.

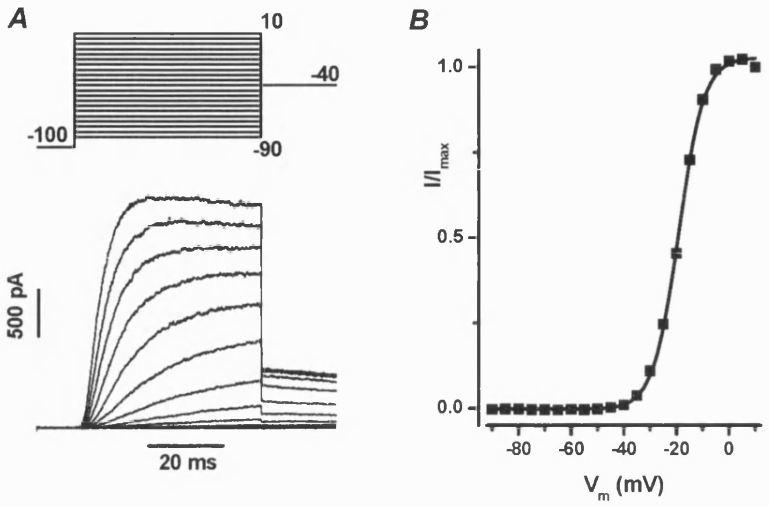

Figure 2.2. ***A***, lower panel demonstrates a representative family of Kv1.5 currents recorded in the inside-outside configuration from a *Xenopus* oocyte membrane patch in response to the protocol shown above. ***B*** illustrates the steady state activation dependence obtained from the normalised tail current reported in ***A***. The continuous line is the fit to the Boltzmann equation [2.8] with V_a = 19.2 mV and k_a = 4.7 mV.

2.6.6.3 The instantaneous I-V protocol

The instantaneous I-V relationship following a pulse that maximally opens Kv channels, can be measured via the following protocol (named the Instantaneous I-V). Figure 2.3 illustrates a schematic representation of the protocol. To maximally activate Kv channels the voltage was set to +20 mV for 20 (Kv1.5) or 100 ms (Kv2.1) (prepulse) and then to various potentials from –100 to +70 mV (Kv1.5) and from –90 to +100 mV (Kv2.1) in 10 mV increments for 10 ms (test pulse). Membrane patches were stimulated every 5 s. A longer duration of the prepulse was required for Kv2.1 since its activation rate is slower than that of the Kv1.5 current. The current amplitude obtained from extrapolation of a single exponential fit of the current elicited by the test pulse was plotted versus the test pulse potential, giving instantaneous I-V. This procedure also allows the precise estimation of reversal potential for the ion that is carrying the current.

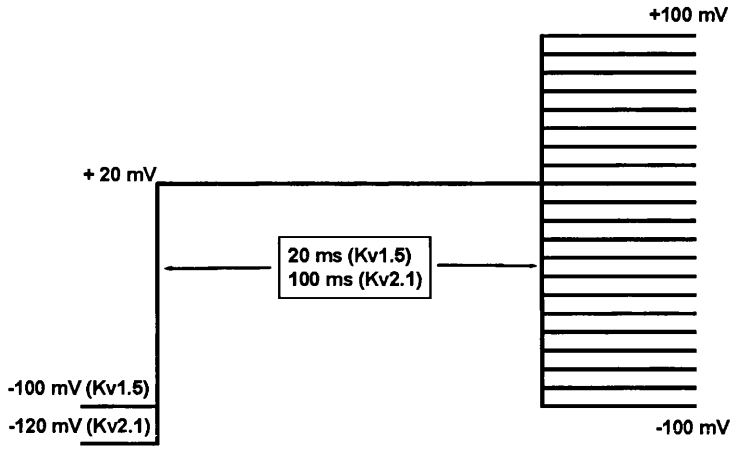

Figure 2.3. The Instantaneous I-V stimulation protocol.

2.6.6.4 The availability protocol

I_{Kv} availability was measured from the peak current amplitude recorded in response to a test pulse to +60 mV following 10 s conditioning pre-pulses (V_c) to various voltages (Fig. 2.4). This protocol allows the determination of the fraction of Kv channels available at each membrane potential after development of the inactivation process. The duration of the conditioning pre-pulse (10 s) was considered to be long enough for inactivation to fully develop. The current amplitude measured at the test potential, proportional to the degree of inactivation that occurred during the prepulse, was plotted against V_c. This relationship was fitted with the modified Boltzmann function:

$$\left(I_{peak} - I_{ss}\right)/\left(\hat{I}_{peak} - I_{ss}\right) = 1/\left(1 + \exp\left(V_c - V_h\right)/k_h\right), \qquad [2.9]$$

where I_{peak} and $\hat{I}_{peak}$ represent the current amplitude measured at the test pulse at different V_c and at the most hyperpolarized V_c, respectively. I_{ss} is the steady state current not inactivated at the most depolarised V_c, V_h is the half-inactivation potential and k_h is the slope factor.

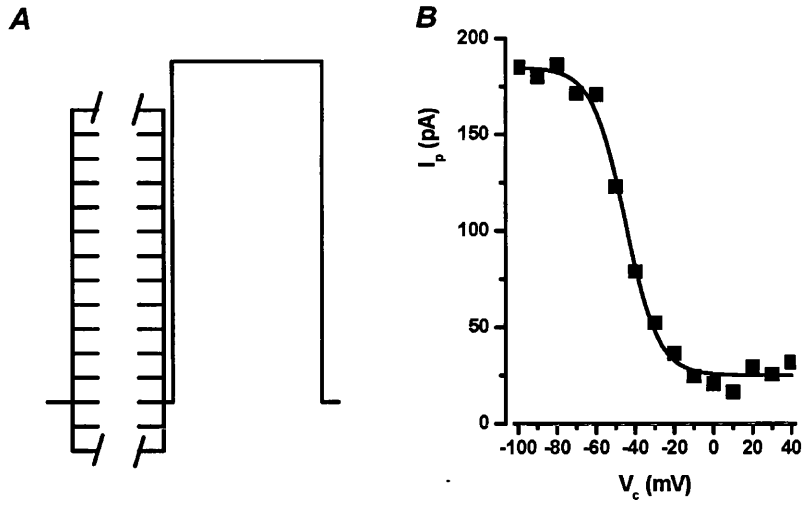

Figure 2.4. The Availability protocol *A*, schematic representation of the voltage protocol. *B* shows an example of the dependence of the I_{Kv} peak amplitude on V_c in a RASMC. A continuous line was drawn according to equation [2.9] with the following parameters: V_h = -45.1 mV, k_h = 8.4 mV I_{peak}=184.8 pA, and the non-inactivating component, I_{ss}, equal to 25.1 pA.

2.6.6.4 Noise analysis

Non-stationary noise analysis (Sigworth, 1980; Heinemann & Conti, 1992) is based upon the fact that a steady state signal, made up from a population of randomly occurring identical unitary events such as single channel currents, exhibits fluctuation or noise around its mean level. Analysis of these fluctuations allows the properties, such as open probability and single channel conductance, of the underlying events to be investigated. To enable this analysis, 50-100 identical depolarising pulses to +20 mV of 50 ms of duration were applied every 3 sec to inside-out patches. The current mean ($\bar{I}$) and variance (σ^2) can then be calculated at identical time points by summing many consecutive responses according to:

$$\bar{I}(t) = \frac{1}{n}\sum_{k=1}^{n} yk(t), \qquad [2.10]$$

$$\sigma^2(t) = \frac{1}{n-1}\sum_{k=1}^{n}\left(yk(t) - \bar{I}(t)\right)^2, \qquad [2.11]$$

where $\bar{I}(t)$ is the mean current at the time t for n records. $\sigma^2(t)$ is the variance at the time t and $yk(t)$ is the signal amplitude of the k^{th} record at time t after the start of the

step. Variance at each time point is then plotted versus the mean current for the same time point. The mean current can be written as:

$$\bar{I} = NP_o i, \qquad [2.12]$$

where N is the number of channels, P_o is the open probability and i is the single channel current. The current variance can be written as:

$$\sigma^2(I) = Ni^2 P_o(1 - P_o), \qquad [2.13]$$

where (1-P_o) is the probability of a channel being closed. Combining equation [2.12] and [2.13]:

$$\sigma^2(I) = i\bar{I} - \left(\frac{\bar{I}^2}{N}\right). \qquad [2.14]$$

Fitting the plot of mean/variance at each time point with this equation gives an estimation of the parameter i and N. The open probability can also be obtained noting that:

$$P_o = \frac{\bar{I}}{Ni}. \qquad [2.15]$$

2.7 Kv channels expression in *Xenopus* oocytes

2.7.1 Molecular biological protocols for cDNA amplification

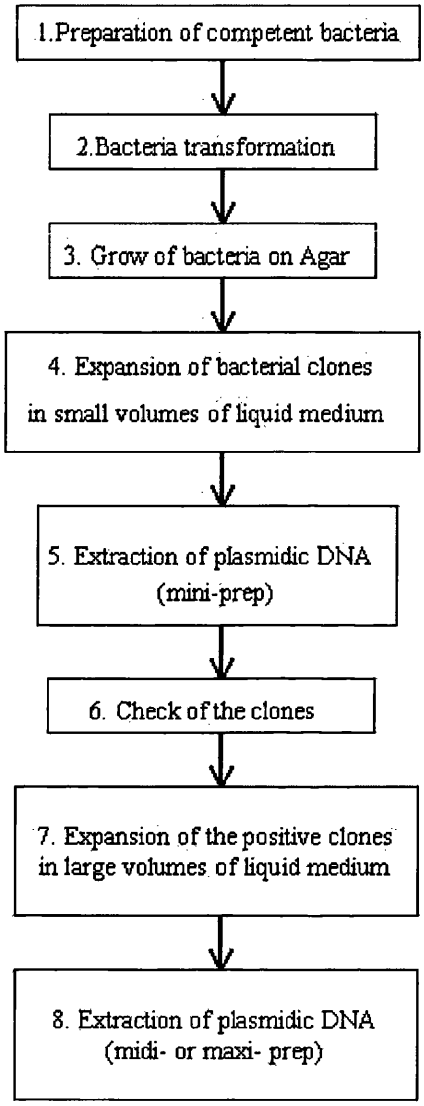

Figure 2.5. Flowchart of the procedures required to amplify plasmidic DNA.

The consecutive steps used for bacteria manipulation and DNA extraction are shown in Fig. 2.5. These are standard protocols and have been applied as described in "Molecular Cloning: a laboratory manual" (Sambrook *et al.*, 1989). Therefore, only the general principles and specific experimental conditions related to my project will be briefly mentioned for each step. All the experimental procedures were carried out according to the European rules (90/219/CEE).

1) *Preparation of competent bacteria.* The bacteria used was XL1 blue type, derived from *Eschierichia coli* and non-infectious and extremely sensitive to UV ray to reduce the risk for the operator. The "$CaCl_2$ method" was used to increase the efficiency of the transformation by making the bacteria "competent". This procedure allowed bacteria to be obtained with an efficiency of transformation $\geq 5 \times 10^8$ bacterial colonies for 1 μg of plasmidic DNA.

2) *Bacteria transformation.* The plasmids used were the p-Gem-A (Promega, Madison WI, USA) and the pBlueScript SK+ (Stratagene, La Jolla CA, USA) for the Kv2.1 Kv1.5 cDNA, respectively. Both vectors contained the bacterial gene "Amp" which gives the resistance to ampicilline to the transformed bacteria. The Kv2.1 cDNA was inserted after the T7 type RNA polymerase recognition site while the Kv1.5 was inserted after the SP6 site. Introduction of a plasmid into bacteria ("transformation") was achieved by rapidly changing the temperature in a suspension of bacteria (a 30 μl volume) in the presence of plasmidic DNA (100 ng). Bacteria effectively transformed acquire the resistance to ampicilline.

3) *Grow of bacteria on Agar.* Transformed bacteria were placed on an agar plate containing ampicilline (50 μg/ml) and left to grow overnight at 37 °C.

4) *Expansion of bacterial clones in small volumes of liquid medium.* Only one colony per plate (one for the Kv1.5 transformed-bacteria plate and another for the Kv2.1 plate) was collected and expanded in 50 ml of liquid medium (in the presence of 50 μg/ml ampicilline). The medium was incubated overnight at 37 °C under continuous shaking.

5) *Extraction of plasmidic DNA (mini-prep).* Small scale-plasmidic DNA extraction ("mini"-prep) were carried out using the commercial kit "Qiagen Plasmid Mini Kit"

(Qiagen, Italy). The procedure yields 10 to 15 μg of DNA extracted from 1.5 ml of bacteria suspension. The kit is based on an initial lysis of bacterial cells with an alkaline solution containing detergents. The plasmidic DNA is then purified using an ionic exchange resin column, eluted using a high ionic force solution and finally precipitated using isopropanol.

6) *Check of the clones*. After purification the DNA was analysed with agarose gel electrophoresis, restriction map analysis and spectroscopy.

Agarose gel electrophoresis allows the separation of molecules of DNA within an electric field on the basis of their diverse mobility in the gel. Double stranded DNA migrates in the agarose gel matrix with a speed that is inversely proportional to: i) the logarithm of its pair base number, ii) the concentration of the agarose, iii) the conformation of the DNA molecule (linear, coil or supercoil), iv) the intensity of the electric field applied, and v) ionic force of the buffer. 0.5 % agarose gel was made in 0.5 x Tris-borate buffer (TBE) containing 0.045 M Tris-borate and 0.001 M EDTA, which was also used as electrophoretic buffer. The gel was placed on a horizontal electrophoresis chamber. 1 μg of DNA was loaded at a final volume of 5 μl, including 1 μl of gel loading buffer type II. The migration occurred at 5 V/cm (measured as the distance between the electrodes) for 10-15 min. To visualise the DNA in the gel, ethidium bromide (0.5 μg/ml) was added to the agarose gel. Ethidium bromide intercalates between DNA bases and fluoresces under UV light.

A restriction map is obtained by treating an aliquote of the previously purified DNA with restriction enzymes that cut the DNA plasmid only in one or few points yielding one or few segments of known dimensions. It is possible to verify the presence of the expected DNA fragments upon their separation with agarose gel electrophoresis. Plasmidic DNA containig Kv1.5 and Kv2.1 cDNA were linearised with the enzyme Not1 (Promega, Madison WI, USA) and their expected size was compared against the DNA marker (range from 100 bp to 10,000 bp. *Gene ruler* DNA Ladder Mix, Fermentas) (Fig. 2.6).

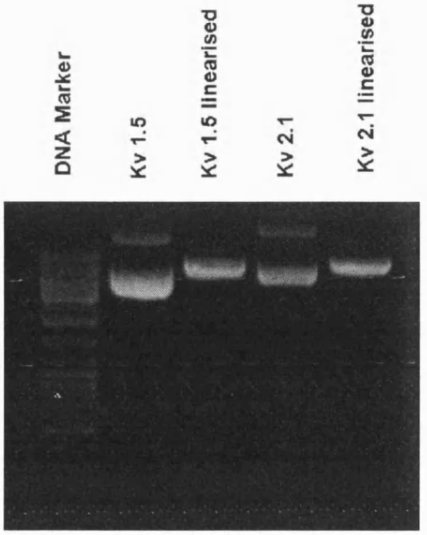

Figure 2.6 Gel electrophoresis. DNA bands in an 0.5 % agarose gel observed under UV light after electrophoresis.

Spectrocopic analysis of the DNA allows the determination of both the purity and the concentration of a DNA sample. DNA samples were examined under two wave lengths: 260 nm and 280 nm. At 260 nm an optical density (OD) of 1 correspond to 50 μg/ml of double strand DNA. The ratio OD_{260}/OD_{280} allows estimation of the purity of the DNA sample. For both Kv1.5 and Kv2.1 cDNA values of ~ 1.8 were obtained indicating a good level of purity. If proteins or phenol were present in the DNA samples this value was lower and the estimation of the DNA concentration via spectroscopic analysis not valid.

7) and 8) *Expansion of positive clones in large volumes of liquid medium* and *extraction of plasmidic DNA (midi- or maxi- prep).* The colonies that contained the desired plasmid were grown in a 50 ml liquid medium (in presence of 50 μg/ml ampicilline) and the plasmidic DNA was extracted with the Quiagen Plasmid Midi Kit according to the manufacturers instructions. This kit is based on the same principles as the mini-prep kit described above. With this procedure about 80 μg of plasmidic DNA was obtained from an initial volume of 50 ml of bacterial suspension.

2.7.2 Transcription in vitro

Transcription of cDNA into RNA was carried out using the commercial kit "mMessage mMachine" (Ambion) according to the manufacturers instructions. Briefly, plasmidic DNA was firstly cut with the NotI restriction enzyme (Promega, Madison WI, USA) at a single point located before the promotor (SP6 or T7) sequence situated in front of the cDNA ATG starting point codon. Then cDNA (1 μg) was mixed with a 20 μl (final volume) solution containing the 4 nucleotides (ATP, CTP, UTP, GTP) (10 μl of 2x *ribonucleotide mix*) and the RNA-polymerase (2μl of 10x *enzyme mix*). Also a polymetil-guanosine was added to the reaction in order to be incorporated by the RNA-polymerase at the 5' end of the RNA. This sequence (called "cap") serves as a recognition sequence for the eucaryotic ribosome.

The presence and integrity of the RNA thus obtained was controlled by gel electrophoresis performed similarly to the DNA gel electrophoresis described above. However, to avoid contamination with RNAase enzymes that could degrade the RNA, the TBE buffer was prepared in RNAase free water and the electrophoretic course was carried out at higher voltage (8-10 mV/cm) to reduce the time of permanence of the loaded RNA sample (1 μl) in the 1% agarose gel. See an example in Figure 2.7.

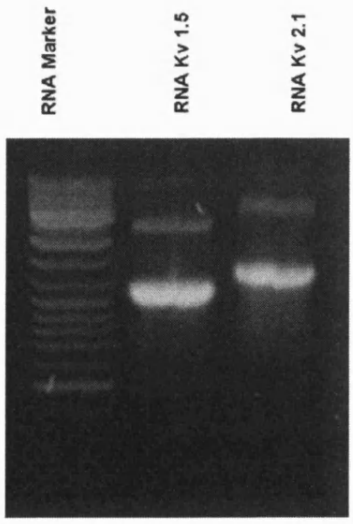

Figure 2.7. RNA gel electrophoresis.

2.7.3 cRNA injection into oocytes and preparation for electrophysiological recordings

Injection pipettes were pulled using a standard pipette puller. The tip of the pipette was broken under a microscope until it had a diameter of about 10 μm and was fire-polished to avoid damaging oocytes. The injection pipette was filled with mineral oil allowing hydraulic connection with a micro-injector (Nanoinject, Drummond) and then filled with 1 μl of RNA solution (which contained ~0.25 μg/μl of Kv1.5 or Kv2.1 cRNA), by suction through the pipette tip. Oocytes were placed in a specialised chamber filled with Barth solution and microinjected (~50 nl each) under a stereoscopic microscope using the microinjector mounted on a micromanipulator. After injection, the oocytes were washed twice in Barth solution containing (100 U/ml) penicillin/streptomycin (Sigma) and incubated at 18°C in multiwell plates (Falcon) for up to 7 days. Oocytes, expressing sufficient quantity of Kv channels (as verified with the TEVC technique) were available for electrophysiological experiments 2 days after injection. To gain access to the plasma membrane with the patch clamp pipette, each oocyte had to be privated of the vitelline membrane. This was achieved by leaving oocytes in the hypertonic "skinning" solution for few minutes. Hypertonicity caused oocytes to contract, resulting in a separation between vitelline and plasma membrane. Vitelline membrane was removed with fine forceps and oocytes could then be used for electrophysiological recordings.

2.8 Immunoblot analysis and immunocytochemistry in vascular smooth muscle cells

2.8.1 Isolation of total proteins, membrane and cytosolic fractions

Prior to protein isolation the lumen of the rat aorta, previously cleaned of the connective tissue, was scraped with a horse hair in order to minimise contamination of the preparation with endothelial cells. Cell lysates were prepared in lysis buffer containing a protease inhibitor cocktail ('Complete', Boehringer Mannheim). The lysis buffer had the following composition (mM): 50 Tris-Cl (pH 7.5), 250 NaCl, 5 EDTA, 5 DTT, 10 NaF, and 0.1% v/v Igepal. Tissue was homogenized using a manual homogenizer and then agitated slowly for 1 hour at 4°C. Cell debris were removed by centrifugation (2,500×*g*, 30 min, 4°C) and supernatant was either used immediately or stored at -70°C.

To separate the particulate (membrane) and cytosolic fractions, a further ultracentrifugation (100,000 g for 1h at 4°C) of the supernatant was performed in the presence of 3 M sucrose. The resulting supernatant was considered as the cytosolic fraction. The pellet (membrane fraction) was resuspended in phosphate buffered saline (PBS) plus 1% Tween and continuous vortexing for 1h at 4°C was carried out.

2.8.2 Western blot

Western blot (Towbin *et al.*, 1979; Burnette, 1981) was carried out according to the protocols described in "Molecular Cloning: a laboratory manual" (Sambrook *et al.*, 1989).

The rate at which a protein migrates in a solution to which an electric field has been applied, is determined by its net charge, size and shape. SDS-PAGE (sodium dodecyl sulfate-polyacrylamide gel electrophoresis) uses a highly cross-linked gel of polyacrylamide as an inert matrix through which the proteins migrate. Proteins are dissolved in a solution containing SDS which binds to the hydrophobic regions of the protein molecules rendering them freely soluble in the detergent solution. 2-mercaptoethanol, a reducing agent, is also added to break any disulphide bridges in the protein molecules so that all of the constituent polypeptides in multi-subunit molecules can be analyzed separately. In the polyacrylamide gel, the negatively charged protein-detergent complexes migrate towards the positively charged electrode with movement of large proteins retarded more than the small polypeptides. SDS-PAGE can be used to separate out all types of proteins, including those which are insoluble in water.

Samples (20-50 μg of protein) were mixed with gel loading buffer and separated using 8% or 15% polyacrylamide gels. The total protein concentration was measured by the Bradford method, and equal amounts of protein were loaded on each gel. Proteins were blotted onto PVDF membranes, and then washed in PBS and PBS containing 0.05% Tween-20 (PBS-T). After blocking in a 5% w/v solution of dried skimmed milk in PBS-T for 1 hour at room temperature, membranes were probed overnight (4°C) with primary antibodies (dilution 1:500 - 1:1000) in 1% milk in PBS-T. Proteins were labelled with a secondary horseradish peroxidase-conjugated goat anti-rabbit antibody

(1:2000) for 1 hour at room temperature. Bound antibodies were detected by the enhaced chemioluminescence (ECL) method (Amersham).

2.8.3 Immunocytochemistry

Affinity–purified commercially available rabbit polyclonal antibodies against PKC α, δ, ε, ζ (Santa Cruz Biotechnology, USA) and against Kv2.1, Kv1.5 and Kv1.2 channel protein (Alomone, USA) were used. A drop of cell suspension was placed on a glass cover slip and left for 20 min at room temperature to allow cells to attach to the glass surface. Cells were then fixed and permeabilized with 4% paraformaldehyde and 0.1% Triton X-100 for 30 min at room temperature. Non-specific staining was blocked with PBS containing 4% normal goat serum (in which secondary antibody against rabbit IgG was made) for 1 h at room temperature. Cell were then washed five times with PBS and exposed to anti–PKC isoforms or anti Kv antibodies (diluted 1:1000) in PBS containing 1% BSA and 0.03% Triton X-100 for 3 hours at room temperature. After incubation and wash (5xPBS), the binding of the primary antibody was detected using a goat anti–rabbit IgG antibodies labelled with Alexa Fluor 488 (Molecular Probes, USA) (1:500). Cells were washed again in PBS and sealed between two coverglasses. Samples were then analysed under a confocal microscope (Fluoview 500, version 3.2, Olympus, UK). Preliminary experiments with both primary and secondary antibodies were carried out to find an optimal dilution of antibodies in order to maximise the signal to noise ratio. Control experiments without primary antibodies were run in parallel to discard a possible non-specific binding of the secondary antibody.

2.9 Data analysis and statistics

Data were analysed and presented using the ClampFit program (Axon Instruments, Foster City, CA), with Origin (Microcal Software, Northampton, MA) and Excel (Microsoft, USA). Noise analysis was performed with the aid of software kindly provided by Dr Michael Pusch (CNR, Genoa, Italy), measurement of the tail currents, estimation of the half time of activation and computation of the Grahame equation (eq. [6.4]) were performed with self-written programs in the Igor (Wavemetrics, Lake Oswego, OR) environment. Contraction data were analysed with Chart v3.6/s software (ADI Instruments, UK). Data are presented as *mean±s.e.m.* (standard error of the mean), unless stated otherwise. Statistical significance was evaluated using a paired or unpaired (as indicated in the text) two-tailed Student *t* test. A probability value of $P<0.05$ was taken as the criteria for a significant difference.

Chapter 3

Electrophysiological and pharmacological characterisation and molecular identity of Kv channel current in single rat aortic myocytes.

Pharmacological, time- and voltage- dependent characteristics of potassium currents in rat aortic myocytes were analysed by evaluating the macroscopic currents evoked by depolarising voltage pulses in the whole-cell configuration of the patch-clamp technique.

In this chapter, the effect of TEA, paxilline and IbTx on the whole cell K^+ currents was examined under conditions in which the free Ca^{2+} concentration in the pipette solution was clamped at 200 nM, using Ca^{2+}-EGTA buffer, in order to mimic elevated intracellular Ca^{2+} levels occurring during agonist- or pressure- induced contractions (Jaggar *et al.*, 1998).

3.1 Pharmacological separation of Kv and BK_{Ca} currents

3.1.1 Effect of K^+ channel inhibitors on whole-cell currents in elevated $[Ca^{2+}]_i$

To compare the potency of BK_{Ca} channel inhibitors on the whole-cell outward currents, a 2 s ramp protocol from -100 to +100 mV was applied every 10 s. Figure 3.1 illustrates I-V relationships derived from this protocol and from the I-V protocol using 300 ms voltage steps (see Materials and Methods). The Figure shows that both the ramp and the I-V protocol produced similar results. However, a slight but significant reduction of the current amplitude between 0 and +100 mV was observed in response to the ramp protocol, possibly due to activation of the current not fully developed and a certain degree of accumulation of inactivation.

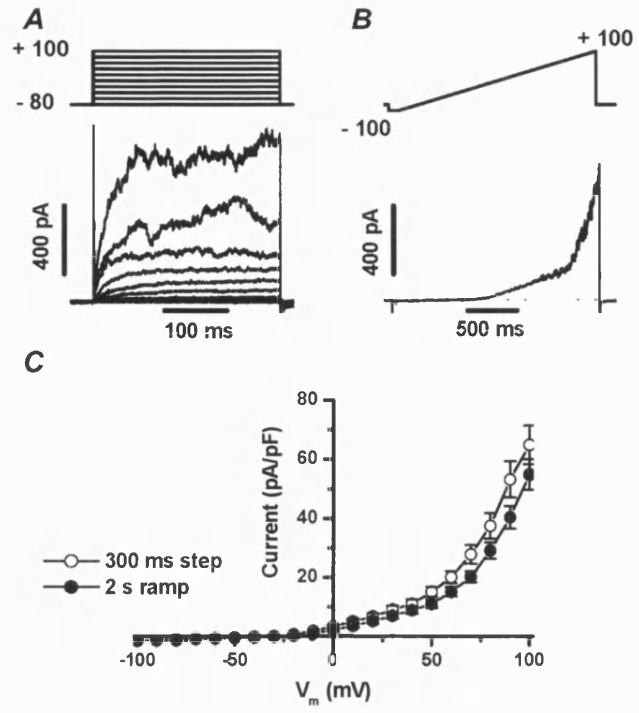

Figure 3.1 Comparison of the I-V and ramp protocols. ***A*** and ***B*** show a family of I_{Kv} and a ramp current recorded from the same RASMC in reponse to the stimulation protocols shown in the upper panels. C_m = 13.8 pA. ***C*** shows the averaged I-V relationships for whole-cell currents recorded from 8 RASMCs and expressed as current density. Holding potential was –80 mV.

Inhibitors were applied cumulatively for 150-200 s. 3-4 current traces recorded with the ramp protocol in the presence of each concentration of the drug were averaged and normalised (I_{NORM}) to that in the absence of the drug (mean of 5-10 traces). The mean IC_{50} for each inhibitor was then calculated according to the following equation:

$$I_{NORM} = \frac{1-A}{1+([Drug]/IC_{50})} + A, \qquad [3.1]$$

where A is the fraction of the residual outward current which remained in the presence of the highest concentration of the drug.

Paxilline, a selective inhibitor of BK_{Ca} channels, at concentrations between 1 and 200 nM progressively suppressed the whole-cell current (Fig. 3.2). It is noteworthy that in the concentration range between 500 nM and 1 μM, the effect of paxilline saturated and no further block was developed (Fig. 3.2*A*). Fitting of the individual data with equation

[3.1] gave the mean IC_{50} value of 97±19 nM (n=7, Fig. 3.2*D*, circles). IbTx, another potent and selective inhibitor of BK_{Ca} channel currents, inhibited the whole-cell current in a similar manner (Fig. 3.2*B*). However, the overall potency of IbTx was ~8 times greater than that of paxilline (mean IC_{50} = 12±5 nM, n=5, P<0.006, Fig. 3.2 *D*, squares). The inhibitory effect of TEA on whole-cell currents was much less potent than paxilline or IbTx with a mean IC_{50} = 273±37 μM (n=6, Fig. 3.2, *C* and *D*, triangles).

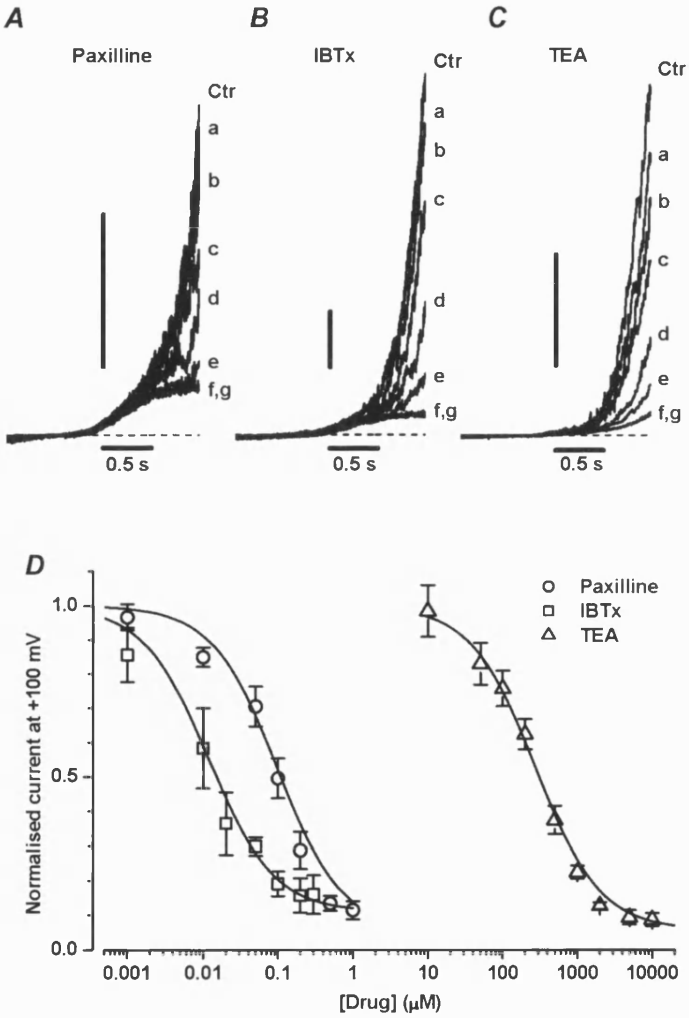

Figure 3.2. Effect of K^+ channel inhibitors on whole-cell K^+ currents in single rat aortic SMCs. ***A***, ***B*** and ***C*** show representative current traces recorded in the presence of various concentrations of paxilline, IbTx and TEA added cumulatively. Traces marked with **a**, **b**, **c**, **d**, **e**, **f** and **g** indicate currents recorded in the presence of 1, 10, 50, 100, 200, 500 and 1000 nM for paxilline (***A***), 1, 10, 20, 50, 100, 200 and 300 nM for IbTx (***B***), and 0.01, 0.2, 0.5, 1, 2 ,5 and 10 mM for TEA (***C***), respectively. Ctr indicates the control current recorded in the absence of the inhibitor. C_m was equal 10.6 (***A***), 14.2 (***B***) and 7.2 (***C***) pF. Vertical bars are 300 pA. ***D*** compares the concentration dependence of the inhibition of K^+ current measured at +100 mV by paxilline (circles, n=7), IbTx (squares, n=5) and TEA (triangles, n=6). Solid lines were drawn according to the equation [3.1] with the mean IC_{50} of 96.5 and 11.7 nM and 273.4 μM and a

residual component A = 0.06, 0.12 and 0.06 for paxilline, IbTx and TEA respectively. Pipette solution contained 200 nM Ca^{2+}.

Figure 3.3*A* compares the mean *I-V* relationship of whole cell currents derived from ramp protocols recorded in the absence (open circles) and presence of 1 μM paxilline (filled circles) from the same cell. The mean slope resistance measured in the linear range (between –60 and –100 mV) of the *I-V* relationship was 7.9±1.1 GΩ (n=15), similar to values I have found in single RASMCs in high buffered $[Ca^{2+}]_i$. As can be seen from the Figure, paxilline blocked the whole-cell current at positive potentials to a significantly greater degree than at negative voltages. For example, the overall inhibition of the current by 1 μM paxilline progressively increased from 35±5% at 0 mV to 64±3% and 95±1% at +50 and +100 mV, respectively (n=15, P<0.0001). To analyse the relative contribution of the paxilline-sensitive and paxilline-insensitive components to the whole cell current over a range of membrane voltages, the I-Vs were leak-corrected and normalised to the current amplitude at +100 mV (Fig. 3.3, *B* and *C*). This comparison clearly shows that the paxilline-insensitive component, representing I_{Kv}, activated at potentials positive to –40 mV, while the paxilline-sensitive current, representing the BK_{Ca} channel component, did not appear until the membrane depolarisation reached potentials above –20 mV (Fig. 3.3*C*). These results strongly suggest that, despite the increased $[Ca^{2+}]_i$, the Kv channel current is the major K^+ current activated close to the resting membrane potential in rat aortic SMCs.

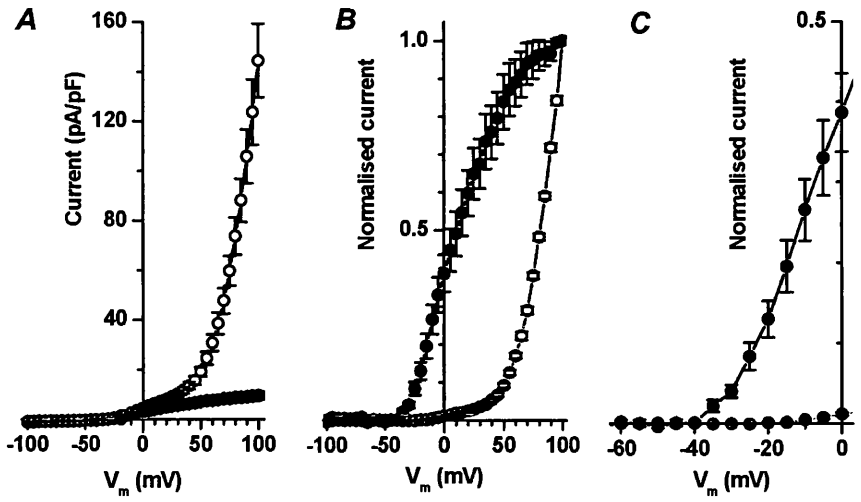

Figure 3.3. Comparison of the activation of the BK_{Ca} (paxilline-sensitive) and Kv (paxilline-resistant) currents in rat aortic myocytes. *A*, *I-V* relationships for the whole-cell current recorded with the ramp protocol in the absence (open circles) and in the presence (filled circles) of 1 μM paxilline in the same cell and expressed as current density (n=15). *B* and *C*, comparison of *I-V* relationship for paxilline-sensitive (open squares, BK_{Ca}) and paxilline-resistant (filled circles, Kv) currents at the full (*B*) and expanded voltage scale (*C*). Paxilline-sensitive current was derived as a difference between the control current and that in the presence of the drug. Currents were corrected for a residual leak calculated from the slope resistance measured in the linear I-V range (between -100 and -60 mV) and then normalised to that at +100 mV for each component.

3.1.2 Inactivation of Kv and BK_{Ca} currents in elevated $[Ca^{2+}]_i$

In spite of a common activation by the membrane potential, BK_{Ca} currents do not inactivate during prolonged depolarisation, while Kv currents tend to decrease if depolarisation is maintained. To evaluate the relative contribution of BK_{Ca} and Kv channels to the whole cell K^+ current in the presence of 200 nM $[Ca^{2+}]_i$, the availability protocol (see Materials and Methods, section 2.6.6.4) was applied (Fig. 3.4). The availability of BK_{Ca} current was measured at +100 mV in PSS, while the Kv availability was assessed at +60 mV in the presence of 1 μM paxilline. As predicted, the Kv current inactivated with V_h = -58.1±2.0 mV, k_h = 9.0±0.4 mV and I_{ss} = 0.080±0.009 (n=15), while the BK_{Ca} current showed practically no inactivation and the small reduction of the BK_{Ca} current seen at positive potentials is likely to be due to inactivation of the Kv component.

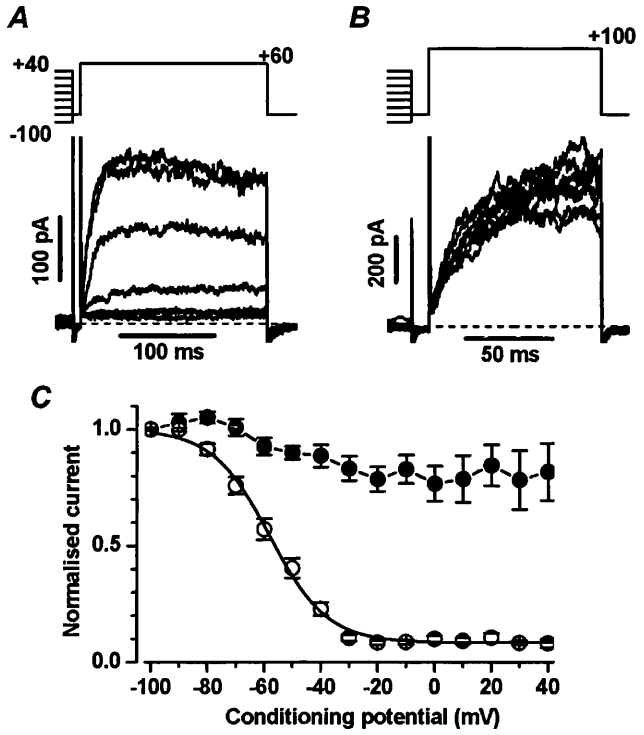

Figure 3.4 Inactivation of I_{Kv} in RASMCs. Inactivation dependency recorded with the availability protocol. The test pulse was at +60 mV or +100 mV for 200 or 100 ms in *A* (1 μM paxilline) and *B* (absence of paxilline), respectively. C_m = 8.4 (*A*) and 10 pF (*B*). In *C*, currents were normalized to the current amplitude elicited by the most hyperpolarized pre-conditioning potential (-100 mV) and plotted versus the potential of the conditioning pre-pulse. Filled and open circles represent BK_{Ca} and Kv currents recorded in the absence and in the presence of 1 μM paxilline, respectively. Pipette solution contained 200 nM Ca^{2+} free. Continuous line through open circle represent the best fit with the Boltzmann function (eq. [2.9]) with V_h = –59.1 mV, k_h = 10.1 mV and I_{ss} = 0.09 (n=15).

3.2 Electrophysiological characterisation of I_{Kv}

The experiments with elevated $[Ca^{2+}]_i$ showed the existence of Kv and BK_{Ca} component in RASMCs. However, as illustrated in Fig. 3.3, the Kv current component is the major contributor to the whole cell K^+ current at membrane potentials close to the resting membrane potential and could therefore have a more relevant physiological meaning. In order to minimise the K^+ current flow through BK_{Ca} channels and study in detail the I_{Kv} properties, the intracellular free $[Ca^{2+}]$ was clamped at ~ 8nM. Moreover, 1 μM paxilline was added to the external solution. In addition, to prevent activation of K_{ATP} channels, 5 mM $MgCl_2$ was replaced with 5 mM MgATP in the intracellular solution and 10 μM glibenclamide was added to the extracellular solution.

3.2.1 The relationship between cell capacitance and I_{Kv} in rat aortic smooth muscle cells

Cell membrane capacitance (C_m), used to estimate the cell membrane area, was calculated as described in Materials and Methods (Section 2.6.3). Since the capacitative current measured in response to a 10 mV depolarizing step is a passive characteristic of the cell membrane, values of C_m recorded from cells perfused with various pipette solutions were combined. The resulting distribution of C_m measured in the 341 cells studied followed a normal distribution with a mean value of 13.05±0.28 pF (n=341) (Fig. 3.5*A*).

Figure 3.5*B* shows the relationship between the peak I_{Kv} measured at +60 mV and C_m recorded in 35 cells in the presence of 5 mM MgATP in the intracellular solution. A good correlation between C_m and I_{Kv} (regression coefficient, R, equal 0.92) suggests that the I_{Kv} amplitude is proportional to the surface area, validating the use of the current density to compare changes in I_{Kv} in RASMCs under different experimental conditions. To the best of my knowledge such a relationship has not been demonstrated for Kv channels in native VSMCs, although current density is routinely used for comparison in most studies.

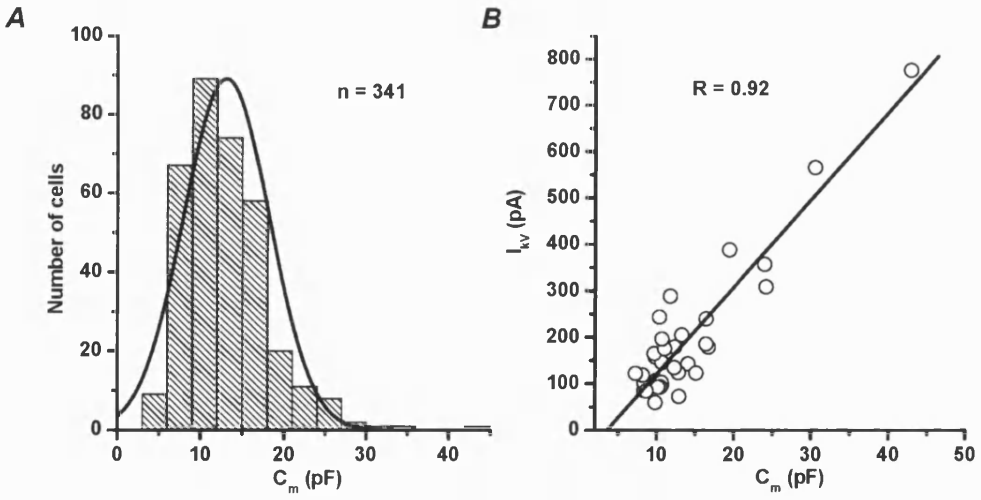

Figure 3.5. Correlation between I_{Kv} and C_m in RASMCs. *A*, distribution of C_m recorded from 341 cells. The continuous line is the normal distribution function with a mean value of 13.5 pF and a standard deviation of 5.13 pF. *B* reports the value of the I_{Kv} peak amplitude recorded in response to +60 mV depolarising pulses and plotted versus C_m in 35 different cells. Continuous line is the linear fit of the data, with slope factor equal to 18.7 (pA/pF) and regression coefficient, *R*, equal to 0.92.

3.2.2 Kinetics of I_{Kv} activation and I_{Kv} steady-state activation

In order to provide a quantitative comparison of the rate of activation of I_{Kv} at different membrane potentials, the rate constant of I_{Kv} activation kinetics was evaluated from a single exponential fit (eq. [2.1]) of the rise of I_{Kv} at each test potential. A representative example of a single exponential fit of activation in a family of current is reported in figure 3.6*A*. Figure 3.6*B* illustrates the potential dependence of τ_a measured at various V_m. τ_a decreased monotonically with membrane depolarisation from 101±15 ms (n=25) at -20 mV to 34±3 ms (n=35), 13±1 ms (n=35) at 0, 50 and 100 mV, respectively.

The I-V relationship for the peak I_{Kv} was derived using the I-V protocol described in Materials and Methods (Section 2.6.6.1) and presented as current density in figure 3.6*C*. I_{Kv} at each membrane potential was corrected for the leak current in each cell, as described in Material and Methods (mean slope resistance in 35 cells studied was equal to 11.0±1.3 GΩ). The leak corrected peak I_{Kv} was converted into conductance (Fig. 3.6*D*) and fitted with the Boltzmann equation (eq. [2.6]) with V_a= 4.12±1.70 mV, k_a = -15.04±0.55 mV, G_{max} = 0.088±0.005 nS/pF in 35 cells studied.

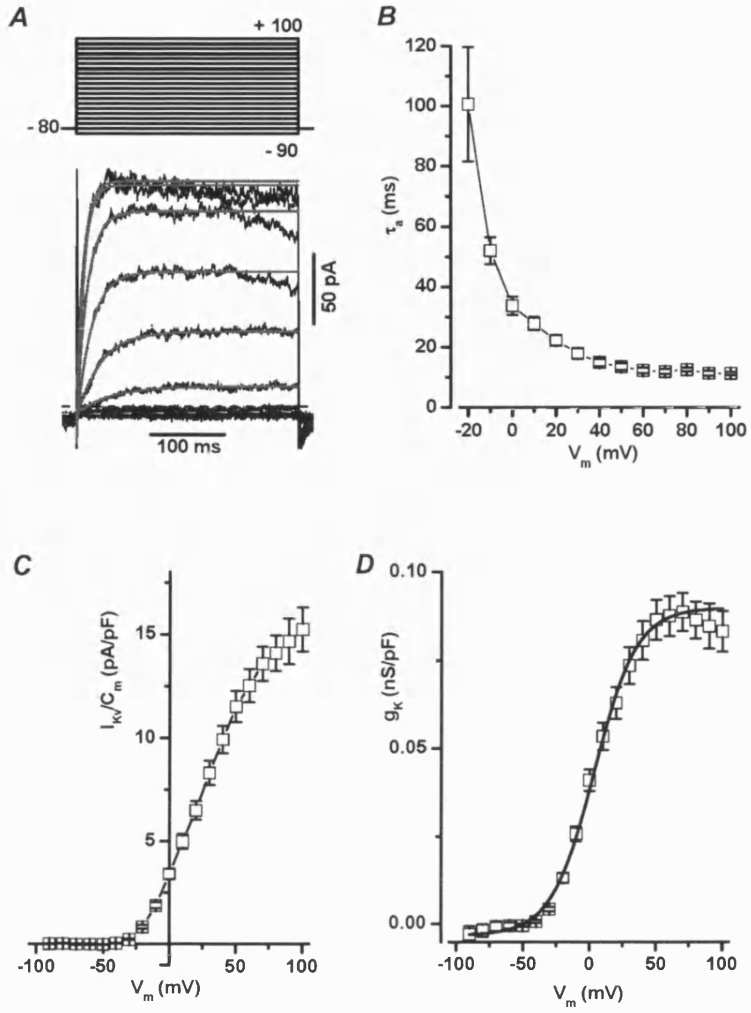

Figure 3.6 Activation of I_{Kv}. *A* shows a family of I_{Kv} recorded from a representative RASMC (C_m = 10.7 pF) in response to 300 ms depolarisation from –90 to +100 mV (only traces every 20 mV are reported). The upper panel illustrates the stimulation protocol. The dotted line represents the zero current. Grey lines are single exponential fits (eq. [2.1]) of the current traces with time constants and an asymptotic values equal to 47.6 ms and 14.5 pA for -10 mV, 32.2 ms and 53.6 pA for 10 mV, 19.6 ms and 93.8 pA for 30 mV, 14.5 ms and 139.5 pA for 50 mV, 9.7 ms and 159.3 pA for 70 mV, 9.0 ms and 167.0 pA for 90 mV, respectively. *B,* potential-dependence of the mean τ_a. *C*, the I-V relationship of the peak I_{Kv} expressed as current density. *D*, dependence of the whole-cell conductance on the membrane potential. Solid line is drawn according the Boltzmann function (eq. [2.6]) with V_a = 3.97 mV, k_a = -15.78 mV and G_{max} = 0.09 nS/pF. Data in *B*, *C* and *D* were obtained from 35 RASMCs.

3.2.3 Kinetics of I_{Kv} inactivation and I_{Kv} availability

During maintained membrane depolarisation, the I_{Kv} amplitude declined monotonically or inactivated to a new steady-state level as illustrated by a representative example in figure 3.6*A*, this process can be fitted with a single exponential function.

The rate of I_{Kv} decay was evaluated at various test pulse potentials each of 5 s duration. The decay phase of I_{Kv} was fitted with a single exponential function of the form:

$$I(t) = a\exp\left(\frac{-t}{\tau_i}\right) + C, \qquad [3.3]$$

where *I(t)* is the current as a function of time (*t*), *a* is a scaling factor, τ_i is the time constant of the current inactivation and *C* represents a non-inactivating fraction of the current (Fig. 3.7). Table 3.1 demonstrates that the time constant of inactivation displays a limited voltage dependence.

Table 3.1. I_{Kv} Inactivation kinetics parameters.

V_m (mV)	τ_i (ms)	% of residual current
-10	1730±263 (n=3)	14.6±8.0 (n=3)
0	1739±170 (n=3)	22.4±1.4 (n=3)
10	1799±125 (n=3)	13.8±3.4 (n=3)
20	1607±161 (n=5)	11.8±2.7 (n=5)
30	1473±114 (n=5)	6.3±4.6 (n=5)
40	1557±116 (n=5)	9.6±4.0 (n=5)
50	1456±149 (n=5)	9.2±4.4 (n=5)
60	1678±139 (n=5)	11.7± 4.5 (n=5)

Using the availability protocol (Materials and Methods, Section 2.6.6.4), the steady-state inactivation of I_{Kv} was analysed (Fig. 3.7*B*). The data were fitted assuming a Boltzmann distribuition (eq. [2.9]). The steady-state inactivation parameters obtained in 27 different RASMCs were V_h = -45.16±1.79 and k_h = 9.20±0.54 mV, $\hat{I}_{peak}$ = 14.04±1.54 pA/pF and I_{ss} = 3.21±0.30 pA/pF.

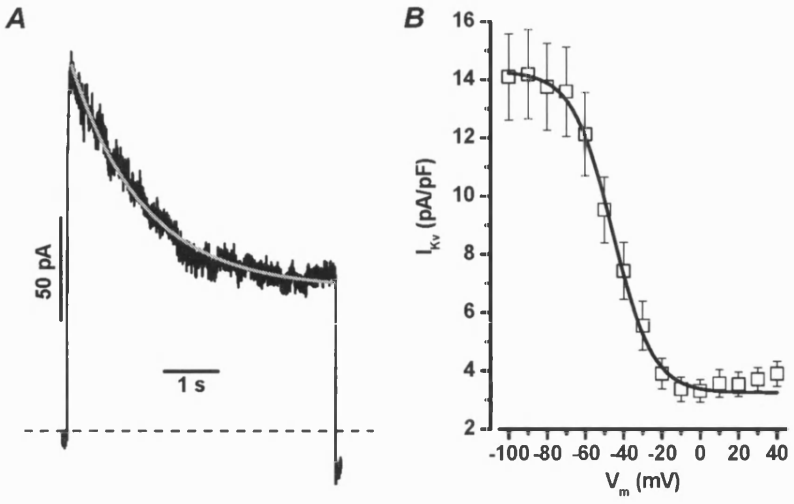

Figure 3.7 I_{Kv} inactivation. *A*, kinetics of I_{Kv} decay. I_{Kv} was elicited by a 5 s pulse to +60 mV. C_m = 11.1 pF. I_{Kv} decay was fitted according to the equation [3.3] with τ_i = 1452 ms and C = 65.5 pA. Dashed line represents zero current. *B*, averaged steady state inactivation dependency from 27 different RASMCs. The continuous line is the fit to the Boltzmann equation (eq. [2.9]) with V_h = -45.7 mV and k_h = 10.4 mV, $\hat{I}_{peak}$ = 14.3 pA/pF and I_{ss} = 3.2 pA/pF.

3.3 Pharmacological profile of I_{Kv}

3.3.1 Sensitivity of I_{Kv} to TEA and 4-AP

The effect of TEA, which inhibits some Kv channels and 4-AP, a non-selective inhibitor of I_{Kv}, was investigated in RASMCs using a test potential of +60 mV applied every 10 s. Cells were superfused continually with increasing concentrations of the TEA (0.1, 0.3, 1, 3, 10 , 20 mM) or 4-AP (0.5, 1, 5, 10, 20 mM). Each subsequent concentration of the drug was applied after equilibrium to the previous dose was achieved (150-200 s). The current amplitude in the presence of each concentration of the drug was normalised to that in the absence of the inhibitor and plotted against the corresponding concentration of the blocker. The averaged concentration dependencies for TEA and 4-AP thus determined are shown in Fig. 3.8. The inhibition of I_{Kv} by TEA was fitted with a modified Langmuir equation (eq. [3.1]). TEA inhibited I_{Kv} in a concentration-dependent manner with the mean IC_{50} of 3.1±0.6 mM and a residual TEA-insensitive component A = 0.1±0.02 (n=3, Fig. 3.8, filled triangles). A similar effect of TEA (IC_{50} = 3.2±0.7 mM, A = 0.1±0.01, n=5), was also observed under conditions where the

pipette solution contained 200 nM instead of 8 nM free Ca^{2+} and in the presence of both 1 μM paxilline and 10 μM glibenclamide (Fig. 3.8, open triangles). This additionally confirms that contamination with other conductances was negligible in elevated $[Ca^{2+}]$. I_{Kv} was also blocked by a moderate (20 mM) concentration of 4-AP, decreasing the I_{Kv} amplitude by 43.0±4.8 % (n=7) (Fig. 3.8).

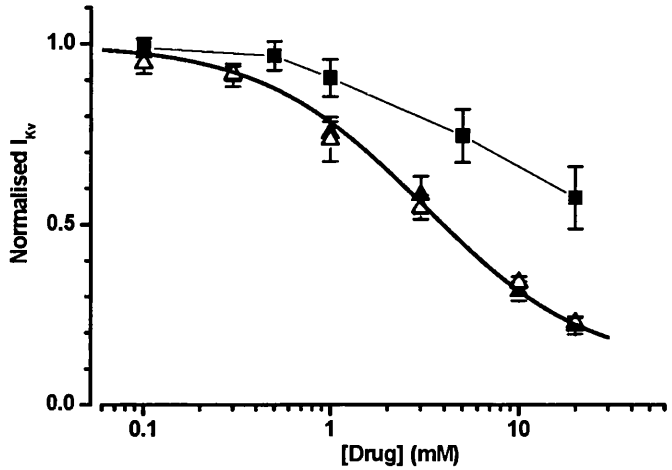

Figure 3.8. Concentration-dependent inhibition of I_{Kv} by TEA and 4-AP. Drugs were added cumulatively and I_{Kv} amplitude in the presence of each concentration of the drug was normalised to that in the absence of the inhibitor. Open and closed triangles show concentration dependent inhibition of the Kv current by TEA in the presence of 200 (n=5) and 8 (n=3) nM free Ca^{2+} in the pipette solution, respectively. The solid line through triangles was drawn according to the equation 3.1 with the mean IC_{50}=3.1 mM and A=0.1 described in the text. Filled squares show the effect of 4-AP.

3.3.2 Sensitivity of I_{Kv} to toxins

The sensitivity of I_{Kv} to specific toxins such as charybdotoxin (ChTx) and dendrotoxin (DTx), which potently inhibit some Kv1 isoforms (Grissmer *et al.*, 1994b), and correolide, a nortriterpene purified from the tree *spachea correae* which blocks Kv1 channels (Felix *et al.*, 1999; Hanner *et al.*, 1999), were also investigated. I_{Kv} was measured at +60 mV and cells were stimulated at 0.1 Hz. Application of 300 nM ChTx and 200 nM DTx did not produce a significant inhibition of the current after 3-5 min (Table 3.2). No significant block of I_{Kv} developed after 5 min of the application of correolide (Table 3.2).

Table 3.2. Toxin sensitivity of I_{Kv} in RASMCs

Toxin	*% of inhibition*
ChTx (300 nM)	5.7 ± 2.4 (n=6)
DTx (200 nM)	1.7 ± 4.9 (n=4)
Correolide (1μM)	4.0 ± 4.0 (n=5)

3.4 Biochemical and immunocytochemical analysis of the Kv channel expression in the rat aorta

The expression of three Kv channel proteins, Kv1.2, Kv1.5 and Kv2.1 was compared using immunoblot and immunocytochemical analysis. Western blot analysis was carried out on total protein extracted from the rat aorta, heart and brain, where heart and brain were used as positive controls. Figure 3.9 shows that all antibodies for the three channels tested gave a positive reaction in both control tissues. Kv2.1 appeared to be the most abundantly expressed channel in the rat aorta. It is noteworthy though that quantitative comparison between different Kv channels is difficult, since the intensity of the band in a gel is not only proportional to the amount of protein present but also depends on affinity of the antibody to the target protein.

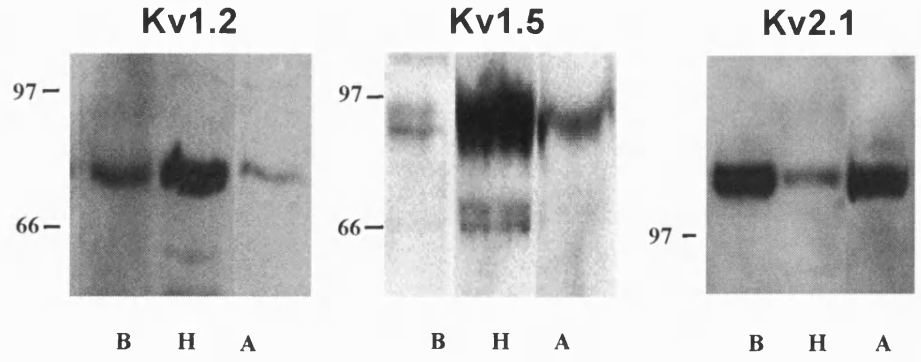

Figure 3.9. Kv channel expression in rat aorta. Representative Western blots for Kv1.2 (75 kDa), Kv1.5 (two bands of 95 and 76 kDa) and Kv2.1 (125 kDa) α-subunit proteins. Numbers on the left correspond to molecular mass standards. B, H and A are abbreviations for brain, heart and aorta protein samples, respectively. Heart and brain tissues served as positive controls.

Moreover, immunoblot analysis does not rule out the possibility that Kv channels were expressed in cells other than SMCs (e.g neuronal cells, Cheong *et al.* 2001) present in the aortic tissue. Therefore, to investigate Kv localisation in aortic myocytes, single aortic SMCs were stained with anti-Kv1.2, anti-Kv2.1 and anti-Kv1.5 antibodies and analysed under confocal microscopy. Representative examples are shown in Figure 3.10. The result of this analysis clearly demonstrated peripheral localisation of Kv2.1 α-protein, in the form of clusters. Also, a distinctive staining for Kv2.1 was observed near the nucleus. However no significant immunostaining with either anti-Kv1.2 or anti-Kv1.5 was detected. Similar results were obtained in another 4 experiments.

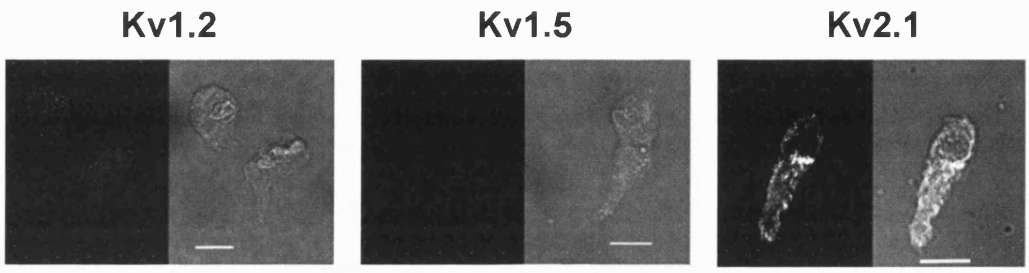

Figure 3.10. Immunocytochemical identification of the Kv2.1 channel expression in the rat aortic myocytes. Single rat aortic myocytes were fixed with paraformaldehyde and stained with the corresponding anti-Kv antibodies as described in Materials and Methods. Horizontal bars are 10 μm.

3.5 Discussion: I_{Kv} in rat aorta

3.5.1 The Kv channel is the main K^+ conductance in rat aortic myocytes

The relative contribution of Kv and BK_{Ca} channel has been initially examined under conditions where the pipette solution contained 200 nM Ca^{2+} in order to mimic the elevated cytosolic Ca^{2+} levels which may occur in response to low doses of PE or KCl. Under these conditions, the whole-cell current at +80 mV was increased 7.5 folds in comparison to that of 14.1±0.8 pA/pF measured in rat aortic SMCs perfused with 8 nM Ca^{2+}. To isolate Kv and BK_{Ca} currents the effect of two specific BK_{Ca} channel

inhibitors, IbTx and paxilline, were characterised and compared to the effect of TEA, which blocks BK_{Ca} and some Kv channels. Both paxilline and IbTx blocked the whole-cell current at +100 mV (mostly BK_{Ca}), with the mean IC_{50}s of 97 and 12 nM, respectively, which are similar to those reported for these inhibitors previously (Li & Cheung, 1999; Kaczorowski & Garcia, 1999). However, block of the whole-cell current by TEA was significantly less potent than that of paxilline and IbTx with IC_{50} of 273 μM, a typical value for the inhibition of BK_{Ca} channels. Despite the difference in potency, the effect of IbTx and paxilline were similar, saturating in the concentration range of 100-300 and 500-1000 nM, respectively. These results indicate that the current through BK_{Ca} channels was selectively suppressed by these concentrations of the blockers. Therefore 1 μM paxilline was used in order to eliminate BK_{Ca} channel components in the subsequent experiments. A comparison of the contribution of BK_{Ca}, expressed as the paxilline-sensitive current, and I_{Kv}, measured as the paxilline-resistant current, revealed that BK_{Ca} currents do not activate until membrane potential reaches approximately -20 mV, whereas I_{Kv} become apparent at membrane potentials more positive than -40 mV (Fig. 3.3). The amplitude of BK_{Ca} current dominates significantly in a non-physiological range of membrane potentials above +50 mV, despite the elevated $[Ca^{2+}]_i$. Interestingly, a similar low activity of BK_{Ca} channels has also been reported in these cells in the presence of 0.1 mM EGTA and 1 μM free Ca^{2+} in the pipette solution (Liu *et al.*, 1997). My results also echoed those obtained in rabbit cerebral arterioles, where I_{Kv} (recorded with a low Ca^{2+}-buffered internal solution) was activated by ~20 mV more negative than the BK_{Ca} current (Cheong *et al.*, 2002). Also, in rat intra-pulmonary arterial SMCs, intracellular perfusion with elevated Ca^{2+} (~ 0.5 μM), caused only small (15-30%) increases in the amplitude of the TEA-sensitive (BK_{Ca}) current at membrane potentials positive to –10 mV (Smirnov *et al.*, 1994; Smirnov & Aaronson, 1994). Although the exact reason for low Ca^{2+} sensitivity of BK_{Ca} currents in some VSMCs is not clear, it is attractive to speculate that lack of expression or functional uncoupling of the existing BK_{Ca} β-subunit, which greatly enhances the Ca^{2+} sensitivity of the BK_{Ca} α-subunit (Tanaka *et al.*, 1997), might be responsible. The existence of BK_{Ca} splice variants with different Ca^{2+} sensitivity (e.g. Sansom & Stockand, 1994) or the spatial distribution of BK_{Ca} channels in VSMCs (e.g. their co-localization with Ry-receptor causing a rapid increase in $[Ca^{2+}]_i$ in the channel vicinity Jaggar *et al.*, 1998) or a combination of these and other yet to be identified factors may also have importance.

3.5.2 Molecular nature of Kv channels in rat aortic myocytes

My experiments showed that I_{Kv} in RASMCs belongs to the delayed rectifier type (Fig. 3.9 and 3.10). Molecular identity of delayed rectifier currents in different types of VSMCs is mostly unknown, although the expression of practically every Kv isoform can be demonstrated, at least at mRNA level, in various types of blood vessels. The expression of Kv1.1, Kv1.2, Kv1.3 Kv 1.5, Kv 1.6, Kv2.1 and to Kv3.1b which encode delayed rectifier currents have been demonstrated in VSMCs, (e.g. Maruoka *et al.*, 2000; Yuan *et al.*, 1998; Osipenko *et al.*, 2000; Patel *et al.*, 1997) including rat aorta (Roberds & Tamkun, 1991; Thorne *et al.*, 2002). Table 3.3 provides a comparison of the pharmacological and electrophysiological properties of these Kv channels. Kv1.1 (Grissmer *et al.*, 1994a), Kv1.6 (Swanson *et al.*, 1990) and Kv3.1b homomultimers are inhibited by a low concentration of TEA (<1mM). Kv3.1b is also potently blocked by micromolar doses of 4-AP (Grissmer *et al.*, 1994). Currents mediated by Kv1.2 and Kv1.5 channels are TEA-insensitive (Grissmer *et al.*, 1994). Therefore Kv1.1, Kv1.2, Kv1.5, Kv1.6, and to Kv3.1b are unlikely to be responsible for I_{Kv} in RASMCs. The insensitivity of I_{Kv} in RASMCs to DTx (200 nM) and ChTx (300 nM) rules out the involvement of Kv1.1, Kv1.2 and Kv1.3 as molecular candidates for I_{Kv} in RASMCs since these rapidly-activating channels are sensitive to one or both toxins. Moreover, the lack of sensitivity of I_{Kv} to 1 μM correolide, a potent inhibitor of all Kv1 channels, rules out a possible significant contribution by any member of the Kv1 subfamily to I_{Kv}. In contrast, Kv2.1 demonstrates a moderate sensitivity to TEA with a half block between 1 and 10 mM (Shi *et al.*, 1994; Roe *et al.*, 1996). Also, relatively slow kinetics of activation of I_{Kv} (see also Chapter 5 where Kv2.1 and Kv1.5 expressed in *Xenopus* oocytes are described) and the sensitivity to 4-AP in the mM range, closely match the characteristics of the cloned Kv2.1 channel, pinpointing this α-subunit as the main carrier of Kv channel current in RASMCs. The western blot analysis (Fig. 3.9) showed the significant presence of Kv2.1 α-protein (compared to a lower expression of Kv1.2 and Kv1.5 α-subunits) in the protein extracts from whole rat aorta. In addition, immunocytochemistry (Fig. 3.10) shows a positive peripheral immunostaining of single RASMCs with anti-Kv2.1 antibodies, but not with anti-Kv1.2 or anti-Kv1.5, providing further evidence that the main functionally active Kv channels are formed predominantly by the Kv2.1 α-subunit in rat aortic SMCs.

Table 5.3 Comparison of electrophysiological and pharmacological properties of I_{Kv} in RASMCs and cloned Kv channels.

	I_{Kv}	$K_v1.1$	$K_v1.2$	Kv1.3	$K_v1.5$	$K_v1.6$	$K_v2.1$	$K_v3.1b$
Rate of activation	Slow	Rapid	Rapid	Rapid	Rapid	Rapid	Slow	Rapid
TEA *	6.0	0.3-0.6	>200	>10-50	>200	4	3-10	0.1-0.2
4 AP *	2.9	0.3-1	0.6-0.8	0.5-1.5	0.2-0.5	0.3	5-100	0.03-0.1

*values are given as K_d and are in mM.

Chapter 4

Role of Kv channels in the regulation of contraction in rat aorta

Patch-clamp experiments described in the previous chapter showed that Kv channel currents dominate in RASMCs in the presence of low (~8 nM) and elevated (~200 nM) intracellular Ca^{2+}. In order to establish whether Kv channels are important in the regulation of resting tension and excitability of the whole tissue, the effect of the Kv and BK_{Ca} channel inhibitors tested in electrophysiological studies, was examined in endothelium-denuded aortic preparations using isometric tension measurements.

4.1 Contribution of Kv channels to the control of resting tension in rat aorta

The effect of K^+ channel inhibitors was evaluated in the presence of 10 mM K^+ to enhance K^+ channel activity. Application of a similar concentration of K^+ produced ~5 mV membrane depolarisation in endothelium-intact rat conduit pulmonary arteries (Chen & Suzuki, 1989) and did not cause significant changes in basal tension in my experiments (data not shown). Cumulative addition of TEA between 1 and 5 mM induced irregular and often transient contractions with superimposed twitch-like oscillations (Fig. 4.1*A*). An increase in the TEA concentration up to 10-20 mM only caused a slight further increase in the amplitude of the maximal contraction. In normal Krebs solution (5.9 mM K^+), contractions to the same concentrations of TEA were observed less frequently (Fig. 4.1*C*). For example, only 3/34 and 5/34 preparations bathed in Krebs solution contracted in response to 1 and 5 mM TEA respectively, in comparison to 3/13 and 8/17 aortic rings maintained in the presence of 10 mM K^+ solution. It is notable that TEA-induced contractions were transient and often developed maximal tension even in the presence of low TEA concentrations. Such behaviour made detailed analysis of the TEA concentration-dependent relationship difficult. Therefore,

the frequency of occurrence of the TEA-induced response, measured as the presence of contraction and/or oscillations normalised to the total number of experiments performed with each dose of TEA, was measured instead. The frequency response demonstrates that TEA-induced contractions are facilitated by higher doses of the drug and in the presence of 10 mM K^+ (Fig. 4.1*C*).

Application of 5 and 10 mM 4-AP also induced contractions similar to those obtained with TEA (data not shown). 5 mM 4-AP triggered contraction in 1/5 and 2/4 preparations in the absence and presence of the 10 mM K^+ solution respectively, whereas 10 mM 4-AP constricted all aortic rings tested (n=6). A lower dose of 4-AP (1 mM), however, did not cause contraction either in the absence (n=5) or in the presence of 10 mM K^+ (n=4).

In the presence of 10 mM K^+, the addition of 1 μM paxilline (Fig. 4.1*B*, n=7) or 10 μM glibenclamide (n=5), a selective inhibitor of ATP-sensitive K^+ (K_{ATP}) channels, or combination of both drugs (n=3) applied for 30 min did not produce contraction (data not shown).

These results strongly support my findings obtained in patch-clamp experiments, suggesting that BK_{Ca} channels do not contribute to the control of resting tone in rat aorta. It is however possible that a contribution of BK_{Ca} channels to the control of cell excitability is raised in active tissue when $[Ca^{2+}]_i$ is significantly increased.

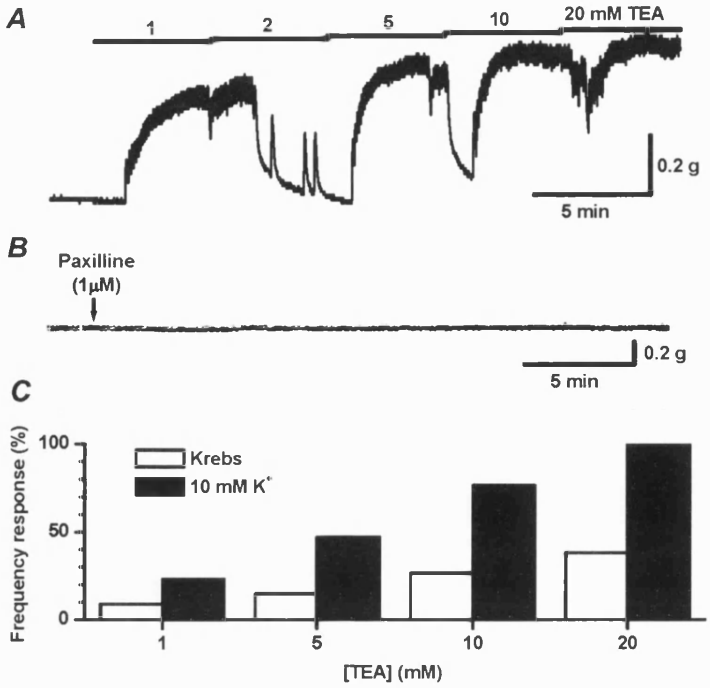

Figure 4.1. The effect of TEA and paxilline on the basal tone in endothelium-denuded rat aorta in the presence of 10 mM K^+. *A*, the effect of cumulative addition of TEA. *B*, the effect of 1 μM paxilline. *C*, comparison of the percentage of preparations eliciting TEA-induced contraction in normal Krebs and 10 mM K^+ solutions. Frequency response was measured as a percentage ratio of contractions appearing in the presence of each concentration of TEA to the total number of applications at that TEA concentration in normal Krebs solution (open bars, total attempts = 34) and in the 10 mM K^+ solution (solid bars, total attempts = 17, except 1 mM where n=13).

4.2 Effect of phenylephrine on the endothelium-denuded rat aorta

To investigate the relative contribution of Kv and BK_{Ca} channels to active tension, aortic rings were stimulated with PE. Since the inhibition of a corresponding K^+ channel would be expected to produce further contraction in intact preparations, 15-40 nM of PE was used. This range of PE concentrations is close to the PE concentration which produce half-maximal response in the endothelium-denuded rat aorta (IC_{50}=31±5 nM, n=13, data not shown). Application of half-maximal concentrations of PE produced a complex contractile activity as illustrated in examples shown in Fig. 4.2 and 4.3. An initial increase in the basal tension was followed by rhythmic contractions superimposed on the PE-induced sustained tension. These contractions (termed oscillatory waves or OWs) were characterized by a marked plateau with superimposed

rhythmic fluctuations probably representing the summation of several shorter twitch-like contractions (Fig. 4.2, inserts). OWs were induced by PE in the concentration range between 15 and 40 nM (except two preparations which required 50 and 80 nM) in 65/73 aortic rings obtained from 25 animals. In the remaining preparations, four showed only periodical twitch-like contractions, and four produced sustained tension with superimposed fluctuations of small amplitude.

To characterise OWs quantitatively the amplitude and duration of OWs were calculated as the difference between the maximal and the minimal amplitudes and as the duration at 50% of the maximal amplitude of OWs respectively, and presented as a mean of at least 3 OWs. The duration of the shortest and the longest OW was 21 and 252 s, respectively, with the mean value of 113±5 ms (n=65). Variations in both the amplitude (range 133-720 mg with the mean value of 359±15 mg) and the frequency (range 0.13-1.32 waves/min with the mean of 0.29±0.02 waves/min) of OWs were also observed (n=65). The mean sustained tension (measured as the difference between the minimum active tension achieved for a given dose of a drug and the resting tension measured in the absence of any stimulants) developed at these concentrations of PE was 0.34±0.02 g (n=65). No correlation between the magnitude of sustained contraction and the amplitude, the frequency or the duration of OWs was found ($0.02<R<0.36$).

OWs were suppressed by 0.2-1 μM diltiazem, a selective inhibitor of L-type VDCCs, and by 1-2 μM ryanodine, which inhibits Ca^{2+} release from ryanodine-sensitive stores, (Fig. 4.2, *A* and *B*, respectively). Both agents blocked OWs in a similar manner, causing an initial shortening of OWs by decreasing the number of individual twitch-like contractions within OWs, followed by complete cessation of OWs (Fig. 4.2, inserts). In addition, OWs were rapidly inhibited by 5-10 μM cyclopiazonic acid (CPA, an inhibitor of SERCA). The effect of CPA was associated with a gradual increase in the sustained tension (Fig. 4.2*C*). It should be noted that no significant inhibition of sustained PE-induced contraction was found in the presence of diltiazem or ryanodine (Fig. 4.2 *A* and *B*), indicating that separate mechanisms contribute to the generation of rhythmic activity and sustained tension. It is noteworthy that OWs were not blocked by 50 μM niflumic acid, an inhibitor of Ca^{2+}-activated Cl^- channels, suggesting that activation of this conductance was not essential for the generation of rhythmic activity under my experimental conditions (data not shown).

4.3 Contribution of Kv channels to active tension in intact rat aorta

The effect of K^+ channel inhibitors (TEA, 4-AP, paxilline, IbTx and correolide) was then investigated on PE-induced tension and OWs. Addition rising concentrations of TEA caused a progressive increase in the amplitude and duration of OWs (Fig. 4.3*A*), as expected from the inhibition of TEA-sensitive K^+ channels participating in the OW relaxation process. Application of 4-AP caused two effects: an initial transient decrease in the sustained PE-induced contraction, and a significant increase in both the amplitude and duration of OWs (Fig. 4.3*B*). Although the reason for the 4-AP-dependent decrease in tension is not clear, we did not observe any relaxing effect of 4-AP on the basal tension measured both in Krebs and 10 mM K^+ solutions, indicating that the development of some tone was required. Nevertheless, the effect of 4-AP on the duration and amplitude of OWs was very similar to that of TEA, suggesting that K^+ conductance involved in the regulation of rhythmic activity is also 4-AP-sensitive. A marked reduction in the frequency of OWs, usually observed in the presence of 4-AP, could be partially due to a decreased level of sustained contraction in the presence of the drug. For example, the sustained tension was decreased by 8±2% (n=7) and 12±2% (n=5) in the presence of 1 and 5 mM 4-AP, respectively. It is interesting to note that a slow decrease in PE-induced sustained tension observed in some preparations with time of incubation, caused a reduction in the frequency of OWs which was also associated with a decrease in duration and amplitude of OWs, effects which are opposite to those observed in the presence of 4-AP. In contrast to TEA and 4-AP, addition of the BK_{Ca} channel inhibitors paxilline (Fig. 4.3*C*) and IbTx (Fig. 4.3*D*) had no significant effect on the amplitude and duration of OWs. Also neither of the BK_{Ca} channel blockers affected the PE-induced contraction, suggesting that contribution of BK_{Ca} currents to the control of aortic activity is negligible under these experimental conditions.

Relative changes in the amplitude and duration of OWs observed in the presence of K^+ channel inhibitors were averaged, expressed as a percentage, and plotted against the corresponding concentration of the drug (Fig. 4.4). The mean changes in both the amplitude and duration of OWs observed in the presence of TEA or 4-AP (both at 5 mM) were significantly different from those measured in the presence of the maximal concentration of BK_{Ca} channel inhibitors ($0.008 < P < 0.03$). In addition, application of 1

μM correolide also did not significantly affect the amplitude (1.6±6.1%) or the duration (-5.9±9.1%) of OWs in 6 aortic rings tested (not shown).

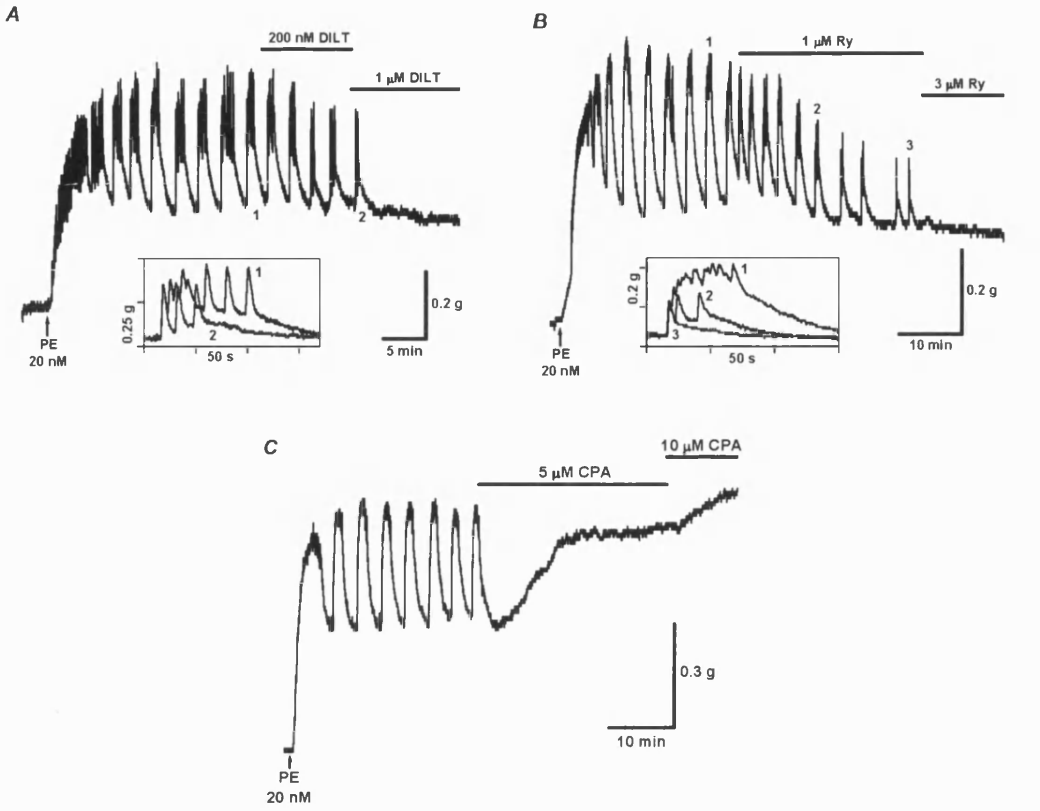

Figure 4.2. Effect of diltiazem (DILT), ryanodine (Ry) and cyclopiazonic acid (CPA) on PE-induced rhythmic contractions in the endothelium-denuded rat aorta. *A*, effect of 200 nM and 1 μM of diltiazem. Insert: two superimposed OWs before (trace 1) and after addition of 200 nM diltiazem (trace 2). Traces were aligned at the beginning of each OW to aid a comparison. *B*, effect of 1 and 3 μM ryanodine on PE-induced OWs. Insert: superimposed traces before (1) and in the presence of 1 μM ryanodine (2 and 3). The baseline in traces 2 and 3 was adjusted by 10 and 40 mg, respectively, for better alignment with trace 1. Note that neither diltiazem nor ryanodine affected the PE-induced sustained contraction while 5 μM CPA are sufficient to cause an increase of the sustained contraction level (*C*). *A* and *B* and *C* were recorded from three different preparations.

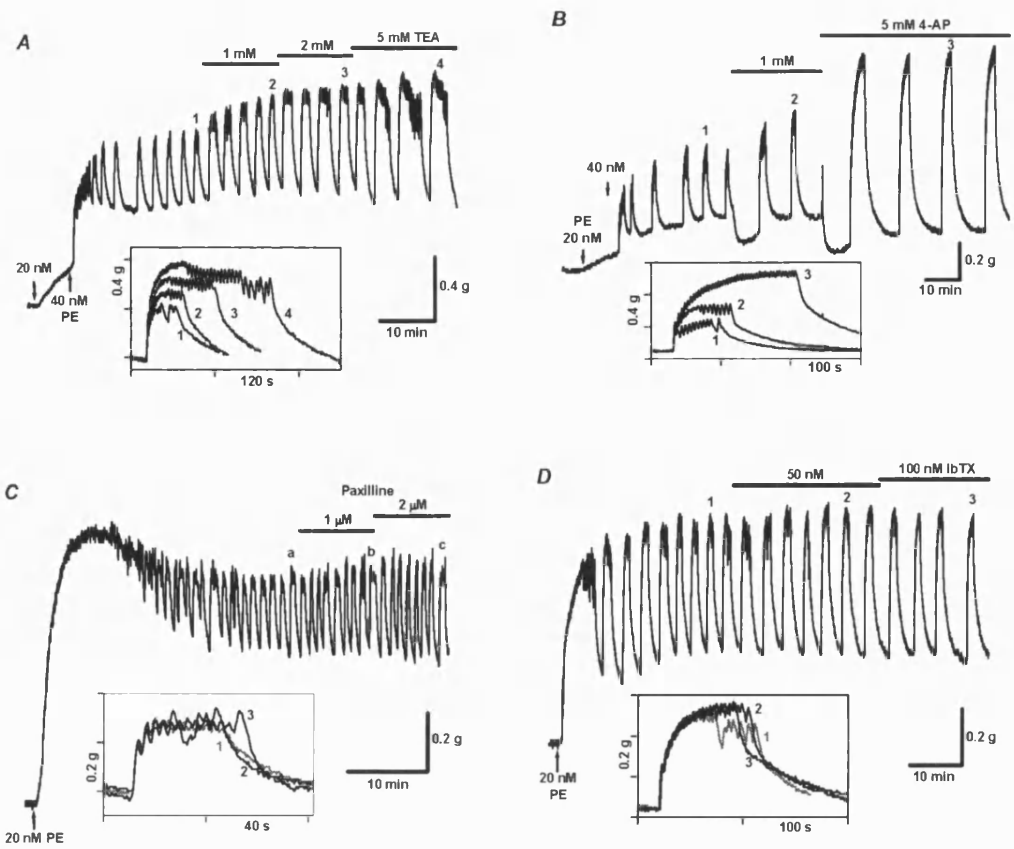

Figure 4.3. The effect of K^+ channel blockers on PE-induced rhythmic activity in the endothelium denuded rat aorta. *A*, *B*, *C* and *D*, the effect of various concentrations of TEA, 4-AP, paxilline and IbTx on OWs, respectively. Inserts: superimposed OWs marked by letters in the absence and presence of the K^+ channel inhibitors. In order to facilitate the comparison, the baseline was adjusted by 96 (trace b), 59 (trace c) and 21 (trace d) mg (*A*), by 90 mg (trace c) (*B*), and by 19 (trace b) and 43 (trace c) mg (*D*).

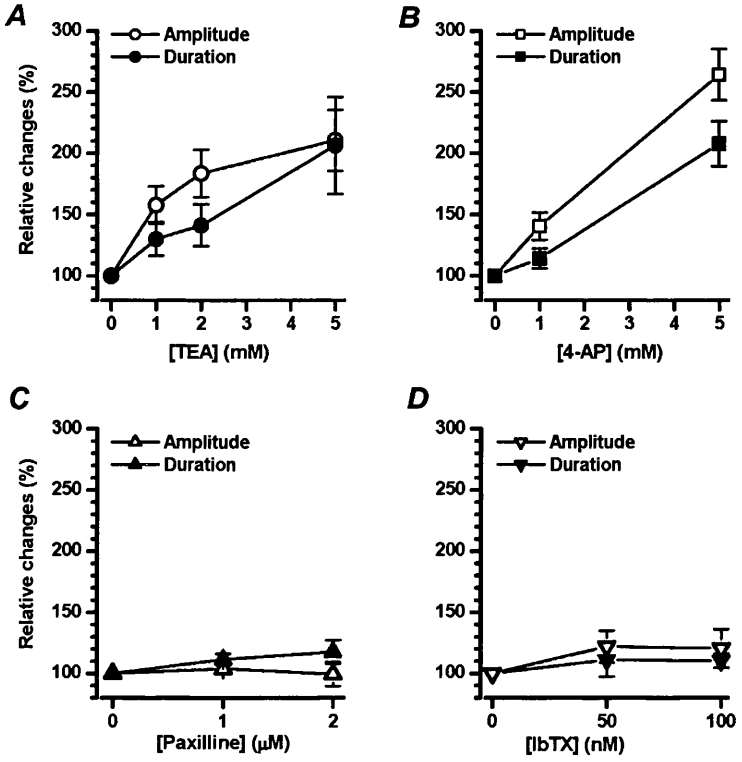

Figure 4.4. Comparison of the effect of K^+ channel inhibitors. *A*, *B*, *C* and *D*, effect of TEA (*A*), 4-AP (*B*), paxilline (*C*) and IbTx (*D*) on the amplitude (open symbols) and the duration (closed symbols) of OWs. The amplitude and the duration of OWs were measured in the presence of each concentration of a K^+ blocker, normalised to that in the absence of the drug and expressed as percentage of relative changes. The control value was measured as the mean of three OWs just before the inhibitor was added to the organ bath and set as 100%. Statistical analysis is given in the text.

4.4 Discussion: rhythmic activity and K^+ channels

4.4.1 The key role of Kv channels in the regulation of the rat aortic contraction

The results of patch-clamp experiments strongly suggest that I_{Kv}, which activates at more negative membrane potentials than BK_{Ca} currents, is one of the major contributors to the regulation of resting membrane potential in rat aorta. Indeed, application of 1-5 mM TEA and 4-AP (K^+ channel inhibitors which block I_{Kv} in rat aortic SMCs), caused a marked contraction of endothelium-denuded rat aortic rings in Krebs solution. Paxilline and/or glibenclamide did not mimic the effects of TEA and 4-AP even at a higher K^+ concentration (10 mM), while the incidence of responses to TEA over the whole range of concentrations tested was increased. An increase in the external K^+

concentration to 10 mM might depolarise the cell membrane by up to 12 mV (assuming the intracellular K^+ concentration is equal to 140 mM), and similar changes in the external K^+ concentration indeed caused membrane depolarisation of rat main pulmonary arterial smooth muscles by ~5 mV in the presence of an intact endothelium (Chen & Suzuki, 1989). Since membrane depolarisation will increase the activity of both L-type VDCC, Kv and BK_{Ca} currents, the ability of Kv inhibitors, but not BK_{Ca} and K_{ATP} blockers, to induce contraction strongly suggest that Kv channel currents control the excitability of rat aorta smooth muscle at rest. Interestingly, potentiation of agonist- and KCl- induced contractions by mM concentrations of 4-AP and TEA were also observed in mouse (Jiang *et al.*, 1999) and rabbit (Cook, 1989) aortas, signifying that activation of a similar type of K^+ conductance might contribute to the control of aorta contractility in other species.

To evaluate a possible contribution of Kv and BK_{Ca} channels on active tension, the effects of TEA, 4-AP, correolide, paxilline and IbTx on the rat aorta stimulated with the α_1-adrenoreceptor agonist PE were investigated. It has been previously shown that stimulation of α_1-adrenoreceptors in addition to release of Ca^{2+} from IP_3-sensitive stores, also causes significant membrane depolarisation of VSMCs (Chen & Rembold, 1995; Mulvany *et al.*, 1982). Under my experimental conditions, application of PE at concentrations close to those which caused half-maximal contraction of the endothelium-denuded rat aorta induced slow rhythmic contractions (termed oscillatory waves or OWs) superimposed on the sustained tension induced by the α-agonist in most preparations. Although shorter twitch-like contractions have been previously reported in the rat aorta (Freeman *et al.* 1995) and observed in some preparations in my study, the type of contraction described in my work has not been previously characterised. The OWs, but not the PE-induced contraction, were blocked by both diltiazem and ryanodine (the inhibitors of L-type VDCCs and ryanodine receptors, respectively), indicating that OWs and sustained tension could be mediated by two separate processes. Based on diltiazem and ryanodine sensitivity of OWs, it is likely that this type of rhythmic activity is triggered by Ca^{2+} entry into SMCs via L-type VDCCs activated by PE-induced depolarisation. L-type VDCC-dependent Ca^{2+} entry causes CICR from ryanodine-sensitive Ca^{2+} store, rise in $[Ca^{2+}]_i$ and muscle contraction. PE-induced sustained tension, on the other hand, probably occurs via the IP_3-dependent mechanism and possibly changes Ca^{2+} sensitivity of contractile proteins. It is worth mentioning that

mechanisms underlying spontaneous rhythmic activity in blood vessels, as well as induced oscillatory activity which generally occurs in large blood vessels are not completely understood. Multiple factors can be responsible in different vascular beds, although the dependence of rhythmic contractions on the L-type VDCC-mediated Ca^{2+} entry has been well characterised in various vascular preparations (reviewed in Gustafsson, 1993 and Shimamura *et al.*, 1999). It is possible that the individual OW occur as a result of temporal/spatial summation of several twitch-like contractions. However, based on the presented experimental data, it is difficult to speculate about the exact intracellular events underlying OWs and further experiments will be required to establish the precise mechanism of this type of rhythmic activity in the rat aorta. Nevertheless, periodical activation of L-type VDCCs, which seems to be necessary for maintaining OWs, requires the presence of a negative feedback mechanism which would hyperpolarise the cell membrane and cause the closure of L-type VDCCs. The most obvious candidate for this role is the BK_{Ca} current which can be activated under these conditions. In this case, application of specific BK_{Ca} channel inhibitors should affect rhythmic activity. Indeed, the development of sustained contraction and either inhibition of oscillatory activity or increase in frequency of oscillations have been previously observed in response to IbTx and/or ChTx (Jiang *et al.*, 1999; Wesselman *et al.*, 1997; Gokina *et al.*, 1996). No effect of IbTx or paxilline (at concentrations which practically eliminate all BK_{Ca} current) either on the basal tension or OWs were found under my experimental conditions, strongly suggesting that BK_{Ca} channels are not involved in the regulation of rhythmic contractions in the rat aorta. On the other hand, the duration and amplitude of OWs was significantly increased in the presence of TEA and 4-AP, which are inhibitors of I_{Kv} in rat aortic SMCs, implying that activation of I_{Kv} is the major K^+ conductance in the negative feedback mechanism controlling OWs. The electrophysiological finding that I_{Kv} activates in a significantly more negative voltage range than BK_{Ca} currents under elevated $[Ca^{2+}]_i$ levels, further supports this suggestion. The lack of any significant effect of 1 μM correolide on OWs indicates that Kv1 channels are not functionally active in the whole tissue preparation, supporting the patch-clamp data obtained in single SMCs after enzymatic treatment. It is important to mention that Ca^{2+} extrusion from the cell and Ca^{2+} reuptake back into Ca^{2+} stores, which represents a negative feedback mechanism for lowering $[Ca^{2+}]_i$ necessary for the relaxation process, have not been taken into consideration, since it seems unlikely that the K^+ channel inhibitors used in this study would specifically affect these processes.

4-AP caused two effects on the PE-stimulated rat aortic rings: an initial decrease in the PE-induced sustained tension and the significant increase in both amplitude and duration of OWs discussed above. It should be pointed out that relaxing effect of 4-AP on the basal tension was not observed in non-stimulated preparation either in Krebs solution or in the presence of 10 mM K^+, suggesting that the tension development was required for the relaxing effect of 4-AP. The exact reason for such effect is difficult to delineate from my experiment. A possibility of release of relaxing neurotransmitters from perivascular nerve endings (similar to the release of noradrenaline in canine saphenous vein (Kun *et al.*, 2002) and neuropeptide Y from non-adrenergic nerves in the isolated jejunum of rabbits (Cheng *et al.*, 1989)) cannot be entirely excluded. Nevertheless, the release of relaxing agents from nerves, even if occurs, cannot explain the second stimulating effect of 4-AP on the amplitude and duration of OWs. Future experiments using tetrodotoxin to block nerve conduction could provide a definite answer to this question.

In conclusion, the data reported in this and in the previous chapter strongly suggest that the voltage-dependent K^+ current through Kv2.1 channels is the main K^+ conductance which controls the resting membrane potential and significantly contributes to the regulation of contractile function and induced rhythmic activity of the rat aorta. Also, the rat aorta could be a useful experimental model to study the mechanism of regulation of the Kv2 type channels expressed in native SMCs during normal and pathological conditions.

Chapter 5

Regulation of Kv channel currents by intracellular Mg^{2+} in the rat vasculature

Preliminary work that led to my PhD project showed that replacement of 5 mM MgATP with 5 mM $MgCl_2$ caused a significant shift to more negative potentials in the steady state inactivation curve of I_{Kv} in RASMCs. Further investigation of this phenomenon showed that omission of $MgCl_2$ from the pipette solution mimicked the effects observed in the presence of 5 mM MgATP. Since ATP is a potent chelator of Mg^{2+}, I hypothesised that intracellular Mg^{2+} and not ATP was the main cause of the shift in the inactivation dependency. Therefore, the effect of intracellular Mg^{2+} on the voltage dependent characteristics of I_{Kv} in RASMCs was investigated in detail.

5.1 Effect of intracellular Mg^{2+} on the voltage-dependent characteristics of I_{Kv} in rat aortic smooth muscle cells

The effects of intracellular Mg^{2+} were studied by adding different concentrations of $MgCl_2$ or MgATP in the pipettes solution (Table 5.1). Free $[Mg^{2+}]_i$, which is influenced by the presence of EGTA, was estimated with the program Maxchelator (Stanford University, CA) and values of $[Mg^{2+}]_i$ which correspond to those of $[MgCl_2]$ in the pipette solution are given in Table 5.1. However, since the Mg^{2+} concentration near the channel mouth cannot be measured directly, I will refer to intracellular $[Mg^{2+}]_i$ as $[MgCl_2]_i$ in the text and figures. PSS in all the experiments reported in this chapter contained 1 μM paxilline and 10 μM glibenclamide.

Table 5.1 Comparison of the pipette [$MgCl_2$] and estimated free [Mg^{2+}].

Concentration (mM)	*Estimated free [Mg^{2+}] (mM)*
0 $MgCl_2$	0
0.5 $MgCl_2$	0.32
5 MgATP	0.58
5 $MgCl_2$	3.48
10 $MgCl_2$	7.30

5.1.1 Current-voltage relationship in different [$MgCl_2$]$_i$

Figure 5.1 compares representative families of I_{Kv} recorded from single RASMCs in the presence of different pipette $[MgCl_2]_i$. It is clear from the Figure that increasing the internal [$MgCl_2$] caused rectification of I_{Kv} at positive membrane potentials, i.e. the I_{Kv} amplitude saturated when the membrane depolarisation increased. The effect became more prominent at $[MgCl_2]_i$ equal 5 and 10 mM. Interestingly changes in the I_{Kv} amplitude in the presence of 0.5 mM $[MgCl_2]_i$ and 5 mM $[MgATP]_i$, which yield an analogous free $[Mg^{2+}]_i$ (Table 5.1), were very similar. Another obvious effect was on the current kinetics at 10 mM $MgCl_2$ in the pipette solution. As summarised in Fig. 5.2, τ_a for I_{Kv} measured between –10 and +100 mV, was significantly larger in the presence of 10 mM $MgCl_2$ (P<0.004) when compared with those at 0 mM.

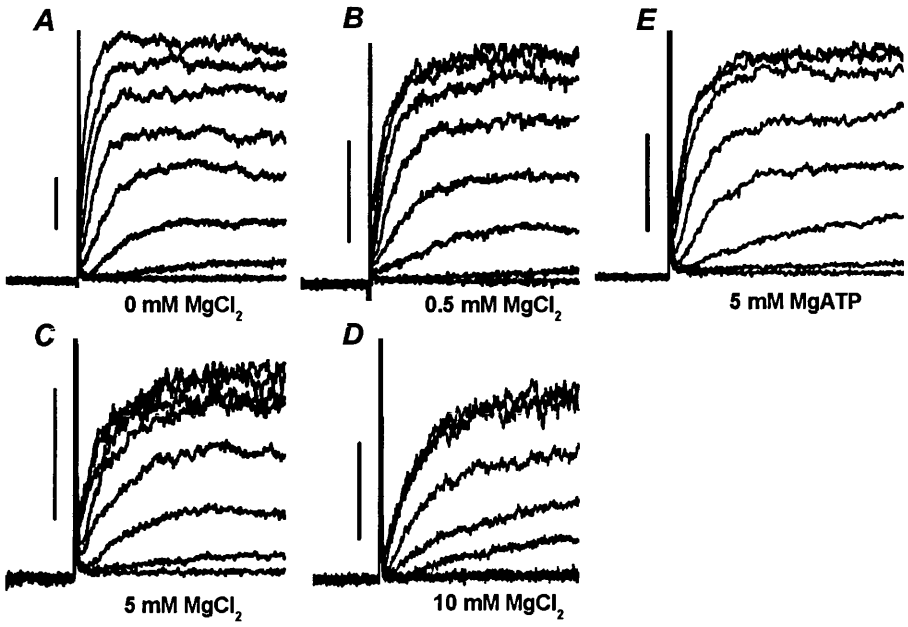

Figure 5.1. Effect of different pipette [$MgCl_2$] and 5 mM MgATP on I_{Kv} in RASMCs. Current traces were recorded in the presence of the concentration of Mg-salt indicated below each family of currents. Only initial 100 ms of 300 ms depolarising pulses applied from –40 to +100 mV in 20 mV steps are shown. C_m was equal to 13.1, 11.7, 12.3, 10.3 and 10.9 pF from *A* to *D*, respectively. Vertical bars are 100 pA.

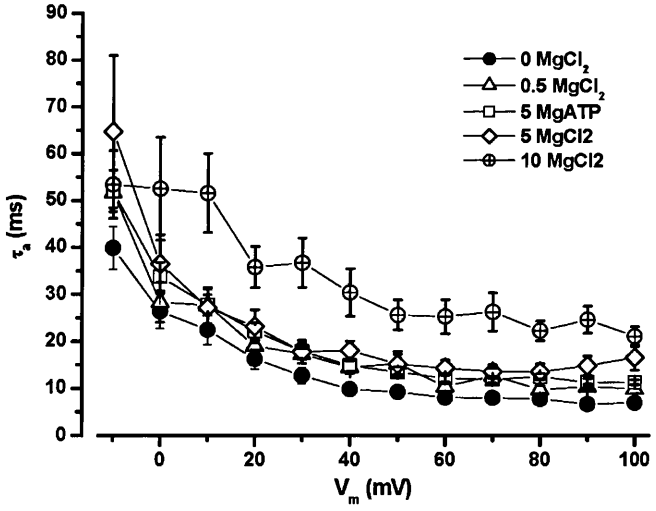

Figure 5.2. Activation time constant (τ_a) in the presence of different [$MgCl_2$] and [MgATP] (in mM). τ_a was calculated as indicated in Materials and Methods. Number of experiments was equal to 15, 12, 21 and 20 for 0, 0.5, 5, 10 mM $MgCl_2$ and 35 for 5 mM MgATP, respectively.

Figure 5.3 compares the averaged I-V relationships for the peak I_{Kv} in different $[MgCl_2]_i$, calculated and leak corrected as described in Materials and Methods. The data were also corrected for the cell size. The analysis clearly shows a progressive decrease in I_{Kv} density with an increase in pipette $[MgCl_2]$. Notably, the peak I_{Kv} also tends to decrease at positive membrane potentials in the presence of 5 and 10 mM $MgCl_2$, showing some rectification at V_m>+70 mV. It is also worth mentioning, that the I-V relationship for I_{Kv} in 5 mM MgATP was similar to those recorded in 0 and 0.5 mM $MgCl_2$ (all solutions that have similar low levels of free $[Mg^{2+}]_i$), indicating that Mg^{2+} and not MgATP determined these effects on I-V relationship for I_{Kv}.

Conductance-voltage relationships derived from the I-V relationships were fitted with equation [2.6] and the maximal conductance (G_{max}) was calculated as indicated in Materials and Methods (section 2.6.6.1). The dependence of the maximum conductance on $[MgCl_2]_i$ is shown in Figure 4.3*B*. Statistical analysis in comparison to that in the absence of $MgCl_2$ shows a significant decrease in G_{max} in 10 mM $MgCl_2$ (P<0.0002).

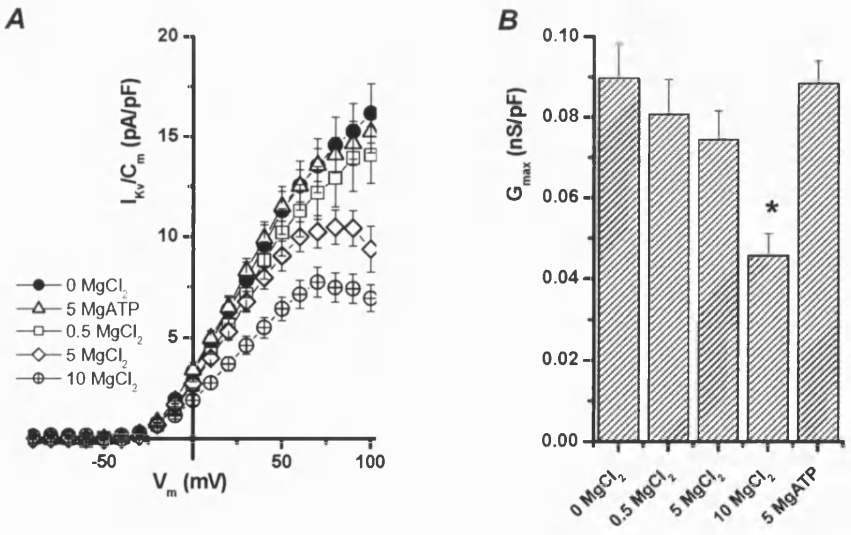

Figure 5.3. I-V relationships for I_{Kv} measured in various pipette $[MgCl_2]$ and 5 mM MgATP. ***A***, peak currents were measured in 15, 12, 21 and 20 cells for 0, 0.5, 5, 10 mM $MgCl_2$ and 35 cells for 5 mM MgATP, respectively, leak corrected and expressed in current density. ***B***, maximum conductance density reported versus the pipette $[MgCl_2]$ and [MgATP] (in mM).

5.1.2 Steady-state activation and availability of I_{Kv} in different $[MgCl_2]_i$

The steady state activation parameters, V_a and k_a, obtained from the fit of individual conductance-voltage relationships derived from the I-V relationships shown in Figure 5.3*A* were averaged and compared in Table 5.2.

Table 5.2. Voltage-dependent activation parameters in various $[MgCl_2]_i$ and $[MgATP]_i$.

Concentration (mM)	V_a (mV)	k_a (mV)	ΔV_a
0 $MgCl_2$	7.9±2.1 (15)	-16.0±0.5 (15)	0
0.5 $MgCl_2$	7.3±1.6 (12)	-15.2±0.5 (12)	-0.6±2.6 (12)
5 MgATP	4.1±1.7 (7)	-15.0±0.5 (7)	-3.8±3.6 (7)
5 $MgCl_2$	3.3±1.8 (21)	-13.6±0.5 (21)	-4.6±3.2 (21)
10 $MgCl_2$	2.9±2.0 (20)	-15.7±1.1 (20)	-5.0±4.2 (20)

ΔV_a indicated mV of difference with respect to the values measured in 0 mM $[MgCl_2]_i$. The error for each ΔV_a was calculated as $\sqrt{(s.e.m.(0))^2 + (s.e.mMg)^2}$ (Taylor, 1997), where *s.e.m.(0)* is the standard error of the mean in 0 $MgCl_2$, and *s.e.m.Mg* is the standard error of the mean for a given $[MgCl_2]_i$.

No significant differences in the obtained V_a and k_a were found in any of these conditions.

I_{Kv} inactivation in various pipette $[MgCl_2]$ or [MgATP] was measured using the availability protocol (Materials and Methods, section 2.6.6.4). Table 5.3 summarises the mean V_h, k_h and I_{ss} obtained from the Boltzmann fit of I_{Kv} availability dependency in each cell.

Table 5.3. Voltage-dependent inactivation parameters in various $[MgCl_2]_i$ and $[MgATP]_i$.

Concentration (mM)	V_h (mV)	K_h (mV)	I_{ss}	ΔV_h
0 $MgCl_2$	-43.5± 1.8 (5)	9.2 ± 0.4 (5)	0.18 ± 0.03 (5)	0
0.5 $MgCl_2$	-45.4 ± 1.7 (6)	8.4 ± 0.5 (6)	0.18 ± 0.04 (6)	-1.9±2.5 (6)
5 MgATP	-45.2 ± 1.8 (27)	9.2 ± 0.5 (27)	0.23 ± 0.02 (27)	-1.7±2.5 (27)
5 $MgCl_2$	-49.6 ± 1.9 (21)	9.3 ± 0.5 (21)	0.19 ± 0.02 (21)	-6.1±2.6 (21)
10 $MgCl_2$	-56.5 ± 3.1 (13)*	9.9 ± 0.5 (13)	0.14 ± 0.02 (13)	-13.0±3.6 (13)

* indicates values significantly different with 0 mM $MgCl_2$ condition. Error for ΔV_h was indicated as in the legend to Table 5.2.

The comparison of the mid-points of I_{Kv} inactivation demonstrated a progressive shift to the right by ~6 and ~13 mV (P<0.03) when the $[MgCl_2]_i$ was increased to 5 and 10 mM, respectively (Fig.5.4*A*). Changes in V_h in $[MgCl_2]_i$ = 10 mM were significantly (P<0.03) different from those measured in 0 or 0.5 mM $MgCl_2$ or 5 mM MgATP (Fig.5.4). Similarly to k_a, the slope factor of inactivation dependency, k_h, was not significantly affected.

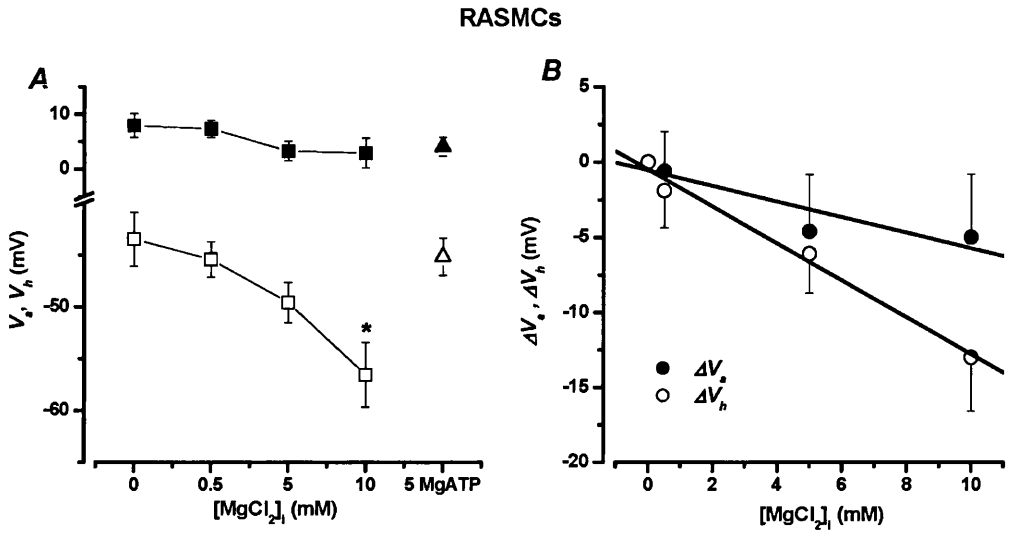

Figure 5.4. Summary of the effect of $[MgCl_2]_i$ and 5 mM MgATP on V_a and V_h in RASMCs. ***A***, Averaged V_a (open symbols) and V_h (filled symbols) are reported versus the corresponding concentration of the Mg-salt applied in the intracellular solution. ***B***, shows the Mg^{2+} dependence of the relative shift in V_a (ΔV_a) and V_h (ΔV_h). Continuous lines are linear fits with slope equal to –0.52 (V_a) and –1.2 (V_h) mV/mM. Asterisks near symbols indicate a significant difference with the control (0 mM $[MgCl_2]_i$).

5.1.3 Effect of intracellular acidification on I_{Kv} activation and inactivation

Changes in intracellular ionic composition can potentially affect the voltage dependent parameters via "screening" of negative surface charges present at the intracellular side of the membrane (Hille, 2001; McLaughlin *et al.*, 1971). The difference in V_a and V_h (Table 5.2 and Fig.5.3) indirectly suggest that the effect of Mg^{2+} on I_{Kv} is unlikely to be due to a simple "screening" of surface charges in the vicinity of the Kv channel intracellular mouth. If this was the case, similar changes of V_a and V_h would be expected. To evaluate whether the Mg^{2+}-dependent shifts in V_h and V_a could be due to an effect of charge screening at the intracellular side of the cell membrane, the effect of intracellular pH on activation and inactivation of I_{Kv} in RASMCs was investigated.

Protons are known to be potent modulator of the voltage dependent characteristics of a number of ion channels due to their interaction with surface charges (Hille *et al.*, 1975; Smirnov *et al.*, 2000; Ahn & Hume, 1997). An increase in intracellular proton concentration was achieved by lowering the pH from 7.2 to 6.2. Figure 5.5*A* shows averaged steady state activation and inactivation dependencies from 12 and 8 cells at pH 7.2 and 6 and 10 cells at pH 6.2, respectively. It is clear that this degree of acidification did not significantly affect the activation nor the inactivation of I_{Kv} with V_a equal to 7.3±1.6 and 8.6±1.5 mV for pH 7.2 and 6.2, respectively and V_h equal to -45.4±1.7 and –46.3±2.3 mV for pH 7.2 and 6.2, respectively. It is noteworthy that the inactivation dependency demonstrated an upward deflection in the current amplitude at $V_m > 10$ mV which resembles the U-shaped inactivation first described for cloned Kv2.1 channel (Klemic *et al.*, 1998).

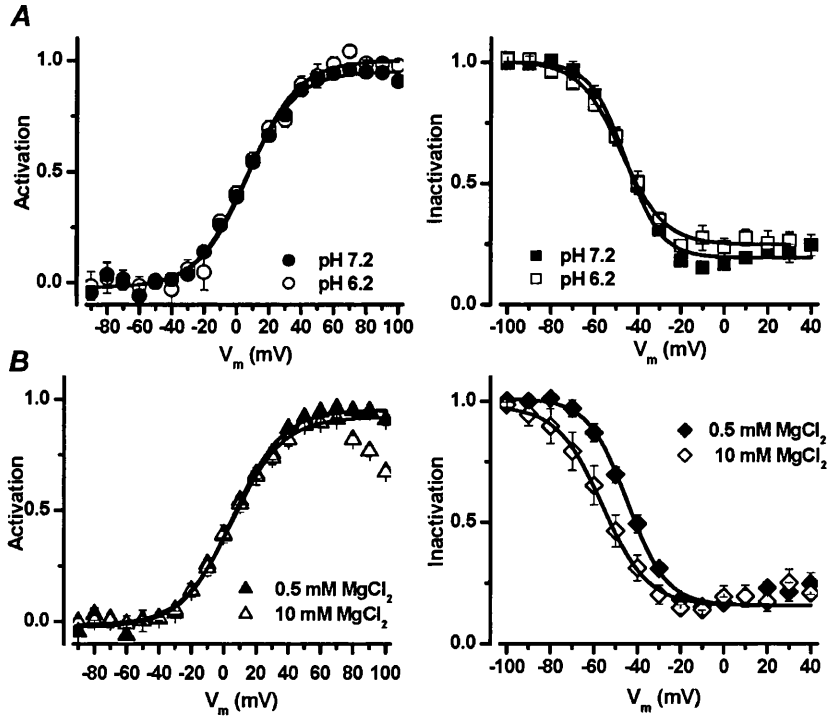

Figure 5.5. Effect of intracellular pH on activation and inactivation dependencies of I_{Kv} in RASMCs. ***A*** shows the averaged activation and inactivation dependencies recorded at pH 7.2 and 6.2. Pipette solution contained 0.5 $MgCl_2$. Continuous lines represent fits with the Boltzmann equation (eq. [2.6] and [2.9] for activation and inactivation, respectively) giving the values of V_a = 5.3 and 7.1 mV, k_a = 15.4 and 15.4 mV for activation and V_h = -45.4 and -47.3 mV, k_h = -8.2 and -9.8 mV, I_{ss} = 0.19 and 0.25 for inactivation at pH 7.2 and 6.2 respectively. ***B***, activation and inactivation curves in presence of 0.5 and 10 mM $[MgCl_2]_i$ at pH 7.2, shown for comparison. The fit with the Boltzmann equation gave the values of V_a = 5.3 and 5.2 mV, k_a = 15.4 and 15.6 mV for activation and V_h = -45.4 and -56.1 mV, k_h = -8.2 and –10.4 mV, I_{ss} = 0.16 and 0.16 for inactivation, in 0.5 and 10 mM $[MgCl_2]_i$, respectively.

5.2 Discussion: effect of intracellular Mg^{2+} on I_{Kv} in rat aortic myocytes

The increase of [$MgCl_2$] in the pipette solution caused several significant effects on I_{Kv} in RASMCs. Firstly the amplitude of I_{Kv} saturated and the maximal conductance was progressively decreased at high (5-10 mM) $[MgCl_2]_i$; secondly, a significant slowing down in I_{Kv} activation kinetics was observed in the presence of different $[MgCl_2]_i$; finally, the inactivation dependence of I_{Kv} was progressively shifted to more negative membrane voltages while no significant effect on the steady-state activation dependency was found. The similarity of the effects on I_{Kv} observed in 0 and 0.5 mM $MgCl_2$ and 5 mM MgATP, which correspond to 0.58 and 0.32 mM free $[Mg^{2+}]_i$ respectively, strongly suggests that these effects are associated with Mg^{2+} and not determined by ATP. The significant reduction of G_{max} in high $[MgCl_2]_i$, together with the inward rectification of the current occurring at higher potentials (see Fig. 5.3*A*), are consistent with a blocking effect that free Mg^{2+} could exert on Kv channels (Hille, 2001). The Mg^{2+}-dependent shift in I_{Kv} inactivation dependency, not coupled with a parallel shift in the activation curve was further investigated. The effects of extracellular and intracellular divalent cations, including Mg^{2+}, on the voltage dependent characteristics of Ca^{2+} and Na^+ and some K^+ channels has been well characterised (for review see Hille, 2001) and it is mainly attributed to the interaction with ("screening") fixed negative surface charges in the close vicinity of the channel mouth (see e.g. Hille *et al.*, 1975). In order to examine the hypothesis that the observed changes in V_h in RASMCs occurred as an effect of surface charge screening by Mg^{2+}, the effect of another cation, the protons, on the voltage dependency of I_{Kv} activation and inactivation were studied. Bringing the pH from 7.2 to 6.2, a degree of acidification that causes shifts in the voltage dependent characteristics of K^+ channels, via interaction with negative surface charges (Ahn & Hume, 1997), did not have any effect on I_{Kv} voltage-dependent characteristics in RASMCs. This observation suggests that the density of intracellular negative charges near the channel with which protons can interact is quite low and the Mg^{2+}-dependent shifts in I_{Kv} inactivation in RASMCs are unlikely to be mediated by this mechanism.

It should be said that an increase of [$MgCl_2$] in the pipette solution to 10 mM changes osmolarity of the solution by 11%. This change in osmolarity can cause cell swelling and potentially affect the interpretation of the observed effect. The activation of various voltage-independent Cl^- and non-selective conductances by reducing tonicity of external

solutions has been demonstrated in endothelial, smooth muscle and other cell types (e.g. (Nilius & Droogmans, 2001; Large, 2002; Baumgarten & Clemo, 2003). Cell swelling induced by 70-60% hypotonic solutions also activated various voltage-dependent conductances including Ca^{2+} channels (Matsuda *et al.*, 1996; Kim *et al.*, 2000) and K^+ channels (Kubota *et al.*, 2002; Zhou *et al.*, 1997). Importantly, no significant effect on voltage-dependent characteristics (e.g. activation and inactivation) was however found (Matsuda *et al.*, 1996; Kim *et al.*, 2000; Kubota *et al.*, 2002), strongly suggesting that the observed changes in activation and inactivation dependencies of Kv currents in rat aortic and pulmonary SMCs under my experimental conditions were not due to a small change in osmolarity of the pipette solution. In addition, no significant effect on the slope conductance was found during cell dialysis with different pipette [$MgCl_2$], suggesting that activation of stretch-activated channels did not occur.

The effect of intracellular Mg^{2+} on I_{Kv} in RASMCs is different from that of Kv channels in canine pulmonary myocytes previously described by Gelband et al. (1992). In this type of SMCs, a marked inhibition of the Kv current in the presence of 20 mM $MgCl_2$ in the pipette solution was found, although no detailed characterisation of the voltage dependent characteristics was presented. The authors also reported a similar inhibition of the Kv currents by 100 μM 2-(2-aminoethyl)pyridine (a H1 receptor agonist) or 10 μM ryanodine, agents that cause an increase in $[Ca^{2+}]_i$ (Gelband & Hume, 1992). Based on their findings, Gelband et al. proposed that Kv channels in canine PA myocytes are directly blocked by divalent cations. Elevation of the pipette $[Ca^{2+}]$ to 200 nM in RASMCs, however, did not affect the I_{Kv} (see Chapter 3). Therefore, the effect of intracellular Mg^{2+} I described in RAMSCs represents a novel mechanism through which Kv channel activity can be modulated. The differences between my findings and those reported by Gelband et al (1992) might rely on the expression of different Kv isoforms or on variable Mg^{2+}-dependent regulatory components in different types of SMCs. To examine the possibility of the former, the effect of intracellular Mg^{2+} was studied in rat main PASMCs, which revealed two sub-types of cells expressing different Kv channel currents. Possible physiological implications of the Mg^{2+}-dependent modulation of I_{Kv} is discussed in Chapter 7.

5.3 Effect of intracellular Mg^{2+} on the voltage-dependent characteristics of I_{Kv} in main pulmonary arterial smooth muscle cells

Before describing the effect of Mg^{2+} on Kv currents in PASMCs, electrophysiological and pharmacological evidence in favour of two sub-populations of SMCs expressing distinct Kv currents are presented in the next section of this chapter.

5.3.1 Two pulmonary arterial cell subtypes expressing different Kv channel currents

I_{Kv} was recorded in the presence of 1 μM paxilline and 10 μM glibenclamide in order to eliminate any residual contamination by BK_{Ca} and/or K_{ATP} channel currents, respectively. Moreover, in these experiments the pipette solution contained 5 mM MgATP. Two types of I_{Kv} were observed under these conditions (Fig. 5.6). In the majority of cells (39/66) (that will be termed I_{K1}), the current was of high amplitude (1574±146 pA at +60 mV) and activated rapidly (Fig. 5.8*A*). In a minority of cells (27/66) (termed I_{K2}), the current activated more slowly, and was much smaller (308±41 pA; $P<0.0001$) (Fig. 5.8*B*). The difference in amplitude was not due to cell size, since the membrane capacitance was not significantly different between two groups of cells (16.5±1.2 pF, n=39, and 19.7±1.8 pF, n=27, respectively). Moreover, the larger current showed very little sensitivity to TEA, even 20 mM caused a little block. On the other hand, in cells with a smaller Kv current, the current was mostly blocked by 20 mM TEA (compare *A* and *B* in Fig. 5.6).

The relationship between the percentage of block by 20 mM TEA has been plotted against the current density and $t_{1/2}$ (the time taken for the current to attain 50% of its maximal amplitude) measured at +60 mV in 59 cells. It is clear that, based on these two characteristics, the currents fall into 2 groups. The amplitude of the peak I_{Kv} in both groups was also significantly different. In the group (n=39) which was more sensitive to 20 mM TEA (> 55% block), the mean $t_{1/2}$ was 7.4±0.4 ms, the mean current density was 17±1.3 pA/pF, and the mean current amplitude was 268±31 pA. In the group which was relatively insensitive to TEA (< 35% block), the mean $t_{1/2}$ was 3.6±0.2 ms, the mean current density was 103±10 pA/pF, and the current amplitude was 1416±147 pA (n=27). For each of these parameters a highly significant difference was seen between the 2 groups of cells ($P<0.003$). Figure 5.6*D* shows the I-V relationships, and the effect of 20

mM TEA in these two groups of cells. TEA significantly blocked the current in both groups (P<0.0001 at +60 mV), but the extent of the block differed greatly between the groups over a wide range of potentials. It is noteworthy that some characteristics of I_{K2}, such as TEA sensitivity, slow activation kinetics and small current density were remarkably similar to those of I_{Kv} in rat aorta recorded under the same experimental conditions. For example, the densitiy of I_{Kv} at +60 mV was 12.5±0.8 pA/pF (n=35) in RASMCs and 14.5±2.7 pA/pF (n=7) in I_{K2} PASMCs and the time constant of activation (τ_a) at +60 mV was 8.1±0.7 ms (n=35) in RASMCs and 9.7±2.9 ms in I_{K2} PASMCs. To stress the similarity between I_{K2} and I_{Kv}, corresponding data for I_{Kv} in RASMCs were compared in Figure 5.6, 5.7, 5.8 and 5.9.

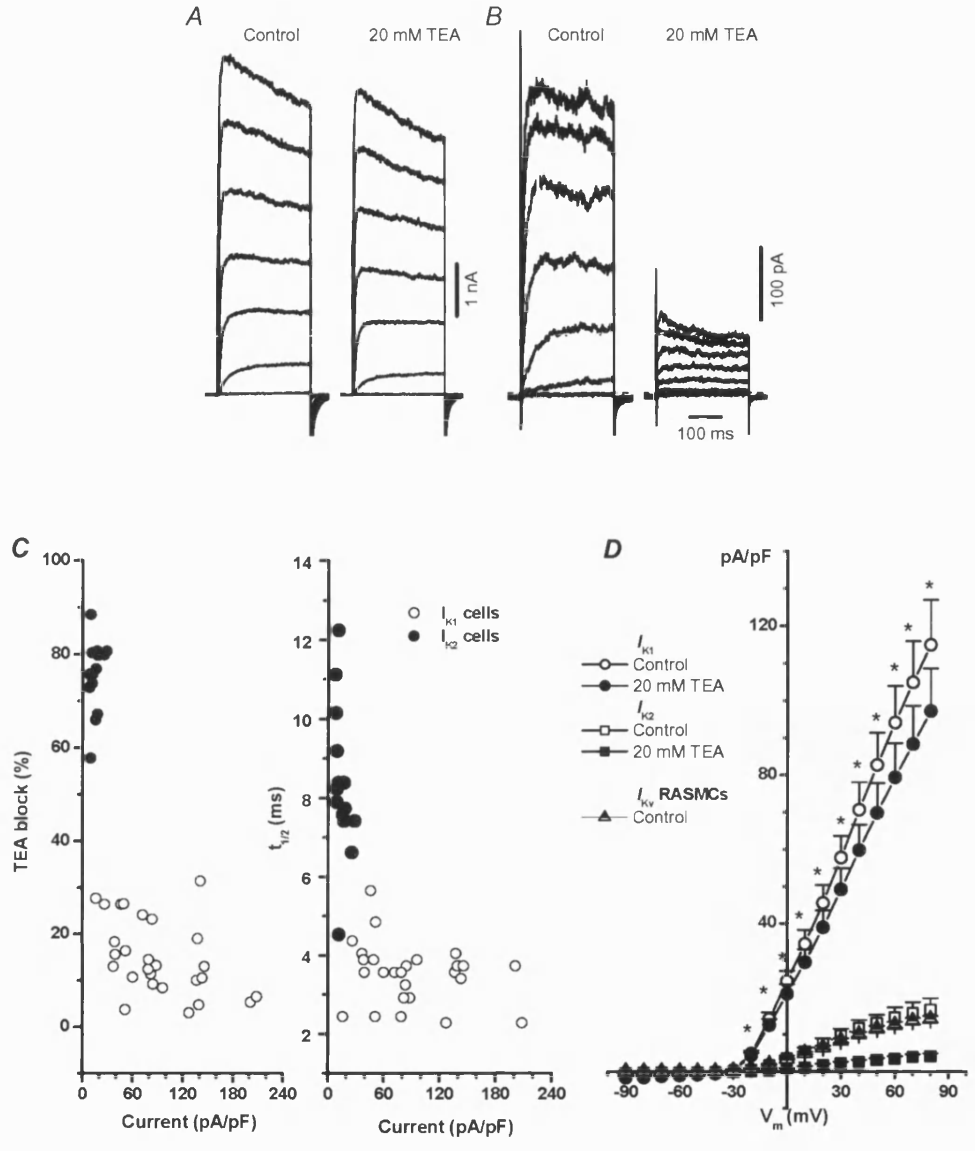

Figure 5.6. Two subpopulations of cells in rat conduit PA. ***A*** and ***B*** show families of I_{Kv} recorded from two representative cells in response to a 300 ms membrane depolarisation between –40 to +80 mV in 20 mV increments and the effect of 20 mM TEA on the current. Holding potential was –80 mV. C_m equal 16.3 (***A***) and 14.4 (***B***) pF. Horizontal dashed lines indicate zero current level. ***C***, relationship between the current density, percentage of TEA (20 mM) block and half-time to the maximum I_{Kv} amplitude ($t_{1/2}$) in 59 rat conduit PASMCs. All parameters were measured at the test potential of +60 mV. ***D***, I-V relationships for I_{K1} (n=26) and I_{K2} (n=7) in two groups of cells in the absence and presence of 20 mM TEA as indicated. Asterisks show significant differences between I_{K1} and I_{K2} densities under both conditions (P<0.003). For comparison, current density measured in 35 RASMCs is plotted as triangles in ***D***.

Another similarity between I_{K2} and I_{Kv} in RASMCs was sensitivity to TEA. TEA blocked I_{K2} with a mean IC_{50} equal to 2.6±0.1 mM (n=6), compared with 3.2±0.7 mM (n=3) for I_{Kv} in RASMCs. As mentioned, I_{K1} was not sensitive to TEA, being blocked by only 18±2.4% (n=26) by 20 mM of the drug (Fig. 5.7*A*). On the other hand, 4-AP potently inhibited I_{K1} with IC_{50} = 99±12 μM (n=6). However, I_{K2} current was suppressed by only 37±3 % (n=5) at 20 mM 4-AP. A similar degree of 4-AP block was also observed in RASMCs (Fig. 5.7*B*).

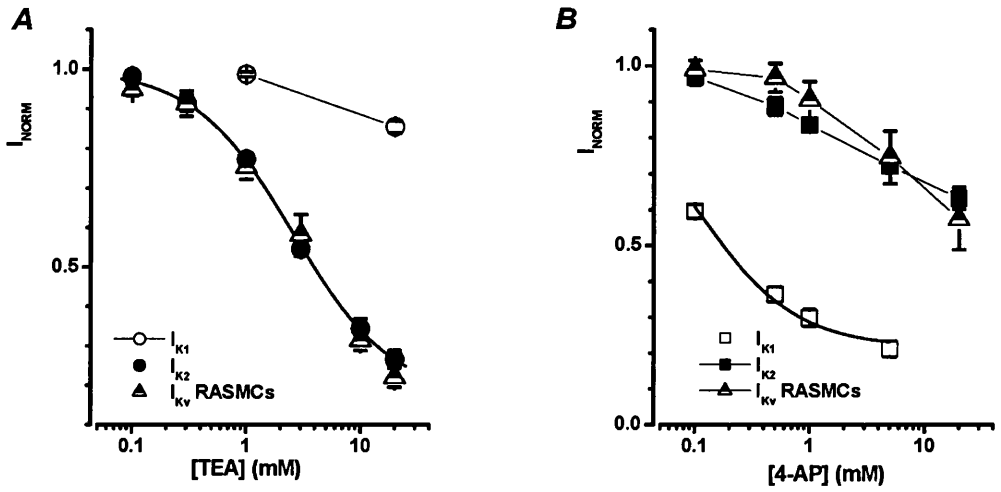

Figure 5.7. Effect of TEA and 4-AP on I_{Kv} in rat conduit PASMCs. *A* shows the inhibition of I_{K2} (solid circles, n=6) and I_{K1} (open circle, n=4 and 26 for 1 and 20 mM, respectively) by various external concentrations of TEA. Solid line through filled circles is drawn according to the equation [3.1], with IC_{50} = 2.6 mM and residual component A equal 0.17. Data for I_{Kv} in RASMCs (n=3) are reported (triangles) for comparison *B*, concentration-dependence of the block of I_{K1} (open squares) and I_{K2} (solid squares) by 4-AP. Solid line through circles is drawn according to the equation [3.1] with IC_{50} = 0.10 mM and residual component A equal 0.21. Data for I_{Kv} in RASMCs (n=6) are reported (triangles) for comparison. The lines through open circles in *A* and through the solid squares and triangles in *B* are drawn by eye.

In both I_{K1} and I_{K2} cells, the kinetics of activation of the outward current could be well fitted by a single exponential function over a wide range of potentials, as shown in Fig. 5.8*A* and *B*. Figure 5.8*C* demonstrates that the resulting time constants of activation of I_{K2} were significantly greater than those for I_{K1} at all test potentials between -20 and +80 mV. Remarkably, τ_a for I_{K2} were also similar to I_{Kv} in rat aortic SMCs (Fig. 5.8*C*).

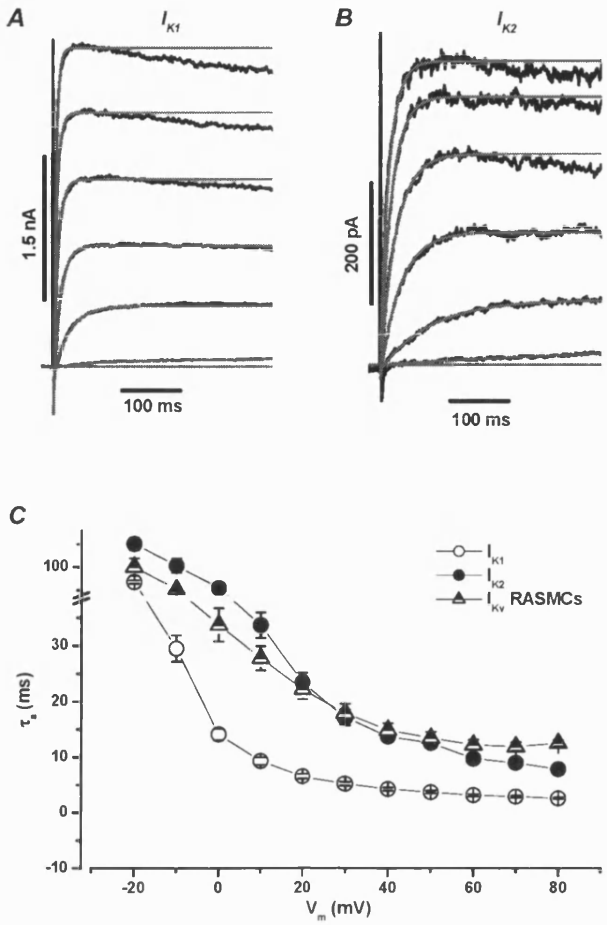

Figure 5.8 Activation of I_{K1} and I_{K2} in rat conduit PASMCs. ***A*** and ***B*** show a family of I_{K1} and I_{K2}, respectively, recorded from two representative cells and fitted with a monoexponential function (eq. [2.1]) (grey lines). C_m was 21 (***A***) and 19.9 (***B***) pF. *C*, illustrates dependence of τ_a for I_{K1} (open circles, n=39 and I_{K2} (filled circles, n=27) on the membrane potential. For comparison, mean τ_a for I_{Kv} in 35 RASMCs are shown as triangles.

The voltage-dependency of current availability in I_{K1} and I_{K2} cells was studied with the availability protocol (Materials and Methods, section 6.2.2.4). Examples of typical experiments are shown in Figure 5.9*A* (I_{K1}) and *B* (I_{K2}), and the mean availabilities derived from a number of similar experiments are depicted in Figure 5.9*C*. I_{K2} inactivated to a greater extent, and over a more negative potential range, compared to I_{K1}. When the data were fitted with the Boltzmann function (eq. [2.9]), V_h, was -39.1±2.3 mV (n=13) in I_{K2} cells, and the maximal degree of inactivation was 77%. In contrast, in I_{K1}, V_h was -20.2 ± 1.6 mV in I_{K1} (n=13, $P < 0.0001$) cells, and the maximal level of inactivation was 62% ($P < 0.0001$). Moreover, as the conditioning potential was

made progressively more positive, the current in I_{K2} cells began to increase again. The U-shaped availability was never observed in I_{K1} cells, however, it was observed in I_{Kv} availabilities in RASMCs. In addition, I_{Kv} in RASMCs was also inactivated in a similar voltage range as I_{K2} (Fig. 5.9*C*).

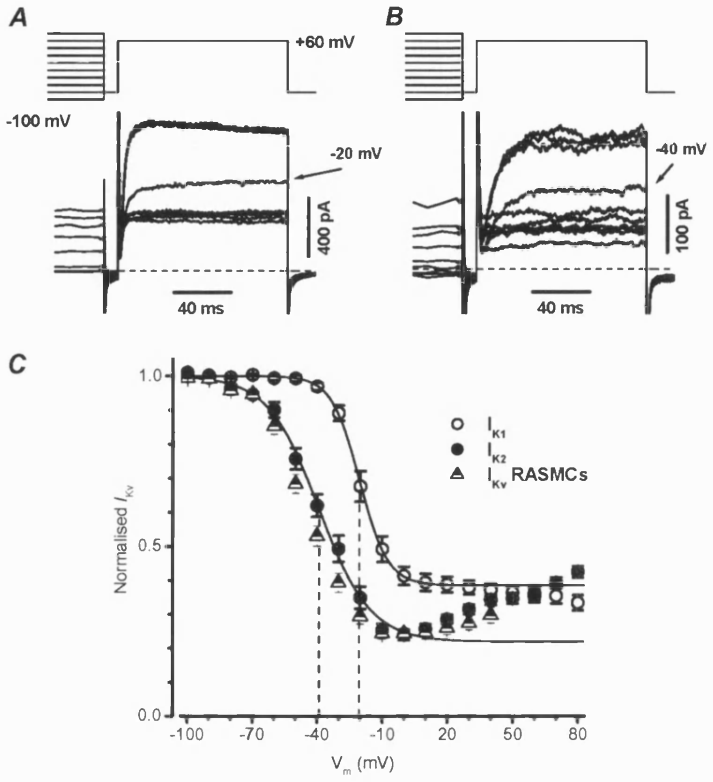

Figure 5.9. Inactivation of I_{K1} and I_{K2} in rat conduit PASMCs. ***A*** and ***B*** show families of I_{K1} (***A***) and I_{K2} (***B***) recorded according to the availability protocol with the conditioning potential (V_m) incremented every 20 mV between –100 and +80 mV. C_m were 15.9 (***A***) and 22.4 (***B***) pF. ***C***, dependence of the normalised I_{K1} (open circles, n=13) and I_{K2} (filled circles, n=13) on V_m. Solid lines were drawn according to the Boltzmann equation (eq. [2.9]) with half-inactivation potential (V_h, shown by dashed lines) equal –20.5 and –39.1 mV, slope factor of 6.5 and 11.9 mV and non-inactivating component I_{ss} equal 0.39 and 0.22 for I_{K1} and I_{K2}, respectively. For comparison, data from 35 RASMCs is reported as triangles.

5.3.2 Effect of intracellular Mg^{2+} on the voltage dependent characteristics of I_{K1} and I_{K2}

5.3.2.1 Current-voltage relationships in different $[MgCl_2]_i$

The comparison of pharmacological and biophysical characteristics of I_{K1} and I_{K2} in rat main PASMCs with those of I_{Kv} in RASMCs, showed a remarkable similarity in properties of I_{K2} and I_{Kv}, which were significantly different from those of I_{K1}. To assess whether changes in intracellular Mg^{2+} have differential effect on the voltage-dependent properties of I_{K1} and I_{K2}, intracellular $[Mg^{2+}]$ was varied by changing $MgCl_2$ in the pipette solution in a similar manner as described for RASMCs. Fig. 510 compares the average peak current (expressed in pA/pF) measured with the I-V protocol in various pipette $[MgCl_2]_i$ for I_{K1} (*A*) and I_{K2} (*B*). The comparison clearly shows that the effect of intracellular $MgCl_2$ on I_{K1} and I_{K2} is different. I_{K1} was strongly suppressed at high $[MgCl_2]_i$. For example, the current density at +100 mV was equal to 153.6±31.6 (n=8), 101.2±21.9 (n=6), 83.1±7.0 (n=9), and to 74.4±11.0 pA/pF for 0, 0.5, 5 and 10 mM $[MgCl_2]_i$, respectively. I_{K2} was inhibited to a lower degree but showed a marked voltage-dependent rectification similary to the effect observed for I_{Kv} in RASMCs (Fig. 5.3*A*). The I_{K2} density at +100 mV was equal to 22.4±1.6 (n=11), 21.8±3.4 (n=13), 17.6±2.3 (n=14) and 15.7±2.1 (n=15) for 0, 0.5, 5 and 10 mM $[MgCl_2]_i$ respectively.

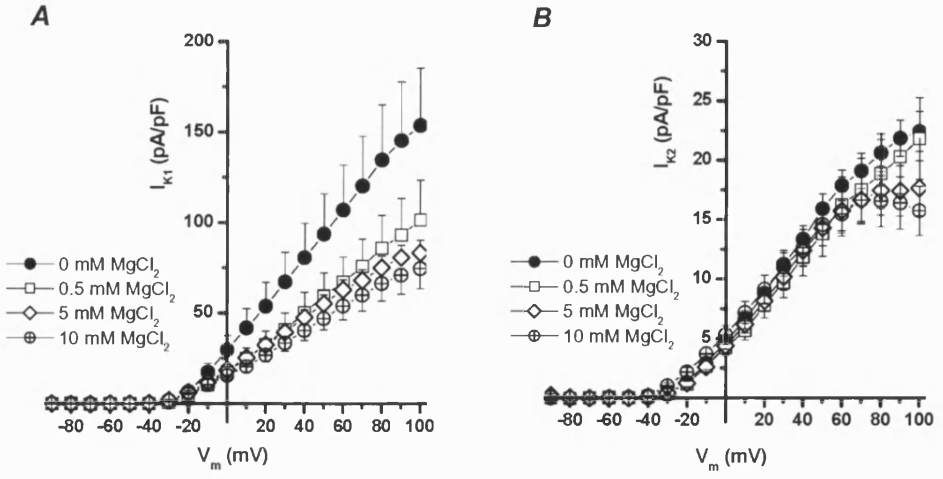

Figure 5.10. I-V relationships for I_{K1} and I_{K2} in various $[MgCl_2]_i$. The peak amplitude of I_{K1} (*A*) and I_{K2} (*B*) (measured using the I-V protocol) was leak corrected and expressed as current density. Number of experiments was equal to 8, 6, 9 and 11 for I_{K1} and 12, 15, 14 and 15 for I_{K2} in 0, 0.5, 5 and 10 mM $[MgCl_2]_i$ respectively.

5.3.2.2 Effect of intracellular Mg^{2+} on I_{K1} and I_{K2} activation

Steady-state activation curves for I_{K1} and I_{K2} cells were recorded using the I-V protocol (Materials and Methods, section 2.6.6.1). Voltage-conductance relationships obtained from the I-Vs recorded in the absence and presence of various $[MgCl_2]_i$ were normalised and fitted according to the Boltzmann equation (eq. [2.6]). Figure 5.11 (*A* and *B*, left panels) compares the averaged potential-conductance dependences in I_{K1} (*A*) and I_{K2} (*B*) cells in the absence (open circles) and in presence (filled circles) of 10 mM $[MgCl_2]_i$. Table 5.4 summarises values of V_a and k_a in various concentrations of pipette $[MgCl_2]$. This analysis clearly shows no significant effect of intracellular Mg^{2+} on the steady-state activation of I_{K1} (~3-4 mV negative shift), while that for I_{K2} was progressively shifted by about 12 mV to more negative potentials. No significant effect of intracellular Mg^{2+} on the slope of potential-conductance dependencies for both Kv currents was found.

Activation kinetics I_{K1} and I_{K2} were analysed in the absence and presence of 10 mM $[MgCl_2]_i$ and compared in Fig. 5.11 (right panels). Although a small increase in the rate of I_{K1} time constant was observed, these differences were not significant. No marked effect on the I_{K2} activation time constant was observed.

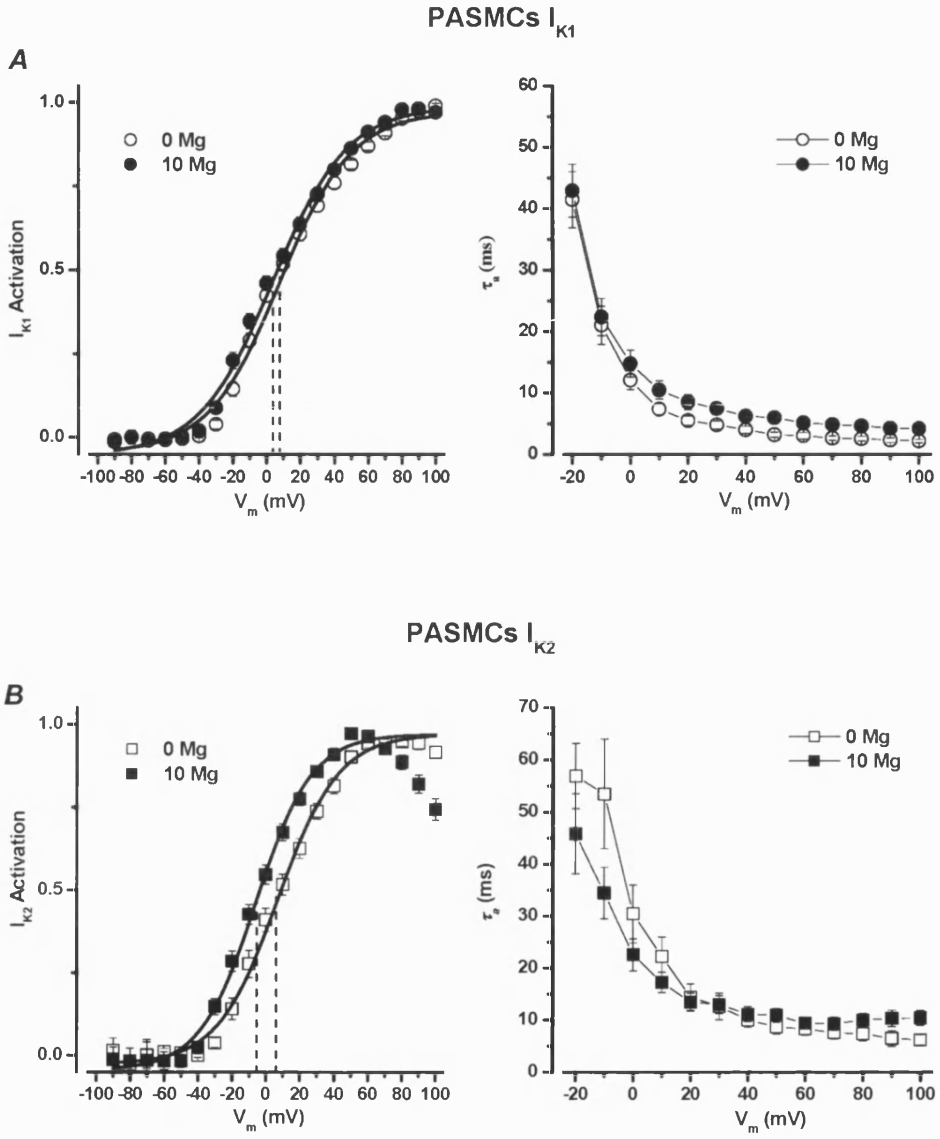

Figure 5.11. Activation in I_{K1} and I_{K2} cells. ***A***, left panel shows the averaged steady-state activation dependencies in the absence (n=11, open circles) and in the presence of 10 mM $[MgCl_2]_i$ (n=11, filled circles) in I_{K1} cells. Continuous lines represent the fit with the equation [2.6], giving V_a equal 7.9 and 3.9 mV and k_a equal –21.4 and –21.9 mV in 0 and 10 mM $[MgCl_2]_i$ respectively. ***B***, in the left panel are the averaged I_{K2} steady-state activation curves in the absence (n=13) and in 10 mM $[MgCl_2]_i$ (n=15). Continuous lines represent the fit with [2.6] giving V_a equal to 7.3 and –4.4 mV and k_a equal to –16.9 and –16.8 mV for 0 and 10 mM $[MgCl_2]_i$ respectively. The right panels in ***A*** and ***B*** show τ_a versus V_m for I_{K1} and I_{K2} respectively measured in the same cells shown in the left panels.

Table 5.4. Comparison of I_{K1} and I_{K2} activation parameters.

	I_{K1}			I_{K2}		
$[Mg^{2+}]$ (mM)	V_a (mV)	k_a (mV)	ΔV_a (mV)	V_a (mV)	k_a (mV)	ΔV_a (mV)
0	9.8±2.0 (11)	-18.8±0.5 (11)	0	7.9±2.5 (13)	-16.6±0.5 (13)	0
0.5	10.5±3.3 (6)	-19.4±0.9 (6)	0.7±3.8 (6)	8.6±3.2 (16)	-16.6±0.7 (16)	0.7±4.1 (16)
5	6.1±2.2 (8)	-17.8±0.8 (8)	-3.7±2.9 (8)	2.5±2.9 (13)	-14.4±0.4 (13)	-5.4±3.9 (13)
10	6.5±2.4 (11)	-19.1±0.7 (11)	-3.3±3.1 (11)	-3.9±2.0 (15) *	-14.7±0.7 (15)	-11.8±3.3 (15)

ΔV_a indicated the relative changes in V_a at a given $[MgCl_2]_i$ in comparison to that at 0 $MgCl_2$. The error for each ΔV_a was calculated as described in the legend to Table 5.2. Asterisks indicate significant difference with the control (0 $MgCl_2$).

5.3.2.3 Effect of intracellular Mg^{2+} on I_{K1} and I_{K2} inactivation

The voltage dependence of I_{K1} and I_{K2} availability was evaluated as described in Materials and Methods (section 2.6.6.4). The current amplitude at the test potential was then plotted against the conditioning prepulse potential and fitted according to the equation (eq. [2.9]). The values of V_h, k_h, I_{ss} obtained in different pipette $[MgCl_2]$ are summarised in Tables 5.5 (I_{K1}) and 5.6 (I_{K2}). The averaged steady-state inactivation dependencies for I_{K1} and I_{K2} obtained in the absence and presence of 10 mM $MgCl_2$ were normalised and compared in Figure 5.12 (see also Fig. 5.13). Analysis of these data clearly shows that increase in the pipette $[MgCl_2]$ caused a large and significant shift ($P<0.0004$) of ~26 mV to the negative voltages for I_{K1} inactivation, while no significant effects on I_{K2} inactivation were observed. Interestingly, the non-inactivated fraction (I_{ss}) was also significantly ($P<0.01$) reduced by ~50% in PASMCs perfused with 10 mM $MgCl_2$.

Table 5.5 Inactivation parameters in I_{K1} cells.

	I_{K1}			
$[Mg^{2+}]$ (mM)	V_h (mV)	K_h (mV)	I_{ss}	ΔV_h (mV)
0	-23.1±1.9 (6)	11.2±2.1 (6)	0.28±0.03 (6)	---
0.5	-22.2±2.6 (7)	9.0±0.5 (7)	0.27±0.03 (7)	0.08±3.24 (7)
5	-33.9±0.6 (11) *	9.1±1.2 (11)	0.25±0.02 (11)*	-10.7±1.9 (11)
10	-49.4±4.8 (6) *	15.3±3.2 (6)	0.13±0.04 (6)*	-26.3±5.2 (6)

Table 5.6. Inactivation parameters in I_{K2} cells.

	I_{K2}			
$[Mg^{2+}]$ (mM)	V_h (mV)	k_h (mV)	I_{ss}	ΔV_h (mV)
0	-53.1±2.5 (8)	8.4±0.7 (8)	0.20±0.02 (8)	---
0.5	-52.1±2.7 (6)	9.4±1.8 (6)	0.18±0.02 (6)	1.04±3.64 (6)
5	-55.7±5.0 (10)	10.2±0.7 (10)	0.16±0.07 (10)	-2.6±5.6 (10)
10	-59.3±3.5 (11)	9.1±0.5 (11)	0.19±0.03 (11)	-6.14±4.32 (6)

In both table *5.5* and *5.6*, the error of the ΔV_h was calculated as described in the legend to Table 5.2. Asterisks indicate any significant difference to the control (0 $MgCl_2$).

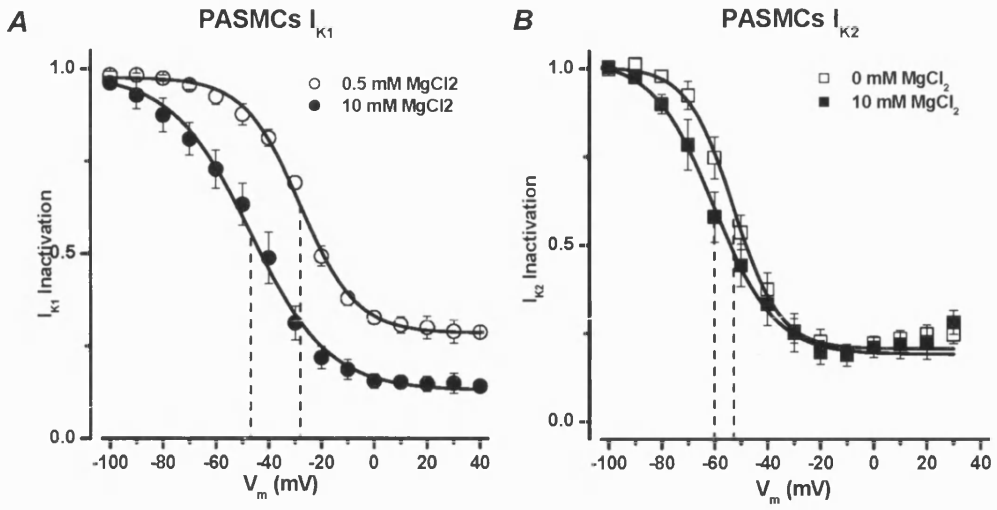

Figure 5.12. Effect of intracellular Mg^{2+} on the I_{K1} and I_{K2} inactivation. ***A*** and ***B*** show the averaged steady state inactivation dependencies for I_{K1} and I_{K2}, respectively, in 0 and 10 mM $[MgCl_2]_i$ as indicated. Fit with the Boltzmann equation (eq. [2.9]) gave the value of V_h=-24.0 and –48.5 mV, k_h=10.6 and 14.9 mV, non-inactivating fraction I_{ss}=0.28 and 0.13 in 0 mM and 10 mM $MgCl_2$, respectively for I_{K1} and V_h=-53.3 and –60.1 mV, k_h=8.2 and 10.5 mV, I_{ss}=0.22 and 0.22 in 0 and 10 mM $MgCl_2$, respectively, for the I_{K2}.

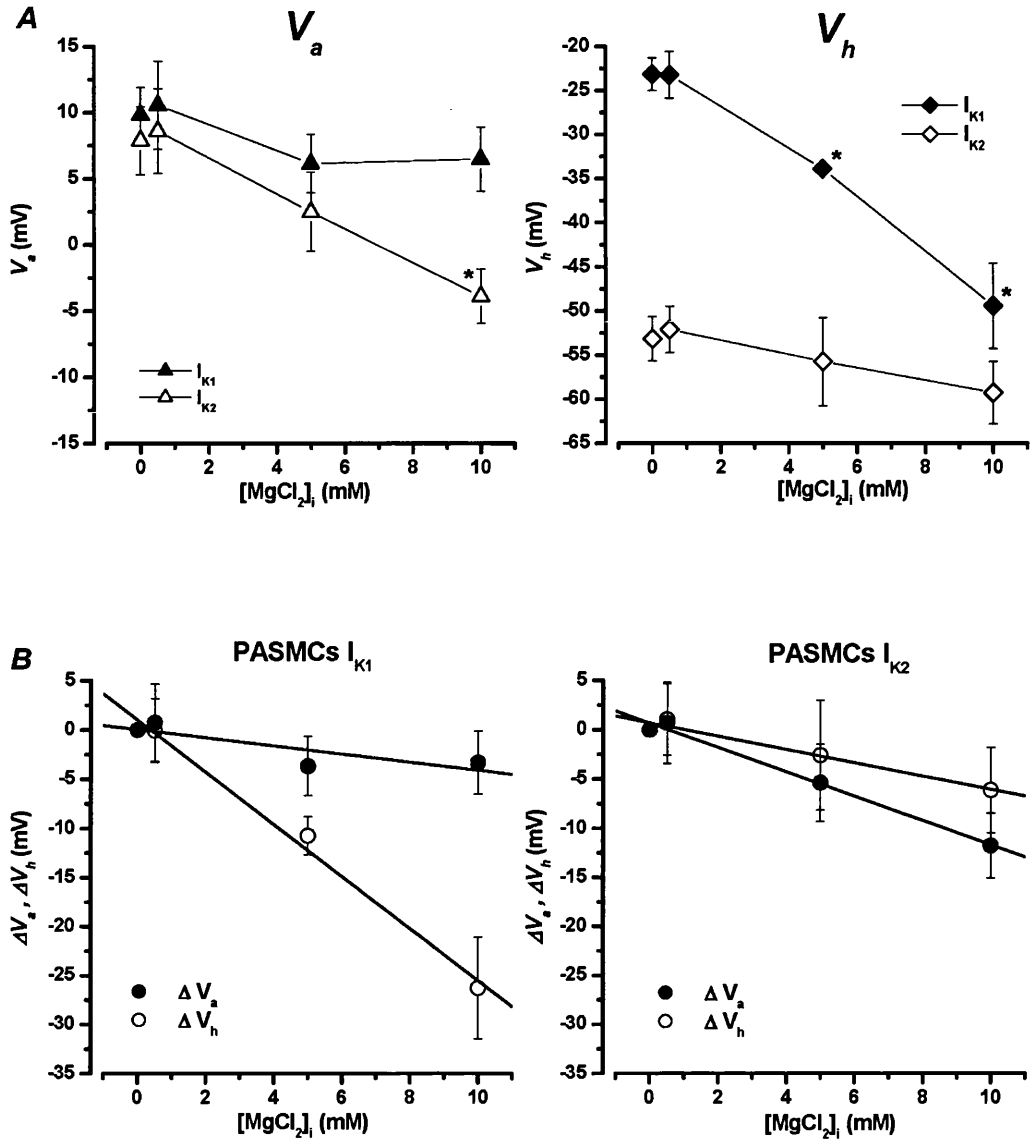

Figure 5.13. Summary of the effect of intracellular Mg^{2+} on the V_a and V_h in I_{K1} and I_{K2} cells. *A* shows the values of V_a (left panel) and V_h (right panel) reported versus the $[MgCl_2]_i$ for I_{K1} and I_{K2} cells. Asterisks near symbols indicate a significant difference with respect to the values measured in absence of $MgCl_2$. *B* shows the Mg^{2+}-dependence of the relative shift in V_a (ΔV_a) and V_h (ΔV_h) parameters for I_{K1} and I_{K2}. Continuous lines represent a simple linear regression fit with a slope of -1.17 mV/mM (ΔV_a) and –2.65 mV/mM (ΔV_h) for I_{K1} (left panel) and –0.85 mV/mM (ΔV_a) and –0.69 mV/mM (ΔV_h) for I_{K2} (right panel). Linear regression lines were drawn to provide a comparison between relative changes in these parameters.

5.4 Discussion: effect of intracellular Mg^{2+} on Kv channel currents in pulmonary artery myocytes

5.4.1 Effect of intracellular Mg^{2+} on I_{K1} and I_{K2}

In this chapter the effects of intracellular Mg^{2+} on the two cells subtypes present in the main pulmonary artery have been compared. An increase in $[MgCl_2]_i$ up to 10 mM produced a significant shift of about -12 mV in I_{K2} activation, while V_a for I_{K1} cells was not significantly different. In both cases the slope of steady-state activation dependencies was not affected. Notably, the inactivation dependencies for Kv currents were also affected differently in the two subpopulations of PASMCs. I_{K1} availability was significantly shifted by about 26 mV in the negative direction in 10 mM $[MgCl_2]_i$ in comparison to that in the absence of $MgCl_2$, while that for I_{K2} was not significantly different. The shift in the voltage dependent inactivation in I_{K2} was similar to that in the activation dependency. An additional selective effect on I_{K1}, but not I_{K2}, observed with an increase of $[MgCl_2]_i$ was a significant and progressive reduction of the non-inactivating component of the current observed with increase in $[MgCl_2]_i$. The differences in Mg^{2+}-sensitivity for activation and inactivation dependency of I_{K1} and I_{K2}, suggest that activation and inactivation gating mechanisms sense Mg^{2+} in a different manner. These results are not consistent with a direct involvement of fixed negative charges on the intracellular side of the membrane (see also discussion to Chapter 6). It is worth mentioning that the effect of intracellular Mg^{2+} on I_{K2} in PASMCs, having a greater effects on inactivation than activation, was opposite to those for I_{Kv} in RASMCs, where only the inactivation dependency was significantly affected. Taking into account that the properties and pharmacological profile of Kv current in I_{K2} cell subtypes in rat PASMCs is very similar to that of I_{Kv} in RASMCs, the differential effects of intracellular Mg^{2+} on voltage dependent parameters might point towards a cell specific regulation of Kv channel currents by this divalent cation. A possible mechanism which might be responsible for this differential intracellular Mg^{2+} sensitivity of Kv channel currents in VSMCs is not clear, however, it is worth noting that Mg^{2+} is an essential cofactor for various enzymes, including some protein phosphatases (Wang *et al.*, 1995; Zhou *et al.*, 2002). Therefore, the possibility that Mg^{2+} can act via this pathway cannot be ruled out.

There are a number of additional differential effects of intracellular Mg^{2+} on Kv currents in PASMCs, including a significant inhibition of the maximal I_{K1} conductance, whereas I_{K2} showed a prominent inward rectification. Interestingly (as will be discussed in Chapter 6), these results mimic the effects of Mg^{2+} on Kv1.5 and Kv2.1 expressed in *Xenopus* oocytes, respectively. A comparison of the effect of intracellular Mg^{2+} on native currents with those of cloned Kv channels could also provide important information about the molecular identity of Kv currents in VSMCs.

5.4.2 Molecular identity of I_{K1} and I_{K2}

Data described at the beginning of this chapter strongly suggested a heterogeneity of Kv channel currents in the rat PA vasculature. About 67% of 85 conduit PASMCs studied demonstrated a large TEA-insensitive and 4-AP-sensitive current termed I_{K1}, whereas a relatively small TEA-sensitive and moderately 4-AP sensitive current, designated as I_{K2}, was recorded in the remaining 33% of conduit PA myocytes. I_{K1} and I_{K2} were also distinct in their kinetics of activation and voltage-dependence of inactivation. In addition to differences in biophysical and pharmacological properties, I_{K1} and I_{K2} had a differential sensitivity to intracellular Mg^{2+}.

The exact molecular identity of Kv channel genes which are responsible for the native Kv currents in pulmonary arteries remains inconclusive although recent evidence strongly suggests that Kv1.2, Kv1.5, Kv2.1 and Kv3.1b α-subunits are the most likely candidates (Coppock *et al.*, 2001). We have demonstrated that Kv1.2, Kv1.5 and Kv2.1 α-subunits were expressed in both conduit and resistance arteries isolated from rat and revealed by immunoblot analysis (published in Smirnov *et al.*, 2001). In addition, comparison of the pharmacological and biophysical profile of I_{K1} and I_{K2} with those reported for cloned delayed rectifier channels suggests that the Kv1.5 channel profile corresponds closely to that of I_{K1}, whereas I_{K2} mimics the properties of the Kv2.1 channel (Table 5.7). Homomultimers of Kv1.1, Kv1.2 and Kv1.6 are unlikely to be responsible for I_{K1}, since the Kv currents in PASMCs were insensitive to high concentrations of DTx (200 nM) and only slightly sensitive to TEA (20 mM), observations which are similar to those described previously for Kv currents in rat resistance PA (Patel *et al.*, 1997; Smirnov *et al.*, 2001). The presence of the Kv1.2 α-subunit protein in conduit arteries is consistent with the possibility that I_{K1} could be

encoded by Kv1.2/Kv1.5 heteromultimers (published in Smirnov *et al.*, 2001). It has been previously shown that Kv1.2/Kv1.5, but not Kv1.1/Kv1.5 (Hatton *et al.*, 2001), heteromultimers become insensitive to DTx and also ChTx (Russell *et al.*, 1994; Hulme *et al.*, 1999). A functional contribution of Kv3.1b to both types of Kv currents in rat PASMCs can be ruled out, since this current is potently blocked by micromolar doses of both TEA and 4-AP (Table 5.7).

Table 5.7. Comparison of some electrophysiological and pharmacological properties of the native Kv currents in rat PASMCs and cloned Kv channels.

	I_{K1}	I_{K2}	Kv1.1 [a,b]	Kv1.2 [a,b]	Kv1.5 [a,b]	Kv1.6 [c]	Kv2.1 [d]	Kv3.1b [a]
Rate of activation	Rapid	Slow	Rapid	Rapid	Rapid	Rapid	Slow	Rapid
U-shape of inactivation	No	Yes	No	No	No	No	Yes [e]	No
TEA†	> 20	2.6	0.3 - 0.6	> 200	> 200	4	3 – 10	0.1 – 0.2
4-AP†	0.23; 0.35	> 20	0.29 - 1	0.6 – 0.8	0.17 – 0.5	0.3	5 - 100	0.03 – 0.1
DTX‡	> 200	> 200	12 - 20	4 – 17	> 1000	9 - 25	ND	> 1000

[a] (Grissmer *et al.*, 1994)

[b] (Stühmer *et al.*, 1989)

[c] (Grupe *et al.*, 1990; Kirsch *et al.*, 1991; Swanson *et al.*, 1990)

[d] (Shi *et al.*, 1994; Patel *et al.*, 1997)

[e] (Kerschensteiner & Stocker, 1999; Klemic *et al.*, 1998)

ND = not determined.

†‡Values are given as IC_{50} in mM† or nM‡.

Chapter 6

Effect of intracellular Mg^{2+} on Kv1.5 and Kv2.1 channels expressed in *Xenopus* oocytes

The differential effect of intracellular Mg^{2+} on two types of Kv current in rat PASMCs could be explained in two ways. One obvious explanation is that intracellular Mg^{2+} directly interacts with different Kv channels in a different manner. Another possibility could be that the effects of Mg^{2+} are mediated via an intermediate mechanism which varies between various types of VSMCs. In order to evaluate the first possibility, the effect of intracellular Mg^{2+} was investigated on two different types of Kv channels, the Kv1.5 and Kv2.1. These channels have different pharmacological and biophysical characteristics (Snyders *et al.*, 1993; Grissmer *et al.*, 1994; Kerschensteiner & Stocker, 1999). Moreover it has been suggested that these Kv isoforms could also form part of the native channels in rat pulmonary artery SMCs (Coppock *et al.*, 2001). My data also suggest that the Kv2.1 α-subunit is likely to contribute to the Kv channel in rat aortic myocytes.

A *Xenopus* oocyte expression system was used to characterise the effects of intracellular Mg^{2+} on the biophysical properties of the Kv1.5 and a Kv2.1 channels. *Xenopus* oocytes contain very few endogenous voltage activated channels and are relatively large (about 1 mm in diameter). They represent a widely used system to study biophysical and pharmacological properties of heterologeously expressed ion channels (Stuhmer, 1992) in a "pure" although "non-physiological" membrane environment, providing a useful database for comparison with those of native Kv currents.

6.1 General features of the Kv1.5 and Kv2.1 channel currents recordings

Heterologous expression of Kv1.5 and Kv2.1 channels result in a fast and slow activating current, with a slow (C-type) inactivation (Hoshi *et al.*, 1991; Klemic *et al.*, 1998). Macroscopic potassium currents were recorded from oocyte membrane patches in inside-out configuration of the patch clamp technique. Each recording was taken at least 3 minutes after the inside-out configuration was established, since preliminary experiments showed that this time was required for the voltage dependent characteristics of the channels be stabilised. A complication in the recordings was due to the tendency of Kv2.1 and, in lesser extent, Kv1.5 channels, to run down within a few minutes after patch excision thus limiting time consuming measurements, such as dose-response or current-voltage relationships. This phenomenon was also observed by other investigators (Lopatin & Nichols, 1994 and Dr Martin Stoker, personal communication). Nevertheless, a reasonable number of patches showed only 10-30% rundown over more than 10-20 minutes, only these patches were used for analysis. Although the presence of Ca^{2+}-activated Cl^- conductances has been reported in *Xenopus* oocytes (Miledi & Parker, 1984), the addition of 2 mM EGTA (Table 2.3) to the intracellular (bath) solution was sufficient to suppress this conductance within membrane potential range used to study Kv channel properties.

Since the intracellular (bath) solution contained 2 mM EGTA, a relatively weak Mg^{2+} chelator (calculated free $[Mg^{2+}]_i$ equal to 4.61 and 9.34 mM in 5 and 10 mM $MgCl_2$-containing bath solutions, respectively), I will refer, in this chapter, to $[MgCl_2]$ as $[Mg^{2+}]_i$, for simplicity.

6.2. Effect of intracellular Mg^{2+} on Kv1.5 and Kv2.1 steady-state activation and activation kinetics

The expression of Kv1.5 and Kv2.1 α-subunit in *Xenopus* oocytes yielded membrane currents which were strikingly different in activation kinetics. Figure 6.1 compares the normalised Kv1.5 and Kv2.1 currents elicited by a 100 ms step depolarisation to +20 mV, demonstrating that Kv2.1 activates to a slower rate than Kv1.5. Slow activation of

Kv2.1 channel current was previously reported (Benndorf *et al.*, 1994; Koopmann *et al.*, 2001).

The onset of Kv currents were described according to the classical Hodgkin-Huxley model (HH-model) (Hodgkin & Huxley, 1952) with the addition of an empirical delay, δt, (Keynes & Rojas, 1974). The time course of the current was fitted by:

$$I_{(t)} = I'\left(1 - \exp\left(-\frac{t-\delta t}{\tau_a}\right)\right)^4, \qquad [6.1]$$

where $I(t)$ is the current at time t and τ_a is the time constant of activation and I' is the asymptotic maximal current at a given potential (equal to $g_{max}(V\text{-}E_K)*n^4$ in the HH-model).

Kinetics of Kv1.5 current were well approximated with the HH-model (Fig. 6.1). However, application of the same routine to the Kv2.1 channel current did not produce a satisfactory fit (Fig. 6.1). Therefore I decided to quantify the activation time course at various voltages by the rise-time to the half maximum current ($t_{1/2}$). This criterion, which is independent of model assumptions, has been previously used by other investigators (Koopmann *et al.*, 2001).

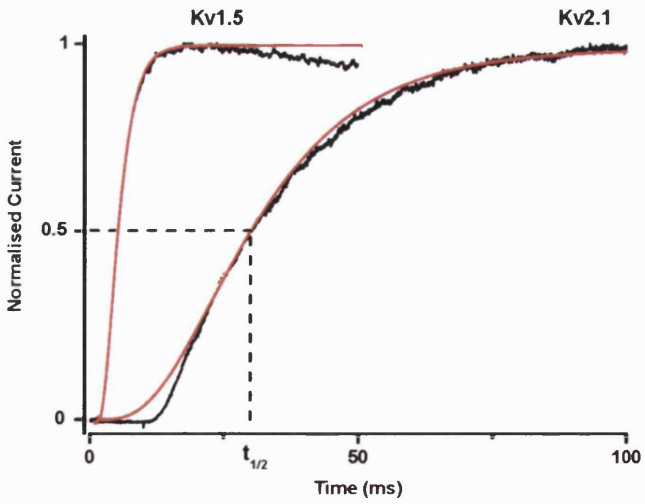

Figure 6.1. Activation kinetics of Kv1.5 and Kv2.1 channel currents. Kv1.5 and Kv2.1 currents were normalised to their peak amplitude and superimposed on the same graph for comparison. Solid red lines represent the best fit to the equation [6.1].

The effect of $[Mg^{2+}]_i$ (0, 5 and 10 mM) on τ_a (Kv1.5) and $t_{1/2}$ (Kv2.1) was then investigated on Kv1.5 and Kv2.1 currents elicited in response to depolarising pulses of 50 ms from –35 to +10 mV (in 5 mV increments) or of 100 ms from – 20 to +50 mV (in 10 mV increments), respectively. In all three $[Mg^{2+}]_i$ both τ_a and $t_{1/2}$ decreased monotonically with membrane depolarization (Fig. 6.2 *B* and *E*). For example, in 0 $[Mg^{2+}]_i$ τ_a was equal to 15.5±0.8 ms (n=12) at +30 mV and 2.7 ±0.2 ms (n=20) at +10 mV while $t_{1/2}$ decreased from 40.0±2.9 ms (n=12) at -20 mV to 19.5±0.9 ms (n=11) at +50 mV. An increase in $[Mg^{2+}]_i$ from 0 to 10 mM, reduced the τ_a at –30 mV by 36.5%, while τ_a at potentials > -5 mV remained virtually unaffected (Fig. 6.2*C*). Similarly, in 10 mM $[Mg^{2+}]_i$ the $t_{1/2}$ at –20 was reduced by about the 25.7%, while the $t_{1/2}$ at + 50 mV was not affected (Fig.6.2*F*). Thus, the comparison of τ_a and $t_{1/2}$ in the absence and presence of 10 mM $[Mg^{2+}]_i$ demonstrated a clear acceleration in the kinetics for both Kv1.5 and Kv2.1 currents with increased intracellular Mg^{2+}. One possible explanation for this phenomenon is that steady-state activation could also be affected, causing this apparent acceleration in the current activation kinetics. Steady-state activation dependencies for Kv1.5 and Kv2.1 were therefore measured in different $[Mg^{2+}]_i$ using the I-V tail protocol as described in Materials and Methods. Normalised I-V dependencies for Kv1.5 and Kv2.1 currents recorded in the absence and presence of 10 mM $[Mg^{2+}]_i$ are shown in Figure 6.2 *A* and *D* respectively. The comparison of V_a derived from the Boltzmann fit showed a significant leftward shift by ~16 (Kv1.5) and ~15 (Kv2.1) mV in activation dependencies in 10 mM versus 0 mM $[Mg^{2+}]_i$. The large changes in V_a for both currents predicts some acceleration in the current kinetics. In order to verify this hypothesis, τ_a and $t_{1/2}$ values at each V_m were corrected for the mean ΔV_a and plotted as diamonds in Figure 6.2 *C* and *F*. This comparison showed that corrected τ_a and $t_{1/2}$ values virtually overlapped with those obtained in the absence of Mg^{2+} indicating that acceleration in the kinetics of activation of both Kv1.5 and Kv2.1 are entirely due to shifts in the steady-state activation dependencies. The absolute values of V_a measured in 0 $[Mg^{2+}]_i$ and ΔV_a measured in paired patches in the absence and presence of a given $[Mg^{2+}]_i$ are compared in Table 6.1 and 6.2 for Kv15 and Kv2.1 respectively. No significant effect on the slope of activation was observed in different $[Mg^{2+}]_i$.

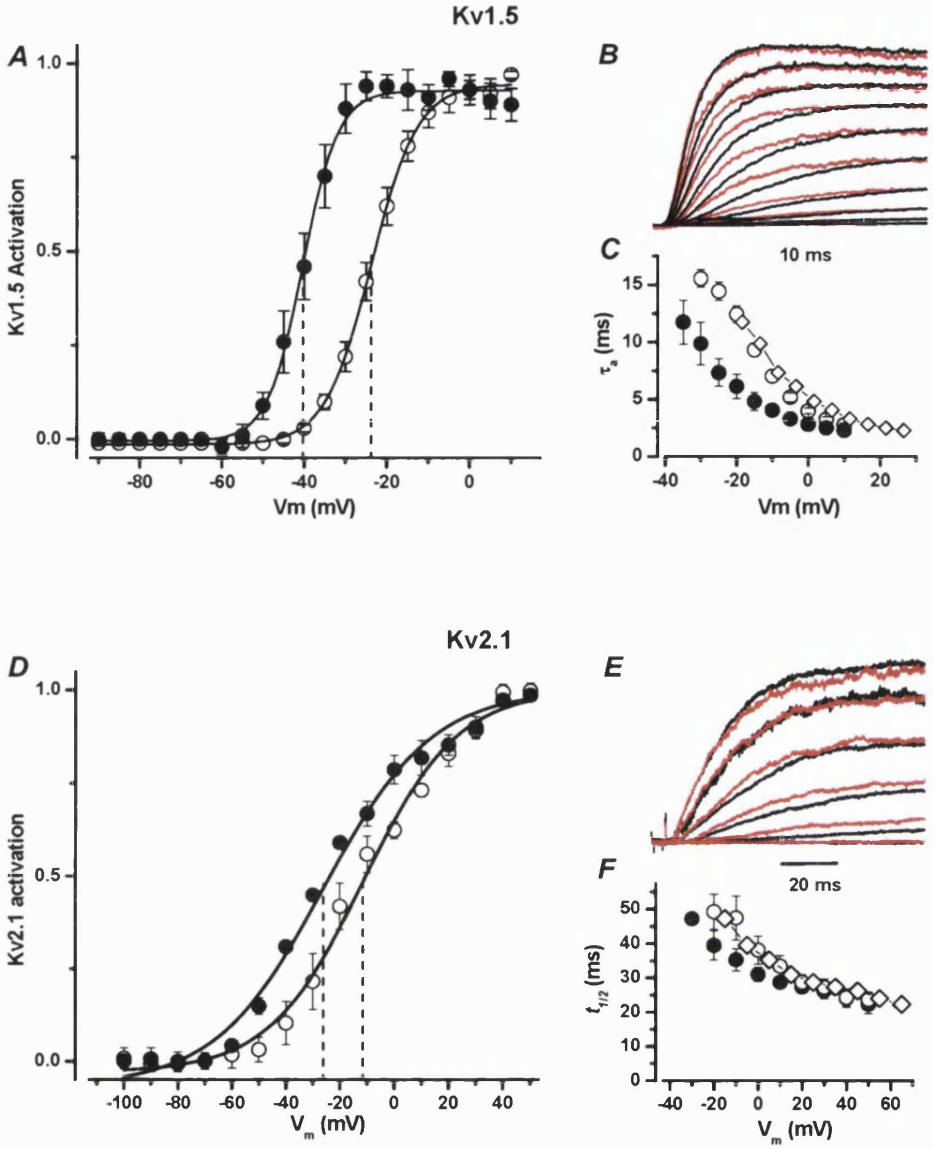

Figure 6.2 Effect of intracellular Mg^{2+} on the steady state activation dependency and activation kinetics of Kv1.5 and Kv2.1 channels. ***A*** (Kv1.5) and ***D*** (Kv2.1) show the averaged steady-state activation curves recorded in the absence (open circles) and in the presence of 10 mM Mg^{2+} (filled circles) from 24 and 8 (Kv1.5) and 4 paired (Kv2.1) patches, respectively. Continuous lines are the fit with the Boltzmann equation (eq. [2.8]) with the mean values reported in table 6.1 and 6.2. ***B*** (Kv1.5) and ***E*** (Kv2.1) are examples of families of normalised currents recorded from the same patch in 0 (black traces) and 10 (red traces) Mg^{2+} in response to 50 ms pulses from -35 to +10 mV in 5 mV steps (Kv1.5) or to 100 ms pulsed from –50 to + 50 mV in 20 mV steps (Kv2.1). Note that for both channels, the current onset is accelerated in the presence of Mg^{2+}. ***C*** (Kv1.5) and ***F*** (Kv2.1) compare the averaged time constant of the current onset (τ_a) or the $t_{1/2}$ measured from the same set of membrane patches as in ***A*** and ***D***.

6.3. Effect of intracellular Mg^{2+} on Kv1.5 and Kv2.1 inactivation

Inactivation of Kv1.5 and Kv2.1 currents were measured using the availability protocol (Materials and Methods, section 2.6.6.4) and the resulting I-V relationships were fitted with the Boltzmann function (eq. [2.9]).

Figure 6.3 compares the averaged inactivation dependencies for Kv1.5 (*A*) and Kv2.1 (*B*) recorded in 0 and 10 mM $[Mg^{2+}]_i$. It can be clearly seen from the Figure that, as for the activation dependencies, the availabilities for Kv1.5 and Kv2.1 currents were also significantly shifted to more negative membrane potentials when intracellular Mg^{2+} was increased. Thus, in the presence of 10 mM $[Mg^{2+}]_i$ the ΔV_h was –16 and –13 mV for Kv1.5 and Kv2.1 respectively, while the slope factor, k_h, was not significantly affected for either channels. The values of the inactivation parameters and their relative changes in the presence of different $[Mg^{2+}]_i$ are reported in Tables 6.1 and 6.2. It should be mentioned that the fraction of the non-inactivating Kv1.5 current, was significantly reduced by ~ 50% ($p<0.001$) in the presence of 10 mM $[Mg^{2+}]_i$. This effect has not been observed for Kv2.1 channels.

Mg^{2+}-dependence of relative changes in activation and inactivation dependencies for Kv1.5 and Kv2.1 were analysed in Fig.6.4. The analysis showed that ΔV_a and ΔV_h varied virtually in an identical manner for the Kv1.5 channel with slopes of –1.58 and –1.50 mV per mM of $[Mg^{2+}]_i$, respectively (Fig.6.4*A*). A similar degree of change in ΔV_a (-1.42 mV/mM) and ΔV_h (-1.27 mV/mM) was found for Kv2.1 channels.

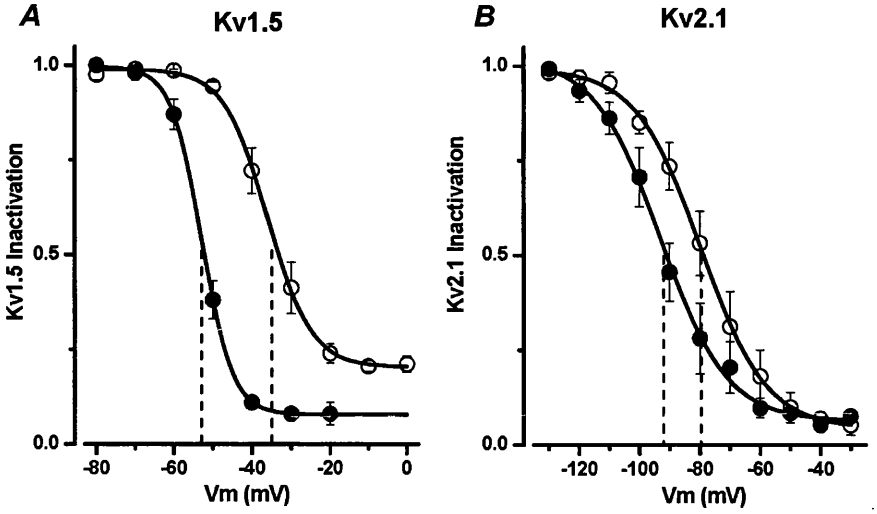

Figure 6.3. Effect of intracellular Mg^{2+} on Kv1.5 (*A*) and Kv2.1 (*B*) inactivation dependencies. Open and filled circles show the averaged steady state inactivation dependencies recorded in the absence and in the presence of 10 mM Mg^{2+}, respectively. Solid lines in *A* represent the best fits to the Boltzmann equation (eq. [2.9]) with of V_h = -36.0 and -52.9 mV, k_h = 5.5 and 3.8 mV and fraction of non-inactivating current I_{ss} = 0.2 and 0.09 in 0 (n=13) and 10 mM (n=5) Mg^{2+}, respectively. Solid lines in *B* were drawn according to the same equation as in *A*, with V_h = -79.6 and –93.0 mV, k_h = 10.8 and 10.9 mV and I_{ss} = 0.004 and 0.006 in 0 (n=6) and 10 (n=6) mM Mg^{2+}, respectively.

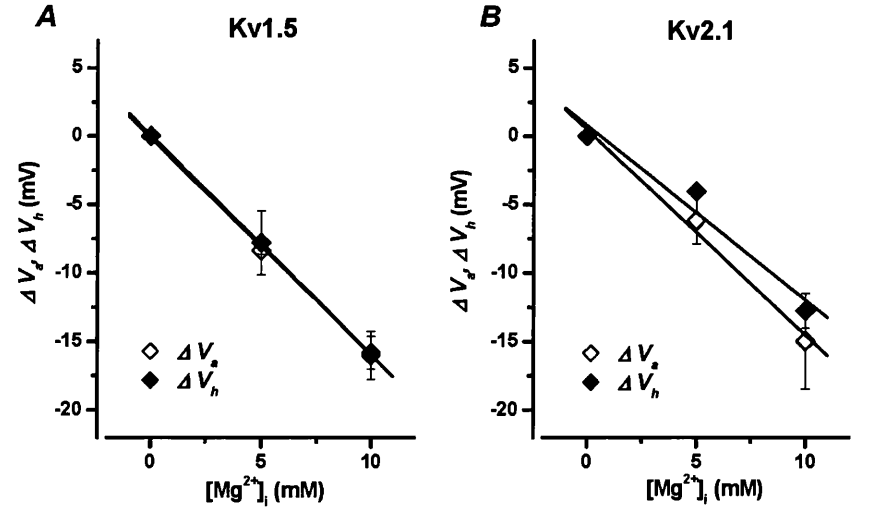

Figure 6.4. The dependence of the relative shifts in activation (ΔV_a) and inactivation (ΔV_h) parameters of Kv1.5 and Kv2.1 channels on $[Mg^{2+}]_i$. Continuous lines are simple linear regression fits with slopes of -1.58 (ΔV_a) and -1.50 mV/mM (ΔV_h) for Kv1.5 channel (*A*) and –1.42 (ΔV_a) and –1.27 mV/mM (ΔV_h) for Kv2.1 channel (*B*). Linear regression lines were drawn to provide a comparison between relative changes in these parameters.

Table 6.1. Comparison of the steady-state activation and inactivation parameters for the Kv1.5 channel in different $[Mg^{2+}]_i$.

$[Mg^{2+}]$ (mM)	V_a (mV)	k_a (mV)	V_h (mV)	k_h (mV)	I_{ss}
0	-23.3±1.1 (23)	-4.2±0.8 (23)	-36.8±1.5 (13)	3.6±0.2 (13)	0.19±0.02 (13)
	ΔV_a (mV)	Δk_a (mV)	ΔV_h (mV)	Δk_h (mV)	ΔI_{ss}
5	-8.3±0.3 (4)*	-0.18±0.37 (4)	-7.8±2.3 (9) *	0.8±0.6 (9)	-0.10±0.04 (9)
10	-15.8±1.2 (6) *	1.29±0.57 (6)	-16.0±1.8 (5) *	0±0.4 (5)	-0.10±0.02 (5)*

Data represents mean±s.e.m. (number of experiments). V_a is the half activation potential, k_a is the maximum e-fold slope of the activation curve, V_h is the half inactivation potential, k_h is the maximum e-fold slope of the inactivation curve, I_{ss} is the non-inactivating current fraction, and ΔV_a and ΔV_h are the shift of V_a and V_h relative to the values measured in absence of Mg^{2+} and calculated in paired patches. Asterisks indicate any significant differences to the control (0 Mg^{2+}).

Table 6.2. Comparison of the steady-state activation and inactivation parameters for the Kv2.1 channels in different $[Mg^{2+}]_i$.

$[Mg^{2+}]$ (mM)	V_a (mV)	k_a (mV)	V_h (mV)	k_h (mV)	I_{ss}
0	-16.4±2.6 (12)	-13.3±0.8 (12)	-83.0±2.3 (15)	7.9±0.4 (15)	0.05±0.02 (15)
	ΔV_a (mV)	Δk_a (mV)	ΔV_h (mV)	Δk_h (mV)	ΔI_{ss}
5	-6.2±1.7 (5) *	-0.71±0.85 (5)	-4.1 (1)	-0.2 (1)	-0.02 (1)
10	-15.0±3.5 (4) *	-0.7±1.6 (4)	-12.8±1.3 (6) *	0.06±1.41 (6)	0.04±0.01 (6)

Symbols have the same meaning that in table 6.1. ΔV_a and ΔV_h were calculated in paired patches.

6.4. Theoretical interpretation of the Mg^{2+}-dependent effect on the voltage dependent characteristics

Similarity in the shifts of the activation and inactivation dependencies for both Kv1.5 and Kv2.1 channels, might indicate that Mg^{2+} interacts with fixed negative charges thereby altering the transmembrane potential. The existence of negatively charged groups at the inner (and outer) surface of the membrane has been demonstrated in various preparations (Hille *et al.*, 1975; McLaughlin *et al.*, 1971; Ohmori & Yoshii, 1977) (see for review McLaughlin, 1989 and Hille, 2001) including smooth muscle (Ganitkevich *et al.*, 1988). Negative surface charges create an electric field (ψ_i) within the membrane additional to the field from the externally applied voltages. The total electric field, with this dual origin, is sensed by the ion channel voltage sensor. Cations can "screen" the surface charges by forming an ionic diffuse double layer at the surface and may also physically neutralise some of the surface charges by forming complexes (binding). Both effects will reduce the negative surface potential; hence cations added to the extracellular side of the membrane will increase the depolarisation needed to bring the field within the membrane to a given value, while cations added to extracellular surface will cause opposite effect. According to other studies (Hille *et al.*, 1975; Ohmori & Yoshii, 1977; Ganitkevich *et al.*, 1988), the measured membrane potential (V_m) between the intracellular compartment and the external bulk phase is composed of the outer surface potential (ψ_o), the genuine transmembrane potential (V_m^*) and the inner surface potential (ψ_i) in series as:

$$V_m = \psi_o + V_m^* - \psi_i, \qquad [6.2]$$

Being ψ_o not varied if the ionic composition of the extracellular solution remains constant, ($\psi_0 + V_m^*$) can be considered a constant value. Thus, at $V_m = V_a$, it can be considered that:

$$V_a = b - \psi_i, \qquad [6.3]$$

where b is a constant value equal to ($\psi_0 + V_m^*$). Therefore V_a can be considered representative of ψ_i. Changes in ψ_i in different concentration of divalent cations could be described by the Gouy-Chapman model with the Grahame equation (Grahame, 1947) (the theory is reviewed in McLaughlin, 1989; Lakshminarayanaiah, 1984 and Hille, 2001).

$$\sigma = \frac{1}{272}\left[\sum_i C_i\left(\exp\frac{-z_i F\psi_i}{RT} - 1\right)\right]^{0.5}, \qquad [6.4]$$

where σ is the presumed surface charge density (considered to be equal to 0.01 $e^-/ Å^2$). C_i is the concentration of the internal ionic species (i). The sum is taken over all ions. R, F, T have their usual meaning and z_i is the valence of ions of species i. This equation relates the surface potential on a side of a planar surface (in this case the intracellular side of the plasma membrane) bearing a uniformly smeared density of a fixed charge (σ) and immersed in an electrolyte. Figure 6.5 compares the theoretically calculated surface potential values obtained by an iterative numerical procedure (the Newton-Raphson method) of the Grahame equation (assuming σ= 0.01 $e^-/ Å^2$) and values of ΔV_a and ΔV_h measured in different $[Mg^{2+}]_i$ for the Kv1.5 and the Kv2.1 channel currents. This comparison demonstrated that: i) Mg^{2+}-dependent changes in voltage-dependent parameters for both channel types are very similar, and ii) they can be explained by screening by $Mg^{2+}$of fixed negative surface charges in the vicinity of channels.

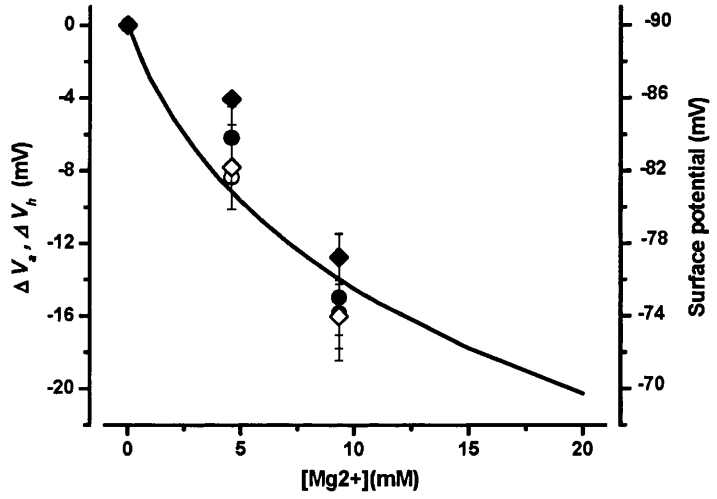

Figure 6.5. Effect on intracellular free Mg^{2+} on relative shifts of the half-activation (ΔV_a, circles) and half-inactivation (ΔV_h, diamonds) potentials for the Kv1.5 (open symbols) and Kv2.1 (filled symbols) channels. The continuous line represents the numerical solution of the Grahame equation of the surface potential, for a surface charge density of 0.01 $e^-/ Å^2$. Right axis reports the values of the estimated surface potential. Free $[Mg^{2+}]_i$ was calculated using the program Maxchelator.

6.5. Concentration dependent block of Kv1.5 and Kv2.1 currents by intracellular Mg^{2+}

Another effect of intracellular Mg^{2+} on both expressed Kv channels was also observed. When Mg^{2+} was added to the intracellular (bath) solution, the Kv1.5 and Kv2.1 currents amplitude elicited by a +20 mV pulse were rapidly reduced (Fig. 6.6*A* and *B*, respectively). This Mg^{2+}-dependent decrease of the current amplitude of both channels was fully reversible. Application of 2, 5 and 10 mM Mg^{2+} reduced the Kv1.5 to a normalized peak current of 0.96±0.011 (n=7), 0.91±0.002 (n=3) and 0.87±0.005 (n=2), respectively. A more pronounced effect of Mg^{2+} was observed for Kv2.1 current, with a reduction to 0.83±0.018 (n=7) and 0.78±0.023 (n=16) seen upon perfusion with 5 and 10 mM Mg^{2+}respectively. Higher concentrations of Mg^{2+} were not tested as significant surface charge screening may alter the gating properties, making the interpretation of the results difficult (Elinder and Arhem, 1999). However, the range of concentrations used allowed the estimation of the apparent dissociation constant for Mg^{2+}, assuming a Michaelis-Menten first order kinetics block:

$$\frac{I}{I_0} = \frac{1}{1 + \frac{[Mg^{2+}]}{Kd_{(20)}}}, \qquad [6.5]$$

where I is the current amplitude measured at various $[MgCl_2]_i$, I_0 is the current measured in $[MgCl_2]_i = 0$, $Kd_{(20)}$ is the apparent dissociation constant at +20 mV. The fit gave a value of $Kd_{(20)}$= 54.2 ± 2.5 mM for the Kv1.5 and 30.7 ± 3.7 mM for the Kv2.1.

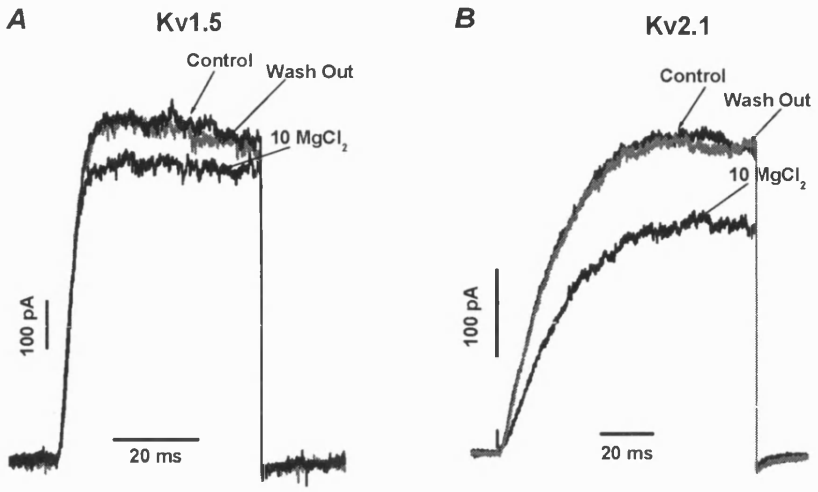

Figure 6.6. Inhibition of the Kv1.5 and Kv2.1 channel currents by intracellular Mg^{2+}. ***A*** and ***B*** illustrate representative current traces elicited by 50 ms (Kv1.5, panel ***A***) or 100 ms (Kv2.1, panel ***B***) depolarising pulses to + 20 mV and recorded from the same patch in the absence ("Control") and in the presence of 10 mM $[Mg^{2+}]_i$. Note the virtually complete recovery of currents after wash-out of Mg^{2+}.

6.6. Voltage dependency of the Mg^{2+} block of Kv1.5 and Kv2.1 currents

Intracellular Mg^{2+} is often reported to act as a voltage dependent open channel blocker in various types of K^+ channels (Ludewig *et al.*, 1993; Lopatin & Nichols, 1994; reviewed in Hille, 2001). I therefore investigated the effect of intracellular Mg^{2+} on Kv1.5 and Kv2.1 currents at the membrane potential of +20 mV, where channels are nearly maximally open. For this purpose, the instantaneous I-V protocol was used (Materials and Methods, section 2.6.6.3) and the resulting current to voltage relationships normalised for the amplitude of the prepulse and corrected for the fraction of the current amplitude reduction observed at +20 mV in various intracellular Mg^{2+} concentrations. Families of tail currents for Kv1.5 (*A*) and Kv2.1 (*B*) and normalised I-Vs recorded in the absence and presence of 10 mM Mg^{2+} are shown in Fig.6.7. The Figure demonstrates that for both Kv1.5 and Kv2.1 channels, the effect of Mg^{2+} is potential dependent, blocking the currents more at positive potentials than at negative voltages. The blocking effect was also increased with a raise in the concentration of Mg^{2+} (Fig. 6.7*C* and *D*). To analyse these changes quantitatively, the Goldman-

Hodgkin-Katz current equation (GHK-current equation) (Goldman, 1943; Hodgkin & Katz, 1949) was used:

$$I = P\frac{V_m F^2}{RT}\frac{1-\exp\left(-\frac{F(V_m - E_K)}{RT}\right)}{1-\exp\left(-\frac{FV_m}{RT}\right)}, \qquad [6.6]$$

that is characterised by the permeability P and the reversal potential E_K; while the remaining symbols have their usual meaning (R is the gas constant, F is the Faraday's constant, T is the absolute temperature). It has to be mentioned that the Kv2.1 and, to a lesser extent, the Kv1.5 currents, showed a downward deflection at higher potential (> ~50 mV) even in the absence of Mg^{2+} (Fig 6.7*C* and *D*, open circles), possibly due to the blocking action of cations such as Na^+ (Lopatin & Nichols, 1994). Therefore, in order to obtain a satisfactory fitting of the data a Boltzmann factor ($P_{block}(V_m)$) was added to the equation [6.6] assuming that a blocking effect by an ion other than Mg^{2+} occurs and follows a Boltzmann distribution (Pusch *et al.*, 1989).

$$P_{block}(V_m) = \frac{1}{1 + A\exp\left(\frac{V_m}{B}\right)}. \qquad [6.7]$$

This factor has an influence on the current amplitude only at positive potentials and was solely added to take into account the rectification of the Kv current at positive potentials and the meaning of the parameters A and B was not interpreted. Parameters A and B were first estimated from the fit of the data in 0 mM Mg^{2+} and then kept constant for the fitting of the data at higher $[Mg^{2+}]_i$, assuming that voltage dependent block by other ions was unaltered by the presence of Mg^{2+}.

To describe quantitatively the concentration and voltage-dependency of the Mg^{2+} block an approach similar to that used by Woodhull (1973) was adopted (Woodhull, 1973). The fraction of channels blocked by Mg^{2+} was expressed as a function of Mg^{2+} concentration and membrane potential, $B_{Mg}([Mg^{2+}],V_m)$, as following:

$$B_{Mg}([Mg^{2+}],V_m) = \frac{1}{1+\frac{[Mg^{2+}]}{Kd_{(0)}}\exp\left(\frac{z\delta FV_m}{RT}\right)} \qquad [6.8]$$

where $Kd_{(0)}$ is the half-maximal blocking concentration at V=0 mV and δ is the relative electric distance of the Mg^{2+}-sensitive site from the internal surface of the membrane, z = 2 is the valence of the blocking particle (Mg^{2+}).

The data were finally fitted with the equation resulting from inclusion of the terms defined in equations [6.7] and [6.8] to the GHK equation described in [6.6]:

$$I = P\frac{V_m F^2}{RT}\frac{1-\exp\left(-\frac{F(V_m - E_K)}{RT}\right)}{1-\exp\left(-\frac{FV_m}{RT}\right)} \times B_{Mg}\left(\left[Mg^{2+}\right]_i, V_m\right) \times P_{block}(V_m). \quad [6.9]$$

Continuous lines in Figure 6.7*C* and *D* are the fit of the experimental data with the equation [6.9] giving a $Kd_{(0)}$ = 64.9±3.2 mM, E_K =79.7±1.0 mV and δ = 0.09±0.01, for the Kv1.5 and $Kd_{(0)}$ = 42.9±4.8 mM, E_K =78.5±1.8 mV and δ = 0.21±0.04 for Kv2.1. The values of the electrical distance δ indicate that a putative Mg^{2+} binding site on the Kv1.5 and Kv2.1 channel proteins are located within a membrane spanning domain, sensing about 10% and 20% of the trans-membrane electric field, respectively.

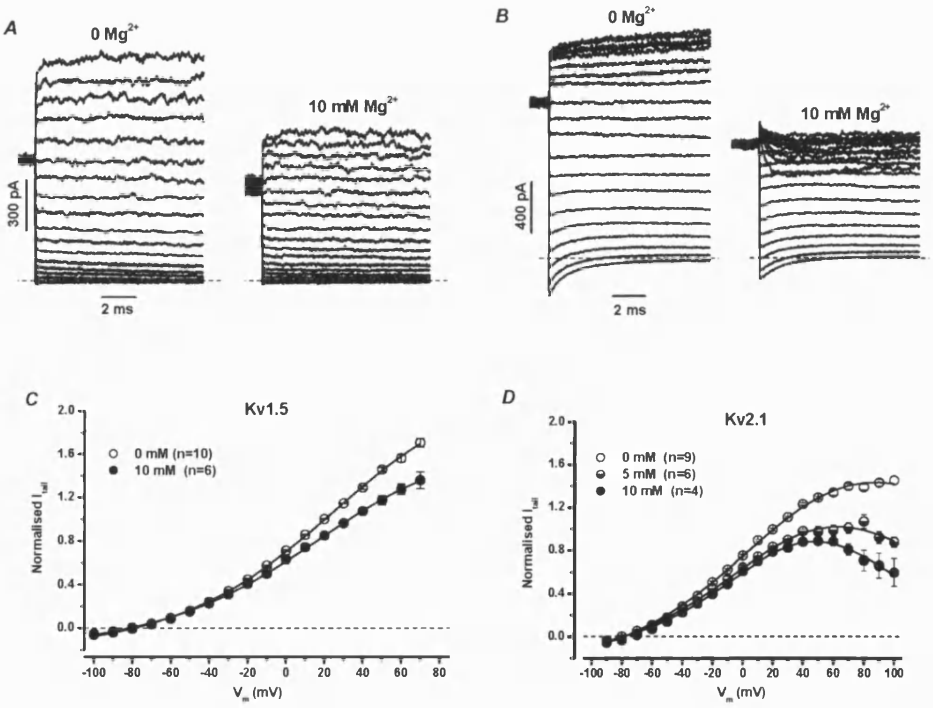

Figure 6.7 Voltage dependency of the Mg^{2+} block of Kv1.5 and Kv2.1 channels. ***A*** and ***B*** show a family of tail currents recorded between –100 and +70 mV (***A***, Kv1.5) and –90 to +100 mV (***B***, Kv2.1) after prepulses to +20 mV in the absence (left panels) and presence (right panels) of 10 mM Mg^{2+}, respectively. Dashed line represent zero current. ***C*** and ***D*** demonstrate averaged tail currents amplitude normalised for the prepulse amplitude as described in the text, for Kv1.5 (***C***) and Kv2.1 (***D***) channels and in the absence and presence of different $[Mg^{2+}]_i$. Continuous lines represent the fit with the equation [6.9]. The number of experiments is shown next to the symbols.

Alternatively, *Kd(0)* and δ can be calculated from the estimation of *Kd* at each membrane potential (*Kd(V)*) according to the Michaelis-Menten equation (eq. [6.5]). The relationships between the *Kd(V)* and membrane potential can be approximated with the following equation (Woodhull, 1973):

$$Kd(V) = Kd_{(0)} \exp\left(\frac{-\delta zVF}{RT}\right) \quad . \qquad [6.10]$$

Figure 6.8 illustrates such potential dependence of *Kd* values calculated from the data points shown in Figure 6.7. Continuous lines represent the fit with equation [6.10] giving a value of *Kd* =69.99±2.5 and 40.5±1.7 mM and a δ = 0.11±0.05 and 0.19±0.08 for Kv1.5 and Kv2.1 channels, respectively. It should be stressed that these values are very similar to those estimated from the fit with the modified GHK equation (eq. [6.9]).

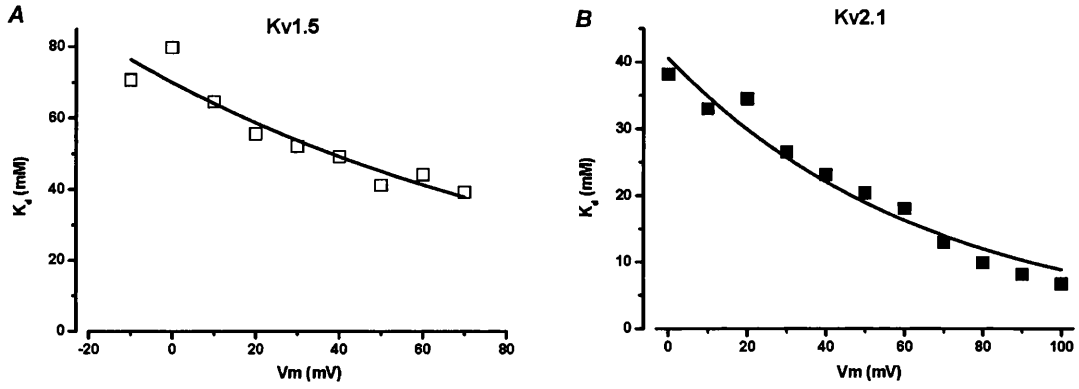

Figure 6.8 Potential dependency of *Kd*. *Kd* was calculated at each potential for the Kv1.5 (*A*, open square) and Kv2.1 (*B*, filled square) currents described in Fig. 6.7. Continuous lines represent the fit with the equation [6.10].

6.7 Additional effects of Mg^{2+} on the Kv1.5 current

Another interesting observation was made when membrane patches expressing Kv1.5 channels were repeatedly stimulated in the absence and presence of Mg^{2+} in the bath solution. In the absence of Mg^{2+} when membrane patches were stimulated with +20 mV depolarising pulses at 0.5 Hz (i.e. every 2 s instead of 5 s) the peak Kv1.5 current was reversibly inhibited (Fig. 6.9*A*, open circles). When patches were stimulated at 0.2 Hz, an addition of 10 mM Mg^{2+} caused a rapid reduction of the peak current amplitude by 11.3±2.0 % (n=3) in response to the first step in the presence of Mg^{2+}. This initial rapid

decrease of the peak amplitude was followed by a progressive inhibition of the current (Fig. 6.9*A*, filled circles). The rate of current inhibition was further increased when the frequency of stimulation was changed to 0.5 Hz. Analysis of the frequency-dependent inhibition rate of Kv1.5 channel currents, measured at 0.5 Hz in different $[Mg^{2+}]_i$ is shown (Fig 6.9*B*). The peak of Kv1.5 current was significantly reduced by 14±9 % (n= 5) and 23±6 % (n=7) after 45 s of stimulation (0.5 Hz) in 5 and 10 mM $[Mg^{2+}]_i$ respectively (P<0.0001 when compared to 5±4 % (n=21) inhibition seen in the absence of Mg^{2+}). The frequency dependent decrease in the Kv1.5 amplitude followed monoexponential time course with time constant equal to 63, 46 and 23 s in the absence and presence of 5 and 10 mM Mg^{2+}. It is noteworthy that, when a similar experimental protocol was applied to membrane patches expressing Kv2.1 channels, no Mg^{2+}-dependent acceleration of the current inhibition was observed. For example, the peak current was equally suppressed by 28.7±4.6 % (n=3) and by 27.9±6.2 % (n=3) after 60s of stimulation (0.3 Hz) in 0 and 10 mM $[Mg^{2+}]_i$, respectively.

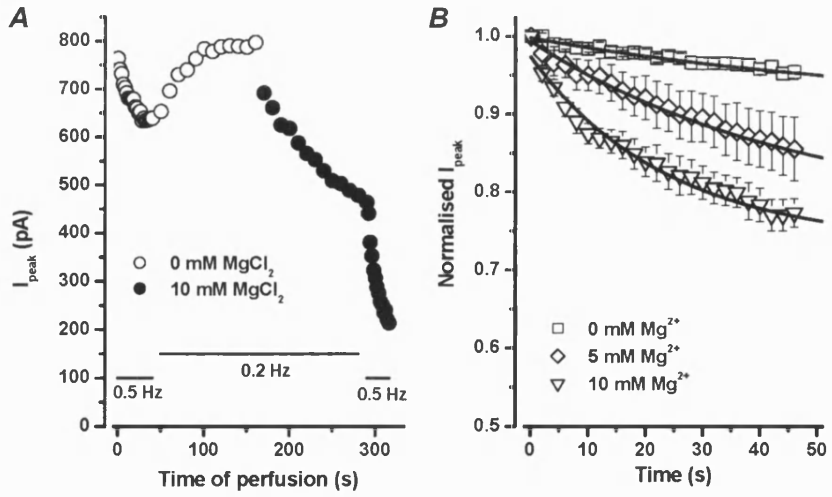

Figure 6.9 Frequency-dependence of the effect of $[Mg^{2+}]_i$ on Kv1.5 current. ***A***, example of the effect of different frequencies of stimulation (as indicated by horizontal bars) in the absence (open circles) and in the presence (filled circles) of 10 mM Mg^{2+}. Test pulse duration was 50 ms, stepped to +20 mV. ***B***, comparison of the time course of Kv1.5 peak current elicited every 2 s (0.5 Hz) in different $[Mg^{2+}]_i$, as indicated. Current amplitude was normalised to that recorded during the first pulse. Number of experiments was equal to 21, 5 and 7 for 0, 5 and 10 mM $[Mg^{2+}]_i$. Continuous lines represent single exponential fits with a time constant of 63, 46 and 23 s for 0, 5 and 10 mM $[Mg^{2+}]_i$, respectively.

6.8 Noise analysis of the Kv1.5 channel current in different $[Mg^{2+}]_i$

Nonstationary noise analysis was applied to study the mechanism of the effect of intracellular Mg^{2+} on Kv1.5 channel. The average and standard deviation at each time point was calculated as described in Materials and Methods. Figure 6.10 illustrates an example of noise analysis carried out in the same patch in the absence (*A*) and presence (*B*) of 10 mM $[Mg^{2+}]_i$. The noise analysis of Kv1.5 currents revealed that neither the single channel conductance nor the open probability was affected by increasing intracellular Mg^{2+}. However, the number of active channels in the patch was significantly reduced (Table 6.3). This observation is consistent with a block of Kv1.5 channels by intracellular Mg^{2+} described in the previous sections. Due to a propensity of the Kv2.1 channel to undergo rundown, noise analysis, which requires a highly stable current, was not performed for this channel.

Table 6.3. Noise analysis of Kv1.5 channel current.

	Contol	10 mM $MgCl_2$	*t-Test*
i (pA)	0.57±0.09 (5)	0.52±0.08 (5)	0.18
ΔN (%)	---	38.7%±11.6 (5)	0.006
P_{max}	0.75±0.05 (5)	0.71±0.05 (5)	0.26

i, ΔN and P_o are single channel current, apparent change in number of channels per patch and open probability. Statistical comparison was performed using a paired *t*-test in 5 patches.

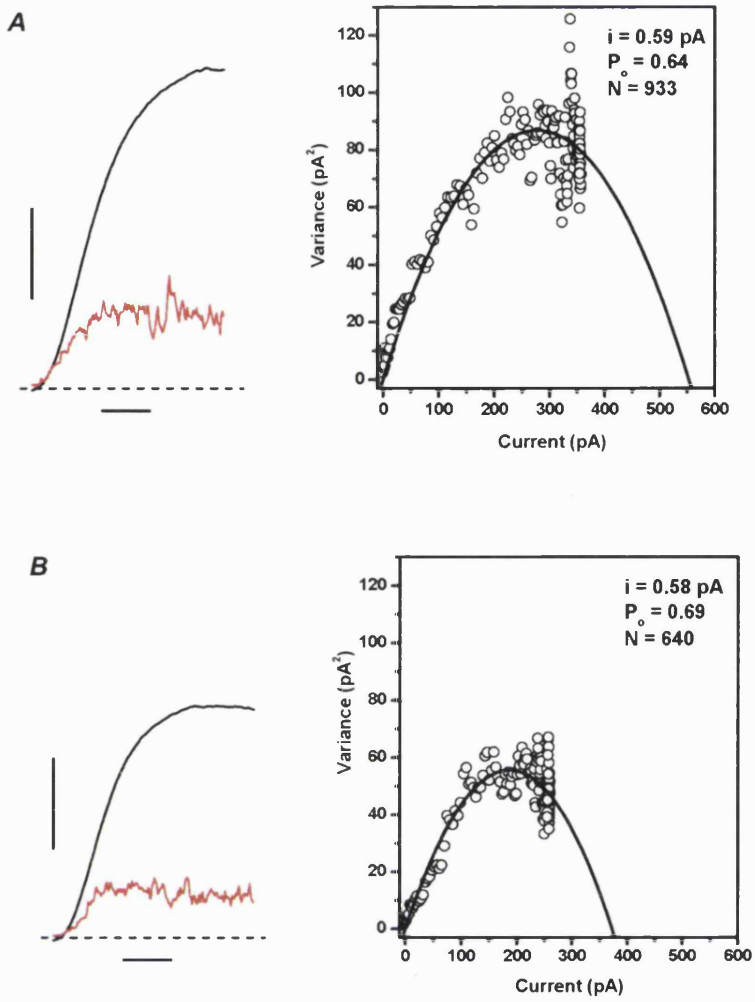

Figure 6.10 Non stationary noise analysis of the Kv1.5 channel currents. The current mean and variance in the absence (***A***) and presence (***B***) of 10 mM $[Mg^{2+}]_i$ were calculated from fifty current traces elicited by 50 ms pulses applied every 2 s. In the left panels in ***A*** and ***B*** the current mean (in pA, black traces) and variance (in pA^2, red traces) are shown. Horizontal bars are 2ms; vertical bars are 100 pA (for current) or pA^2 (for variance). The right panels show the variance plotted versus the mean. Continuous lines are fits with the equation [2.14] as described in Materials and Methods with the parameters i , N, P_o shown at the top of each panel.

6.9 Discussion: effect of intracellular Mg^{2+} on Kv1.5 and Kv2.1 channels

Comparison of the effect of intracellular Mg^{2+} on Kv1.5 and Kv2.1 currents revealed a complex mechanism of action of the divalent cation on these Kv channels. Kv1.5 and Kv2.1 α-subunits encode two different types of Kv currents, mediating a rapidly and a slowly activating current respectively (Snyders *et al.*, 1993; Grissmer *et al.*, 1994; Kerschensteiner & Stocker, 1999), properties also observed in my experiments. Changes in intracellular Mg^{2+} caused several significant effects on the Kv1.5 and Kv2.1 currents. A pronounced effect on activation and inactivation dependency was observed. Similar shifts in the steady-state activation of Kv1.5 and Kv2.1 channels in response to an increase in intracellular Mg^{2+}, suggest that the voltage sensor of both channels detected changes in $[Mg^{2+}]_i$ in a similar manner. Parallel shifts in activation and inactivation dependencies for various types of ion channels in response to changes in the intracellular or extracellular ionic composition has been previously demonstrated (e.g. Hille *et al.*, 1975; McLaughlin *et al.*, 1971; Ohmori & Yoshii, 1977; Ganitkevich *et al.*, 1988; Zamponi & French, 1995; Elinder & Arhem, 1999; Boccaccio *et al.*, 1998) and can be interpreted in terms of the Gouy-Chapman theory, which describes interaction of ions with fixed charged groups on the surface of biological membranes. There are two principal ways by which ions, mainly divalent cations, could interact with fixed negative charges in the cell membrane: screening and forming complexes with the fixed charges (binding), both processes will lead to changes in the transmembrane electric field (McLaughlin, 1989). Assuming that Mg^{2+} can only act via a screening mechanism, the relative changes in V_a for Kv1.5 and Kv2.1 in different $[Mg^{2+}]_i$, were relatively well described by the Grahame equation, with an estimated density of fixed charges equal to $0.01e^-/Å^2$, a value chosen arbitrary but close to values used in similar studies in smooth muscle (Ganitkevich *et al.*, 1988). The negative shift in activation dependencies also explained the apparent acceleration of the Kv1.5 and Kv2.1 current activation rate observed in high $[Mg^{2+}]_i$ (Fig. 6.2). It is noteworthy that the half-inactivation potential, V_h, was affected by intracellular Mg^{2+} similarly to V_a. This is in line with the intrinsic voltage independent nature of the C-type inactivation, whose apparent voltage dependency is given by the process of activation (Pardo *et al.*, 1992; Lopez-Barneo *et al.*, 1993; Yellen, 1998). Overall, the effect of Mg^{2+} on steady state voltage dependent characteristics of Kv1.5 and Kv2.1 channels expressed in *Xenopus* oocytes can be explained by the presence of negatively charged groups in the close

vicinity to the voltage sensor, which are screened by increased $[Mg^{2+}]_i$. In arterial SMCs, however, similar changes in intracellular $[Mg^{2+}]_i$, caused a differential effect on activation and inactivation dependencies, depending on the type of the Kv current and the cell type (Chapter 5). Importantly, I_{K1} and I_{K2}, which have similar kinetics and pharmacological profile as Kv1.5 and Kv2.1, respectively, responded differently to increases in $[Mg^{2+}]_i$. Interestingly, a suppression of the non-inactivating component (I_{ss}) of the Kv1.5, but not of Kv2.1 channels (Fig. 6.3) echoes that on I_{K1}, but not I_{K2}, currents in PASMCs (Fig. 5.12). Although the exact reason for differential effects of Mg^{2+} on native currents is not clear, it seems unlikely that they are determined by the expression of different types of Kv α-subunits among SMCs, since Kv1.5 and Kv2.1 channels, which belong to different Kv subfamilies, responded in similar ways to changes in $[Mg^{2+}]_i$. One possible explanation for the differences in the effects of Mg^{2+} on native and expressed Kv channel currents, might be that in SMCs a complex structure of Kv channels can alter the Mg^{2+} sensitivity. For example, one would expect that the presence of auxiliary Kv β-subunits might have a significant effect on the intracellular negatively charges which interact with Mg^{2+}. The heteromeric structure of the Kv channel in VSMCs could also potentially alter its sensitivity to Mg^{2+}. It is believed that Kv1.5 is expressed in mesenteric arterial SMCs as a complex with the Kv1.2 (Kerr *et al.*, 1923), while the Kv2.1 α-subunit is likely to interact with the "silent" Kv9.3 isoform, forming heteromultimeric channels (Patel *et al.*, 1997). How it will affect the Mg^{2+} sensitivity is not known and could be the subject of future experimental work. Also, a possibility that Mg^{2+}-sensing sites in the Kv channels may be modified by a phosphorylation/dephosphorylation process to a different degree in various types of SMCs, cannot be excluded.

Another interesting observation was that intracellular Mg^{2+} blocked the expressed channels in a voltage- and dose- dependent manner. The potential dependent blockage became apparent at potentials > +50 mV and was more pronounced for the Kv2.1 than for the Kv1.5 channel. Since this blocking effect was obvious only at very positive potentials, its physiological significance is not clear. However, it may serve as a useful experimental tool for investigation of the molecular identity of native Kv currents.

A different mechanism of modulation of the Kv1.5-mediated current by Mg^{2+} was also observed. The Kv1.5 steady-state inactivation did not inactivate fully in the absence of

Mg^{2+}. However, the fraction of non-inactivating current (I_{ss}) was greatly reduced in the presence of Mg^{2+} suggesting a Mg^{2+}-dependent facilitation of the Kv1.5 channels to undergo to the inactivated state. The Mg^{2+}-dependent reduction of the Kv1.5 current amplitude upon continuous (0.5 Hz) stimulation with 50 ms depolarizing pulses is also consistent with this hypothesis. Interestingly an analogous current reduction was not observed for the Kv2.1 channel current. It is noteworthy that in Kv1.5 channel, the most prevalent form of slow inactivation is C-type (Hoshi *et al.*, 1991; Stuhmer *et al.*, 1989), which is thought to result from a constriction of the outer mouth of the pore (Liu *et al.*, 1996; Yellen, 1998). Permeable ions produce very strong effects on the extent of the rate of C-type inactivation, e.g. elevated extracellular K^+ slows down the channel inactivation rate (Lopez-Barneo *et al.*, 1993). It is also believed that amino acid residues in the S6 or the outer part of pore could be important in the control of C-type inactivation. Ludewig et al. (1993) demonstrated that the single point mutation K533Y, located in the pore region of the Kv1.4 (RCK4) channel, which creates homology with the Kv1.2 channel, confers to the Kv1.4 properties of Mg^{2+} sensitivity proper of the Kv1.2 channel and also modulates the inactivation of the channel (Ludewig *et al.*, 1993). They proposed that this mutation alters the channel occupancy by K^+ and thereby indirectly affects internal Mg^{2+} block and channel inactivation. My experiments show a possible complementary relationship between intracellular Mg^{2+} and inactivation properties of the channel. Interruption of ionic flux by intracellular block of the current would alter the channel occupancy by K^+, modifying the inactivation.

Chapter 7

Physiological relevance of Mg^{2+}-dependent modulation of I_{Kv} in vascular smooth muscle

The results described in Chapter 5 demonstrate that intracellular Mg^{2+} differentially alters the activation and inactivation dependencies of Kv channel currents in aortic and pulmonary arterial myocytes. Therefore, a possible physiological significance of the modulatory effects of Mg^{2+} has been examined using a theoretical prediction and experimental approach.

7.1 Effect of intracellular Mg^{2+} on Kv "window currents" in rat aortic and pulmonary myocytes

The dependence of the open probability of any voltage-dependent channel, including Kv, on the membrane potential can be described by two processes, activation and inactivation. Membrane depolarisation has two effects: it promotes the open state of the channel (activation) and promotes a long-lived closed state (inactivation). Thus, for a channel to be open, it has to be activated and not inactivated. This can be expressed as the product of two probabilities:

$$Po = Pa \times (1 - Pi), \qquad [7.1]$$

where, at a given potential, *Po* is the probability for the channel to be open, *Pa* is the probability to be activated and *Pi* the probability to be inactivated. Thus *(1-Pi)* is the probability of not being in the inactivated state. The plot of *Po* versus the V_m is called "window current" because it provides a range ("window") of membrane potentials where ion channels should be always open. The *Pa* and *(1-Pi)* dependencies on membrane potential can be derived from the Boltzmann parameters acquired from the fit of steady-state activation dependencies and availabilities of Kv currents.

To evaluate whether $[Mg^{2+}]_i$ has a significant effect on the open probability of Kv channels in rat VSMCs, window currents for I_{K1} and I_{K2} in PASMCs and I_{Kv} in RASMCs, measured in different free $[Mg^{2+}]_i$, were constructed. In order to generate window currents Boltzmann parameters for I_{K1} and I_{K2} (Tables 5.4, 5.5, 5.6) and I_{Kv} (tables 5.2 and 5.3) activation and inactivation dependencies, measured in different pipette $[MgCl_2]$, were utilised. The effect of an increase in $[MgCl_2]_i$ on window currents for three types of native Kv currents is shown in Figure 7.1. As can be seen from this comparison, the open probability of I_{K1} (panel *A*) and I_{Kv} (panel *C*) was significantly suppressed, while that for I_{K2} (panel *B*) was increased as Mg^{2+} was increased. It is noteworthy that the non-inactivating component of the Kv current was not taken into account in these simulations. In order to compare changes over a range of free $[Mg^{2+}]_i$ absolute values of V_a and V_h for the three types of Kv currents obtained in different pipette $[MgCl_2]$ were plotted against the free $[Mg^{2+}]_i$ (calculated as described in Materials and Methods and presented in Table 5.1). Dependencies of V_a and V_h versus on $[Mg^{2+}]_i$ were linearly approximated with slopes equal to –0.56 (I_{K1}), -1.69 (I_{K2}) and -0.70 (I_{Kv}) mV/mM for V_a and –3.6 (I_{K1}), -0.92 (I_{K2}) and –1.68 (I_{Kv}) mV/mM for V_h (Fig 7.2*A-C*). Since no significant changes in slope factors for activation and inactivation dependencies for the Kv currents in PA and RA myocytes were observed, k_a and k_h obtained in different pipette $[MgCl_2]$ were averaged for each current type and mean values were used for 3D modelling of the window currents shown in Fig. 7.2 (*D-F*). As in the previous simulation, the non-inactivating current component has been neglected. A comparison of open probabilities over the range of $[Mg^{2+}]_i$ suggests that relatively small changes in intracellular Mg^{2+} could cause a profound decrease in open probability of one type of Kv channel current (e.g. I_{K1} and I_{Kv}), while another Kv current could be increased (e.g. I_{K2}) in the physiological range of membrane potentials between –60 and –40 mV.

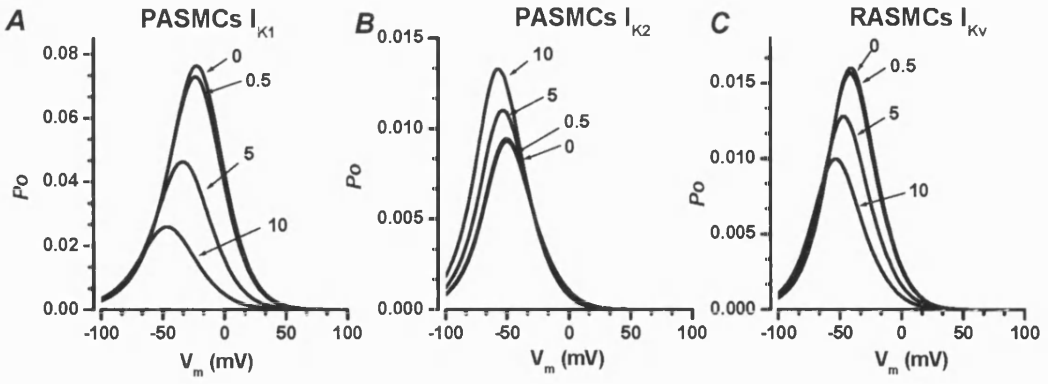

Figure 7.1. Window currents for PASMCs I_{K1} (***A***), PASMCs I_{K2} (***B***), RASMCs I_{Kv} (***C***) in various pipette [$MgCl_2$].

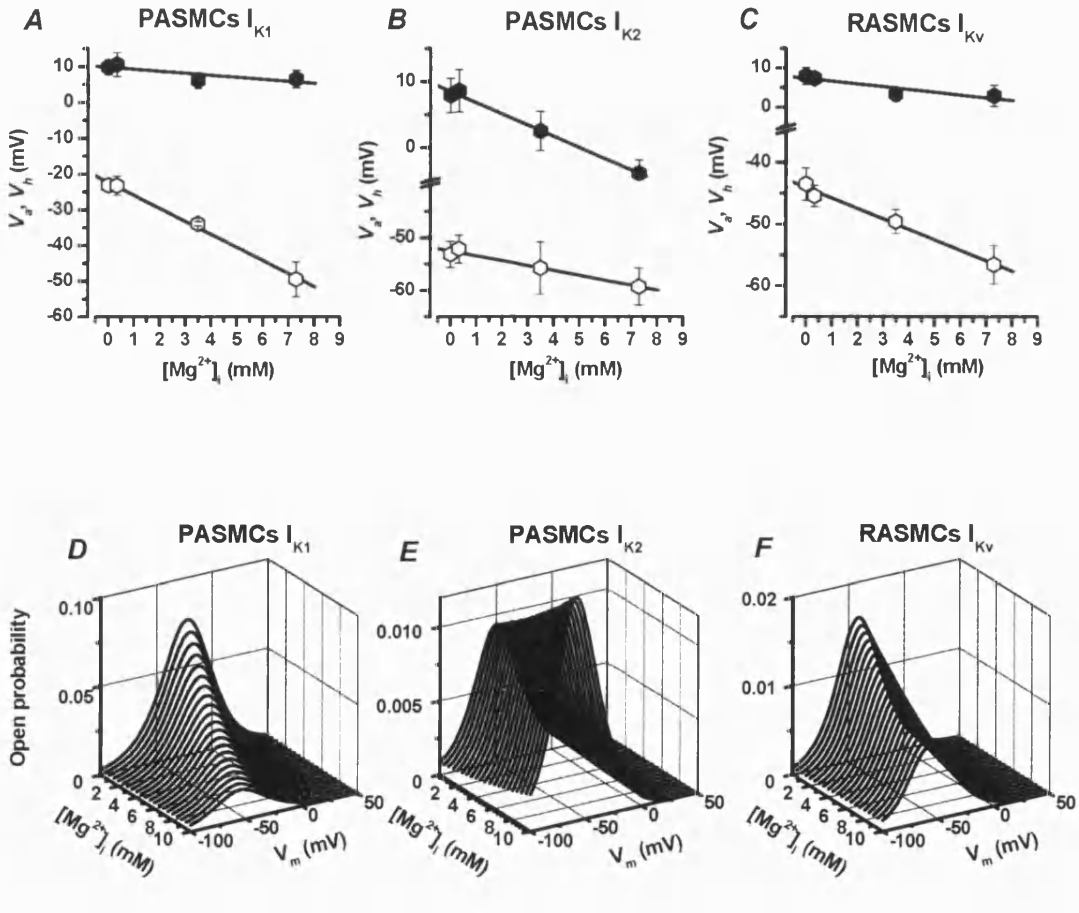

Figure 7.2. ***A***, ***B***, ***C*** are the averaged V_a (filled circles) and V_h (open circles) reported versus calculated free $[Mg^{2+}]_i$ (see Table 5.1). Continuous lines represents linear regression fits with slopes equal to –0.56, -1.69, -0.70 mV/mM for V_a and –3.6, -0.92 and –1.68 for V_h in ***A*** (PASMCs I_{K1}), ***B*** (PASMCs I_{K2}) and ***C*** (RASMCs I_{Kv}), respectively. ***D***, ***E***, ***F*** are predicted changes in the open probability of Kv channels on $[Mg^{2+}]_i$ in rat VSMCs. Window currents for I_{K1} (***D***) and I_{K2} (***E***) PASMCs and I_{Kv} (***F***) in RASMCs were computed using V_a and V_h parmeters determined from the slopes depicted in panels ***A***, ***B*** and ***C***.

7.2 Effect of Mg^{2+}-loading on KCl-dependent contraction in intact rat aorta

The theoretical simulation of the effect of $[Mg^{2+}]_i$ on Kv currents predicts that elevation of intracellular $[Mg^{2+}]_i$ should increase tissue excitability in rat aorta and possibly in main PA. Since an interpretation of the results in PA tissue might be complicated by the presence of two subpopulations of cells, the theoretical prediction was tested experimentally at whole tissue level in endothelium denuded aortic preparations. To elevate $[Mg^{2+}]_i$ in rat aortic smooth muscle an adapted procedure based on the methods reported by Handy *et al.*, 1996 was carried out. The methods, described in Materials and Methods (section 2.1), rely upon the fact that $[Mg^{2+}]_i$ can be increased above the resting level by superfusing an intact tissue with a Na^+-free medium containing high Mg^{2+} concentration (30 mM). Under this condition the Na^+/Mg^{2+} antiport is forced to transport Mg^{2+} inside the myocytes. The effect can then be reversed by application of a solution with normal ionic composition.

To compare whether Mg^{2+}-loading procedures will affect the excitability of rat aortic smooth muscle, endothelium-denuded aortic rings were subjected to various KCl concentrations before and after loading of the tissue with Mg^{2+}. These experiments were performed in the absence of Na^+ in the bath solution (containing 1.2 $MgCl_2$ and 2 mM $CaCl_2$, Table 2.1 in Materials and Methods). After 25 min of incubation in "Na^+-free buffer" no significant effect on basal tension was observed (compare 0.68±0.03 g in Krebs solution and 0.68±0.02 g in "Na^+-free buffer, 8 preparations, 2 rats). A contraction response to various KCl concentrations (10, 15, 20, 40 and 100 mM each applied for 10 min) was then constructed (Fig. 7.3*A*). Contractile response appeared at 15 mM KCl and tension saturated at 40-100 mM KCl (Fig.7.3*A*). The mean concentration response was then plotted in Fig.7.4 (circles). Tissue was subsequently incubated in "Mg^{2+}-loading buffer" (Table 2.1, Materials and Methods) for 30 min in order to increase $[Mg^{2+}]_i$ in the cytosol of SMCs. This treatment did not produce changes in the level of tension, calculated as 0.68±0.03 (n=8) before Mg^{2+}-loading and 0.67±0.02 (n=8) after the treatment. The "Mg^{2+}-loading buffer" was replaced with the "Na^+-free buffer" for 20 min (to wash out extracellular Mg^{2+}) and a concentration-response to KCl was performed in a similar manner of that described above. Figure 7.3*B* shows that after the Mg^{2+}-loading procedure, the tissue became significantly more sensitive to KCl. The threshold of the contractile response shifted to 10 mM KCl with

15 mM producing a similar degree of contraction as 20 mM KCl before Mg^{2+}-loading (Fig. 7.4 squares). It is noteworthy that the maximal contraction at 40 and 100 mM KCl was not significantly changed after Mg^{2+}-loading of aortic tissue. Aortic preparations were washed in Krebs and then maintained in a solution containing Na^{+} and normal (1.2 mM) Mg^{2+} ("Na^{+}-buffer", Table 2.1, Materials and Methods) for 30 min in order to re-establish normal levels of $[Mg^{2+}]_i$ inside the cells. After this incubation, the concentration response to KCl was measured in the "Na^{+}-buffer" (Fig. 7.3*C*). Although the effect of Mg^{2+}-loading was completely reversible it was found that contraction to low concentration of KCl (15-20 mM) was smaller than that in comparison to similar concentrations before Mg^{2+}-loading (Fig. 7.4, triangles). Another effect seen in "Na^{+}-buffer" was a significant increase in the maximal level of contraction at 40 and 100 mM KCl in comparison to those measured in NMDG-based buffers (Fig. 7.3*C* and Fig.7.4)

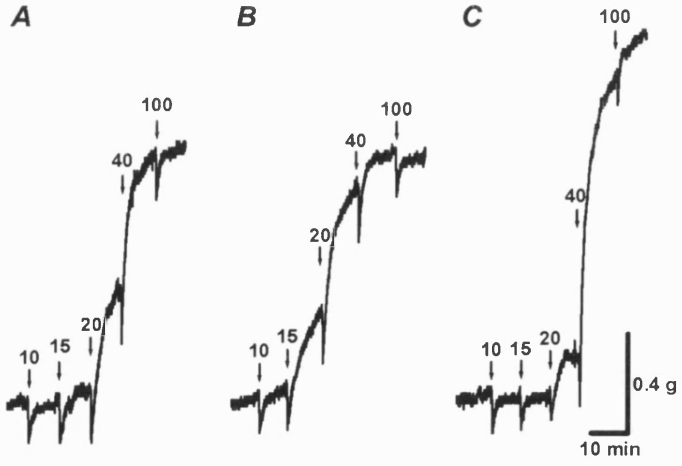

Figure 7.3. Effect of Mg^{2+}-loading on KCl-induced contraction. Different KCl concentrations were applied (as indicated in mM above the arrows) in "Na^{+}-free buffer" before (***A***) and after (***B***) Mg^{2+}-loading of aortic tissue and in "Na^{+}-buffer" after wash-out of excess of external Mg^{2+} (***C***). The data shown are representative traces recorded from the same endothelium-denuded aortic preparation.

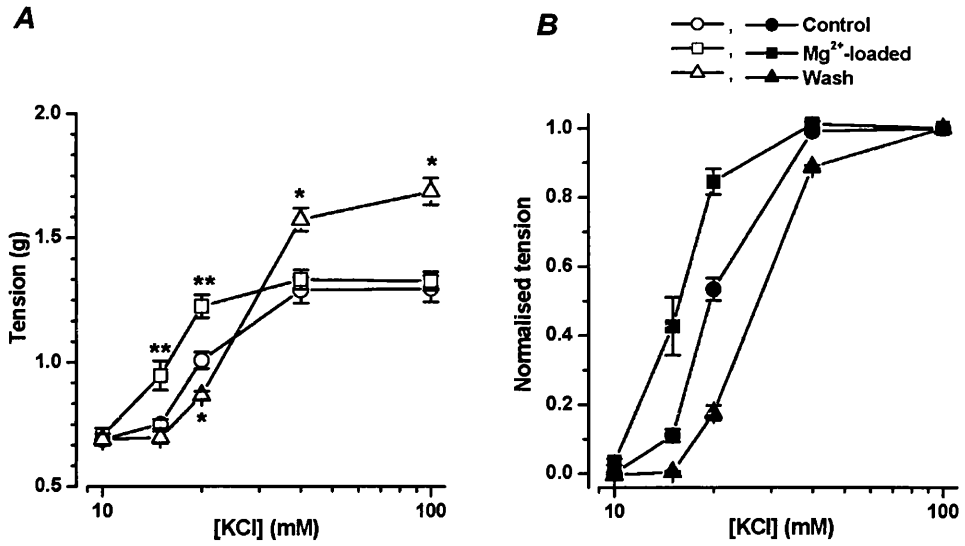

Figure 7.4. KCl-induced responses before, after Mg^{2+} loading and after wash out of elevated Mg^{2+}. ***A***, data were averaged from 8 endothelium-denuded aortic rings from 2 rats and expressed as grams of tension. In panel ***B*** contraction at each KCl concentration was corrected for the basal tension and then normalised to that at 100 mM KCl. ** indicates significant difference between Mg^{2+}-loaded and control condition ($P<0.003$, paired *t*-test). * indicates significant difference ($P<0.0008$, paired *t*-test) between the maximal contractions during wash out in "Na^+-buffer" and in "Na^+-free buffer".

7.3 Discussion: effect of intracellular Mg^{2+} on I_{Kv} "window currents"

In this chapter the theoretical prediction that an increase in $[Mg^{2+}]_i$ should reduce the open probability of I_{Kv} and I_{K1} and thus increase excitability of VSMCs was tested in endothelium-denuded rat aortic preparation. Tissue was loaded with Mg^{2+} using previously described methods (Handy *et al.*, 1996). In this set of experiments KCl was chosen as the stimulator, since it mainly acts via membrane depolarisation and activation of VDCCs. If excitability is increased in Mg^{2+}-loaded preparations then responses to KCl ought to be potentiated. Indeed this was observed in these experiments supporting the proposed hypothesis.

Several factors that may influence the interpretation of the results obtained in Mg^{2+} loaded preparations have to be considered. i) It is unknown to what degree $[Mg^{2+}]_i$ was increased. Direct measurements of changes in $[Mg^{2+}]_i$, using, for example, Mg^{2+}-sensitive fluorescent dyes, should be performed. Although such direct measurements have not been performed in the present study, Handy et al. (1996), using mag-fura dye, demonstrated that $[Mg^{2+}]_i$ significantly increased in cardiac myocytes after a similar Mg^{2+}-loading procedure. ii) Removal of Na^+ from the extracellular solution may affect the activity of Na^+-K^+ ATPase. Future experiments in the presence of ouabaine could give useful information concerning this point. iii) A significant contribution of Na^+/Ca^{2+} exchanger to increased sensitivity of aortic tissue to KCl seems unlikely. If the Na^+/Ca^{2+} exchanger is active at basal levels, then one would expect the removal of external Na^+ to stimulate the exchanger leading to increased $[Ca^{2+}]_i$ and subsequent facilitation of KCl-induced contraction. However, no significant changes in the basal tension were found when Krebs solution was replaced by a Na^+-free solution.

Another important factor which may alter the interpretation of the results is the effect of Mg^{2+} on the L-type VDCCs, whose potentiation would also facilitate KCl-induced contraction. Although we did not directly investigate the effects of intracellular Mg^{2+} on L-type VDCCs in RASMCs, White & Hartzell (1988) previously showed that within few mM range intracellular Mg^{2+} is acting as a potent voltage dependent blocker of L-type VDCCs (White & Hartzell, 1988). If this was the case in RASMCs, then inhibition and not potentiation of KCl-induced contraction would be likely to occur. In addition, if

L-type VDDCs were activated by increased $[Mg^{2+}]_i$, then the maximal contraction to KCl in Mg^{2+}-loaded preparation should be also increased. This effect was not observed.

It is also noteworthy that Mg^{2+}-loading did not cause changes in the level of maximal contraction *per se* (Fig. 7.4*A*), suggesting that the direct effect of Mg^{2+} on the contractile machinery (Erdodi *et al.*, 1988; Sato & Ogawa, 2001) is not significant under these conditions .

The exact reason for the increased degree of maximal contraction to KCl observed after wash out of aortic preparation with "Na^+-buffer" is not clear. Further experiments will be required to clarify the reason for this enhanced contraction.

Chapter 8

Modulation of I_{Kv} by protein kinase C in rat aortic smooth muscle cells

In chapters 5 and 6 I demonstrated that the effects of intracellular Mg^{2+} on the functional properties of I_{Kv} currents in VSMCs differ from those in an heterologous expression system. As mentioned in the discussion to chapters 5 and 6, one reason could be due to the presence of a specific Mg^{2+}-dependent regulatory mechanism in VSMCs that is not present in *Xenopus* oocytes. Preliminary data leading to this project, demonstrated that PKC could be involved in the regulation of Kv channels in rat aortic myocytes. Interestingly, the involvement of Mg^{2+} as a possible modulator of PKC activity has been previously reported (Hannun & Bell, 1990; Bazzi & Nelsestuen, 1992). Moreover, Mg^{2+} is an essential cofactor for some protein phosphatases (Wang *et al.*, 1995) and it could affect Kv channel functional properties via this pathway (e.g. (Zhou *et al.*, 2002)). Therefore, a possible contribution of PKC to the regulation of Kv channels was investigated in rat aortic smooth muscle cells.

8.1 Western blot and immunocytochemical analysis of expression and distribution of various PKC isoforms in rat aortic smooth muscle

The presence of four PKC isoforms PKCα, PKCγ, PKCζ and PKCε has been demonstrated previously in VSMCs (Assender *et al.*, 1994; Walsh *et al.*, 1994; Liou & Morgan, 1994). Therefore, the expression of these isoforms and their distribution between cytosolic and particulate (membrane) fractions in RASMCs was investigated using western blot and immunocytochemistry. A representative western blot analysis of the total protein extract is shown in Fig 8.1 (upper panel), where a marked expression of PKCα, PKCγ, and PKCζ but not PKCε isoforms in rat aortic smooth muscle is shown. Interestingly, only one high molecule band was detected for PKCζ, whereas in rat brain sample (used as a positive control) two specific bands were present. Immunoblot

analysis of membrane and cytosolic fractions demonstrated a prevalent distribution of PKCα and PKCδ in the membrane fraction. Surprisingly, the PKCζ isoform, markedly expressed in the total protein, was present only as a weak band of a lower molecular weight in the membrane fraction. At present, the reason for this discrepancy is not clear. PKCε was not detected in neither the membrane nor cytosolic fractions, which is consistent with the total protein analysis.

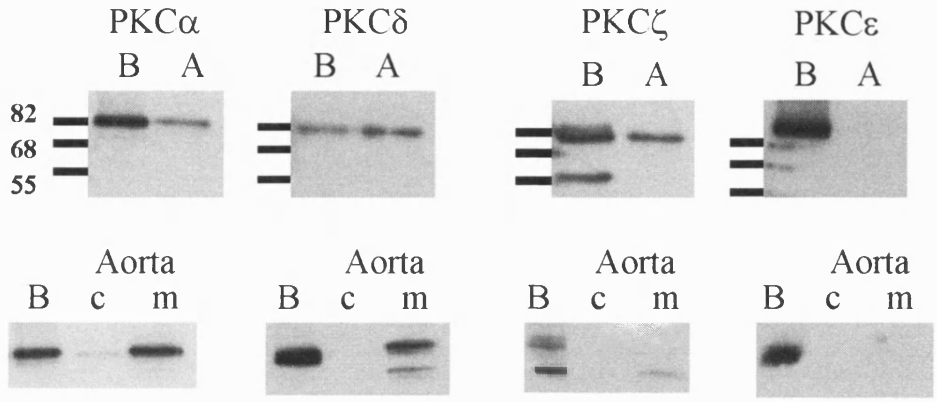

Figure 8.1 Expression and distribution of various PKC isoforms in rat aortic smooth muscle. B and A indicate total rat brain (used as positive controls), and aorta proteins, respectively. c and m are cytosolic and particulate (membrane) fractions of the total protein, correspondingly.

Intracellular distribution of the PKC isoforms was studied with immunocytochemical analysis in single RASMCs, fixed, permeabilised and stained with specific anti-PKC antibodies. Figure 8.2 illustrates representative immunofluorescent images obtained using confocal microscopy (shown on the right of each panel) and superimposed immunofluorescent and transmitted light images. This analysis shows that PKCα is predominantly expressed close to the plasma membrane, while PKCδ was localised more around the nuclear membrane. The expression of PKCε and PKCζ isoforms was not detectable under our experimental conditions.

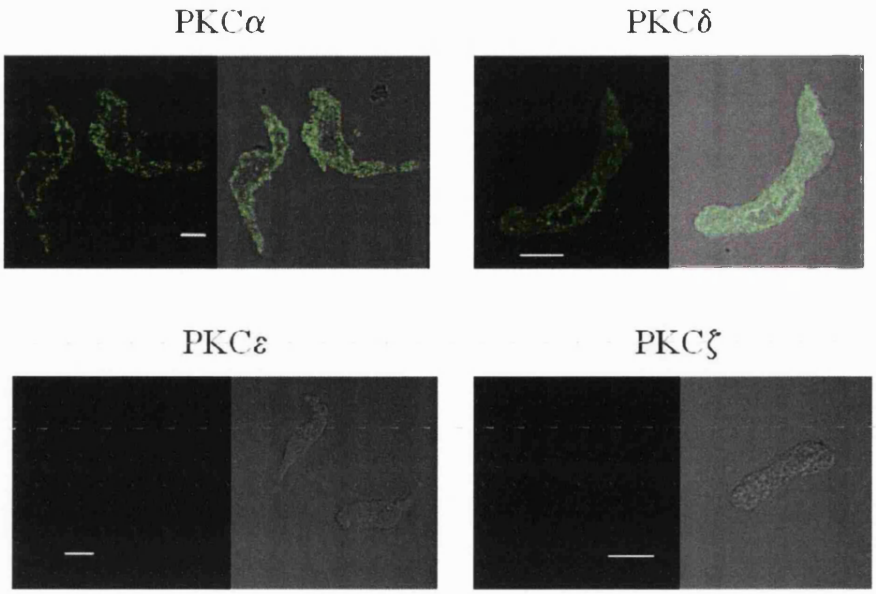

Figure 8.2 Intracelllular distribuition of various PKC isoforms in single rat aortic smooth muscle cells. Each panel shows a fluorescent image (left) and superimposed fluorescent and transmitted light images (right). Bars are 5 μM.

8.2 Effect of bisindolylmaleimide I (BIM) on I_{Kv}

The expression of the PKCα isoform in the vicinity of the plasma membrane suggests that this isoform could potentially be involved in regulation of the native Kv2.1 channel current in RASMCs. To verify such a possibility, the effect of BIM, a specific PKC inhibitor, which selectively blocks the PKCα isoform with an IC_{50} of 10 nM (Toullec *et al.*, 1991), on I_{Kv} was investigated. Two different experimental protocols were used. In one protocol, termed "acute" application, BIM (100 nM) was applied for 5 min while I_{Kv} was recorded in the whole cell mode. In another protocol, termed "pre-treatment", RASMCs were pre-incubated in 100 nM BIM for 5-10 min before patch-clamp recording started. All experiments were performed in the presence of 1 μM paxilline and 10 μM glibenclamide. The pipette solution contained 5 mM MgATP and $[Ca^{2+}]$ was kept at ~8 nM using Ca^{2+}-EGTA buffer.

8.2.1. Acute application of BIM

8.2.1.1 Time-dependence of the effect of BIM

Time-dependence of the acute effect of BIM (100 nM) was studied using the following experimental protocol. I_{Kv} was recorded for 100 s initially in the absence of BIM using a 300 ms step depolarisation to +60 mV applied every 10 s, and then in the presence of 100 nM BIM applied for 5 min. The insert in Figure 8.3*A* shows that the peak amplitude of I_{Kv} was only marginally affected by the drug, but the current measured at the end of the test pulse was significantly reduced. Figure 8.4 summarises the effect of BIM on peak I_{Kv} recorded in RASMCs. To illustrate the time course of the effect of BIM, I_{Kv} amplitude at the end of the each pulse was normalised to that measured before the treatment and plotted against the time of the drug application (Fig. 8.2*A*). The reduction of the I_{Kv} amplitude was seen more clearly during prolonged depolarisation (Fig. 8.2*B*). The decrease of the I_{Kv} amplitude at +60 mV followed a single exponential function (eq. [3.3]) with a time constant equal to 1817.1±102.6 (n=12) and 668.1±57.7 ms (n=8) for control and 100 nM BIM, respectively.

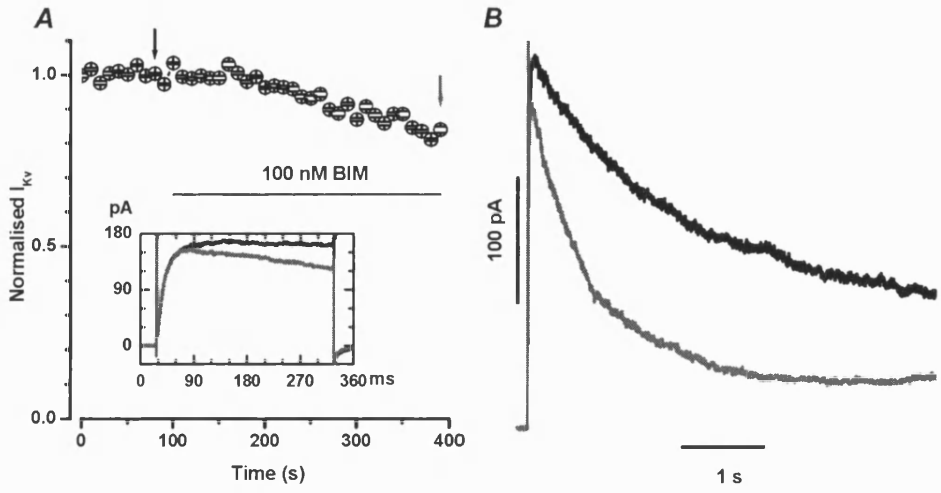

Figure 8.3 Time-dependence of the effect of the acute application of BIM on I_{Kv}. ***A*** time course of the I_{Kv} amplitude measured at 300 ms at a test pulse of +60 mV applied avery 10 s. The I_{Kv} amplitude in the presence of BIM was normalised to the mean I_{Kv} (average of 5-10 traces) before the application of the drug (n=15) The insert shows superimposed I_{Kv} traces recorded from a representative cell in the absence and presence of 100 nM BIM at the time indicated by arrows. C_m=9.7 pF ***B***, the effect of BIM on the current decay during prolonged depolarisation (5 s test pulse to +60 mV).

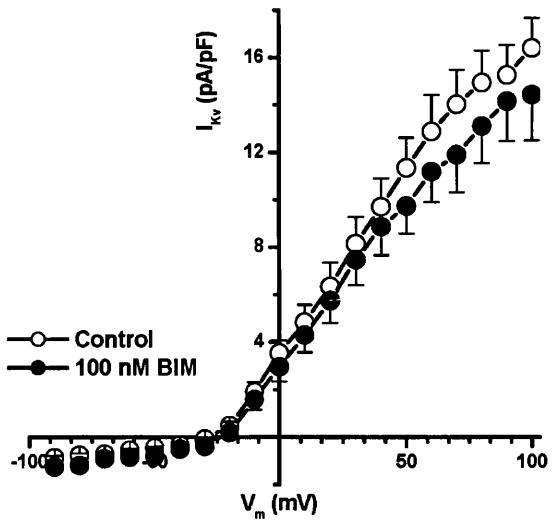

Figure 8.4 Comparison of the acute effect of BIM on I_{Kv} on the mean I-V relationships. The peak current was estimated from the single exponential fit (with the equation [2.1]) of the rising phase of the current and plotted versus V_m. Point represent means for 21 (control) and 7 (100 nM BIM) cells.

8.2.1.2. Effect of BIM on I_{Kv} steady-state activation and inactivation

I_{Kv} steady-state activation and inactivation were analysed as described in Materials and Methods (sections 2.6.6.1 and 2.6.6.4) and the mean Boltzmann parameters obtained in 8 paired RASMCs before and after the acute application of 100 nM BIM are compared in Table 8.1. No significant differences in the steady-state activation and availability parameters were found, apart from a significant reduction of the G_{max} during the acute application of the drug.

Table 8.1. Effect of acute application of BIM on voltage dependence of activation and inactivation of I_{Kv} in RASMCs.

	Control	*Acute (BIM 100 nM)*	*Significance*
V_a *(mV)*	9.3 ± 4.7	4.4 ± 2.8.	N.S.
k_a*(mV)*	-17.5 ± 2.3	-16.4 ± 2.6	N.S.
Gmax (nS/pF)	0.08±*0.01*	0.07±*0.01*	P<0.004
V_h*(mV)*	-39.5 ± 0.7	-39.5 ± 0.8	N.S.
k_h*(mV)*	6.3 ± 2.5	9.5 ± 2.7	N.S.
Iss	0.12±0.06	0.15±0.01	N.S.

V_a and V_h are half-activation and half-inactivation potentials, and k_a and k_h are slope factors for the activation and inactivation, respectively. N.S. means not significant.

8.2.1.3 Use dependence of the effect of BIM

The lack of effect of BIM on I_{Kv} inactivation dependency might suggest that acceleration of I_{Kv} decay is due to a direct effect of the drug on the channel. To assess this possibility further use-dependency of the inhibition of I_{Kv} by 100 nM BIM was studied with 200 ms depolarising pulses to +60 mV applied at three different frequencies, 0.5, 1 and 2 Hz, from the holding potential of –80 mV. In the absence of the PKC inhibitor, the peak of I_{Kv} progressively decreased as the frequency of stimulation was increased. For example, after 20 s of stimulation, the peak I_{Kv} was decreased by 5.5±1.4 % (n=4), 10.7±2.5 % (n = 3) and 33±3.8% (n = 3) at frequencies of 0.5, 1 and 2 Hz, respectively. The inhibition of the current was significantly more pronounced in the presence of the inhibitor, decreasing the I_{Kv} peak amplitude by 24.8± 3.7 (n=8), 42.6±3.2 (n=8) and 62.9±1.8 (n=7) in 0.5, 1 and 2 Hz respectively (P<0.007) (Fig.6.5). These effects suggest that the effect of BIM is use-dependent.

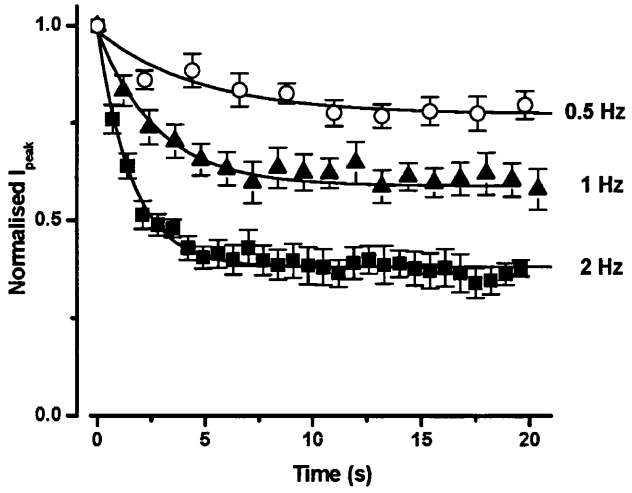

Figure 8.5. The use-dependency of the effect of 100 nM BIM. 200 ms depolarising pulses of +60 mV were applied at the indicated frequencies in the presence of 100 nM BIM. The peak amplitude of I_{Kv} at each pulse was normalised to that measured at the first pulse and then plotted against the time of stimulation. Solid lines represent single exponential fits of the experimental data with time constants of 4.5, 2.4 and 1.6 s for 0.5, 1 and 2 Hz, respectively.

8.2.1.4 Dose dependency of I_{Kv} inhibition by BIM

Concentration dependence of the effect of BIM was studied using depolarising test pulses applied every 5 s. Different concentrations of BIM (100, 200, 500 and 1000 nM) were added cumulatively to the extracellular solution for 5 min each. Representative I_{Kv} recordings in the presence and absence of 0.5 and 1 μM BIM are shown in Fig 8.6*A*. In the presence of 1 μM BIM, the peak I_{Kv} was reduced only by 18.5±5.7 % (n=6). The steady state current measured at the end of a 1 s pulse to +60 mV was affected more significantly, being reduced by 19.9±9.7 % (n=4), 41.7±23 % (n=2), 73.0±2.7 % (n=8) and 88.1±1.9 (n=5) in the presence of 100, 200, 500 and 1000 nM BIM, respectively.

To characterise quantitatively the interaction kinetics between the drug and the channel on the basis of a first order kinetics mechanism (Snyders & Yeola, 1995), the apparent affinity constant, *Kd*, and the Hill coefficient, *n*, were obtained by fitting concentration dependence data to the following equation:

$$I_{NORM} = \frac{1}{1+(Kd/[BIM])^n}, \qquad [8.1]$$

where I_{NORM} is the current normalised to that in the absence of BIM at a test potential (+60 mV).

A non-linear least-squares fit of the equation [8.1] of the concentration-response to BIM yielded an apparent *Kd* of 0.25 ± 0.01 μM and a Hill coefficient, *n*, equal 1.47 ± 0.01 (Fig. 8.6*B*).

The apparent rate constant of association, k_{+1}, and dissociation, k_{-1}, of the drug with the channel were obtained from the following equations:

$$1/\tau_d = k_{+1}[BIM] + k_{-1}, \qquad [8.2]$$

$$Kd = k_{-1}/k_{+1}, \qquad [8.3]$$

where τ_d is the drug induced time constant, which can be determined from the kinetics of the current decay in the presence of the inhibitor.

τ_d in different BIM concentrations was determined from approximation of I_{Kv} decay with the equation [3.3] during 1s pulses to +60 mV, where the current decay in the absence of the drug was negligible. The plot of the reciprocal of τ_d versus each concentration yielded an apparent association rate constant k_{+1} of 3.90±1.90 $\mu M^{-1}s^{-1}$ and a dissociation rate constant k_{-1} of 1.22±0.53 s^{-1} (Fig.8.6*C*). The theoretical *Kd* value derived from equation [8.3] is equal 0.31 μM, which is similar to the value of 0.25 μM obtained from the concentration-response curve shown in Figure 8.6*B*.

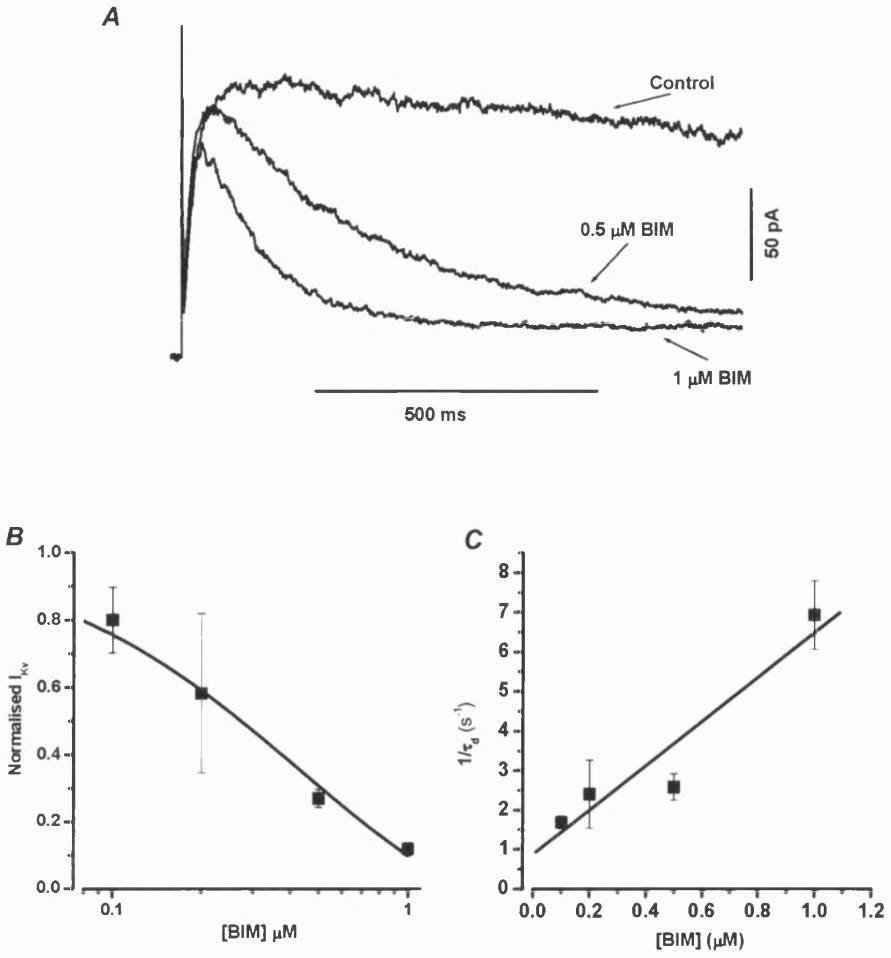

Figure 8.6 Characterisation of the concentration-dependent inhibition of I_{Kv} by BIM. ***A***, current traces (average of 3 traces each) recorded in response to 1 s depolarising pulses to +60 mV from the same RASMC in the absence (control) and in the presence of 0.5 and 1μM BIM in the extracellular solution. Various doses of BIM were applied for 5 min each. C_m = 12.6 pF. ***B***, normalised I_{Kv} amplitude measured at the end of a 1 s pulses to +60 mV in the presence of different [BIM] and reported versus [BIM]. Tha continuous line represents the fit with equation [8.1], giving an apparent *Kd* equal to 0.25 μM and the Hill coefficient *n* equal 1.47. ***C***, dependence of the inversed time constant ($1/\tau_d$) reported versus [BIM]. Continuous line is the fit with equation [8.3] giving k_{+1} and k_{-1} equal to 3.90 $\mu M^{-1}s^{-1}$ and 1.22 s^{-1}, respectively.

8.2.1.5 Changes in I_{Kv} activation kinetics

During the analysis of the rate of I_{Kv} activation at various membrane potentials (derived from individual I-Vs) in the presence and absence of the drug a trend for the rate of I_{Kv} kinetics to increase after acute application of 100 nM BIM was noticed (Fig. 8.7*A*),

although no significance between data pooled from different RASMCs was observed. In order to examine this effect more closely, the rate of I_{Kv} activation was measured at a single potential (+60 mV). To reduce the noise and facilitate a comparison, at least 5 current traces in the absence of BIM and 3-5 traces after 5 min in the presence of 100 nM BIM were averaged and the mean currents were fitted to a single exponential function (eq. [2.1]) (Fig.8.7*B*). This analysis showed a consistent acceleration of the I_{Kv} kinetics with a time constant reduced from 12.5±1.0 ms to 10.9±0.6 ms (n=16, $P<0.03$) (Fig. 8.7*C*).

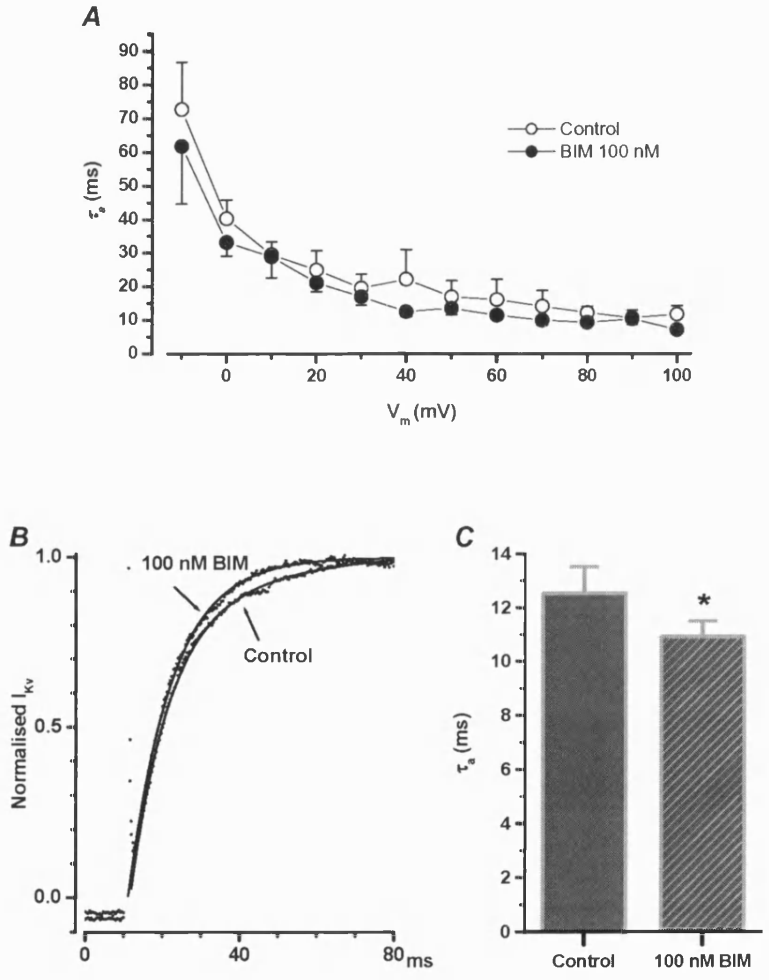

Figure 8.7 Effect of BIM on the kinetics of I_{Kv} activation. ***A***, time constant of activation, τ_a, reported versus V_m in the presence (open squares) and in the absence (filled squares) of 100 nM BIM in 8 paired cells. ***B***, I_{Kv} were elicited by 300 ms, +60 mV pulses in the absence and presence of the drug, averaged and normalised to their peaks as described in the text. Solid lines represent a single exponential fit with time constants (τ_a) of 13.7 and 11.2 ms. ***C***, summary of the effect of BIM on τ_a in 8 paired cells. Asterisk indicates $P<0.03$.

8.2.2 Pre-treatment with BIM

In this set of experiments, 100 nM BIM was continually present 5 min before the beginning of the patch-clamp recording and during the 5 min of equilibration period after the whole cell configuration was achieved. The total duration of the exposure to BIM before I_{Kv} properties were characterised was therefore ≥ 10 min.

8.2.2.1 Effect of BIM pre-treatment on I_{Kv} steady-state activation and inactivation

Figure 8.8*A* compares the effect of the pre-treatment on the I-V relationships for the I_{Kv} peak. The mean I-V relationship for I_{Kv} in RASMCs *acutely* treated with BIM is also shown for comparison. The pre-treatment with BIM significantly reduced the maximal I_{Kv} conductance without significant changes in the steady state activation dependency (Fig. 8.8*A* and *B*, Table 8.2). Also, a significant shift in I_{Kv} availability to more negative membrane potentials and a slight but significant decrease in the non-inactivating current fraction (I_{ss}) was observed after the pre-treatment procedure (Fig. 8.8*C* and Table 8.2).

Table 8.2. Comparison of the effect of the BIM pre-treatment on the voltage-dependent parameters for I_{Kv}

	Control	*Pre-treatment (BIM 100 nM)*	*Significance*
V_a *(mV)*	6.5 ± 2.2 (21)	4.0 ± 1.9 (27)	N.S.
k_a *(mV)*	-14.7± 0.9 (21)	-13.4 ± 0.5 (27)	N.S.
G_{max} *(nS/pF)*	0.09 ± 0.006 (21)	0.06 ± 0.003 (27)	$P < 0.0006$
V_h *(mV)*	-43.8 ± 2.6 (12)	-54.6 ± 1.7 (7)	$P < 0.003$
k_h *(mV)*	8.9 ± 0.63 (12)	11.1 ± 1.0 (7)	N.S.
I_{ss}	0.24±0.02 (12)	0.19±0.02 (12)	$P < 0.02$

Abbreviations are as previously defined. N.S. indicates not significant. P was determined using unpaired *t*-test.

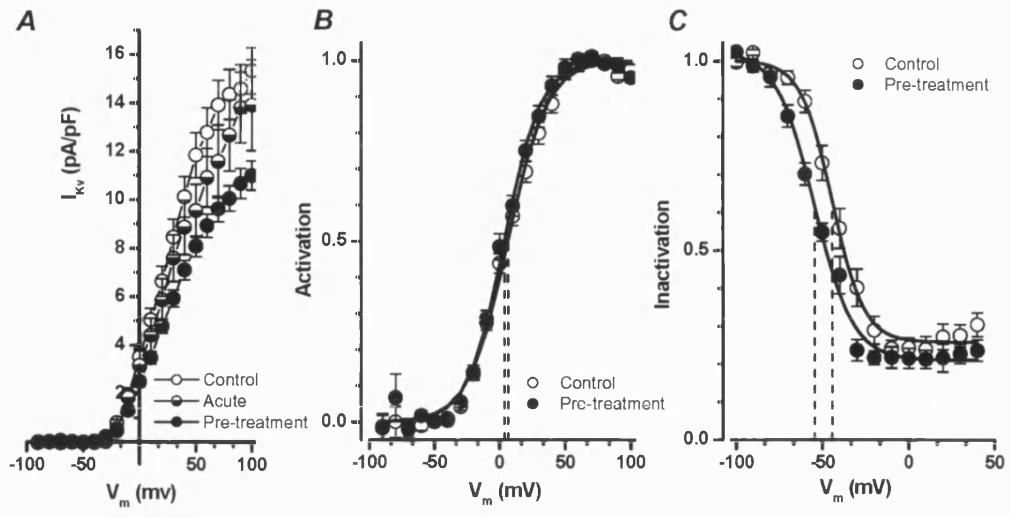

Figure 8.8 The effect of the pre-treatment with BIM (100 nM) on I_{Kv}. ***A***, comparison of the I-V relationship of the I_{Kv} peak after pre-treatment (n=27), after the acute application (n=7) and in the absence of the drug (control) (n=21). Voltage-dependency of the activation ***B*** and inactivation ***C*** in control and pre-treated RASMCs. Continuous lines represent the fit with the Boltzmann equation (eq. [2.6] and [2.9] for activation and inactivation, respectively) giving the values of V_a equal 6.3 and 3.6 mV, k_a equal –14.9 and –13.8 mV, V_h equal –44.2 and –54.5 mV, k_h equal 9.1 and 11.1 mV for control and pretreatment, respectively.

Similar to the comparison of τ_a derived from I-Vs during the acute application of the drug, no significant differences in the rate of I_{Kv} activation after pre-treatment with BIM was observed (Fig.8.9*A*). The rate of I_{Kv} decay measured during 5 s depolarisation to +60 mV after BIM pre-treatment was similar to that recorded during the acute application of 100 nM BIM (Fig. 8.9*B*), indicating that no additional direct effect of the drug on the channel was developed during prolonged exposure.

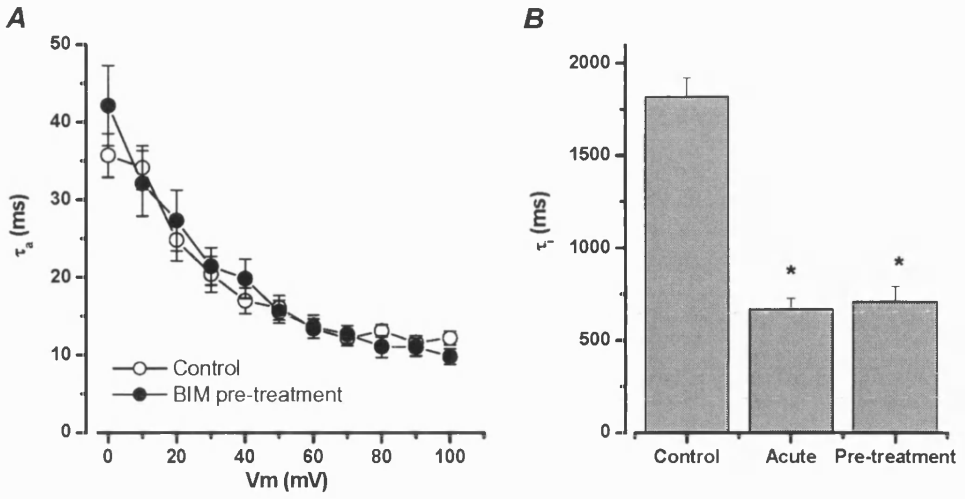

Figure 8.9. Time constant of activation (τ_a) and inactivation (τ_i) in control and pre-treated cells. ***A***, comparison of the potential-dependence of τ_a in control (n=21) and pre-treated RASMCs with 100 nM BIM (n = 27). τ_a were determined from the fit with the equation [2.1]. ***B***, comparison of the time constant of I_{Kv} decay measured during 5 sec pulses to +60 mV using the equation [3.3] in 12 (control), 8 (acute) and 10 (pre-treated) RASMCs. Asterisks indicate values significantly ($P<0.01$) different from that recorded in the absence of BIM.

8.2.3 Effect of BIM on Kv2.1 channels expressed in Xenopus oocytes

The effect of BIM on the Kv2.1 channel, the proposed molecular candidate for I_{Kv}, heterologously expressed in *Xenopus* oocytes was also examined. Application of 1 μM BIM to the intracellular side of the inside-out patch reduced the Kv2.1 current elicited by a 1s depolarising pulse to +60 mV by 49.7±1.3 % (n=3). This effect was rapidly developed (within ~ 10 s) and was fully reversible (Fig.8.10*B*). The current decay was greatly accelerated in the presence of the drug. The ratio of the current measured at the end of the pulse and that measured at the peak was equal 0.61±0.08 and 0.09±0.01 in 2 different patches, analysed in the absence and presence of 1 μM BIM, respectively. It is noteworthy that, in contrast to I_{Kv} in RASMCs, the activation rate, measured as the time required to reach the half peak current amplitude, $t_{1/2}$, was not significantly affected by the drug, being equal to 17.4±2.0 ms (Control) and 14.0±2.6 ms (1 μM BIM) in 3 paired patches.

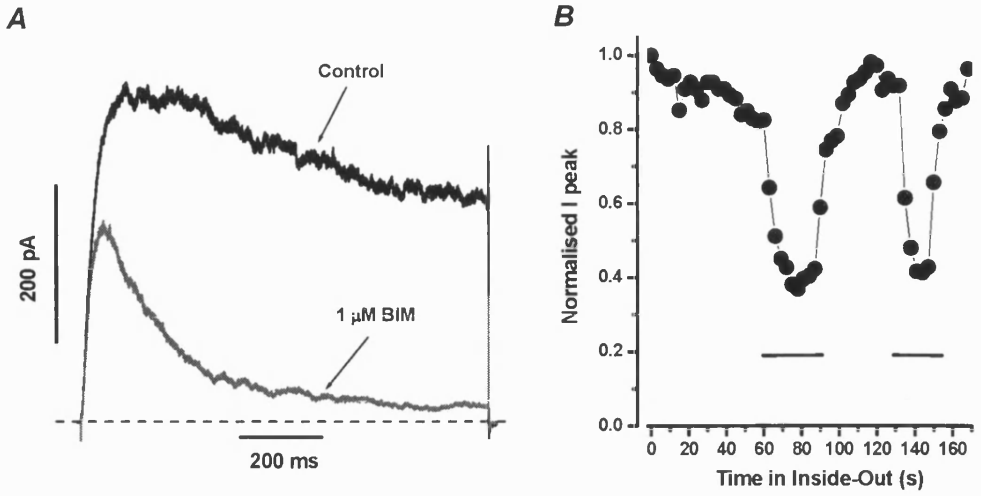

Figure 8.10 Effect of BIM on Kv2.1 mediated current expressed in *Xenopus* oocytes. ***A*** reports representative traces recorded in the absence (black trace) and in the presence (grey trace) of 1 μM BIM in the intracellular solution. Current traces were recorded in inside-out configuration in response to 1 s depolarising pulses to +60 mV. ***B*** shows time dependency of the effect of BIM (1 μM, horizontal bars) on the normalised peak current amplitude in response to 100 ms pulses to +60 mV acquired every 5 s.

8.3. Effect of phorbol 12-myristate 13-acetate (PMA) on I_{Kv}

The protocols of acute application of 100 nM PMA, a specific PKC activator, and the pre-treatment with PMA were the same as those described for BIM. Mean current traces recorded from a representative cell are shown in Figure 8.11*A*. No significant changes in the time constant of the I_{Kv} activation were observed during the acute application of PMA. τ_a was equal to 15.8±3.9 and 15.0±3.6 ms and in three paired RASMCs studied before and 5 min after acute application of PMA, respectively. However, wash out of PMA (100 nM) after the pre-treatment procedure caused a marked effect on the I_{Kv} activation kinetcs (Fig. 8.11*B*). In order to analyse the kinetics of I_{Kv} activation, an analysis similar to that of BIM was applied. 10 current traces in the presence of 100 nM PMA and 5 traces recorded 5 min after the removal of the drug were averaged and the mean traces were fitted to a single exponential function (eq. [2.1]) with the time constant equal to 15.1±1.8 ms (n=6) (PMA) and 10.7±1.3 ms (n=6) (wash-out) (Fig. 8.11*B*, $P<0.03$), showing a significant acceleration of the I_{Kv} activation kinetics after wash out of PMA.

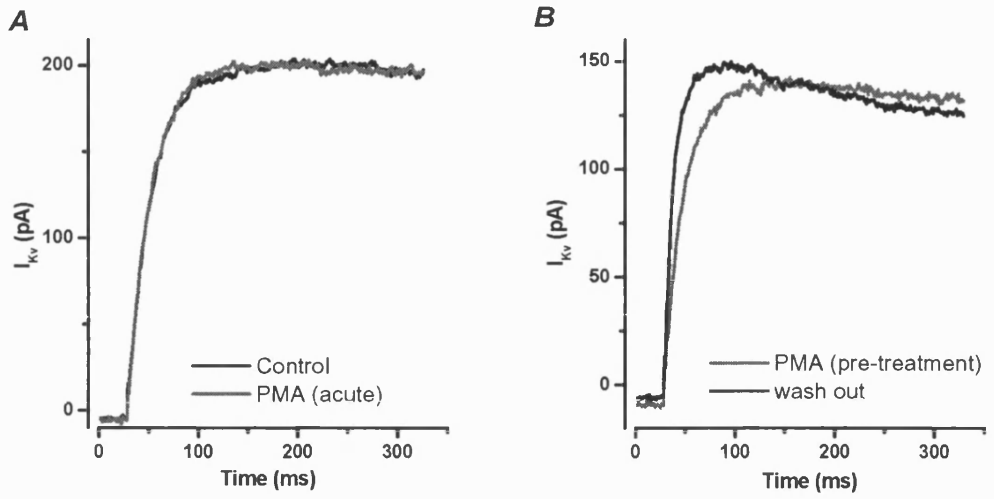

Figure 8.11. The effect of PMA on I_{Kv} activation kinetics. ***A***, the acute application of 100 nM PMA. I_{Kv} was compared before and after 5 min of continuous superfusion with the drug. C_m= 13.9 pF. ***B***, the effect of wash out of PMA after pre-treatment with the drug. PMA was washed out for 5 min and the current was analysed as described in the text. C_m=12.3 pF.

8.4 Effect of chelerythrine on I_{Kv} availability

The effect exhibited by another potent and selective PKC inhibitor, chelerythrine, on the I_{Kv} availability was investigated in RASMCs. I_{Kv} availabilities were recorded at 5 min intervals, in the absence and presence of 2 mM chelerythrine and after wash out of the drug. I_{Kv} availability was analysed using the Boltzmann function (eq. [2.9]) and V_h values were then compared in Fig. 8.12. It is clearly seen that chelerythrine caused a progressive negative shift of ~10 mV in the availability after ~10 min of incubation with the PKC inhibitor. The effect was completely reversible after removal of the drug. Similar results were obtained in 2 other RASMCs. The averaged negative shift of V_h was equal –1.8±1.0 mV and –6.4±2.5 mV after 5 and 10 min in 2 μM chelerythirine, respectively. It has to be mentioned that these experiments were performed in the presence of 5 mM $MgCl_2$, and not MgATP, in the pipette solution.

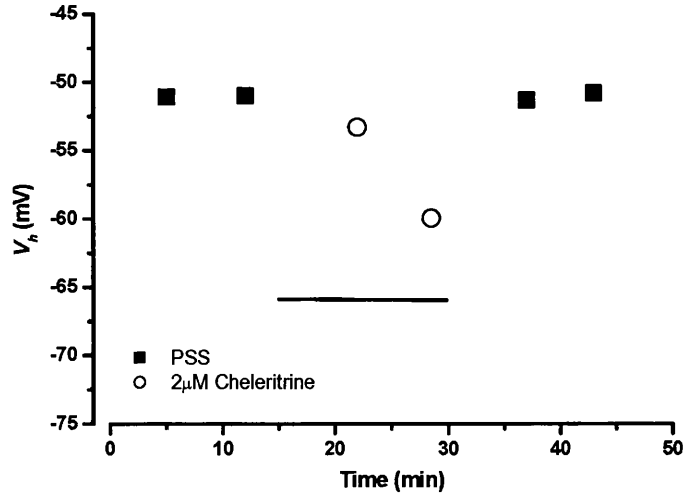

Figure 8.12. Effect of the acute application of chelerythrine on the half inactivation potential, V_h. C_m=13.1 pF. Pipette solution contained 5 mM $MgCl_2$.

8.5 Discussion: regulation of I_{Kv} by PKC

8.5.1 Biochemical detection of PKC isoforms in rat aorta

Western blot and immunocytochemistry showed that different PKC isoforms are unequally distributed in RASMCs. Thus, although both PKCα and PKCδ were found in the membrane fractions, their intracellular distribution was dissimilar. Only PKCα was localised close to the plasma membrane, whereas the PKCδ isoform was mostly localised near the nuclear membrane. This distribution of PKCδ has not been reported previously in VSMCs. PKCε and PKCζ were not detectable in my immunocytochemical experiments.

It is interesting to mention that an additional band for PKCδ appears after fractionation of the total protein fraction. Also, the band in the membrane fraction for PKCζ is "shifted" to low molecular weights as a consequence of protein fractionation. Although the exact reason for this difference is not clear, it is possible that partial protein degradation occurring during the fractionation might be responsible.

The distribution of the PKCα isoform near the plasma membrane makes this isoform the most likely candidate involved in the regulation of I_{Kv} in RASMCs, although other

isoenzymes, e.g. PKCζ, cannot be entirely excluded at this stage. It was for these reasons that BIM was chosen as an inhibitor with high specificity for PKCα (Toullec *et al.*, 1991).

8.5.2 Effect of PKC inhibition and activation on I_{Kv}

A number of PKC isoform specific inhibitors have been developed. One group of PKC inhibitors, bisindolylmaleimides, which are derived from staurosporine, are widely used for studying signal transduction pathways in various cell systems. BIM (I) is a less potent but more selective inhibitor for PKC than staurosporine. It has a half inhibition value of 10 nM for PKC and 2 μM for PKA, whereas staurosporine has a value of 0.7 nM for PKC and 7nM for PKA (Toullec *et al.*, 1991). BIM competes with ATP for the PKC ATP-binding site. On the other hand, both staurosporine and bisindolylmaleimides were found to suppress cloned Kv1.3 and Kv1.5 channels expressed in Chinese hamster ovary cells directly, and not via PKC-dependent pathways (Choi *et al.*, 1999; Choi *et al.*, 2000). The analysis of the acute action of BIM on I_{Kv} in RASMCs suggests that it also blocks I_{Kv} via a similar mechanism. Evidence for a preferential interaction of BIM with the open state (usually termed "open channel block") are: 1) BIM caused acceleration of the rate of I_{Kv} decay without a significant effect on the I_{Kv} peak amplitude; 2) BIM did not affect the inactivation dependency, suggesting that it does not interact with the inactivated state of the channel; and 3) BIM blocked I_{Kv} in a use-dependent manner. This possibility was confirmed by experiments performed on the Kv2.1 channel expressed in *Xenopus* oocytes. As proposed earlier the Kv2.1 α-subunit is one of the major components of I_{Kv} in RASMCs. The fact that BIM exerted its effects when applied intracellularly (in inside-out patches), suggests that its binding site in the open channel might be located at the intracellular side of the channel.

Assuming the direct effect of BIM on I_{Kv}, the PKC-independent block of Kv channel currents in native and heterologously expressed systems by BIM can be described using the following scheme:

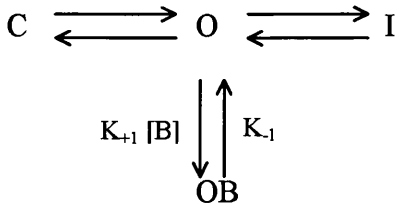

Where C represents the closed state of the channel, O is the open state, OB is the drug-bound open state, and I is the inactivated state.

The predominant open channel blockage of I_{Kv} by BIM made it difficult to dissect a possible PKC-dependent action of this drug. Nevertheless, a small but significant change in the activation time course, caused by the acute application of 100 nM BIM, was observed. This effect cannot be explained on the basis of the drug interaction with the open channel and might reflect a PKC-dependent process. Also, application of a 10 times higher concentration of BIM on the Kv2.1 channel current did not significantly affect the activation rate, indirectly supporting this suggestion. It is noteworthy that slowing down of current kinetics by PMA was observed only when intact cells were pre-incubated with the drug, but not when PMA was acutely applied after the whole-cell configuration was established, suggesting that a direct (non PKC-mediated) effect of PMA on Kv channel currents in RASMCs is unlikely. The similar effect of PMA and BIM on I_{Kv} activation kinetics is difficult to explain. It is possible that PMA stimulates the same PKC by enhancing autophosphorylation of the enzyme. In this case, the removal of the PKC activator may mimic the effect of the PKC inhibitor. The involvement of different PKC isoenzymes targeted by BIM and PMA also cannot be excluded. A comparison of the results obtained with acute application of BIM and PMA and those obtained after pre-treatment with these agents suggests that an intermediate factor, which is removed or inactivated during cell perfusion in whole-cell, could be important in this process. Indeed, a significant negative shift of ~10 mV on the I_{Kv} inactivation dependencies and a significant decrease of the current non-inactivating component (I_{ss}) were observed after pre-treatment with BIM. Current conductance was also significantly reduced by ~30% in comparison to control. It is important to mention that the effect of the pre-treatment with BIM on the kinetics of I_{Kv} inactivation was virtually identical to that of acute application of the drug, suggesting a similar degree of the open channel block under both conditions. Interestingly, chelerythrine, which is a

substrate specific PKC inhibitor, also caused significant shift in inactivation dependency when applied acutely. Interestingly, Chelerythrine did not cause acceleration of the kinetics of I_{Kv} decay as BIM did, suggesting the absence of open channel blockage effect. For this reason, chelerythrine could be a more suitable pharmacological tool in the investigation of PKC-dependent regulation of Kv currents in VSMCs.

It is noteworthy that pre-treatment with BIM did not significantly affect I_{Kv} activation voltage dependency, in contrast to the inactivation dependency that was negatively shifted. As previously discussed (Chapter 7), such differential changes in activation and inactivation dependencies can significantly alter the number of Kv channels opened near to the resting membrane potential and increase excitability. To examine this possibility, Kv window currents in the absence of BIM and after pre-treatment with the drug were constructed in a similar manner to that described in Chapter 7 (Fig. 8.13). The analysis predicts ~ 50% reduction in the fraction of Kv channels opened at –50 mV.

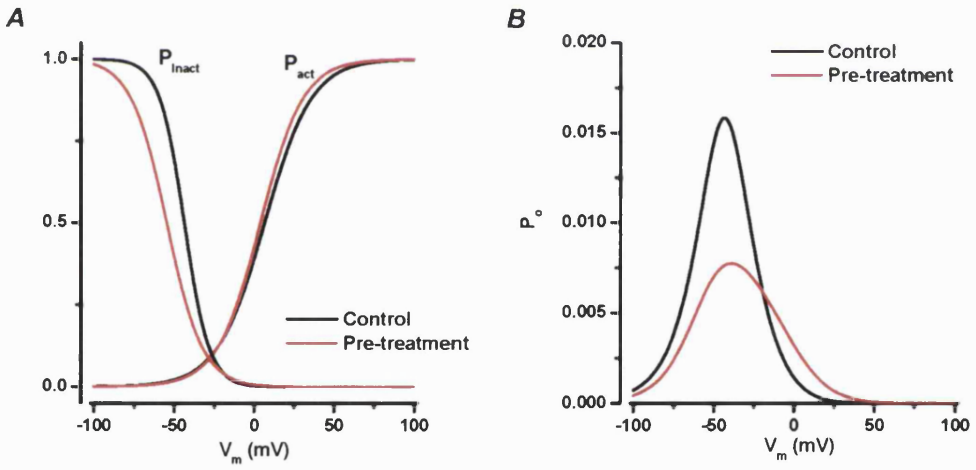

Figure 8.13. The effect of pre-treatment with BIM on the I_{Kv} window current. ***A***, normalised activation and inactivation curves derived for the parameters reported in Table 8.2. ***B***, theoretical I_{Kv} window currents constructed as indicated in Chapter 7.

The results of experiments with PKC inhibitors strongly suggest that in RASMCs I_{Kv} is regulated by PKC, possibly by the PKCα isoform, though the precise mechanism is not clear. Also, similarity between the effect of PKC inhibitors and changes in intracellular

[Mg^{2+}] might indicate possible cross talk between the two novel phenomena I have discovered and characterised in the rat aorta. Further experimental evidence will be required to draw the full picture of the complex regulation of the Kv currents in rat aorta.

Summary and conclusions

The main aim of my thesis was to investigate the functional role of Kv channel currents and the mechanisms which might control their activity in VSMCs. This aim was based on the recently emerging evidence that Kv channels could play a pivotal role in the control of vascular smooth muscle tone. During my study I have learned and successfully applied a range of experimental techniques, including the patch-clamp and two microelectrode voltage clamp techniques on single isolated smooth muscle cells and *Xenopus* oocytes, isometric tension measurements in intact vascular smooth muscle preparations, immunoblot analysis of whole tissue protein and confocal analysis of immunocytochemical images forintracellular localisation of Kv channel α-subunits and PKC isoforms. The results of my work can be summarised as followed:

1. It was demonstrated that, in rat aortic SMCs, Kv currents, and not BK_{Ca}, are the main contributor to the whole-cell K^+ currents activated in a physiological range of membrane potentials between -60 and -20 mV. The Kv conductance dominated both in low and increased intracellular [Ca^{2+}] levels. This conclusion was supported by isometric tension measurements in rat aortic rings, as non-stimulated preparations contracted in response to application of TEA and 4-AP (inhibitors which blocked Kv currents in this type of VSMCs) but not of paxilline (a selective and potent BK_{Ca} inhibitor) or glibenclamide (a specific K_{ATP} channel inhibitor). In addition, rhythmic contractions induced by PE and termed oscillatory waves were characterised for the first time in intact rat aortas. It was suggested that oscillatory waves could be mediated by PE-induced membrane-depolarisation and activation of L-type VDCCs which trigger CICR from ryanodine-sensitive intracellular Ca^{2+} stores. Modulation of rhythmic activity by TEA and 4-AP, but not IbTx and paxilline, suggests that Kv channels play a key role in this process as a negative feedback mechanism. Therefore, the results of patch-clamp and isometric tension studies strongly support the central role of the Kv channels in the regulation of excitability and active contraction of the rat aortic smooth muscle.

2. The molecular identity of Kv channels in rat aortic SMCs was assessed based on pharmacological and electrophysiological profiles of I_{Kv} and biochemical and

immunocytochemical characterisation of the expression of Kv isoforms using specific anti-Kv antibodies. Moderate TEA and 4-AP sensitivity and insensitivity to charybdotoxin, α-dendrotoxin and correolide (inhibitors of Kv1 channel subtypes) together with relatively slow activation kinetics and a negative U-shaped inactivation dependency, fit the profile of the Kv2 subfamily of Kv channels. Abundant expression of Kv2.1 isoform in the whole aorta protein lysate and clustering sub-plasmalemmal localisation of Kv2.1 channels in single RASMCs suggest that Kv2.1 α-subunit is a major molecular component of the native Kv channel in rat aortic SMCs.

3. The novel observation that changes in intracellular Mg^{2+} have specific effects on voltage-dependent characteristics (such as steady-state activation and inactivation dependencies) of I_{Kv} was made in RASMCs. An increase in $[Mg^{2+}]_i$ caused a significant negative shift in the inactivation, but not activation, of I_{Kv}. Such shift should reduce open probability of Kv channels near the resting membrane potential, therefore leading to increased tissue excitability. This prediction was confirmed in experiments measuring isometric tension in Mg^{2+}-loaded endothelium-denuded rat aortic rings, as concentration-response to KCl was significantly potentiated.

4. The effect of intracellular Mg^{2+} on Kv currents was also studied in rat conduit pulmonary arterial SMCs, where two electrophysiologically distinct cell subtypes (termed I_{K1} and I_{K2}), were identified and characterised. It was proposed that I_{K1} and I_{K2} channels are probably formed by members of the Kv1 and Kv2 subfamilies, respectively. An increase in $[Mg^{2+}]_i$ caused opposite effects on the voltage-dependent characteristics, significantly shifting the inactivation dependency of I_{K1}, but not of I_{K2}, to more negative voltages. In contrast, the steady-state activation of I_{K2} was more affected by intracellular Mg^{2+} compared to that of I_{K1}. Also, additional differential effects were observed on the whole-cell conductance of both Kv channels. Comparison of the effect of $[Mg^{2+}]_i$ on Kv1.5 and Kv2.1 channels (representative of the Kv1 and Kv2 channel sub-families) heterologously expressed in *Xenopus* oocytes revealed a similar effect on the voltage-dependent characteristics, shifting both steady-state activation and inactivation dependencies to a similar degree. Comparison of the results obtained in different types of VSMCs and in a heterologously expression system, suggests the existence of a specific Mg^{2+}-dependent mechanism which differentially modulates Kv channel activity in VSMCs.

5. The involvement of PKC in the regulation of I_{Kv} in rat aortic SMCs was investigated using selective PKC inhibitors (BIM and chelerythrine). During this work, it was found that BIM, but not chelerythrine, acts as an open channel blocker, therefore the pre-treatment of RASMCs with BIM was utilised, whereas chelerythrine was applied acutely. Both PKC inhibitors caused a negative shift in inactivation dependency I_{Kv}, thus mimicking the effects of $[Mg^{2+}]_i$ on the current. Western blot analysis demonstrated the presence of PKCα, PKCδ and PKCζ, but not PKCε, isoforms in the whole tissue lysate. PKCα and PKCδ were chiefly present in the particulate (membrane) fraction. Confocal image analysis of single RASMCs stained with anti-PKCα and anti-PKCδ antibodies clearly demonstrated that PKCα is distributed close to the cell plasma membrane, while PKCδ is localised close to the nucleus, suggesting a potential involvement of the PKCα isoform in the regulation of I_{Kv} in RASMCs.

In conclusion, I have demonstrated that Kv currents, mediated mainly by Kv2.1 α-isoform, play the key role in the regulation of excitability and contractile activity of rat aortic smooth muscle. I have discovered that Kv channel currents are regulated by intracellular Mg^{2+} in a manner specific for a particular type of VSMCs, which could differentially modulate blood vessel reactivity. Similarity between the effects of intracellular Mg^{2+} and inhibition of PKC activity observed in rat aortic SMCs points towards a complex crosstalk between these two processes. The understanding of a complex mechanism regulating Kv channel currents by intracellular second messengers in VSMCs is far from complete and therefore represents an important goal for further studies.

References

Aaronson, P. I., Bolton, T. B., Lang, R. J., & MacKenzie, I. (1988). Calcium currents in single isolated smooth muscle cells from the rabbit ear artery in normal-calcium and high-barium solutions. *J.Physiol.* **405**, 57-75.

Aaronson, P. I. & Smirnov, S. V. (1996a). Membrane ion channels in vascular smooth muscle excitation-contraction coupling. In *Pharmacology of Vascular Smooth Muscle*, eds. Garland, C. J. & Angus, J. A., pp. 136-159. Oxford University Press, Oxford - New York - Tokyo.

Aaronson, P. I. & Smirnov, S. V. (1996b). Regulation of voltage-gated K^+ channels in vascular smooth muscle cells. In *Smooth Muscle Excitation*, eds. Bolton, T. B. & Tomita, T., pp. 63-73. Academic Press, London - San Diego - New York - Boston - Sydney - Tokyo - Toronto.

Aaronson, P. I., Smirnov, S. V., Robertson, T. P., & Ward, J. P. T. (1994). Reduction of delayed rectifier K^+ current in rat pulmonary artery cells during chronic hypoxia. In *The Resistance Arteries. Integration of the Regulatory Pathways*, eds. Halpern, W., Bevan, J., Brayden, J., Dustan, H., Nelson, M., & Osol, G., pp. 103-113. Humana Press, Totowa, New Jersey.

Aaronson, P. I. & Ward, J. P. (1999). *The Cardiovascular System at a Glance*, 1 ed. Blackwell Science (UK).

Ahn, D. S. & Hume, J. R. (1997). pH regulation of voltage-dependent K^+ channels in canine pulmonary arterial smooth muscle cells. *Pflugers.Arch.* **433**, 758-765.

Aiello, E. A., Clément-Chomienne, O., Sontag, D. P., Walsh, M. P., & Cole, W. C. (1996). Protein kinase C inhibits delayed rectifier K^+ current in rabbit vascular smooth muscle cells. *Am.J.Physiol.* **271**, H109-H119.

Aiello, E. A., Walsh, M. P., & Cole, W. C. (1995). Phosphorylation by protein kinase A enhances delayed rectifier K^+ current in rabbit vascular smooth muscle cells. *Am.J.Physiol.* **268**, H926-H934.

Akaike, N., Kanaide, H., Kuga, T., Nakamura, M., Sadoshima, J., & Tomoike, H. (1989). Low-voltage-activated calcium current in rat aorta smooth muscle cells in primary culture. *J.Physiol.* **416**, 141-160.

Albelda, S. M. & Buck, C. A. (1990). Integrins and other cell adhesion molecules. *FASEB J* **4**, 2868-2880.

Allen, B. G. & Walsh, M. P. (1994). The biochemical basis of the regulation of smooth-muscle contraction. *Trends.Biochem.Sci.* **19**, 362-368.

Altura, B. M. & Altura, B. T. (1984). Magnesium, electrolyte transport and coronary vascular tone. *Drugs* **28**, 120-142.

Amedee, T., Benham, C. D., Bolton, T. B., Byrne, N. G., & Large, W. A. (1990). Potassium, chloride and non-selective cation conductances opened by noradrenaline in rabbit ear artery cells. *J Physiol* **423**, 551-568.

Archer, S. L., Huang, J. M. C., Reeve, H. L., Hampl, V., Tolarova, S., Michelakis, E., Weir, E. K., & Huang, J. M. (1996). Differential distribution of electrophysiologically distinct myocytes in conduit and resistance arteries determines their response to nitric oxide and hypoxia. *Circ.Res.* **78**, 431-442.

Archer, S. L., London, B., Hampl, V., Wu, X., Nsair, A., Puttagunta, L., Hashimoto, K., Waite, R. E., & Michelakis, E. D. (2001). Impairment of hypoxic pulmonary vasoconstriction in mice lacking the voltage-gated potassium channel Kv1.5. *FASEB J.* **15**, 1801-1803.

Archer, S. L., Souil, E., Dinh-Xuan, A. T., Schremmer, B., Mercier, J. C., El, Y., Nguyen-Huu, L., Reeve, H. L., & Hampl, V. (1998). Molecular identification of the role of voltage-gated K^+ channels, Kv1.5 and Kv2.1, in hypoxic pulmonary vasoconstriction and control of resting membrane potential in rat pulmonary artery myocytes. *J Clin Invest* **101**, 2319-2330.

Armstrong, C. M., Bezanilla, F., & Rojas, E. (1973). Destruction of sodium conductance inactivation in squid axons perfused with pronase. *J Gen Physiol* **62**, 375-391.

Ashcroft, F. M. (2000). *Ion Channels and Disease* Academic Press.

Ashcroft, F. M. & Gribble, F. M. (1998). Correlating structure and function in ATP-sensitive K+ channels. *Trends.Neurosci.* **21**, 288-294.

Ashida, T. & Blaustein, M. P. (1987). Regulation of cell calcium and contractility in mammalian arterial smooth muscle: the role of sodium-calcium exchange. *J Physiol* **392**, 617-635.

Assender, J. W., Kontny, E., & Fredholm, B. B. (1994). Expression of protein kinase C isoforms in smooth muscle cells in various states of differentiation. *FEBS Lett.* **342**, 76-80.

Balzer, M., Lintschinger, B., & Groschner, K. (1999). Evidence for a role of Trp proteins in the oxidative stress-induced membrane conductances of porcine aortic endothelial cells. *Cardiovasc Res* **42**, 543-549.

Barbe, C., Dubuis, E., Rochetaing, A., Kreher, P., Bonnet, P., & Vandier, C. (2002). A 4-AP-sensitive current is enhanced by chronic carbon monoxide exposure in coronary artery myocytes. *Am.J.Physiol.Heart.Circ.Physiol.* **282**, H2031-H2038.

Baron, A., Frieden, M., Chabaud, F., & Beny, J. L. (1996). Ca^{2+}-dependent non-selective cation and potassium channels activated by bradykinin in pig coronary artery endothelial cells. *J Physiol* **493**, 691-706.

Barry, P. H. & Lynch, J. W. (1991). Liquid junction potentials and small cell effects in patch-clamp analysis. *J.Membr.Biol.* **121**, 101-117.

Baumgarten, C. M. & Clemo, H. F. (2003). Swelling-activated chloride channels in cardiac physiology and pathophysiology. *Prog Biophys Mol Biol* **82**, 25-42.

Bazzi, M. D. & Nelsestuen, G. L. (1992). Autophosphorylation of protein kinase C may require a high order of protein-phospholipid aggregates. *J Biol Chem* **267**, 22891-22896.

Beech, D. J. & Bolton, T. B. (1989). A voltage-dependent outward current with fast kinetics in single smooth muscle cells isolated from rabbit portal vein. *J Physiol* **412**, 397-414.

Beech, D. J., Cheong, A., Flemming, R., Guibert, C., & Xu, S. Z. (2001). Modulation of Vascular K+ Channels by Extracellular Messengers. In *Potassium Channels in Cardiovascular Biology*, eds. Archer, S. L. & Rusch, N. J., pp. 457-483. Academic/Plenum, New York.

Beech, D. J., Zhang, H., Nakao, K., & Bolton, T. B. (1993). K channel activation by nucleotide diphosphates and its inhibition by glibenclamide in vascular smooth muscle cells. *Br.J.Pharmacol.* **110**, 573-582.

Belevych, A. E., Beck, R., Tammaro, P., Poston, L., & Smirnov, S. V. (2002). Developmental changes in the functional characteristics and expression of voltage-gated K+ channel currents in rat aortic myocytes. *Cardiovasc.Res.* **54**, 152-161.

Benham, C. D., Hess, P., & Tsien, R. W. (1987). Two types of calcium channels in single smooth muscle cells from rabbit ear artery studied with whole-cell and single-channel recordings. *Circ.Res.* **61**, I10-I16.

Benham, C. D. & Tsien, R. W. (1987a). A novel receptor-operated Ca^{2+}-permeable channel activated by ATP in smooth muscle. *Nature* **328**, 275-278.

Benham, C. D. & Tsien, R. W. (1987b). Calcium-permeable channels in vascular smooth muscle: voltage-activated, receptor-operated, and leak channels. *Society of General Physiologists Series* **42**, 45-64.

Benndorf, K., Koopmann, R., Lorra, C., & Pongs, O. (1994). Gating and conductance properties of a human delayed rectifier K^+ channel expressed in frog oocytes. *J Physiol* **477**, 1-14.

Beny, J. L. (1990). Endothelial and smooth muscle cells hyperpolarized by bradykinin are not dye coupled. *Am.J.Physiol.* **258**, H836-H841.

Beny, J. L. & Pacicca, C. (1994). Bidirectional electrical communication between smooth muscle and endothelial cells in the pig coronary artery. *Am.J.Physiol.* **266**, H1465-H1472.

Benzing, T., Fleming, I., Blaukat, A., Muller-Esterl, W., & Busse, R. (1999). Angiotensin-converting enzyme inhibitor ramiprilat interferes with the sequestration of the B2 kinin receptor within the plasma membrane of native endothelial cells. *Circulation* **99** , 2034-2040.

Berk, B. C. & Alexander, R. W. (1989). Vasoactive effects of growth factors. *Biochem Pharmacol* **38**, 219-225.

Bezanilla, F. (2002). Voltage sensor movements. *J Gen Physiol* **120**, 465-473.

Bhullar, I. S., Li, Y. S., Miao, H., Zandi, E., Kim, M., Shyy, J. Y., & Chien, S. (1998). Fluid shear stress activation of IkappaB kinase is integrin-dependent. *J Biol Chem* **273**, 30544-30549.

Birnbaumer, L., Zhu, X., Jiang, M., Boulay, G., Peyton, M., Vannier, B., Brown, D., Platano, D., Sadeghi, H., Stefani, E., & Birnbaumer, M. (1996). On the molecular basis and regulation of cellular capacitative calcium entry: roles for Trp proteins. *Proc.Natl.Acad.Sci.U S A* **93**, 15195-15202.

Bkaily, G., d'Orleans-Juste, P., Naik, R., Perodin, J., Stankova, J., Abdulnour, E., & Rola-Pleszczynski, M. (1993). PAF activation of a voltage-gated R-type Ca^{2+} channel in human and canine aortic endothelial cells. *Br J Pharmacol* **110**, 519-520.

Boccaccio, A., Moran, O., & Conti, F. (1998). Calcium dependent shifts of Na^+ channel activation correlated with the state dependence of calcium-binding to the pore. *Eur.Biophys.J.* **27**, 558-566.

Bolotina, V. M., Najibi, S., Palacino, J. J., Pagano, P. J., & Cohen, R. A. (1994). Nitric oxide directly activates calcium-dependent potassium channels in vascular smooth muscle. *Nature* **368**, 850-853.

Bolton, T. B. (1979). Mechanisms of action of transmitters and other substances on smooth muscle. *Physiol.Rev.* **59**, 606-718.

Bonev, A. D. & Nelson, M. T. (1996). Vasoconstrictors inhibit ATP-sensitive K^+ channels in arterial smooth muscle through protein kinase C. *J.Gen.Physiol.* **108**, 315-323.

Brayden, J. E. (1990). Membrane hyperpolarization is a mechanism of endothelium-dependent cerebral vasodilation. *Am.J.Physiol.* **259**, H668-H673.

Brayden, J. E. & Nelson, M. T. (1992a). Regulation of arterial tone by activation of calcium-dependent potassium channels. *Science* **256**, 532-535.

Brehm, P. & Eckert, R. (1978). Calcium entry leads to inactivation of calcium channel in Paramecium. *Science* **202**, 1203-1206.

Bruzzone, R., Haefliger, J. A., Gimlich, R. L., & Paul, D. L. (1993). Connexin40, a component of gap junctions in vascular endothelium, is restricted in its ability to interact with other connexins. *Mol Biol Cell* **4**, 7-20.

Burnette, W. N. (1981). "Western blotting": electrophoretic transfer of proteins from sodium dodecyl sulfate-polyacrylamide gels to unmodified nitrocellulose and radiographic detection with antibody and radioiodinated protein A. *Anal Biochem* **112**, 195-203.

Busse, R., Luckhoff, A., & Mulsch, A. (1991). Cellular mechanisms controlling EDRF/NO formation in endothelial cells. *Basic Res Cardiol* **86 Suppl 2**, 7-16.

Byrne, N. G. & Large, W. A. (1987). Membrane mechanism associated with muscarinic receptor activation in single cells freshly dispersed from the rat anococcygeus muscle. *Br J Pharmacol* **92**, 371-379.

Casella, C. & Taglietti, V. (1996). *Principi di Fisiologia* La Goliardica Pavese, Pavia.

Celermajer, D. S. (1997). Endothelial dysfunction: does it matter? Is it reversible? *J Am Coll Cardiol* **30**, 325-333.

Chad, J. E. & Eckert, R. (1986). An enzymatic mechanism for calcium current inactivation in dialysed Helix neurones. *J Physiol* **378**, 31-51.

Chen, G. & Suzuki, H. (1989). Some electrical properties of the endothelium-dependent hyperpolarization recorded from rat arterial smooth muscle cells. *J.Physiol.* **410**, 91-106.

Chen, X. L. & Rembold, C. M. (1995). Phenylephrine contracts rat tail artery by one electromechanical and three pharmacomechanical mechanisms. *Am.J.Physiol.* **268**, H74-H81.

Cheng, J. T., Hsu, S. Y., & Shen, C. L. (1989). 4-Aminopyridine induces the release of neuropeptide Y (NPY) to produce an atropine- and tetrodotoxin-resistant contraction in rabbit isolated jejunum. *Eur.J.Pharmacol.* **174**, 1-7.

Cheong, A., Dedman, A. M., Xu, S. Z., & Beech, D. J. (2001). $K_V\alpha 1$ channels in murine arterioles: differential cellular expression and regulation of diameter. *Am.J.Physiol.* **281**, H1057-H1065.

Cheong, A., Quinn, K., Dedman, A. M., & Beech, D. J. (2002). Activation thresholds of Kv, BK and Cl_{Ca} channels in smooth muscle cells in pial precapillary arterioles. *J.Vasc.Res.* **39**, 122-130.

Choi, B. H., Choi, J. S., Jeong, S. W., Hahn, S. J., Yoon, S. H., Jo, Y. H., & Kim, M. S. (2000). Direct block by bisindolylmaleimide of rat Kv1.5 expressed in Chinese hamster ovary cells. *J.Pharmacol.Exp.Ther.* **293**, 634-640.

Choi, J. S., Hahn, S. J., Rhie, D. J., Jo, Y. H., & Kim, M. S. (1999). Staurosporine directly blocks Kv1.3 channels expressed in Chinese hamster ovary cells. *Naunyn Schmiedeberg's Arch.Pharmacol.* **359**, 256-261.

Christie, M. J., North, R. A., Osborne, P. B., Douglass, J., & Adelman, J. P. (1990). Heteropolymeric potassium channels expressed in Xenopus oocytes from cloned subunits. *Neuron* **4**, 405-411.

Clapham, D. E. (2004). TRP channels as cellular sensors. *Nature* **426**, 517-524.

Clapp, L. H., Davey, R., & Gurney, A. M. (1993). ATP-sensitive K^+ channels mediate vasodilation produced by lemakalim in rabbit pulmonary artery. *Am.J.Physiol.* **264**, H1907-H1915.

Clapp, L. H. & Gurney, A. M. (1991). Outward currents in rabbit pulmonary artery cells dissociated with a new technique. *Exp Physiol* **76**, 677-693.

Clapp, L. H. & Tinker, A. (1998). Potassium channels in the vasculature. *Current Opinion in Nephrology & Hypertension* 7, 91-98.

Clark, J. D., Schievella, A. R., Nalefski, E. A., & Lin, L. L. (1995). Cytosolic phospholipase A2. *J Lipid Mediat Cell Signal* **12**, 83-117.

Cole, W. C., Carl, A., & Sanders, K. M. (1989). Muscarinic suppression of Ca^{2+}-dependent K current in colonic smooth muscle. *Am.J.Physiol.* **257**, C481-C487.

Colyer, J. (1998). Phosphorylation states of phospholamban. *Ann N Y Acad Sci* **853**, 79-91.

Conforti, L., Bodi, I., Nisbet, J. W., & Millhorn, D. E. (2000). O_2-sensitive K^+ channels: role of the Kv1.2 α-subunit in mediating the hypoxic response. *J.Physiol.* **524**, 783-793.

Cook, N. S. (1989). Effect of some potassium channel blockers on contractile responses of the rabbit aorta. *J.Cardiovasc.Pharmacol.* **13**, 299-306.

Coppock, E. A., Martens, J. R., & Tamkun, M. M. (2001). Molecular basis of hypoxia-induced pulmonary vasoconstriction: role of voltage-gated K^+ channels. *Am.J.Physiol.* **281**, L1-L12.

Cowan, C. L., Palacino, J. J., Najibi, S., & Cohen, R. A. (1993). Potassium channel-mediated relaxation to acetylcholine in rabbit arteries. *J Pharmacol Exp Ther* **266**, 1482-1489.

Cunningham, S. A., Awayda, M. S., Bubien, J. K., Ismailov, I. I., Arrate, M. P., Berdiev, B. K., Benos, D. J., & Fuller, C. M. (1995). Cloning of an epithelial chloride channel from bovine trachea. *J Biol Chem* **270**, 31016-31026.

Curtis, B. M. & Catterall, W. A. (1984). Purification of the calcium antagonist receptor of the voltage-sensitive calcium channel from skeletal muscle transverse tubules. *Biochemistry* **23**, 2113-2118.

Dart, C. & Standen, N. B. (1995). Activation of ATP-dependent K^+ channels by hypoxia in smooth muscle cells isolated from the pig coronary artery. *J.Physiol.* **483**, 29-39.

Daut, J., Standen, N. B., & Nelson, M. T. (1994). The role of the membrane potential of endothelial and smooth muscle cells in the regulation of coronary blood flow. *J Cardiovasc Electrophysiol* **5**, 154-181.

Davie, C. S., Kubo, M., & Standen, N. B. (1998). Potassium channel activation and relaxation by nicorandil in rat small mesenteric arteries. *Br.J.Pharmacol.* **125**, 1715-1725.

Davies, P. F. (1995). Flow-mediated endothelial mechanotransduction. *Physiol.Rev.* **75**, 519-560.

Davies, P. F., Olesen, S. P., Clapham, D. E., Morrel, E. M., & Schoen, F. J. (1988). Endothelial communication. State of the art lecture. *Hypertension* **11**, 563-572.

Davies, P. F. & Tripathi, S. C. (1993). Mechanical stress mechanisms and the cell. An endothelial paradigm. *Circ Res* **72**, 239-245.

de LeonM, Wang, Y., Jones, L., Perez-Reyes, E., Wei, X., Soong, T. W., Snutch, T. P., & Yue, D. T. (1995). Essential Ca^{2+}-binding motif for Ca^{2+}-sensitive inactivation of L-type Ca^{2+} channels. *Science* **270**, 1502-1506.

Dejana, E., Corada, M., & Lampugnani, M. G. (1995). Endothelial cell-to-cell junctions. *FASEB J* **9**, 910-918.

Denning, G. M., Ostedgaard, L. S., Cheng, S. H., Smith, A. E., & Welsh, M. J. (1992). Localization of cystic fibrosis transmembrane conductance regulator in chloride secretory epithelia. *J Clin Invest* **89**, 339-349.

Dolor, R. J., Hurwitz, L. M., Mirza, Z., Strauss, H. C., & Whorton, A. R. (1992). Regulation of extracellular calcium entry in endothelial cells: role of intracellular calcium pool. *Am.J.Physiol.* **262**, C171-C181.

Dora, K. A. & Garland, C. J. (2001). Properties of smooth muscle hyperpolarization and relaxation to K^+ in the rat isolated mesenteric artery. *Am.J.Physiol.Heart.Circ.Physiol.* **280**, H2424-H2429.

Dora, K. A., Sandow, S. L., Gallagher, N. T., Takano, H., Rummery, N. M., Hill, C. E., & Garland, C. J. (2003). Myoendothelial gap junctions may provide the pathway for EDHF in mouse mesenteric artery. *J.Vasc.Res.* **40**, 480-490.

Edwards, F. R., Hirst, G. D., & Silverberg, G. D. (1988). Inward rectification in rat cerebral arterioles; involvement of potassium ions in autoregulation. *J Physiol* **404**, 455-466.

Edwards, F. R. & Hirst, G. D. S. (1988). Inward rectification in submucosal arterioles of guinea-pig ileum. *J.Physiol.* **404**, 437-454.

Edwards, G., Dora, K. A., Gardener, M. J., Garland, C. J., & Weston, A. H. (1998). K^+ is an endothelium-derived hyperpolarizing factor in rat arteries. *Nature* **19;396**, 269-272.

Ekhterae, D., Platoshyn, O., Krick, S., Yu, Y., McDaniel, S. S., & Yuan, J. X. (2001). Bcl-2 decreases voltage-gated K^+ channel activity and enhances survival in vascular smooth muscle cells. *Am.J.Physiol.* **281**, C157-C165.

Elam, T. R. & Lansman, J. B. (1995). The role of Mg^{2+} in the inactivation of inwardly rectifying K^+ channels in aortic endothelial cells. *J Gen Physiol* **105**, 463-484.

Elinder, F. & Arhem, P. (1999). Role of individual surface charges of voltage-gated K channels. *Biophys.J.* **77**, 1358-1362.

Emeis, J. J., van, d. S., van, d., de, P., Westmuckett, A., & Lupu, F. (1997). An endothelial storage granule for tissue-type plasminogen activator. *J Cell Biol* **139**, 245-256.

Erdodi, F., Rokolya, A., Barany, M., & Barany, K. (1988). Phosphorylation of the 20,000-Da myosin light chain isoforms of arterial smooth muscle by myosin light chain kinase and protein kinase C. *Arch Biochem Biophys* **266**, 583-591.

Fanger, C. M., Ghanshani, S., Logsdon, N. J., Rauer, H., Kalman, K., Zhou, J., Beckingham, K., Chandy, K. G., Cahalan, M. D., & Aiyar, J. (1999). Calmodulin mediates calcium-dependent activation of the intermediate conductance K_{Ca} channel, $IK_{Ca}1$. *J Biol Chem* **274**, 5746-5754.

Faraci, F. M. & Heistad, D. D. (1998). Regulation of the cerebral circulation: role of endothelium and potassium channels. *Physiol.Rev.* **78**, 53-97.

Fasolato, C. & Nilius, B. (1998). Store depletion triggers the calcium release-activated calcium current (ICRAC) in macrovascular endothelial cells: a comparison with Jurkat and embryonic kidney cell lines. *Pflugers.Arch.* **436**, 69-74.

Felix, J. P., Bugianesi, R. M., Schmalhofer, W. A., Borris, R., Goetz, M. A., Hensens, O. D., Bao, J. M., Kayser, F., Parsons, W. H., Rupprecht, K., Garcia, M. L., Kaczorowski, G. J., & Slaughter, R. S. (1999). Identification and biochemical characterization of a novel nortriterpene inhibitor of the human lymphocyte voltage-gated potassium channel, Kv1.3. *Biochemistry* **38**, 4922-4930.

Feron, O., Smith, T. W., Michel, T., & Kelly, R. A. (1997). Dynamic targeting of the agonist-stimulated m2 muscarinic acetylcholine receptor to caveolae in cardiac myocytes. *J Biol Chem* **272**, 17744-17748.

Forsyth, S. E., Hoger, A., & Hoger, J. H. (1997). Molecular cloning and expression of a bovine endothelial inward rectifier potassium channel. *FEBS Lett* **409**, 277-282.

Forsythe, I. D., Linsdell, P., & Stanfield, P. R. (1992). Unitary A-currents of rat locus coeruleus neurones grown in cell culture: rectification caused by internal Mg^{2+} and Na^{+}. *J Physiol* **451**, 553-583.

Fransen, P. F., Demolder, M. J., & Brutsaert, D. L. (1995). Whole cell membrane currents in cultured pig endocardial endothelial cells. *Am.J.Physiol.* **268**, H2036-H2047.

Frech, G. C., VanDongen, A. M., Schuster, G., Brown, A. M., & Joho, R. H. (1989). A novel potassium channel with delayed rectifier properties isolated from rat brain by expression cloning. *Nature* **340**, 642-645.

Freeman, K. A., Mao, A., Nordberg, L. O., Pak, J., & Tallarida, R. J. (1995). The relationship between vessel wall tension and the magnitude and frequency of oscillation in rat aorta. *Life Sci.* **56**, PL129-PL134.

Freichel, M., Schweig, U., Stauffenberger, S., Freise, D., Schorb, W., & Flockerzi, V. (1999). Store-operated cation channels in the heart and cells of the cardiovascular system. *Cell Physiol Biochem* **9**, 270-283.

Ganitkevich, V. Y. & Isenberg, G. (1993). Membrane potential modulates inositol 1,4,5-trisphosphate-mediated Ca^{2+} transients in guinea-pig coronary myocytes. *J Physiol* **470**, 35-44.

Ganitkevich, V. Y., Shuba, M. F., & Smirnov, S. V. (1988). Saturation of calcium channels in single isolated smooth muscle cells of guinea-pig taenia caeci. *J Physiol* **399**, 419-436.

Ganitkevich, V. Ya. & Isenberg, G. (1990). Contribution of two types of calcium channels to membrane conductance of single myocytes from guinea-pig coronary artery. *J.Physiol.* **426**, 19-42.

Gelband, C. H. & Hume, J. R. (1992). Ionic currents in single smooth muscle cells of the canine renal artery. *Circ Res* **71**, 745-758.

Gericke, M., Droogmans, G., & Nilius, B. (1993a). Thapsigargin discharges intracellular calcium stores and induces transmembrane currents in human endothelial cells. *Pflugers.Arch.* **422**, 552-557.

Gericke, M., Droogmans, G., & Nilius, B. (1993b). Thimerosal induced changes of intracellular calcium in human endothelial cells. *Cell Calcium* **14**, 201-207.

Gibson, A., McFadzean, I., Tucker, J. F., & Wayman, C. (1994). Variable potency of nitrergic-nitrovasodilator relaxations of the mouse anococcygeus against different forms of induced tone. *Br J Pharmacol* **113**, 1494-1500.

Gibson, A., McFadzean, I., Wallace, P., & Wayman, C. P. (1998). Capacitative Ca2+ entry and the regulation of smooth muscle tone. *Trends Pharmacol Sci* **19**, 266-269.

Gokina, N. I., Wellman, T. D., Bevan, R. D., Walters, C. L., Penar, P. L., & Bevan, J. A. (1996). Role of Ca^{2+}-activated K^+ channels in the regulation of membrane potential and tone of smooth muscle in human pial arteries. *Circ.Res.* **79**, 881-886.

Goldman, D. E. (1943). Potential, impedance, and rectification in mebranes. *J Gen Physiol* 37-60.

Gollasch, M., Hescheler, J., Quayle, J. M., Patlak, J. B., & Nelson, M. T. (1992). Single calcium channel currents of arterial smooth muscle at physiological calcium concentrations. *Am.J.Physiol.* **263**, C948-C952.

Gonzalez, J. M., Jost, L. J., Rouse, D., & Suki, W. N. (1996). Plasma membrane and sarcoplasmic reticulum Ca-ATPase and smooth muscle. *Miner.Electrolyte.Metab.* **22**, 345-348.

Grahame, D. C. (1947). The electrical double layer and the theory of electrocapillarity. *Chem Rev* **41**, 441-501.

Graier, W. F., Paltauf-Doburzynska, J., Hill, B. J., Fleischhacker, E., Hoebel, B. G., Kostner, G. M., & Sturek, M. (1998). Submaximal stimulation of porcine endothelial cells causes focal Ca^{2+} elevation beneath the cell membrane. *J Physiol* **506**, 109-125.

Graier, W. F., Simecek, S., & Sturek, M. (1995). Cytochrome P450 mono-oxygenase-regulated signalling of Ca^{2+} entry in human and bovine endothelial cells. *J Physiol* **482**, 259-274.

Grissmer, S., Nguyen, A. N., Aiyar, J., Hanson, D. C., Mather, R. J., Gutman, G. A., Auperin, D. D., & Chandy, K. G. (1994a). Pharmacological characterization of five

cloned voltage-gated K^+ channels, types Kv1.1, 1.2, 1.3, 1.5, and 3.1, stably expressed in mammalian cell lines. *Mol.Pharmacol.* **45**, 1227-1234.

Grissmer, S., Nguyen, A. N., Aiyar, J., Hanson, D. C., Mather, R. J., Gutman, G. A., Karmilowicz, M. J., Auperin, D. D., & Chandy, K. G. (1994b). Pharmacological characterization of five cloned voltage-gated K^+ channels, types Kv1.1, 1.2, 1.3, 1.5, and 3.1, stably expressed in mammalian cell lines. *Mol Pharmacol* **45**, 1227-1234.

Groschner, K., Graier, W. F., & Kukovetz, W. R. (1992). Activation of a small-conductance Ca^{2+}-dependent K^+ channel contributes to bradykinin-induced stimulation of nitric oxide synthesis in pig aortic endothelial cells. *Biochim Biophys Acta* **1137**, 162-170.

Groschner, K., Graier, W. F., & Kukovetz, W. R. (1994). Histamine induces K^+, Ca^{2+}, and Cl^- currents in human vascular endothelial cells. Role of ionic currents in stimulation of nitric oxide biosynthesis. *Circ Res* **75**, 304-314.

Groschner, K. & Kukovetz, W. R. (1992). Voltage-sensitive chloride channels of large conductance in the membrane of pig aortic endothelial cells. *Pflugers.Arch.* **421**, 209-217.

Grunder, S., Thiemann, A., Pusch, M., & Jentsch, T. J. (1992). Regions involved in the opening of CIC-2 chloride channel by voltage and cell volume. *Nature* **360**, 759-762.

Grupe, A., Schröter, K. H., Ruppersberg, J. P., Stocker, M., Drewes, T., & Beckh, S. (1990). Cloning and expression of a human voltage-gated potassium channel. A novel member of the RCK potassium channel family. *EMBO J.* **9**, 1749-1756.

Guo, W., Kamiya, K., & Toyama, J. (1997). Roles of the voltage-gated K^+ channel subunits, Kv 1.5 and Kv 1.4, in the developmental changes of K^+ currents in cultured neonatal rat ventricular cells. *Pflugers.Arch.* **434**, 206-208.

Gurney, A. M., Osipenko, O. N., MacMillan, D., & Kempsill, F. E. (2002). Potassium channels underlying the resting potential of pulmonary artery smooth muscle cells. *Clin Exp Pharmacol Physiol* **29**, 330-333.

Gustafsson, H. (1993). Vasomotion and underlying mechanisms in small arteries. An in vitro study of rat blood vessels. *Acta Physiol.Scand.* **614 (Suppl.)**, 1-44.

Haburcak, M., Wei, L., Viana, F., Prenen, J., Droogmans, G., & Nilius, B. (1997). Calcium-activated potassium channels in cultured human endothelial cells are not directly modulated by nitric oxide. *Cell Calcium* **21**, 291-300.

Hamill, O. P., Marty, A., Neher, E., Sakmann, B., & Sigworth, F. J. (1981). Improved patch-clamp techniques for high-resolution current recording from cells and cell-free membrane patches. *Pflugers.Arch.* **391**, 85-100.

Handy, R. D., Gow, I. F., Ellis, D., & Flatman, P. W. (1996). Na-dependent regulation of intracellular free magnesium concentration in isolated rat ventricular myocytes. *J Mol Cell Cardiol* **28**, 1641-1651.

Hanner, M., Schmalhofer, W. A., Green, B., Bordallo, C., Liu, J., Slaughter, R. S., Kaczorowski, G. J., & Garcia, M. L. (1999). Binding of correolide to Kv1 family potassium channels. Mapping the domains of high affinity interaction. *J.Biol.Chem.* **274**, 25237-25244.

Hannun, Y. A. & Bell, R. M. (1990). Rat brain protein kinase C. Kinetic analysis of substrate dependence, allosteric regulation, and autophosphorylation. *J Biol Chem* **265**, 2962-2972.

Harder, D. R. (1984). Pressure-dependent membrane depolarization in cat middle cerebral artery. *Circ Res* **55**, 197-202.

Harvey, R. D. & Ten, E. (1989). On the role of sodium ions in the regulation of the inward-rectifying potassium conductance in cat ventricular myocytes. *J Gen Physiol* **94**, 329-348.

Hassessian, H., Bodin, P., & Burnstock, G. (1993). Blockade by glibenclamide of the flow-evoked endothelial release of ATP that contributes to vasodilatation in the pulmonary vascular bed of the rat. *Br J Pharmacol* **109**, 466-472.

Hatton, W. J., Mason, H. S., Carl, A., Doherty, P., Latten, M. J., Kenyon, J. L., Sanders, K. M., & Horowitz, B. (2001). Functional and molecular expression of a voltage-dependent K^+ channel (Kv1.1) in interstitial cells of Cajal. *J.Physiol.* **533**, 315-327.

He, P. & Curry, F. E. (1991). Depolarization modulates endothelial cell calcium influx and microvessel permeability. *Am.J.Physiol.* **261**, H1246-H1254.

He, P. & Curry, F. E. (1994). Endothelial cell hyperpolarization increases $[Ca^{2+}]_i$ and venular microvessel permeability. *J.Appl.Physiol.* **76**, 2288-2297.

Hecker, M., Mulsch, A., Bassenge, E., & Busse, R. (1993). Vasoconstriction and increased flow: two principal mechanisms of shear stress-dependent endothelial autacoid release. *Am.J.Physiol.* **265**, H828-H833.

Heinemann, S. H. (1995). Guide to Data Acquisition and Analysis. In *Single-Channel Recording*, eds. Sakmann, B. & Neher, E., pp. 53-90. Plenum Press, New York and London.

Heinemann, S. H. & Conti, F. (1992). Non-stationary noise analysis and its application to patch clamp recordings. In *Ion Channels, Methods in Enzymology*, eds. Ridy, B. & Iverson, L. E., pp. 131-138. Academic Press, San Diego.

Herlitze, S., Hockerman, G. H., Scheuer, T., & Catterall, W. A. (1997). Molecular determinants of inactivation and G protein modulation in the intracellular loop connecting domains I and II of the calcium channel alpha1A subunit. *Proc.Natl.Acad.Sci.U S A* **94**, 1512-1516.

Hille, B. (2001). *Ion Channels of Excitable Membranes*, 3 ed. Sinauer Associates.

Hille, B., Woodhull, A. M., & Shapiro, B. I. (1975). Negative surface charge near sodium channels of nerve: divalent ions, monovalent ions, and pH. *Philos.Trans.R.Soc.Lond.B.Biol.Sci.* **270**, 301-318.

Himmel, H. M., Rasmusson, R. L., & Strauss, H. C. (1994). Agonist-induced changes of $[Ca^{2+}]_i$ and membrane currents in single bovine aortic endothelial cells. *Am.J.Physiol.* **267**, C1338-C1350.

Himmel, H. M., Whorton, A. R., & Strauss, H. C. (1993). Intracellular calcium, currents, and stimulus-response coupling in endothelial cells. *Hypertension* **21**, 112-127.

Himpens, B., De, S., Droogmans, G., & Casteels, R. (1992). Differences in regulation between nuclear and cytoplasmic Ca^{2+} in cultured smooth muscle cells. *Am.J.Physiol.* **263**, C95-105.

Himpens, B., Missiaen, L., & Casteels, R. (1995). Ca^{2+} homeostasis in vascular smooth muscle. *J.Vasc.Res.* **32**, 207-219.

Hirst, G. D. & Edwards, F. R. (1989a). Sympathetic neuroeffector transmission in arteries and arterioles. *Physiol.Rev.* **69**, 546-604.

Hirst, G. D., Silverberg, G. D., & van, H. (1986). The action potential and underlying ionic currents in proximal rat middle cerebral arterioles. *J Physiol* **371**, 289-304.

Hockerman, G. H., Peterson, B. Z., Johnson, B. D., & Catterall, W. A. (1997). Molecular determinants of drug binding and action on L-type calcium channels. *Annu Rev Pharmacol Toxicol* **37**, 361-396.

Hodgkin, A. L. & Huxley, A. F. (1952). A quantitative description of membrane current and its application to conduction and excitation in nerve. *J.Physiol.(Lond.)* 500-544.

Hodgkin, A. L. & Katz, B. (1949). The effect of sodium ions on the electrical activity of the giant axon of the squid. *J.Physiol.(Lond.)* 37-77.

Hoshi, T., Zagotta, W. N., & Aldrich, R. W. (1990). Biophysical and molecular mechanisms of Shaker potassium channel inactivation. *Science* **250**, 533-538.

Hoshi, T., Zagotta, W. N., & Aldrich, R. W. (1991). Two types of inactivation in Shaker K+ channels: effects of alterations in the carboxy-terminal region. *Neuron* **7**, 547-556.

Hosoki, E. & Iijima, T. (1994). Chloride-sensitive Ca^{2+} entry by histamine and ATP in human aortic endothelial cells. *Eur.J.Pharmacol.* **266**, 213-218.

Hosoki, E. & Iijima, T. (1995). Modulation of cytosolic Ca^{2+} concentration by thapsigargin and cyclopiazonic acid in human aortic endothelial cells. *Eur.J.Pharmacol.* **288**, 131-137.

Hoyer, J., Distler, A., Haase, W., & Gogelein, H. (1994). Ca^{2+} influx through stretch-activated cation channels activates maxi K^+ channels in porcine endocardial endothelium. *Proc.Natl.Acad.Sci.U S A* **91**, 2367-2371.

Hoyer, J., Popp, R., Meyer, J., Galla, H. J., & Gogelein, H. (1991). Angiotensin II, vasopressin and GTPγ-s inhibit inward-rectifying K^+ channels in porcine cerebral capillary endothelial cells. *J.Membr.Biol.* **123**, 55-62.

Hughes, A. D. (1995). Calcium channels in vascular smooth muscle cells. *J.Vasc.Res.* **32**, 353-370.

Hulme, J. T., Coppock, E. A., Felipe, A., Martens, J. R., & Tamkun, M. M. (1999). Oxygen sensitivity of cloned voltage-gated K^+ channels expressed in the pulmonary vasculature. *Circ.Res.* **85**, 489-497.

Hutcheson, I. R. & Griffith, T. M. (1994). Heterogeneous populations of K^+ channels mediate EDRF release to flow but not agonists in rabbit aorta. *Am.J.Physiol.* **266**, H590-H596.

Inagaki, N., Gonoi, T., Clement, J. P., Wang, C. Z., Aguilar-Bryan, L., Bryan, J., & Seino, S. (1996). A family of sulfonylurea receptors determines the pharmacological properties of ATP-sensitive K^+ channels. *Neuron* **16**, 1011-1017.

Inagami, T., Naruse, M., & Hoover, R. (1995). Endothelium as an endocrine organ. *Annu Rev Physiol* **57**, 171-189.

Inazu, M., Zhang, H., & Daniel, E. E. (1994). Properties of the LP-805-induced potassium currents in cultured bovine pulmonary artery endothelial cells. *J Pharmacol Exp Ther* **268**, 403-408.

Ishii, T. M., Silvia, C., Hirschberg, B., Bond, C. T., Adelman, J. P., & Maylie, J. (1997). A human intermediate conductance calcium-activated potassium channel. *Proc.Natl.Acad.Sci.U S A* **94**, 11651-11656.

Ishikawa, T., Hume, J. R., & Keef, K. D. (1993). Regulation of Ca^{2+} channels by cAMP and cGMP in vascular smooth muscle cells. *Circ.Res.* **73**, 1128-1137.

Ishizaka, H. & Kuo, L. (1997). Endothelial ATP-sensitive potassium channels mediate coronary microvascular dilation to hyperosmolarity. *Am.J.Physiol.* **273**, H104-H112.

Islam, M. O., Yoshida, Y., Koga, T., Kojima, M., Kangawa, K., & Imai, S. (1996). Isolation and characterization of vascular smooth muscle inositol 1,4,5-trisphosphate receptor. *Biochem.J.* **316**, 295-302.

Jacob, M. P., Badier-Commander, C., Fontaine, V., Benazzoug, Y., Feldman, L., & Michel, J. B. (2001). Extracellular matrix remodeling in the vascular wall. *Pathol Biol (Paris)* **49** , 326-332.

Jacob, R., Merritt, J. E., Hallam, T. J., & Rink, T. J. (1988). Repetitive spikes in cytoplasmic calcium evoked by histamine in human endothelial cells. *Nature* **335**, 40-45.

Jacobs, E. R., Cheliakine, C., Gebremedhin, D., Birks, E. K., Davies, P. F., & Harder, D. R. (1995). Shear activated channels in cell-attached patches of cultured bovine aortic endothelial cells. *Pflugers.Arch.* **431**, 129-131.

Jaggar, J. H., Porter, V. A., Lederer, W. J., & Nelson, M. T. (2000). Calcium sparks in smooth muscle. *Am.J.Physiol.* **278**, C235-C256.

Jaggar, J. H., Stevenson, A. S., & Nelson, M. T. (1998a). Voltage dependence of Ca^{2+} sparks in intact cerebral arteries. *Am.J.Physiol.* **274**, C1755-C1761.

Jaggar, J. H., Wellman, G. C., Heppner, T. J., Porter, V. A., Perez, G. J., Gollasch, M., Kleppisch, T., Rubart, M., Stevenson, A. S., Lederer, W. J., Knot, H. J., Bonev, A. D., & Nelson, M. T. (1998b). Ca^{2+} channels, ryanodine receptors and Ca^{2+}-activated K^+

channels: a functional unit for regulating arterial tone. *Acta Physiol.Scand.* **164**, 577-587.

Jan, L. Y. & Jan, Y. N. (1992). Structural elements involved in specific K^+ channel functions. *Annu Rev Physiol* **54**, 537-555.

Janigro, D., West, G. A., Gordon, E. L., & Winn, H. R. (1993). ATP-sensitive K^+ channels in rat aorta and brain microvascular endothelial cells. *Am.J.Physiol.* **265**, C812-C821.

Jiang, J., Thoren, P., Caligiuri, G., Hansson, G. K., & Pernow, J. (1999). Enhanced phenylephrine-induced rhythmic activity in the atherosclerotic mouse aorta *via* an increase in opening of K_{Ca} channels: relation to K_v channels and nitric oxide. *Br.J.Pharmacol.* **128**, 637-646.

Jiang, Y., Ruta, V., Chen, J., Lee, A., & MacKinnon, R. (2003). The principle of gating charge movement in a voltage-dependent K^+ channel. *Nature* **423**, 42-48.

Jow, F. & Numann, R. (2000). Histamine increases $[Ca^{2+}]_i$ and activates Ca-K and nonselective cation currents in cultured human capillary endothelial cells. *J.Membr.Biol.* **173** , 107-116.

Kaczorowski, G. J. & Garcia, M. L. (1999). Pharmacology of voltage-gated and calcium-activated potassium channels. *Curr Opin Chem Biol* **3**, 448-458.

Kajimura, M. & Curry, F. E. (1999). Endothelial cell shrinkage increases permeability through a Ca^{2+}-dependent pathway in single frog mesenteric microvessels. *J Physiol* **518**, 227-238.

Kamouchi, M., Mamin, A., Droogmans, G., & Nilius, B. (1999). Nonselective cation channels in endothelial cells derived from human umbilical vein. *J.Membr.Biol.* **169**, 29-38.

Kamouchi, M., Trouet, D., De, G., Droogmans, G., Eggermont, J., & Nilius, B. (1997a). Functional effects of expression of hslo Ca^{2+}-activated K^+-channels in cultured macrovascular endothelial cells. *Cell Calcium* **22**, 497-506.

Kamouchi, M., Van, D., Eggermont, J., Droogmans, G., & Nilius, B. (1997b). Modulation of inwardly rectifying potassium channels in cultured bovine pulmonary artery endothelial cells. *J Physiol* **504**, 545-556.

Katnik, C. & Adams, D. J. (1995). An ATP-sensitive potassium conductance in rabbit arterial endothelial cells. *J Physiol* **485**, 595-606.

Katnik, C. & Adams, D. J. (1997). Characterization of ATP-sensitive potassium channels in freshly dissociated rabbit aortic endothelial cells. *Am.J.Physiol.* **272**, H2507-H2511.

Keen, J. E., Khawaled, R., Farrens, D. L., Neelands, T., Rivard, A., Bond, C. T., Janowsky, A., Fakler, B., Adelman, J. P., & Maylie, J. (1999). Domains responsible for constitutive and Ca^{2+}-dependent interactions between calmodulin and small conductance Ca^{2+}-activated potassium channels. *J.Neurosci.* **19**, 8830-8838.

Kerr, P. M., Clement-Chomienne, O., Thorneloe, K. S., Chen, T. T., Ishii, K., Sontag, D. P., Walsh, M. P., & Cole, W. C. (1923). Heteromultimeric Kv1.2-Kv1.5 channels underlie 4-aminopyridine-sensitive delayed rectifier K^+ current of rabbit vascular myocytes. *Circ Res* **89**, 1038-1044.

Kerschbaum, H. H. & Cahalan, M. D. (1999). Single-channel recording of a store-operated Ca2+ channel in Jurkat T lymphocytes. *Science* **283**, 836-839.

Kerschensteiner, D. & Stocker, M. (1999a). Heteromeric assembly of Kv2.1 with Kv9.3: effect on the state dependence of inactivation. *Biophys.J.* **77**, 248-257.

Keynes, R. D. & Rojas, E. (1974). Kinetics and steady-state properties of the charged system controlling sodium conductance in the squid giant axon. *J Physiol* **239**, 393-434.

Khakh, B. S. (2001). Molecular physiology of P2X receptors and ATP signalling at synapses. *Nat.Rev.Neurosci.* **2**, 165-174.

Khan, S. A., Mathews, W. R., & Meisheri, K. D. (1993). Role of calcium-activated K^+ channels in vasodilation induced by nitroglycerine, acetylcholine and nitric oxide. *J Pharmacol Exp Ther* **267**, 1327-1335.

Kim, C. H., Rhee, P. L., Rhee, J. C., Kim, Y. I., So, I., Kim, K. W., Park, M. K., Uhm, D. Y., & Kang, T. M. (2000). Hypotonic swelling increases L-type calcium current in smooth muscle cells of the human stomach. *Exp Physiol* **85**, 497-504.

Kirsch, G. E., Drewe, J. A., Verma, S., Brown, A. M., & Joho, R. H. (1991). Electrophysiological characterization of a new member of the RCK family of rat brain K^+ channels. *FEBS Lett.* **278**, 55-60.

Klemic, K. G., Shieh, C. C., Kirsch, G. E., & Jones, S. W. (1998a). Inactivation of Kv2.1 potassium channels. *Biophys.J.* **74**, 1779-1789.

Klockner, U. (1993). Intracellular calcium ions activate a low-conductance chloride channel in smooth-muscle cells isolated from human mesenteric artery. *Pflugers.Arch.* **424**, 231-237.

Knaus, H. G., Eberhart, A., Kaczorowski, G. J., & Garcia, M. L. (1994a). Covalent attachment of charybdotoxin to the beta-subunit of the high conductance Ca^{2+}-activated K+ channel. Identification of the site of incorporation and implications for channel topology. *J Biol Chem* **269**, 23336-23341.

Knaus, H. G., Folander, K., Garcia-Calvo, M., Garcia, M. L., Kaczorowski, G. J., Smith, M., & Swanson, R. (1994b). Primary sequence and immunological characterization of beta-subunit of high conductance Ca^{2+}-activated K^+ channel from smooth muscle. *J Biol Chem* **269**, 17274-17278.

Knot, H. J. & Nelson, M. T. (1995). Regulation of membrane potential and diameter by voltage-dependent K^+ channels in rabbit myogenic cerebral arteries. *Am.J.Physiol.* **269**, H348-H355.

Kofuji, P., Davidson, N., & Lester, H. A. (1995). Evidence that neuronal G-protein-gated inwardly rectifying K^+ channels are activated by G beta gamma subunits and function as heteromultimers. *Proc.Natl.Acad.Sci.U S A* **92**, 6542-6546.

Koliwad, S. K., Elliott, S. J., & Kunze, D. L. (1996). Oxidized glutathione mediates cation channel activation in calf vascular endothelial cells during oxidant stress. *J Physiol* **495**, 37-49.

Koopmann, R., Scholle, A., Ludwig, J., Leicher, T., Zimmer, T., Pongs, O., & Benndorf, K. (2001). Role of the S2 and S3 segment in determining the activation kinetics in Kv2.1 channels. *J.Membr.Biol.* **182**, 49-59.

Kozlowski, R. (2000). *Chloride channels* Isis Medical Media Limited Feb.

Krapivinsky, G., Gordon, E. A., Wickman, K., Velimirovic, B., Krapivinsky, L., & Clapham, D. E. (1995). The G-protein-gated atrial K^+ channel IKACh is a heteromultimer of two inwardly rectifying K-channel proteins. *Nature* **374**, 135-141.

Krick, S., Platoshyn, O., Sweeney, M., Kim, H., & Yuan, J. X. (2001). Activation of K^+ channels induces apoptosis in vascular smooth muscle cells. *Am.J.Physiol.* **280**, C970-C979.

Kubo, M., Nakaya, Y., Matsuoka, S., Saito, K., & Kuroda, Y. (1994). Atrial natriuretic factor and isosorbide dinitrate modulate the gating of ATP-sensitive K^+ channels in cultured vascular smooth muscle cells. *Circ.Res.* **74**, 471-476.

Kubo, M., Quayle, J. M., & Standen, N. B. (1997). Angiotensin II inhibition of ATP-sensitive K^+ currents in rat arterial smooth muscle cells through protein kinase C. *J.Physiol.* **503**, 489-496.

Kubota, T., Horie, M., Takano, M., Yoshida, H., Otani, H., & Sasayama, S. (2002). Role of KCNQ1 in the cell swelling-induced enhancement of the slowly activating delayed rectifier K current. *Jpn J Physiol* **52**, 31-39.

Kume, H., Graziano, M. P., & Kotlikoff, M. I. (1992). Stimulatory and inhibitory regulation of calcium-activated potassium channels by guanine nucleotide-binding proteins. *Proc.Natl.Acad.Sci.U S A* **89**, 11051-11055.

Kume, H. & Kotlikoff, M. I. (1991). Muscarinic inhibition of single KCa channels in smooth muscle cells by a pertussis-sensitive G protein. *Am.J.Physiol.* **261**, C1204-C1209.

Kume, H., Takai, A., Tokuno, H., & Tomita, T. (1989). Regulation of Ca^{2+}-dependent K^+-channel activity in tracheal myocytes by phosphorylation. *Nature* **341**, 152-154.

Kun, A., Pataricza, J., Krassoi, I., Szecsi, M., Hohn, J., Varro, A., & Papp, J. G. (2002). Low 4-aminopyridine concentration-induced contraction is mediated by neuronal noradrenaline in canine saphenous vein. *Vascul Pharmacol* **39**, 7-11.

Kuriyama, H., Kitamura, K., & Nabata, H. (1995). Pharmacological and physiological significance of ion channels and factors that modulate them in vascular tissues. *Pharmacol.Rev.* **47**, 387-573.

Kuromaru, O. & Sakai, K. (1986). Effects of nicorandil on the rhythmic contractile response of isolated miniature pig coronary artery to 3,4-diaminopyridine: comparison with nitroglycerin. *Arch Int Pharmacodyn Ther* **283**, 272-281.

Kuschinsky, W., Wahl, M., Bosse, O., & Thurau, K. (1972). Perivascular potassium and pH as determinants of local pial arterial diameter in cats. A microapplication study. *Circ Res* **31**, 240-247.

Lakshminarayanaiah, N. (1984). *Equations of membrane biophysics* Academic Press.

Langheinrich, U., Mederos, y., & Daut, J. (1998). Ca^{2+}-transients induced by K^+ channel openers in isolated coronary capillaries. *Pflugers.Arch.* **435**, 435-438.

Lansman, J. B., Hallam, T. J., & Rink, T. J. (1987). Single stretch-activated ion channels in vascular endothelial cells as mechanotransducers? *Nature* **325**, 811-813.

Large, W. A. (2002). Receptor-operated Ca^{2+}-permeable nonselective cation channels in vascular smooth muscle: a physiologic perspective. *J Cardiovasc Electrophysiol* **13**, 493-501.

Large, W. A. & Wang, Q. (1996). Characteristics and physiological role of the Ca^{2+}-activated Cl^- conductance in smooth muscle. *Am.J.Physiol.* **271**, C435-C454.

Lawson, K. (2000). Potassium channel openers as potential therapeutic weapons in ion channel disease. *Kidney International* **57**, 838-845.

Leavesley, D. I., Schwartz, M. A., Rosenfeld, M., & Cheresh, D. A. (1993). Integrin beta 1- and beta 3-mediated endothelial cell migration is triggered through distinct signaling mechanisms. *J Cell Biol* **121**, 163-170.

Lesh, R. E., Nixon, G. F., Fleischer, S., Airey, J. A., Somlyo, A. P., & Somlyo, A. V. (1998). Localization of ryanodine receptors in smooth muscle. *Circ Res* **82**, 175-185.

Leung, Y. M., Kwan, C. Y., & Daniel, E. E. (2000). Block of inwardly rectifying K^+ currents by extracellular Mg^{2+} and Ba^{2+} in bovine pulmonary artery endothelial cells. *Can J Physiol Pharmacol* **78**, 751-756.

Levick, J. R. (1995). *An Introduction to Cardiovascular Physiology*, 2 ed. Butterworth-Heinemann, Oxford.

Li, C. & Xu, Q. (2000). Mechanical stress-initiated signal transductions in vascular smooth muscle cells. *Cell Signal* **12**, 435-445.

Li, G. & Cheung, D. W. (1999). Effects of paxilline on K^+ channels in rat mesenteric arterial cells. *Eur.J.Pharmacol.* **372**, 103-107.

Ling, B. N. & O'Neill, W. C. (1992). Ca^{2+}-dependent and Ca^{2+}-permeable ion channels in aortic endothelial cells. *Am.J.Physiol.* **263**, H1827-H1838.

Liou, Y. M. & Morgan, K. G. (1994). Redistribution of protein kinase C isoforms in association with vascular hypertrophy of rat aorta. *Am.J.Physiol.* **267**, C980-C989.

Little, T. L., Beyer, E. C., & Duling, B. R. (1995). Connexin 43 and connexin 40 gap junctional proteins are present in arteriolar smooth muscle and endothelium in vivo. *Am.J.Physiol.* **268**, H729-H739.

Liu, Y., Jurman, M. E., & Yellen, G. (1996). Dynamic rearrangement of the outer mouth of a K+ channel during gating. *Neuron* **16**, 859-867.

Liu, Y., Pleyte, K., Knaus, H. G., & Rusch, N. J. (1997). Increased expression of Ca^{2+}-sensitive K^+ channels in aorta of hypertensive rats. *Hypertension* **30**, 1403-1409.

Loirand, G., Mironneau, C., Mironneau, J., & Pacaud, P. (1989). Two types of calcium currents in single smooth muscle cells from rat portal vein. *J Physiol* **412**, 333-349.

Long, W., Zhang, L., & Longo, L. D. (2000). Cerebral artery K_{ATP}- and K_{Ca}-channel activity and contractility: changes with development. *Am.J.Physiol.* **279**, R2004-R2014.

Lopatin, A. N., Makhina, E. N., & Nichols, C. G. (1994). Potassium channel block by cytoplasmic polyamines as the mechanism of intrinsic rectification. *Nature* **372**, 366-369.

Lopatin, A. N. & Nichols, C. G. (1994). Internal Na^+ and Mg^{2+} blockade of DRK1 (Kv2.1) potassium channels expressed in Xenopus oocytes. Inward rectification of a delayed rectifier. *J Gen Physiol* **103**, 203-216.

Lopez-Barneo, J., Hoshi, T., Heinemann, S. H., & Aldrich, R. W. (1993). Effects of external cations and mutations in the pore region on C-type inactivation of Shaker potassium channels. *Receptors Channels* **1**, 61-71.

Ludewig, U., Lorra, C., Pongs, O., & Heinemann, S. H. (1993). A site accessible to extracellular TEA and K^+ influences intracellular Mg^{2+} block of cloned potassium channels. *Eur.Biophys.J.* **22**, 237-247.

Lytton, J., Westlin, M., & Hanley, M. R. (1991). Thapsigargin inhibits the sarcoplasmic or endoplasmic reticulum Ca-ATPase family of calcium pumps. *J Biol Chem* **266**, 17067-17071.

Malek, A. M. & Izumo, S. (1994). Molecular aspects of signal transduction of shear stress in the endothelial cell. *J Hypertens* **12**, 989-999.

Manolopoulos, V. G., Liekens, S., Koolwijk, P., Voets, T., Peters, E., Droogmans, G., Lelkes, P. I., De, C., & Nilius, B. (2000). Inhibition of angiogenesis by blockers of volume-regulated anion channels. *Gen Pharmacol* **34**, 107-116.

Marchenko, S. M. & Sage, S. O. (1993). Electrical properties of resting and acetylcholine-stimulated endothelium in intact rat aorta. *J Physiol* **462**, 735-751.

Marchenko, S. M. & Sage, S. O. (1994). Smooth muscle cells affect endothelial membrane potential in rat aorta. *Am.J.Physiol.* **267**, H804-H811.

Marijic, J., Li, Q., Song, M., Nishimaru, K., Stefani, E., & Toro, L. (2001). Decreased expression of voltage- and Ca^{2+}-activated K^+ channels in coronary smooth muscle during aging. *Circ.Res.* **88**, 210-216.

Martel, J., Dupuis, G., Deschenes, P., & Payet, M. D. (1998). The sensitivity of the human Kv1.3 (hKv1.3) lymphocyte K^+ channel to regulation by PKA and PKC is partially lost in HEK 293 host cells. *J.Membr.Biol.* **161**, 183-196.

Maruoka, N. D., Steele, D. F., Au, B. P., Dan, P., Zhang, X., Moore, E. D., & Fedida, D. (2000). α-Actinin-2 couples to cardiac Kv1.5 channels, regulating current density and channel localization in HEK cells. *FEBS Lett.* **473**, 188-194.

Matsuda, H., Saigusa, A., & Irisawa, H. (1987). Ohmic conductance through the inwardly rectifying K channel and blocking by internal Mg^{2+}. *Nature* **325**, 156-159.

Matsuda, J. J., Volk, K. A., & Shibata, E. F. (1990). Calcium currents in isolated rabbit coronary arterial smooth muscle myocytes. *J.Physiol.* **427**, 657-680.

Matsuda, N., Hagiwara, N., Shoda, M., Kasanuki, H., & Hosoda, S. (1996). Enhancement of the L-type Ca^{2+} current by mechanical stimulation in single rabbit cardiac myocytes. *Circ Res* **78**, 650-659.

Mazzanti, M. & DiFrancesco, D. (1989). Intracellular Ca modulates K-inward rectification in cardiac myocytes. *Pflugers.Arch.* **413**, 322-324.

McCannel, C. A., Scanlon, P. D., Thibodeau, S., & Brubaker, R. F. (1992). A study of aqueous humor formation in patients with cystic fibrosis. *Invest Ophthalmol Vis Sci* **33**, 160-164.

McCarron, J. G. & Halpern, W. (1990). Potassium dilates rat cerebral arteries by two independent mechanisms. *Am.J.Physiol.* **259**, H902-H908.

McLaughlin, S. (1989). The electrostatic properties of membranes. *Annu Rev Biophys Biophys Chem* **18**, 113-136.

McLaughlin, S. G., Szabo, G., & Eisenman, G. (1971). Divalent ions and the surface potential of charged phospholipid membranes. *J Gen Physiol* **58**, 667-687.

McManus, O. B., Helms, L. M., Pallanck, L., Ganetzky, B., Swanson, R., & Leonard, R. J. (1995). Functional role of the beta subunit of high conductance calcium-activated potassium channels. *Neuron* **14**, 645-650.

Mendelowitz, D., Bacal, K., & Kunze, D. L. (1992). Bradykinin-activated calcium influx pathway in bovine aortic endothelial cells. *Am.J.Physiol.* **262**, H942-H948.

Miao, K., Wondergem, R., Hossler, F. E., & Joyner, W. L. (1993). Contributions of K+, Na+, and Cl- to the membrane potential of intact hamster vascular endothelial cells. *J Cell Physiol* **156**, 550-559.

Miledi, R. & Parker, I. (1984). Chloride current induced by injection of calcium into Xenopus oocytes. *J Physiol* **357**, 173-183.

Miller, A. L., Morales, E., Leblanc, N. R., & Cole, W. C. (1993). Metabolic inhibition enhances Ca^{2+}-activated K^+ current in smooth muscle cells of rabbit portal vein. *Am.J.Physiol.* **265**, H2184-H2195.

Minami, K., Fukuzawa, K., Nakaya, Y., Zeng, X. R., & Inoue, I. (1993). Mechanism of activation of the Ca^{2+}-activated K^+ channel by cyclic AMP in cultured porcine coronary artery smooth muscle cells. *Life Sci.* **53**, 1129-1135.

Miyoshi, H. & Nakaya, Y. (1993). Activation of ATP-sensitive K^+ channels by cyclic AMP-dependent protein kinase in cultured smooth muscle cells of porcine coronary artery. *Biochem.Biophys.Res.Commun.* **193**, 240-247.

Miyoshi, Y. & Nakaya, Y. (1991). Angiotensin II blocks ATP-sensitive K^+ channels in porcine coronary artery smooth muscle cells. *Biochem.Biophys.Res.Commun.* **181**, 700-706.

Miyoshi, Y., Nakaya, Y., Wakatsuki, T., Nakaya, S., Fujino, K., Saito, K., & Inoue, I. (1992). Endothelin blocks ATP-sensitive K^+ channels and depolarizes smooth muscle cells of porcine coronary artery. *Circ.Res.* **70**, 612-616.

Moore, E. D., Etter, E. F., Philipson, K. D., Carrington, W. A., Fogarty, K. E., Lifshitz, L. M., & Fay, F. S. (1993). Coupling of the N^{a+}/Ca^{2+} exchanger, Na^+/K^+ pump and sarcoplasmic reticulum in smooth muscle. *Nature* **365**, 657-660.

Moran, O. (1996). Patch-clamp technique. In *Experimental Techniques in Bioelectrochemistri*, eds. Brabec, V., Walz, D., & Milazzo, G., pp. 527-555. Birkhauser Verlag, Basel/ Switzerland.

Moran, O., Conti, F., & Tammaro, P. (2003). Sodium channel heterologous expression in mammalian cells and the role of the endogenous beta1-subunits. *Neurosci.Lett.* **336**, 175-179.

Mueller, E. & van Breemen, C. (1979). Role of intracellular Ca^{2+} sequestration in beta-adrenergic relaxation of a smooth muscle. *Nature* **281**, 682-683.

Mulvany, M. J., Nilsson, H., & Flatman, J. A. (1982). Role of membrane potential in the response of rat small mesenteric arteries to exogenous noradrenaline stimulation. *J.Physiol.* **332**, 363-373.

Muraki, K., Imaizumi, Y., Ohya, S., Sato, K., Takii, T., Onozaki, K., & Watanabe, M. (1997). Apamin-sensitive Ca^{2+}-dependent K^+ current and hyperpolarization in human endothelial cells. *Biochem Biophys Res Commun* **236**, 340-343.

Murakoshi, H., Shi, G., Scannevin, R. H., & Trimmer, J. S. (1997). Phosphorylation of the Kv2.1 K+ channel alters voltage-dependent activation. *Mol Pharmacol* **52**, 821-828.

Nag, S. (1990). Ultracytochemical localisation of Na^+/K^+-ATPase in cerebral endothelium in acute hypertension. *Acta Neuropathol (Berl)* **80**, 7-11.

Nakache, M. & Gaub, H. E. (1988). Hydrodynamic hyperpolarization of endothelial cells. *Proc.Natl.Acad.Sci.U S A* **85**, 1841-1843.

Nakazawa, M. & Mustafa, S. J. (1988). Effects of adenosine and calcium entry blockers on 3,4-diaminopyridine-induced rhythmic contractions in dog coronary artery. *Eur.J.Pharmacol.* **149**, 345-349.

Neher, E. (1992). Correction for liquid junction potentials in patch clamp experiments. *Methods Enzymol.* **207**, 123-131.

Neher, E. & Sakmann, B. (1995). *Single-Channel Recording*, 2 ed. Plenum Press, New York and London.

Neild, T. O. & Keef, K. (1985). Measurements of the membrane potential of arterial smooth muscle in anesthetized animals and its relationship to changes in artery diameter. *Microvasc Res* **30**, 19-28.

Nelson, M. T., Cheng, H., Rubart, M., Santana, L. F., Bonev, A. D., Knot, H. J., & Lederer, W. J. (1995). Relaxation of arterial smooth muscle by calcium sparks. *Science* **270**, 633-637.

Nelson, M. T., Huang, Y., Brayden, J. E., Hescheler, J., & Standen, N. B. (1990a). Arterial dilations in response to calcitonin gene-related peptide involve activation of K^+ channels. *Nature* **19;344**, 770-773.

Nelson, M. T., Patlak, J. B., Worley, J. F., & Standen, N. B. (1990b). Calcium channels, potassium channels, and voltage dependence of arterial smooth muscle tone. *Am.J.Physiol.* **259**, C3-18.

Nelson, M. T. & Quayle, J. M. (1995). Physiological roles and properties of potassium channels in arterial smooth muscle. *Am.J.Physiol.* **268**, C799-C822.

Neylon, C. B. (2002). Potassium channels and vascular proliferation. *Vascul Pharmacol* **38**, 35-41.

Neylon, C. B., Lang, R. J., Fu, Y., Bobik, A., & Reinhart, P. H. (1999). Molecular cloning and characterization of the intermediate-conductance Ca^{2+}-dependent K^+ channel in vascular smooth muscle: relationship between K_{Ca} channel diversity and smooth muscle cell function. *Circ Res* **85**, e33-e43.

Nilius, B. (1990). Permeation properties of a non-selective cation channel in human vascular endothelial cells. *Pflugers.Arch.* **416**, 609-611.

Nilius, B. & Droogmans, G. (2001). Ion channels and their functional role in vascular endothelium. *Physiol.Rev.* **81**, 1415-1459.

Nilius, B., Droogmans, G., Gericke, M., & Schwarz, G. (1993a). Nonselective ion pathways in human endothelial cells. *EXS* **66**, 269-280.

Nilius, B. & Riemann, D. (1990). Ion channels in human endothelial cells. *Gen.Physiol.Biophys.* **9**, 89-111.

Nilius, B., Schwartz, G., Oike, M., & Droogmans, G. (1993b). Histamine-activated, non-selective cation currents and Ca^{2+} transients in endothelial cells from human umbilical vein. *Pflugers.Arch.* **424**, 285-293.

Nilius, B., Schwarz, G., & Droogmans, G. (1993c). Modulation by histamine of an inwardly rectifying potassium channel in human endothelial cells. *J Physiol* **472**, 359-371.

Nilius, B., Viana, F., & Droogmans, G. (1997). Ion channels in vascular endothelium. *Annu Rev Physiol* **59**, 145-170.

Nixon, G. F., Mignery, G. A., & Somlyo, A. V. (1994). Immunogold localization of inositol 1,4,5-trisphosphate receptors and characterization of ultrastructural features of the sarcoplasmic reticulum in phasic and tonic smooth muscle. *J Muscle Res Cell Motil* **15**, 682-700.

Ogden, D. (1994). *Microelectrode Techniques. The plymouth Workshop Handbook*, 2 ed. Company of Biologists.

Ohmori, H. & Yoshii, M. (1977). Surface potential reflected in both gating and permeation mechanisms of sodium and calcium channels of the tunicate egg cell membrane. *J Physiol* **267**, 429-463.

Ohno, M., Gibbons, G. H., Dzau, V. J., & Cooke, J. P. (1993). Shear stress elevates endothelial cGMP. Role of a potassium channel and G protein coupling. *Circulation* **88**, 193-197.

Oike, M., Droogmans, G., Casteels, R., & Nilius, B. (1993). Electrogenic Na^+/K^+-transport in human endothelial cells. *Pflugers.Arch.* **424**, 301-307.

Oike, M., Droogmans, G., & Nilius, B. (1994a). Mechanosensitive Ca^{2+} transients in endothelial cells from human umbilical vein. *Proc.Natl.Acad.Sci.U S A* **91**, 2940-2944.

Oike, M., Gericke, M., Droogmans, G., & Nilius, B. (1994b). Calcium entry activated by store depletion in human umbilical vein endothelial cells. *Cell Calcium* **16**, 367-376.

Okabe, K., Kitamura, K., & Kuriyama, H. (1988). The existence of a highly tetrodotoxin sensitive Na channel in freshly dispersed smooth muscle cells of the rabbit main pulmonary artery. *Pflügers Arch.* **411**, 423-428.

Okada, K., Ishikawa, S., & Saito, T. (1992). Cellular mechanisms of vasopressin and endothelin to mobilize $[Mg^{2+}]_i$ in vascular smooth muscle cells. *Am.J.Physiol.* **263**, C873-C878.

Okano, M. & Yoshida, Y. (1993). Influence of shear stress on endothelial cell shapes and junction complexes at flow dividers of aortic bifurcations in cholesterol-fed rabbits. *Front Med Biol Eng* **5**, 95-120.

Osipenko, O. N., Tate, R. J., & Gurney, A. M. (2000). Potential role for Kv3.1b channels as oxygen sensors. *Circ.Res.* **86**, 534-540.

Osol, G. (1995). Mechanotransduction by vascular smooth muscle. *J.Vasc.Res.* **32**, 275-292.

Pacaud, P., Loirand, G., Gregoire, G., Mironneau, C., & Mironneau, J. (1992). Calcium-dependence of the calcium-activated chloride current in smooth muscle cells of rat portal vein. *Pflugers.Arch.* **421**, 125-130.

Pal, S., Hartnett, K. A., Nerbonne, J. M., Levitan, E. S., & Aizenman, E. (1915). Mediation of neuronal apoptosis by Kv2.1-encoded potassium channels. *J.Neurosci.* **23**, 4798-4802.

Parcej, D. N., Scott, V. E., & Dolly, J. O. (1992). Oligomeric properties of alpha-dendrotoxin-sensitive potassium ion channels purified from bovine brain. *Biochemistry* **31**, 11084-11088.

Pardo, L. A., Heinemann, S. H., Terlau, H., Ludewig, U., Lorra, C., Pongs, O., & Stuhmer, W. (1992). Extracellular K^+ specifically modulates a rat brain K^+ channel. *Proc.Natl.Acad.Sci.U S A* **89**, 2466-2470.

Parekh, A. B. & Penner, R. (1997). Store depletion and calcium influx. *Physiol.Rev.* **77**, 901-930.

Park, M. K., Lee, S. H., Ho, W. K., & Earm, Y. E. (1995). Redox agents as a link between hypoxia and the responses of ionic channels in rabbit pulmonary vascular smooth muscle. *Exp.Physiol.* **80**, 835-842.

Pasyk, E., Mao, Y. K., Ahmad, S., Shen, S. H., & Daniel, E. E. (1992). An endothelial cell-line contains functional vasoactive intestinal polypeptide receptors: they control inwardly rectifying K+ channels. *Eur.J.Pharmacol.* **212**, 209-214.

Patel, A. J. & Honore, E. (2001). Properties and modulation of mammalian 2P domain K^+ channels. *Trends.Neurosci.* **24**, 339-346.

Patel, A. J. & Honoré, E. (2001). Molecular physiology of oxygen-sensitive potassium channels. *European Respiratory Journal* **18**, 221-227.

Patel, A. J., Lazdunski, M., & Honore, E. (1997a). Kv2.1/Kv9.3, a novel ATP-dependent delayed-rectifier K^+ channel in oxygen-sensitive pulmonary artery myocytes. *EMBO.J.* **16**, 6615-6625.

Patel, A. J., Lazdunski, M., & Honoré, E. (1997b). Kv2.1/Kv9.3, a novel ATP-dependent delayed-rectifier K^+ channel in oxygen-sensitive pulmonary artery myocytes. *EMBO J.* **16**, 6615-6625.

Pennefather, P. S. & DeCoursey, T. E. (1994). A scheme to account for the effects of Rb^+ and K^+ on inward rectifier K channels of bovine artery endothelial cells. *J Gen Physiol* **103**, 549-581.

Pfau, S., Leitenberg, D., Rinder, H., Smith, B. R., Pardi, R., & Bender, J. R. (1995). Lymphocyte adhesion-dependent calcium signaling in human endothelial cells. *J Cell Biol* **128** , 969-978.

Pili, R., Corda, S., Passaniti, A., Ziegelstein, R. C., Heldman, A. W., & Capogrossi, M. C. (1993). Endothelial cell Ca^{2+} increases upon tumor cell contact and modulates cell-cell adhesion. *J Clin Invest* **92**, 3017-3022.

Post, J. M., Hume, J. R., Archer, S. L., & Weir, E. K. (1992). Direct role for potassium channel inhibition in hypoxic pulmonary vasoconstriction. *Am.J.Physiol.* **262**, C882-C890.

Proudfoot, D. & Shanahan, C. M. (2001). Biology of calcification in vascular cells: intima versus media. *Herz* **26**, 245-251.

Pusch, M., Conti, F., & Stuhmer, W. (1989). Intracellular magnesium blocks sodium outward currents in a voltage- and dose-dependent manner. *Biophys.J.* **55**, 1267-1271.

Quayle, J. M., Bonev, A. D., Brayden, J. E., & Nelson, M. T. (1994). Calcitonin gene-related peptide activated ATP-sensitive K^+ currents in rabbit arterial smooth muscle via protein kinase A. *J.Physiol.* **475**, 9-13.

Quayle, J. M., McCarron, J. G., Brayden, J. E., & Nelson, M. T. (1993). Inward rectifier K+ currents in smooth muscle cells from rat resistance-sized cerebral arteries. *Am.J.Physiol.* **265**, C1363-C1370.

Quayle, J. M., Nelson, M. T., & Standen, N. B. (1997). ATP-sensitive and inwardly rectifying potassium channels in smooth muscle. *Physiol.Rev.* **77**, 1165-1232.

Quinn, M. T., Parthasarathy, S., Fong, L. G., & Steinberg, D. (1987). Oxidatively modified low density lipoproteins: a potential role in recruitment and retention of monocyte/macrophages during atherogenesis. *Proc.Natl.Acad.Sci.U S A* **84**, 2995-2998.

Ran, S. & Benos, D. J. (1992). Immunopurification and structural analysis of a putative epithelial Cl- channel protein isolated from bovine trachea. *J Biol Chem* **267**, 3618-3625.

Reed, K. E., Westphale, E. M., Larson, D. M., Wang, H. Z., Veenstra, R. D., & Beyer, E. C. (1993). Molecular cloning and functional expression of human connexin37, an endothelial cell gap junction protein. *J Clin Invest* **91**, 997-1004.

Reimann, F. & Ashcroft, F. M. (1999). Inwardly rectifying potassium channels. *Curr Opin Cell Biol* **11**, 503-508.

Rembold, C. M. & Murphy, R. A. (1993). Models of the mechanism for crossbridge attachment in smooth muscle. *J Muscle Res Cell Motil* **14**, 325-334.

Rettig, J., Heinemann, S. H., Wunder, F., Lorra, C., Parcej, D. N., Dolly, J. O., & Pongs, O. (1994). Inactivation properties of voltage-gated K^+ channels altered by presence of beta-subunit. *Nature* **369**, 289-294.

Richard, S., Neveu, D., Carnac, G., Bodin, P., Travo, P., & Nargeot, J. (1992). Differential expression of voltage-gated Ca^{2+}-currents in cultivated aortic myocytes. *Biochim.Biophys.Acta* **1160**, 95-104.

Roberds, S. L. & Tamkun, M. M. (1991). Cloning and tissue-specific expression of five voltage-gated potassium channel cDNAs expressed in rat heart. *Proc.Natl.Acad.Sci.USA* **88**, 1798-1802.

Robertson, B. E. & Nelson, M. T. (1994). Aminopyridine inhibition and voltage dependence of K^+ currents in smooth muscle cells from cerebral arteries. *Am.J.Physiol.* **267**, C1589-C1597.

Robertson, B. E., Schubert, R., Hescheler, J., & Nelson, M. T. (1993). cGMP-dependent protein kinase activates Ca-activated K channels in cerebral artery smooth muscle cells. *Am.J.Physiol.* **265**, C299-C303.

Roe, M. W., Worley, J. F. 3., Mittal, A. A., Kuznetsov, A., DasGupta, S., Mertz, R. J., Witherspoon, S. M. 3., Blair, N., Lancaster, M. E., McIntyre, M. S., Shehee, W. R., Dukes, I. D., & Philipson, L. H. (1996). Expression and function of pancreatic β-cell delayed rectifier K^+ channels. Role in stimulus-secretion coupling. *J.Biol.Chem.* **271**, 32241-32246.

Ross, R. (1999). Atherosclerosis--an inflammatory disease. *N Engl J Med* **340**, 115-126.

Rubanyi, G. M., Freay, A. D., Kauser, K., Johns, A., & Harder, D. R. (1990). Mechanoreception by the endothelium: mediators and mechanisms of pressure- and flow-induced vascular responses. *Blood Vessels* **27**, 246-257.

Rudy, B. (1988). Diversity and ubiquity of K channels. *Neuroscience* **25**, 729-749.

Rusko, J., Tanzi, F., van, B., & Adams, D. J. (1992). Calcium-activated potassium channels in native endothelial cells from rabbit aorta: conductance, Ca^{2+} sensitivity and block. *J Physiol* **455**, 601-621.

Russell, S. N., Overturf, K. E., & Horowitz, B. (1994). Heterotetramer formation and charybdotoxin sensitivity of two K^+ channels cloned from smooth muscle. *Am.J.Physiol.* **267**, C1729-C1733.

Sackin, H. (1995). Mechanosensitive channels. *Annu Rev Physiol* **57**, 333-353.

Sadoshima, J., Akaike, N., Kanaide, H., & Nakamura, M. (1988a). Cyclic AMP modulates Ca-activated K channel in cultured smooth muscle cells of rat aortas. *Am.J.Physiol.* **255**, H754-H759.

Sadoshima, J., Akaike, N., Kanaide, H., & Nakamura, M. (1988b). Cyclic AMP modulates Ca-activated K channel in cultured smooth muscle cells of rat aortas. *Am.J.Physiol.* **255**, H754-H759.

Sambrook, J., Fritsch, E. F., & Maniatis, T. (1989). *Molecular cloning: a laboratory manual.*, 2 ed. Cold Spring Harbour Laboratory Press, London.

Sansom, S. C. & Stockand, J. D. (1994). Differential Ca^{2+} sensitivities of BK_{Ca} isochannels in bovine mesenteric vascular smooth muscle. *Am.J.Physiol.* **266**, C1182-C1189.

Sato, O. & Ogawa, Y. (2001). Myosin assembly critical for the enzyme activity of smooth muscle myosin phosphatase: effects of MgATP, ionic strength, and Mg^{2+}. *J Biochem (Tokyo)* **129**, 881-889.

Sauve, R., Chahine, M., Tremblay, J., & Hamet, P. (1990). Single-channel analysis of the electrical response of bovine aortic endothelial cells to bradykinin stimulation: contribution of a Ca^{2+}-dependent K^+ channel. *J Hypertens Suppl* **8**, S193-S201.

Sauve, R., Parent, L., Simoneau, C., & Roy, G. (1988). External ATP triggers a biphasic activation process of a calcium-dependent K^+ channel in cultured bovine aortic endothelial cells. *Pflugers.Arch.* **412**, 469-481.

Schlessinger, J. & Ullrich, A. (1992). Growth factor signaling by receptor tyrosine kinases. *Neuron* **9**, 383-391.

Schnitzler, M. M., Derst, C., Daut, J., & Preisig-Muller, R. (2000). ATP-sensitive potassium channels in capillaries isolated from guinea-pig heart. *J Physiol* **525 Pt 2**, 307-317.

Schubert, R. & Nelson, M. T. (2001). Protein kinases: tuners of the BK_{Ca} channel in smooth muscle. *Trends Pharmacol.Sci.* **22**, 505-512.

Schwartz, M. A., Brown, E. J., & Fazeli, B. (1993). A 50-kDa integrin-associated protein is required for integrin-regulated calcium entry in endothelial cells. *J Biol Chem* **268**, 19931-19934.

Schwarz, G., Callewaert, G., Droogmans, G., & Nilius, B. (1992a). Shear stress-induced calcium transients in endothelial cells from human umbilical cord veins. *J Physiol* **458**, 527-538.

Schwarz, G., Droogmans, G., & Nilius, B. (1992b). Shear stress induced membrane currents and calcium transients in human vascular endothelial cells. *Pflugers.Arch.* **421**, 394-396.

Scornik, F. S., Codina, J., Birnbaumer, L., & Toro, L. (1993). Modulation of coronary smooth muscle KCa channels by Gs alpha independent of phosphorylation by protein kinase A. *Am.J.Physiol.* **265**, H1460-H1465.

Scornik, F. S. & Toro, L. (1992). U46619, a thromboxane A2 agonist, inhibits K_{Ca} channel activity from pig coronary artery. *Am.J.Physiol.* **262**, C708-C713.

Seidler, N. W., Jona, I., Vegh, M., & Martonosi, A. (1989). Cyclopiazonic acid is a specific inhibitor of the Ca^{2+}-ATPase of sarcoplasmic reticulum. *J Biol Chem* **264**, 17816-17823.

Shamotienko, O. G., Parcej, D. N., & Dolly, J. O. (1997). Subunit combinations defined for K+ channel Kv1 subtypes in synaptic membranes from bovine brain. *Biochemistry* **36**, 8195-8201.

Shi, G., Kleinklaus, A. K., Marrion, N. V., & Trimmer, J. S. (1994). Properties of Kv2.1 K^+ channels expressed in transfected mammalian cells. *J.Biol.Chem.* **269**, 23204-23211.

Shi, G., Nakahira, K., Hammond, S., Rhodes, K. J., Schechter, L. E., & Trimmer, J. S. (1996). Beta subunits promote K^+ channel surface expression through effects early in biosynthesis. *Neuron* **16**, 843-852.

Shieh, C. C., Coghlan, M., Sullivan, J. P., & Gopalakrishnan, M. (2000). Potassium channels: molecular defects, diseases, and therapeutic opportunities. *Pharmacol.Rev.* **52**, 557-594.

Shimamura, K., Sekiguchi, F., & Sunano, S. (1999). Tension oscillation in arteries and its abnormality in hypertensive animals. *Clin.Exp.Pharmacol.Physiol.* **26**, 275-284.

Sigworth, F. J. (1980). The variance of sodium current fluctuations at the node of Ranvier. *J Physiol* **307**, 97-129.

Silver, M. R. & DeCoursey, T. E. (1990). Intrinsic gating of inward rectifier in bovine pulmonary artery endothelial cells in the presence or absence of internal Mg^{2+}. *J Gen Physiol* **96**, 109-133.

Silver, M. R., Shapiro, M. S., & DeCoursey, T. E. (1994). Effects of external Rb^{+} on inward rectifier K^{+} channels of bovine pulmonary artery endothelial cells. *J Gen Physiol* **103**, 519-548.

Smirnov, S. V. & Aaronson, P. I. (1992a). Ca^{2+}-activated and voltage-gated K^{+} currents in smooth muscle cells isolated from human mesenteric arteries. *J Physiol* **457**, 431-454.

Smirnov, S. V. & Aaronson, P. I. (1992b). Ca^{2+} currents in single myocytes from human mesenteric arteries: evidence for a physiological role of L-type channels. *J.Physiol.* **457**, 455-475.

Smirnov, S. V. & Aaronson, P. I. Calcium currents in smooth muscle cells isolated from human mesenteric arteries measured in solutions containing normal and elevated calcium concentrations. Journal of Physiology 446, 483P. 1992c.

Smirnov, S. V. & Aaronson, P. I. (1994). Alteration of the transmembrane K^{+} gradient during development of delayed rectifier in isolated rat pulmonary arterial cells. *J.Gen.Physiol.* **104**, 241-264.

Smirnov, S. V., Beck, R., Tammaro, P., Ishii, T., & Aaronson, P. I. (2001). Electrophysiologically distinct smooth muscle cell subtypes in rat conduit and resistance pulmonary arteries. *J.Physiol.* **538**, 867-878.

Smirnov, S. V., Knock, G. A., Belevych, A. E., & Aaronson, P. I. (2000). Mechanism of effect of extracellular pH on L-type Ca^{2+} channel currents in human mesenteric arterial cells. *Am.J.Physiol.Heart.Circ.Physiol.* **279**, H76-H85.

Smirnov, S. V., Robertson, T. P., Ward, J. P., & Aaronson, P. I. (1994a). Chronic hypoxia is associated with reduced delayed rectifier K+ current in rat pulmonary artery muscle cells. *Am.J.Physiol.* **266**, H365-H370.

Smirnov, S. V., Robertson, T. P., Ward, J. P. T., & Aaronson, P. I. (1994b). Chronic hypoxia is associated with reduced delayed rectifier K^{+} current in rat pulmonary artery muscle cells. *Am.J.Physiol.* **266**, H365-H370.

Smirnov, S. V., Zholos, A. V., & Shuba, M. F. (1992). Potential-dependent inward currents in single isolated smooth muscle cells of the rat ileum. *J Physiol* **454**, 549-571.

Snutch, T. P. & Reiner, P. B. (1992). Ca^{2+} channels: diversity of form and function. *Curr Opin Neurobiol* **2**, 247-253.

Snyders, D. J., Tamkun, M. M., & Bennett, P. B. (1993). A rapidly activating and slowly inactivating potassium channel cloned from human heart. Functional analysis after stable mammalian cell culture expression. *J.Gen.Physiol.* **101**, 513-543.

Snyders, D. J. & Yeola, S. W. (1995). Determinants of antiarrhythmic drug action. Electrostatic and hydrophobic components of block of the human cardiac hKv1.5 channel. *Circ Res* **77**, 575-583.

Somlyo, A. V., Bond, M., Somlyo, A. P., & Scarpa, A. (1985). Inositol trisphosphate-induced calcium release and contraction in vascular smooth muscle. *Proc.Natl.Acad.Sci.U S A* **82** , 5231-5235.

Somlyo, A. V. & Somlyo, A. P. (1968). Electromechanical and pharmacomechanical coupling in vascular smooth muscle. *J Pharmacol Exp Ther* **159**, 129-145.

Song, Y. & Simard, J. M. (1995). β-Adrenoceptor stimulation activates large-conductance Ca^{2+}- activated K^+ channels in smooth muscle cells from basilar artery of guinea pig. *Pflügers Arch.* **430**, 984-993.

Standen, N. B. & Quayle, J. M. (1998a). K^+ channel modulation in arterial smooth muscle. *Acta Physiol Scand* **164**, 549-557.

Standen, N. B. & Quayle, J. M. (1998b). K^+ channel modulation in arterial smooth muscle. *Acta Physiol.Scand.* **164**, 549-557.

Steinberg, D., Parthasarathy, S., Carew, T. E., Khoo, J. C., & Witztum, J. L. (1989). Beyond cholesterol. Modifications of low-density lipoprotein that increase its atherogenicity. *N Engl J Med* **320**, 915-924.

Stromer, M. H. (1998). The cytoskeleton in skeletal, cardiac and smooth muscle cells. *Histol Histopathol* **13**, 283-291.

Stuhmer, W. (1992). Electrophysiological recordings of *Xenopus* oocytes. In *Methods in Enzymology: Ion Channels* pp. 319-339. Academic Press, London.

Stuhmer, W., Ruppersberg, J. P., Schroter, K. H., Sakmann, B., Stocker, M., Giese, K. P., Perschke, A., Baumann, A., & Pongs, O. (1989). Molecular basis of functional diversity of voltage-gated potassium channels in mammalian brain. *EMBO.J.* **8**, 3235-3244.

Stull, J. T., Gallagher, P. J., Herring, B. P., & Kamm, K. E. (1991). Vascular smooth muscle contractile elements. Cellular regulation. *Hypertension* **17**, 723-732.

Sturek, M. & Hermsmeyer, K. (1986). Calcium and sodium channels in spontaneously contracting vascular muscle cells. *Science* **233**, 475-478.

Stühmer, W., Ruppersberg, J. P., Schröter, K. H., Sakmann, B., Stocker, M., Giese, K. P., Perschke, A., Baumann, A., & Pongs, O. (1989). Molecular basis of functional diversity of voltage-gated potassium channels in mammalian brain. *EMBO J.* **8**, 3235-3244.

Suh, S. H., Vennekens, R., Manolopoulos, V. G., Freichel, M., Schweig, U., Prenen, J., Flockerzi, V., Droogmans, G., & Nilius, B. (1999). Characterisation of explanted endothelial cells from mouse aorta: electrophysiology and Ca^{2+} signalling. *Pflugers.Arch.* **438**, 612-620.

Sun, X. P., Supplisson, S., Torres, R., Sachs, G., & Mayer, E. (1992). Characterization of large-conductance chloride channels in rabbit colonic smooth muscle. *J Physiol* **448**, 355-382.

Swanson, R., Marshall, J., Smith, J. S., Williams, J. B., Boyle, M. B., Folander, K., Antanavage, J., Oliva, C., Buhrow, S. A., Bennett, C., Stein, R. B., & Kaczmarek, L. K. (1990). Cloning and expression of cDNA and genomic clones encoding three delayed rectifier potassium channels in rat brain. *Neuron* **4**, 929-939.

Szucs, G., Buyse, G., Eggermont, J., Droogmans, G., & Nilius, B. (1996a). Characterization of volume-activated chloride currents in endothelial cells from bovine pulmonary artery. *J.Membr.Biol.* **149**, 189-197.

Szucs, G., Heinke, S., De, G., Raeymaekers, L., Eggermont, J., Droogmans, G., & Nilius, B. (1996b). The volume-activated chloride current in endothelial cells from bovine pulmonary artery is not modulated by phosphorylation. *Pflugers.Arch.* **431**, 540-548.

Takaya, J., Higashino, H., & Kobayashi, Y. (2000). Can magnesium act as a second messenger? Current data on translocation induced by various biologically active substances. *Magnes.Res.* **13**, 139-146.

Tammaro, P., Conti, F., & Moran, O. (2002). Modulation of sodium current in mammalian cells by an epilepsy-correlated beta 1-subunit mutation. *Biochem.Biophys.Res.Commun.* **291**, 1095-1101.

Tanaka, Y., Meera, P., Song, M., Knaus, H. G., & Toro, L. (1997). Molecular constituents of maxi KCa channels in human coronary smooth muscle: predominant alpha + beta subunit complexes. *J Physiol* **502**, 545-557.

Taylor, J. R. (1997). *An Introduction to Error Analysis: The Study of Uncertainties in Physical Measurements*, 2 ed. University Science, Sausalito, CA.

Thiemann, A., Grunder, S., Pusch, M., & Jentsch, T. J. (1992). A chloride channel widely expressed in epithelial and non-epithelial cells. *Nature* **356**, 57-60.

Thorne, G. D., Conforti, L., & Paul, R. J. (2002). Hypoxic vasorelaxation inhibition by organ culture correlates with loss of Kv channels but not Ca^{2+} channels. *Am.J.Physiol.Heart.Circ.Physiol.* **283**, H247-H253.

Toro, L., Amador, M., & Stefani, E. (1990a). ANG II inhibits calcium-activated potassium channels from coronary smooth muscle in lipid bilayers. *Am.J.Physiol.* **258**, H912-H915.

Toro, L., Amador, M., & Stefani, E. (1990b). ANG II inhibits calcium-activated potassium channels from coronary smooth muscle in lipid bilayers. *Am.J.Physiol.* **258**, H912-H915.

Toullec, D., Pianetti, P., Coste, H., Bellevergue, P., Grand-Perret, T., Ajakane, M., Baudet, V., Boissin, P., Boursier, E., Loriolle, F., & et, a. (1991). The bisindolylmaleimide GF 109203X is a potent and selective inhibitor of protein kinase C. *J Biol Chem* **266**, 15771-15781.

Towbin, H., Staehelin, T., & Gordon, J. (1979). Electrophoretic transfer of proteins from polyacrylamide gels to nitrocellulose sheets: procedure and some applications. *Proc.Natl.Acad.Sci.U S A* **76**, 4350-4354.

Treharne, K. J., Marshall, L. J., & Mehta, A. (1994). A novel chloride-dependent GTP-utilizing protein kinase in plasma membranes from human respiratory epithelium. *Am.J.Physiol.* **267**, L592-L601.

Triggle, D. J. (1998). The physiological and pharmacological significance of cardiovascular T-type, voltage-gated calcium channels. *Am J Hypertens* **11**, 80S-87S.

Tseng, H., Peterson, T. E., & Berk, B. C. (1995). Fluid shear stress stimulates mitogen-activated protein kinase in endothelial cells. *Circ Res* **77**, 869-878.

Tucker, S. J., Gribble, F. M., Zhao, C., Trapp, S., & Ashcroft, F. M. (1997). Truncation of Kir6.2 produces ATP-sensitive K^+ channels in the absence of the sulphonylurea receptor. *Nature* **387**, 179-183.

Ueda, S., Lee, S. L., & Fanburg, B. L. (1990). Chloride efflux in cyclic AMP-induced configurational change of bovine pulmonary artery endothelial cells. *Circ Res* **66**, 957-967.

Vaca, L., Gurrola, G. B., Possani, L. D., & Kunze, D. L. (1993). Blockade of a KCa channel with synthetic peptides from noxiustoxin: a K^+ channel blocker. *J.Membr.Biol.* **134**, 123-129.

Vaca, L., Schilling, W. P., & Kunze, D. L. (1992). G-protein-mediated regulation of a Ca^{2+}-dependent K^+ channel in cultured vascular endothelial cells. *Pflugers.Arch.* **422**, 66-74.

van Hinsbergh, VW. (1992). Arteriosclerosis. Impairment of cellular interactions in the arterial wall. *Ann N Y Acad Sci* **673**, 321-330.

Van, R. & Lazdunski, M. (1992). A small-conductance charybdotoxin-sensitive, apamin-resistant Ca^{2+}-activated K^+ channel in aortic smooth muscle cells (A7r5 line and primary culture). *Pflugers.Arch.* **420**, 417-423.

Van, R., Vigne, P., & Frelin, C. (1995). A charybdotoxin-sensitive, Ca^{2+}-activated K^+ channel with inward rectifying properties in brain microvascular endothelial cells: properties and activation by endothelins. *J Neurochem* **65**, 1274-1281.

Vandorpe, D. H., Shmukler, B. E., Jiang, L., Lim, B., Maylie, J., Adelman, J. P., de, F., Cappellini, M. D., Brugnara, C., & Alper, S. L. (1998). cDNA cloning and functional characterization of the mouse Ca^{2+}-gated K^+ channel, mIK1. Roles in regulatory volume decrease and erythroid differentiation. *J Biol Chem* **273**, 21542-21553.

Vargas, F. F., Caviedes, P. F., & Grant, D. S. (1994). Electrophysiological characteristics of cultured human umbilical vein endothelial cells. *Microvasc Res* **47**, 153-165.

Vergara, C., Latorre, R., Marrion, N. V., & Adelman, J. P. (1998). Calcium-activated potassium channels. *Curr Opin Neurobiol* **8**, 321-329.

Verin, A. D., Gilbert-McClain, L. I., Patterson, C. E., & Garcia, J. G. (1998). Biochemical regulation of the nonmuscle myosin light chain kinase isoform in bovine endothelium. *Am J Respir Cell Mol Biol* **19**, 767-776.

Voets, T., Szucs, G., Droogmans, G., & Nilius, B. (1995). Blockers of volume-activated Cl- currents inhibit endothelial cell proliferation. *Pflugers.Arch.* **431**, 132-134.

Volk, K. A., Matsuda, J. J., & Shibata, E. F. (1991). A voltage-dependent potassium current in rabbit coronary artery smooth muscle cells. *J Physiol* **439**, 751-768.

von, B., Dittrich, M., Klieber, H. G., & Daut, J. (1996). Inwardly rectifying K^+ channels in freshly dissociated coronary endothelial cells from guinea-pig heart. *J Physiol* **491**, 357-365.

Wakatsuki, T., Nakaya, Y., & Inoue, I. (1992). Vasopressin modulates K^+-channel activities of cultured smooth muscle cells from porcine coronary artery. *Am.J.Physiol.* **263**, H491-H496.

Wallner, M., Meera, P., & Toro, L. (1996). Determinant for beta-subunit regulation in high-conductance voltage-activated and Ca^{2+}-sensitive K^+ channels: an additional transmembrane region at the N terminus. *Proc.Natl.Acad.Sci.U S A* **93**, 14922-14927.

Walsh, M. P., Andrea, J. E., Allen, B. G., Clément-Chomienne, O., Collins, E. M., & Morgan, K. G. (1994). Smooth muscle protein kinase C. *Can.J.Physiol.Pharmacol.* **72**, 1392-1399.

Wang, J., Juhaszova, M., Rubin, L. J., & Yuan, X. J. (1997). Hypoxia inhibits gene expression of voltage-gated K^+ channel alpha subunits in pulmonary artery smooth muscle cells. *J Clin Invest* **100**, 2347-2353.

Wang, Y., Santini, F., Qin, K., & Huang, C. Y. (1995). A Mg^{2+}-dependent, Ca^{2+}-inhibitable serine/threonine protein phosphatase from bovine brain. *J Biol Chem* **270**, 25607-25612.

Watanabe, M., Yumoto, K., & Ochi, R. (1994). Indirect activation by internal calcium of chloride channels in endothelial cells. *Jpn J Physiol* **44 Suppl 2**, S233-S236.

Wellman, G. C., Quayle, J. M., & Standen, N. B. (1998). ATP-sensitive K^+ channel activation by calcitonin gene-related peptide and protein kinase A in pig coronary arterial smooth muscle. *J Physiol* **507**, 117-129.

Wesselman, J. P., Schubert, R., VanBavel, E. D., Nilsson, H., & Mulvany, M. J. (1997). K_{Ca}-channel blockade prevents sustained pressure-induced depolarization in rat mesenteric small arteries. *Am.J.Physiol.* **272**, H2241-H2249.

White, C. R. & Brock, T. A. (1994). Calcium-mobilizing agonists stimulate anion fluxes in cultured endothelial cells from human umbilical vein. *J.Membr.Biol.* **142**, 171-179.

White, R. E. & Hartzell, H. C. (1988). Effects of intracellular free magnesium on calcium current in isolated cardiac myocytes. *Science* **239**, 778-780.

Wilcox, J. N. & Scott, N. A. (1996). Potential role of the adventitia in arteritis and atherosclerosis. *Int J Cardiol* **54 Suppl**, S21-S35.

Willeit, J. & Kiechl, S. (2000). Biology of arterial atheroma. *Cerebrovasc Dis* **10 Suppl 5**, 1-8.

Williams, C. P., Hu, N., Shen, W., Mashburn, A. B., & Murray, K. T. (2002). Modulation of the human Kv1.5 channel by protein kinase C activation: role of the Kvbeta1.2 subunit. *J Pharmacol Exp Ther* **302**, 545-550.

Wonderlin, W. F. & Strobl, J. S. (1996). Potassium channels, proliferation and G1 progression. *J.Membr.Biol.* **154**, 91-107.

Woodhull, A. M. (1973). Ionic blockage of sodium channels in nerve. *J Gen Physiol* **61**, 687-708.

Wu, S., Moore, T. M., Brough, G. H., Whitt, S. R., Chinkers, M., Li, M., & Stevens, T. (2000). Cyclic nucleotide-gated channels mediate membrane depolarization following activation of store-operated calcium entry in endothelial cells. *J Biol Chem* **275**, 18887-18896.

Xia, X. M., Fakler, B., Rivard, A., Wayman, G., Johnson-Pais, T., Keen, J. E., Ishii, T., Hirschberg, B., Bond, C. T., Lutsenko, S., Maylie, J., & Adelman, J. P. (1998). Mechanism of calcium gating in small-conductance calcium-activated potassium channels. *Nature* **395**, 503-507.

Xie, H. Q. & Hu, V. W. (1994). Modulation of gap junctions in senescent endothelial cells. *Exp Cell Res* **214**, 172-176.

Xu, X., Rials, S. J., Wu, Y., Marinchak, R. A., & Kowey, P. R. (1999). The properties of the inward rectifier potassium currents in rabbit coronary arterial smooth muscle cells. *Pflugers.Arch.* **438**, 187-194.

Yaghi, A., Mehta, S., & McCormack, D. G. (2002). Delayed rectifier potassium channels contribute to the depressed pulmonary artery contractility in pneumonia. *J.Appl.Physiol.* **93**, 957-965.

Yamamoto, K., Korenaga, R., Kamiya, A., Qi, Z., Sokabe, M., & Ando, J. (2000). P2X(4) receptors mediate ATP-induced calcium influx in human vascular endothelial cells. *Am.J.Physiol.Heart.Circ.Physiol.* **279**, H285-H292.

Yao, X., Leung, P. S., Kwan, H. Y., Wong, T. P., & Fong, M. W. (1999). Rod-type cyclic nucleotide-gated cation channel is expressed in vascular endothelium and vascular smooth muscle cells. *Cardiovasc Res* **41**, 282-290.

Yatani, A., Seidel, C. L., Allen, J., & Brown, A. M. (1987). Whole-cell and single-channel calcium currents of isolated smooth muscle cells from saphenous vein. *Circ.Res.* **60**, 523-533.

Yellen, G. (1998). The moving parts of voltage-gated ion channels. *Q.Rev.Biophys.* **31**, 239-295.

Yu, F. H. & Catterall, W. A. (2003). Overview of the voltage-gated sodium channel family. *Genome Biol* **4**, 207.

Yu, S. P. & Choi, D. W. (2000). Ions, cell volume, and apoptosis. *Proc.Natl.Acad.Sci.USA* **97**, 9360-9362.

Yuan, X.-J., Sugiyama, T., Goldman, W. F., Rubin, L. J., & Blaustein, M. P. (1996). A mitochondrial uncoupler increases K_{Ca} currents but decreases K_V currents in pulmonary artery myocytes. *Am.J.Physiol.* **270**, C321-C331.

Yuan, X.-J., Wang, J., Juhaszova, M., Golovina, V. A., & Rubin, L. J. (1998). Molecular basis and function of voltage-gated K^+ channels in pulmonary arterial smooth muscle cells. *Am.J.Physiol.* **274**, L621-L635.

Yuan, X. J., Goldman, W. F., Tod, M. L., Rubin, L. J., & Blaustein, M. P. (1993). Ionic currents in rat pulmonary and mesenteric arterial myocytes in primary culture and subculture. *Am.J.Physiol.* **264**, L107-L115.

Yumoto, K., Watanabe, M., Yamaguchi, H., & Ochi, R. (1994). ATP-induced chloride current and tonic increase of internal Ca^{2+} concentration in vascular endothelial cells. *Jpn J Physiol* **44 Suppl 2**, S241-S243.

Zamponi, G. W. & French, R. J. (1995). Sodium current inhibition by internal calcium: a combination of open-channel block and surface charge screening? *J.Membr.Biol.* **147**, 1-6.

Zhang, H. & Bolton, T. B. (1995). Activation by intracellular GDP, metabolic inhibition and pinacidil of a glibenclamide-sensitive K-channel in smooth muscle cells of rat mesenteric artery. *Br.J.Pharmacol.* **114**, 662-672.

Zhang, H., Inazu, M., Weir, B., & Daniel, E. (1994). Endothelin-1 inhibits inward rectifier potassium channels and activates nonspecific cation channels in cultured endothelial cells. *Pharmacology* **49**, 11-22.

Zhou, S. S., Takai, A., & Okada, Y. (2002). Regulation of cardiac CFTR Cl^- channel activity by a Mg^{2+}-dependent protein phosphatase. *Pflugers.Arch.* **444**, 327-334.

Zhou, X. B., Ruth, P., Schlossmann, J., Hofmann, F., & Korth, M. (1996). Protein phosphatase 2A is essential for the activation of Ca2+-activated K+ currents by cGMP-dependent protein kinase in tracheal smooth muscle and Chinese hamster ovary cells. *J Biol Chem* **271**, 19760-19767.

Zhou, Y. Y., Yao, J. A., & Tseng, G. N. (1997). Role of tyrosine kinase activity in cardiac slow delayed rectifier channel modulation by cell swelling. *Pflugers.Arch.* **433**, 750-757.

Zhuchenko, O., Bailey, J., Bonnen, P., Ashizawa, T., Stockton, D. W., Amos, C., Dobyns, W. B., Subramony, S. H., Zoghbi, H. Y., & Lee, C. C. (1997). Autosomal dominant cerebellar ataxia (SCA6) associated with small polyglutamine expansions in the alpha 1A-voltage-dependent calcium channel. *Nat Genet* **15**, 62-69.

Zunkler, B. J., Henning, B., Grafe, M., Bass, R., Hildebrandt, A. G., & Fleck, E. (1995). Electrophysiological properties of human coronary endothelial cells. *Basic Res Cardiol* **90**, 435-442.

Zylinska, L., Guerini, D., Gromadzinska, E., & Lachowicz, L. (1998). Protein kinases A and C phosphorylate purified Ca^{2+}-ATPase from rat cortex, cerebellum and hippocampus. *Biochim Biophys Acta* **19;1448**, 99-108.

Publications

Papers:

- Smirnov S.V, Beck R., **Tammaro P.**, Ishii T. and Aaronson P. (2002). Electrophysiologically distinct smooth muscle cell subtypes in rat conduit and resistance pulmonary arteries. *J. Physiol.* **538**, 867-878.
- Belevych A.E., Beck R., **Tammaro P.**, Poston L., Smirnov S.V. (2002). Developmental changes in the functional characteristics and expression of voltage gated K^+ channel currents in rat aortic myocytes *Cardiov. Res.* **54**, 152-161.
- Smirnov S.V., **Tammaro P.**, Hutchings R.S. and Smith A.L. (2003). Role of voltage-gated K^+ (Kv) channels in vascular function *Neurophysiology* **35**, 262-275.

Abstracts:

Posters:

- **Tammaro P.**, Aaronson P.I., Smirnov S.V. Modulation of the native Kv2.1 channel by phosphorylation in rat aortic myocites. 45th Biophysical Society annual meeting. 17-21 February 2001, Boston, Massachusetts, U.S.A. *Biophys. J.* **80**, A1872.
- Smirnov S.V., Beck R., **Tammaro P.**, Aaronson P.I.. Differing voltage-gated K^+ currents in rat conduit and resistance pulmonary arteries. 45th Biophysical Society annual meeting. 17-21 February 2001, Boston, Massachusetts, U.S.A. *Biophys. J.* **80**, A848.
- **Tammaro P.**, Smirnov S.V. Modulation of Kv channel currents by bisindolylmaleimide I (BIM), a selective PKC inhibitor, in rat aortic myocytes. 46th Biophysical Society annual meeting. 23-27 February 2002, San Francisco, California, U.S.A. *Biophys. J.* **82**, A1380.
- **Tammaro P.**, Smirnov S.V. Dual effect of Bisindolylmaleimide I (BIM), a selective PKC inhibitor, on Kv channel currents in rat aortic myocites. XVI National Congress of the Italian Society for Pure and Applied Biophysics and 1st Italian-Slovenian Workshop of Biophysics. 11-14 September 2002, Trento, Italy.

- **Tammaro P.,** Smirnov S.V. Modulation of voltage-gated K^+ (Kv) channel currents by intracellular Mg^{2+} in rat vasculature. 47th Biophysical Society annual meeting 1-5 March 2003, San Antonio, Texas, U.S.A. *Biophys. J.* **84**, A2040.

Oral communication:

- **Tammaro P.,** Smirnov S.V. Modulation of the voltage-gated potassium (Kv) channel currents by intracellular Mg^{2+} in rat aortic smooth muscle cells (RASMCs). Scientific Meeting of the Physiological Society. 17-20 December 2002 University College London, U.K. (2003) *J. Physiol.* 547P,C47.